Therapeutic Targeting of the Leukaemic Fusion Genes

Hasan Issa

Student No: 140615502

Thesis submitted to the Faculty of Medical Sciences, Newcastle University

In partial fulfilment of the requirements for the degree of

Doctor of Philosophy

October 2019

Supervisor: Prof. Olaf Heidenreich

Wolfson Childhood Cancer Research Centre, Northern Institute for Cancer research, Newcastle University. NE1 7RU, UK

Declaration

I hereby declare that the work reported in this thesis was performed by myself from January 2015 until May 2018. The laboratory work was performed in the Leukaemic Stem Cell group under the supervision of Prof. Olaf Heidenreich at the Northern Institute for Cancer research, Newcastle University.

Except where clearly indicated and referenced, the laboratory work was performed by myself.

Hasan Issa

Student No: 140615502

October 2019

Abstract

The translocation t(8;21) stands out as a paradigm of genomic aberrations in which it's fusion product (RUNX1/ETO) initiates and maintains the leukaemogenic transformation of haematopoietic stem cells. Like all leukaemias, t(8;21)-positive AML is characterised by extensive hyperproliferation and aberrant self-renewal. Here, in this thesis we show that silencing *RUNX1/ETO* by siRNA dysregulates the leukaemic molecular programme, restrains leukaemia expansion and ablates clonogenicity, suggesting therapeutic potentials.

Aiming to develop a specific targeted therapy, we relied on the RNAi machinery to specifically knockdown *RUNX1/ETO* by a chemically modified siRNA encapsulated into a lipid nanoparticle.

To enhance the efficacy of si*RUNX1/ETO,* we have introduced a combination of 2'-sugar and phosphodiester backbone modifications and proved the robustness of the gene knockdown *in vitro*. Then, we have utilised a state-of-the-art microfluidic system to encapsulate the siRNA into a novel lipid nanoparticle that is approved for clinical use. The lipid nanoparticles provided a long-lasting *RUNX1/ETO* knockdown *in vitro* in cell lines, and in t(8;21) patient primary cells and PDXs in a co-culture system. The gene knockdown was also associated with irreversible changes in RUNX1/ETO transcriptional network and induced a cytostatic phenotype characterised by G1 cell cycle arrest and senescence.

To gain insight into the pharmacokinetics and biodistribution of the nanoparticles, we have developed a protocol to label the lipid nanoparticles with a NIR dye that is compatible with *in vivo* imaging. Systemic administration of a single dose of the labelled nanoparticles caused a global body distribution in immunocompromised hosts, including leukaemic tissues and CNS. Our in-house optimised labelling protocol transforms the nanoparticles into a platform for tissue-specific delivery by substituting the dye with targeting motifs.

Using comprehensive experimental settings *in vivo*, we have successfully achieved *RUNX1/ETO* knockdown in t(8;21) murine xenotransplantation model and proved the on-target effect of the nanoparticles. Further *ex vivo* testing revealed that

RUNX1/ETO repression triggers cellular senescence and initiates a myeloid differentiation programme, which were affirmed by RNA-seq analysis obtained from *RUNX1/ETO* knockdown mice.

Our study, for the first time, shows that *RUNX1/ETO* depletion *in vivo* in a clinically relevant setting significantly prolongs the survival of leukaemic mice. Our novel approach for gene knockdown revealed that depleting *RUNX1/ETO* severely impairs clonogenicity and self-renewal, as well as prevents leukaemia propagation in secondary recipients.

To exploit the therapeutic benefits of combinational chemotherapies with *RUNX1/ETO* knockdown, we carried *in vitro* drug toxicity assays and *in vivo* treatment. The combination of *RUNX1/ETO* depletion with DNA damage agents treatment resulted in a lost sensitivity to those chemotherapies. On the contrary, *RUNX1/ETO* knockdown enhanced the pharmacological inhibition of BCL2 with a small molecule inhibitor *in vitro* but not *in vivo*.

Overall, this thesis developed a potent siRNA-based drug for *RUNX1/ETO* knockdown, which brings gene therapy from the lab closer to bedside. The thesis supports the notion that RUNX1/ETO guards the reservoir of leukaemic initiating cells, and shows how targeting the fusion transcript with siRNA significantly reduces the number of the long-term repopulating leukaemic stem cells providing an effective second-line therapy to prevent relapse in AML.

Acknowledgements

At first, I would like to thank the ‘’*Mother Nature”* who taught me modesty. I have learnt the lesson that is when I think I am clever and making progress, she would pick me up and hit me to the wall to remind me that I still have a lot to learn.

Thanks to Olaf who did not throw me from the 6th floor each time I told him that I can feel and see the knockdown in the mice, although the control group was surviving longer than the knockdown group!

Many thanks for my funders, AKF-ISP, AKF-EB-UK and Olaf. Without their support, I would not be able to complete my degree.

Many thanks to all OTH et al group members, Helen for the great training, encouragement and strict monitoring during the animal work. I feel privileged that I learnt animal work under her supervision. Hesta for not hating me (maybe!) when I ask for processing my samples or sorting them at midnight. Thanks to Ricky, Asmida, Yuzhi, Meline, Melanie, Ed and Katarzyna for the unforgettable 4 years, although nobody agreed to count my colonies! Anja for always legally stealing my PFA stock and lending her pre-historic Western blotting system. Mojgan for the special support and help during and after the move to Germany. Natalia for the help at the beginning of my PhD, and the foodies’ tour guide in the snowy Madrid! Natalie for the 30th birthday prank. The genius Alex, Frida, Vicky, and Dan for the instructions and protocols. Martina my lab dude for all the on-going and never-ending fruitful discussions. Finally, Alessandro for not hiring a hitman to get rid of me while I was teaching him the proper science.

Special thanks to my friends, Kamal and Alaa for the long sessions on the phone and sharing our PhD difficulties. Karam for the frequent late-night teatime in Quilliam. To pre-Prof. Dr^2. T Gomes for saving me from falling in the darkest valley, for listening, listening and listening. For not crushing us from the highest mountain in the Lake District in his first time to drive a red car in the UK, for the unforgettable trip to Scotland and the ticks crisis, for the lab salads, movies and many other random stuff.

Finally, many thanks for my parents and extended grand-family in Syria for all the support regardless of our loss and the pressure of the war. Ziad, my brother, who

made it finally to UCL and managed to put my bank account under a strict diet and my nerve on the edge of explosion.

List of Abbreviations

Acute myeloid leukemia	AML
Acute lymphoblastic leukemia	ALL
Argonaute 2	AGO2
Cell-penetrating peptides	CPP
Chronic lymphocytic leukemia	CML
Colony formation assay	CFA
Core binding factor	CBF
Critical micelle concentration	CMC
Cytosine arabinoside	AraC
Dimethylamine	DMA
Dynamic light scattering	DLS
Fluorescence activated cell sorting	FACS
Food and drug administration	FDA
French American British classification	FAB
Granulocyte-macrophage colony-stimulating factor	GM-CSF
Haematopoietic stem cells	HSC
Lipid nanoparticle	LNP
Nervy homology regions	NHR
Polyethylene glycol	PEG
Polyethylenimine	PEI
Reverse transcription polymerase chain reaction	RT-PCR
RNA-induced silencing complex	RISC
RNA interference	RNAi
Runt-homology domain	RHD
Small interfering ribonucleic acid	siRNA
Toll-like receptors	TLR
Transmission electron microscopy	TEM

List of Tables

List of figures

Table of Contents

Chapter 1.

Introduction

1.1 Acute Myeloid Leukaemia

1.1.1 Haematopoiesis and haematopoietic stem cell

Pluripotent haematopoietic stem cells (HSCs) generate the adult haematopoietic system providing long-term production and maintenance of all blood cell types. In adults, HSCs comprise less than 0.1% of the bone marrow (BM) cells. The origin of the pluripotent HSCs is traced back to the Aorta-Gonad-Mesonephros (AGM) region during early embryogenesis (Fig 1-1A-B) (Thomson and Meyskens 1982, Bizzari and Mackillop 1985, Mendelson and Frenette 2014).

Embryonic development of human HSCs (Fig 1-1C) begins at day 19 of gestation when the endothelial lining of the dorsal aorta upregulates the HSCs marker CD34. By the end of the third week of gestation, lymphoid and myeloid multilineage stem cells CD34+/CD45+ can be found in the intraembryonic coelom (Fig 1-1B) (Hirschi 2012, Cao, Spielmann et al. 2019) . The first wave of haematopoiesis (pre-circulation) starts in the yolk sac (YS) at day 27 of gestation. The haematopoietic trajectory in the YS has a mesoderm origin where a group of mesenchymal stem cells (MSCs) differentiate into primitive erythroblasts, and occasionally to primitive megakaryocytes and macrophages. At this stage, the haemogenic endothelium (HE) in the AGM region generates clusters of HSCs, which adhere to the ventral wall of the dorsal aorta. The second wave of haematopoiesis (circulation) in the YS produces definitive myeloid, megakaryocytes, erythroid and multipotent progenitors, which seed the foetal liver. The endothelial-to-haematopoietic migration (detachment of the HSCs from the HE) and colonising the foetal liver marks the transition to hepatic haematopoiesis by the end of the fourth week of gestation. Foetal liver remains the primary niche for HSCs maintenance and differentiation until birth. In parallel with hepatic haematopoiesis, bone marrow formation and osteogenesis mark the end of embryogenesis by the end of the second month of gestation when CD34-/CD45+/CD68+ macrophages invade the bone marrow and facilitate chondrolysis. Finally, the definitive BM niche hosts and maintains the haematopoietic progenitors and HSCs throughout life (Bloom and Bartelmez 1940, Bertrand, Giroux et al. 2005, Hirschi 2012, Beaudin, Boyer et al. 2016, Ivanovs, Rybtsov et al. 2017, Cao, Spielmann et al. 2019).

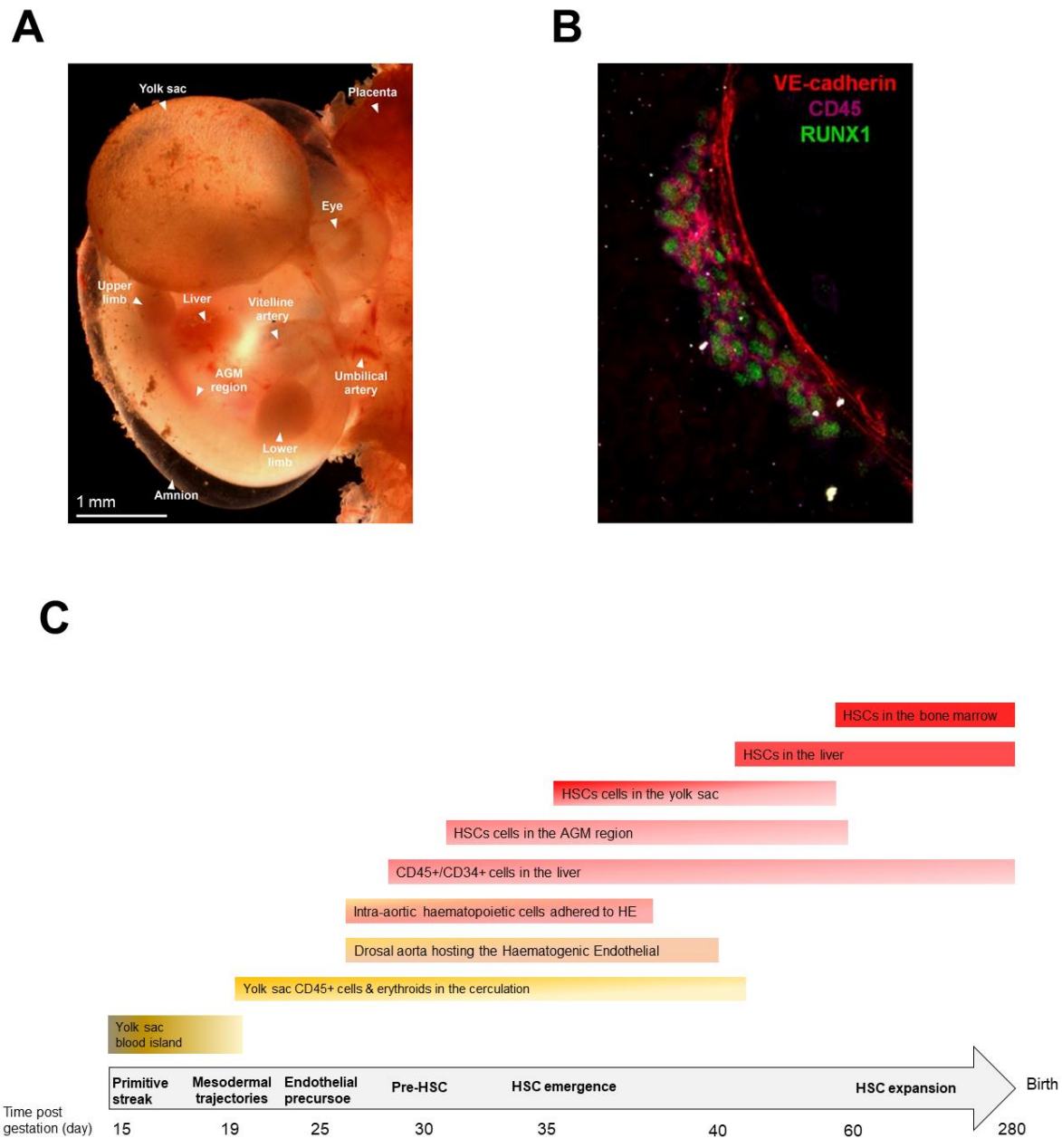

Fig 1-1: Human haematopoiesis during embryogenesis and development. (A) The localisation of the yolk sac, AGM region, liver, placenta and other embryonic tissues in a 33 days old human embryo. (B) Ventral wall of the dorsal aorta of a 38 days old human embryo showing the intra-aortic haematopoietic clusters expressing CD45, RUNX1 and VE-cadherin. (C) Chronology of human haematopoiesis. The first primitive haematopoietic cells, monocytes and macrophages are produced in the yolk sac. Blood circulation starts at day 21 after the onset of cardiac contractions, and at day 27 the ventral wall of the dorsal aorta hosts the CD34+/CD45+ cells, which are also disseminated into the liver. HSCs emerge in the AGM region at day 30 until day 42, then in the yolk sac at day 35, the liver around day 40 and finally HSCs enter the expansion phase in the bone marrow at day 60. Fading of the coloured rectangles represents the extinction of the process. Scale bar: 1 mm in A. Adapted from (Bertrand, Giroux et al. 2005, Ivanovs, Rybtsov et al. 2017).

HSCs undergo two progressive series, either self-renewal and maintaining the pluripotency or differentiation into more mature progenitor cells (Fig 1-2A, B). Haematopoietic development is a highly orchestrated process where the multipotent immature progenitors are committed to differentiate into lymphoid, myeloid, erythroid or megakaryocytic precursors in the bone marrow (Sabbath, Ball et al. 1985, Blair, Hogge et al. 1998). The multipotent myeloid and lymphoid precursors are highly proliferative and express specific receptors for growth, survival, and colony-stimulation factors. During their differentiation, precursors follow successive stages until they lose the ability to divide further and become mature blood cells (Bertrand, Giroux et al. 2005, Amabile, Welner et al. 2013).

Recent studies have showon significant HSCs heterogeneity resulting in a continuous segregation of lineage-specific features (Fig 1-2C). The new model of haematopoiesis challenges the classical model of lineage commitment and proposes a lineage-biased HSCs paradigm for blood cells formation and emergence of haematological malignancies (Haas, Trumpp et al. 2018). Moreover, there is evidence of progenitor reversibility and lineage switch between the lymphoid and myeloid progenitors, mostly in rare AML relapse cases (Ryotokuji, Yamaguchi et al. 2016). The drivers for such a switch are still under investigation, and the new lineage-biased model of HSCs might deliver new insights into the regulation of lineage switch, leukaemia propagation, and disease origin.

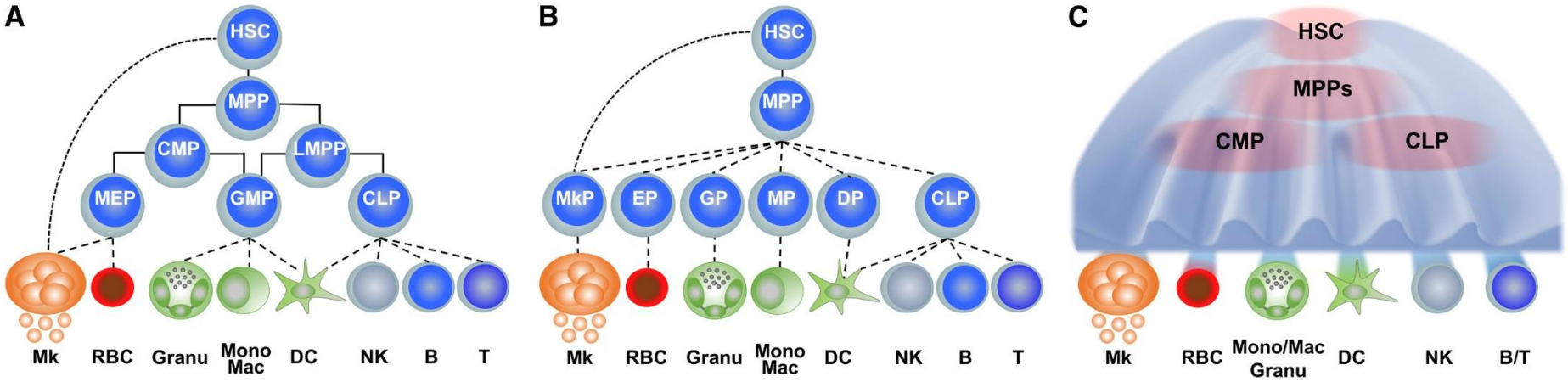

Fig 1-2: Normal human haematopoiesis models. (A) HSC classical model of lineage commitment. HSC undergoes a series of intermediate differentiation stages where HSC first generates the common myeloid and common lymphoid progenitors, which later give rise to all blood cell types. Direct shortcut from HSC to megakaryocytes was recently proposed. (B) HSC early split model where the lineage separation occurs in early stages. (C) Latest HSC lineage-bias commitment model where the HSC does not follow distinct intermediate stages of differentiation but is proposed to acquire transcriptional lineage priming features leading to a continuous Waddington-like model (Haas, Trumpp et al. 2018).

1.1.2 Leukaemogenesis

As normal haematopoiesis undergoes a highly orchestrated hierarchy of HSCs differentiation programmes, changes can lead to a transient or prolonged dysregulation of haematopoiesis. Leukaemia is defined as a condition of disordered haematopoiesis due to the acquisition of mutations in the haematopoietic progenitors, which favours their self-renewing, proliferative and survival properties and weakens their differentiation potential (Bonnet and Dick 1997, Hope, Jin et al. 2004).

Since antiquity, haematological disorders such as malaria and anaemia were noted to be associated with the spleen and liver. The first recorded description of the blood clotting dysfunction or ‘’haemophilia’’ goes back to 300-500 AD and comes from the Babylonian Talmud. Nine years after the development of the microscope by Hooke, the first description of red blood cells was made Anton van Leeuwenhoek during the Dutch Golden Age in 1674. White blood cells were later described as the “globuli albicantes” by Josef Lieutaud in 1749 (Buess 1959), while in the same year Jean-Baptiste de Sénac also describes the colourless and nucleated cells of the blood (Senac 1926). Leukaemia was finally described by Cullen in 1811 when he noticed an increased amount of white blood cells in a 35 years old patient (Cullen 1811). Before the end of the 19th century, several cases of patients with an excessive amount of white blood cells had been reported, and some authors were even able to predict that the disease were caused by increased circulation of immature blood cells (Piller 2001). Nevertheless, the term “leukaemia” was only coined by Rudolf Virchow, a German pathologist, in 1855, based on the Greek word for “white blood” to describe the leukaemic cells (Virchow 1855).

1.1.3 Acute myeloid leukaemia landscape

Acute myeloid leukaemia (AML) occurs when myeloid progenitors accumulate in the bone marrow disrupting blood production and commonly causing anaemia, immunodeficiency with recurrent infections and haemostasis deficiency with increased haemorrhagic risk. AML is a heterogeneous clonal disease which mainly affects elderly with a median age at diagnosis around 65 years (Lapidot, Sirard et al. 1994, Bonnet and Dick 1997, Hope, Jin et al. 2004). Interestingly, some myeloid conditions can evolve into acute leukaemia including disorders such as granulocytopenia, thrombocytopenia and transient abnormal myelopoiesis.

Acute myeloid leukaemia is classically diagnosed based on cytomorphological features of myeloblasts observed in samples of peripheral blood and bone marrow stained with Wright-Giemsa. Leukaemic cells display a distinctive nucleoli in a large irregular-round nuclei surrounded by a small cytoplasm (Strobel and Brandt 1986, Woronzoff-Dashkoff 2002). The French-American-British (FAB) classification (Table 1-1) categories AML into eight subtypes (M0-M7) based on the cell differentiation status and type.

Acute myeloid leukaemia	
M0	Undifferentiated acute myeloblastic leukaemia
M1	Acute myeloblastic leukaemia with minimal maturation
M2	Acute myeloblastic leukaemia with maturation
M3	Acute promyelocytic leukaemia
M4	Acute myelomonocytic leukaemia
M5	Acute monocytic leukaemia
M6	Acute erythroid leukaemia (Di or Guglielmo syndrome)

M7	Acute megakaryoblastic leukaemia (AMKL)

Table 1-1: FAB classification of AML. Adapted from (Bennett, Catovsky et al. 1976).

Leukaemia is defined by the presence of 30% or more of blasts but genetic testing is required to distinguish AML from other conditions of ineffective haematopoiesis such as myelodysplastic syndrome (MDS) or AML-related MDS (Piller 2001). In this regard, the World Health Organisation (WHO) revised the old FAB classification and introduced cytogenetic subgroups to the standard morphology classification (Table 1-2).

AML with recurrent genetic abnormalities
AML with inv(16)(p13.1q22) or t(16;16)(p13.1;q22); CBFB-*MYH11*
AML with t(8;21)(q22;q22); *RUNX1-RUNX1T1*
Acute promyelocytic leukaemia (APL) with t(15;17)(q22;q12); *PML-RARA*
AML with t(6;9)(p23;q34); *DEK-NUP214*
AML with t(9;11)(p22;q23); *MLLT3-MLL*
AML with inv(3)(q21q26.2) or t(3;3)(q21;q26.2); *RPN1-EVI1*
AML (megakaryoblastic) with t(1;22)(p13;q13); *RBM15-MKL1*
Provisional entity: AML with mutated *CEBPA*
Provisional entity: AML with mutated *NPM1*
AML with myelodysplasia-related change
Therapy-related myeloid neoplasms

AML, not otherwise specified:
Undifferentiated AML (M0)
AML with minimal differentiation (M1)
AML without maturation (M2)
Acute promyelocytic leukaemia (APL) (M3)
Acute myelomonocytic leukaemia (AMoL) (M4)
Acute erythroid leukaemia (AEL) (M5)
Erythroleukaemia, erythroid/myeloid (M6)
Pure erythroid leukaemia (M6b)
Acute megakaryoblastic leukaemia (AMKL) (M7)
Acute basophilic leukaemia (ABL)
Myeloid proliferations related to Down syndrome:
Transient abnormal myelopoiesis (TAM)
Myeloid leukaemia associated with Down syndrome (DS-AML)
Blastic plasmacytoid dendritic cell neoplasm (BPDCN)
Acute panmyelosis with myelofibrosis (APMF)
Myeloid sarcoma

Table 1-2: WHO classifications of AML and neoplasms. Adapted from (Falini, Tiacci et al. 2010)

1.1.4 AML chromosomal alterations

Chromosomal rearrangements are key indicators of haematopoietic malignancies, and 60% of AML patients carry abnormal karyotypes. Core binding factors (CBFs) are direct targets for gene rearrangements, and mutations in CBFs lead to acute leukaemia. The translocation between chromosome 8 and 21, or t(8;21)(q22;q22), was the first to be described in AML, and it affects the target genes *RUNX1* and *CBFB*. For over 40 years, t(8;21) has been considered a milestone in understanding AML genetics (Burel, Harakawa et al. 2001, Singh, Mandoli et al. 2017). Since then, AML has been associated with a growing number of other frequent genetic abnormalities, including chromosomal translocations and other aberrations (Table 1-3). Currently, the most common chromosomal abnormalities in AML are t(8;21)(q22;q22) detected in 15% of cases, followed by the inv(16)(p13;q22) and t(15;17), which are present in 12% and 8% of AML cases respectively. In paediatric AML, about 19% of the cases are Mixed-Lineage Leukaemia (MLLr) caused by rearrangements affecting the *MLL1* gene in 11q23, which lead to the expression of MLL fusion proteins. AML Mixed-lineage leukaemia is typically associated with poorer prognosis and a higher risk of relapse. Genetics of AML is complex disease but can be widely classified into three risk groups for prognostic purposes as having a favourable, intermediate and adverse impact on prognosis (Burnett, Hills et al. 2010, Dohner, Estey et al. 2010, Falini, Tiacci et al. 2010). Table 1-3 shows the Medical Research Council (MRC) classification of AML according to patients' outcome (Burnett, Hills et al. 2010).

Favourable Risk	t(8;21)(q22;q22) t(15;17)(q22;q22) inv(16)(p13.1q22); t(16;16)(p13.1q22)
Intermediate Risk	Normal karyotype or other cytogenetic abnormalities not classified as favourable or adverse.

Adverse Risk	inv(3)(q21;q26.2); t(3;3)(q21;q26.1) abnormal (3q), excluding t(3;5)(q21~25;q31~35) -7, add(7q)/del(7q) -5, add(5q)/del(5q) -17/abnormal(17p) t(10;11)(p11~13;q23) t(6;11)(q27;q23) t(9;22)(q34; q11) t(11q23), excluding t(9;11)(p21~22;q23) and t(11;19)(q23;p13) Complex karyotype of more than 4 independent chromosomal abnormalities.

Table 1-3: MRC classification of AML. Adapted from (Burnett, Hills et al. 2010, Grimwade, Hills et al. 2010).

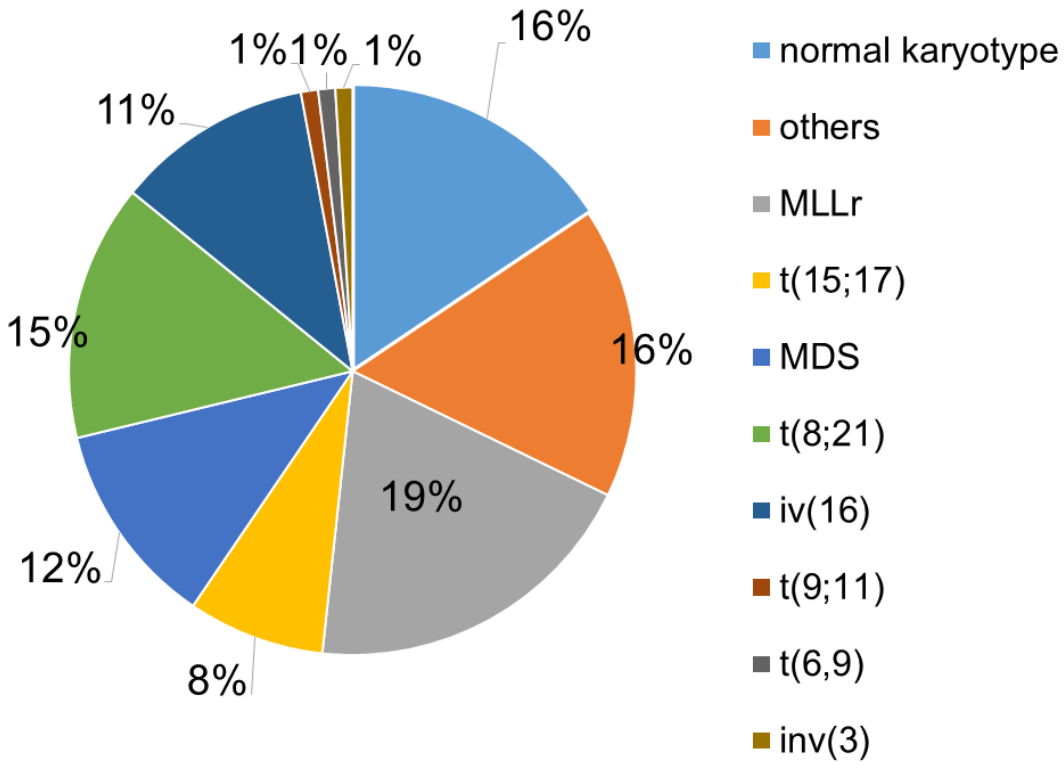

Fig 1-3: MRC cytogenetic classification of AML. Distribution of cytogenetic abnormalities in AML from 59% of 5876 patient cases in the MRC trials 2010. Adapted from (Burnett, Hills et al. 2010, Dohner, Estey et al. 2010).

1.1.5 AML mutational landscape

Alongside the chromosomal aberrations, which can be detected by cytogenetic techniques, genome screening of somatic mutations that can predispose or influence the development and progression of AML can also be very informative to estimate prognosis (Burnett, Hills et al. 2010, Falini, Tiacci et al. 2010). Curiously, the genome of an AML case was the first human cancer to be fully sequenced. In the advent of next-generation sequencing (NGS) and high-throughput protocols, the number of mutations known to be associated with AML has been increasing (Taussig, Vargaftig et al. 2010, Thol, Kolking et al. 2012). Recent studies have identified several novel mutations associated with AML in genes such as *RAS*, *FLT3*, *NPM1, and DNMT3A* (Fig 1-4).

The clonal composition and expansion are crucial for the clinical outcome of AML. Point mutations account for two-thirds of mutation capable of driving AML, and most of them are associated with an intermediate risk outcome. To increase complexity, one-third of AML patients carry co-mutations, and some of these are exclusive of specific hotspots within certain genes. For instance, patients with *NPM1* mutation have a high occurrence of $NRAS^{G12/13}$ but not $NRAS^{Q61}$,and those patients have intermediate risk (Shen, Zhu et al. 2011, Vaskova, Dubayova et al. 2015). Furthermore, some paediatric acute leukaemias can be associated with other genetic disorders and atypical driver mutations. For example, neonates and young children with trisomy 21 (Down syndrome, DS) carrying mutations on *GATA1* have a 500-fold increased risk of developing megakaryoblastic leukaemia (AMKL or DS-AML) (Reinhardt, Reinhardt et al. 2012). Up to 10% of neonates with DS suffer from transient abnormal myelopoiesis (TAM) but only 30% of them progresses to AMKL within the first four years of life. In the absence of trisomy 21 genetic background, *GATA1* mutations alone do not lead to leukaemia, and other cooperating mutations are always required to transform TAM to AMKL (Klusmann, Godinho et al. 2010, Scheer, Kratz et al. 2016, Uffmann, Rasche et al. 2017, Gialesaki, Mahnken et al. 2018).

AML undergoes ordered evolutionary trajectories, where mutations might occur or drive different stages during disease development (Hope, Jin et al. 2004). Mutations that affect epigenetic modifier genes such as *IDH1/2*, *TET2* and *ASXL1* are often present in elderly patients and increase the risk of developing leukaemia. Such mutations are acquired or present in the earliest stages of haematopoietic disruption and can be usually detected in the founder clones of AML, but are not sufficient for leukaemia transformation (Shen, Zhu et al. 2011). On the other hand, mutations in tyrosine kinases usually occur at later stages and often multiple mutations in these genes can be detected in different clones of the same patient. Secondary mutations such as in *NPM1* followed by *IDH1* and *DNMT3A* are associated with progression to full-blown leukaemia (Thol, Kolking et al. 2012).

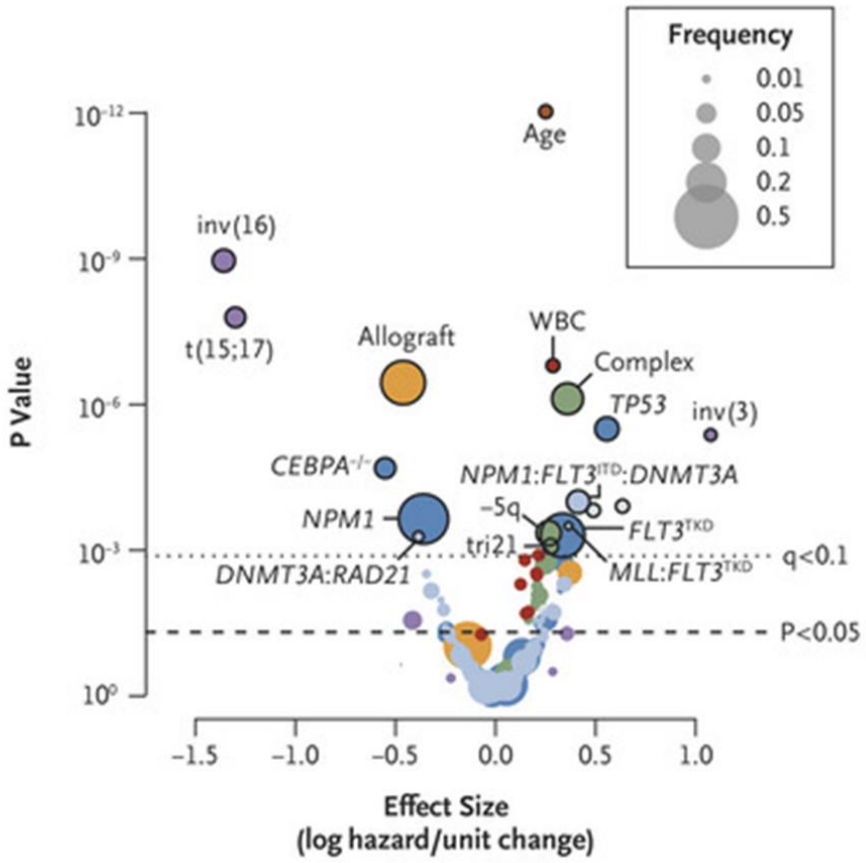

Fig 1-4: Common mutation in AML and their frequencies. Distribution of cytogenetic abnormalities in AML from 59% of 5876 patient cases in the MRC trials 2010. Adapted from (Vaskova, Dubayova et al. 2015)

1.1.6 AML molecular pathogenesis

As described, AML has complex and heterogeneous cytogenetics and results from a sequential acquisition of mutations and/or genomic alterations. The old FAB classification categorised AML mutations into two main classes. Class I mutations enhance the proliferation and survival via the activation of several signal transduction pathways such as *FLT3*, *NRAS*, and *KIT*. Class II mutations block the differentiation of myeloid progenitors by interfering with transcription factors such as *RUNX1, CEPBA, and GATA1/2* (Garg, Nagata et al. 2015, Ryotokuji, Yamaguchi et al. 2016). However, this classification is continuously under revision, and some newly

discovered mutations either fit both or none of the classic classes. Consequently, new models of classifying AML according to mutations and genomic abnormalities have become ever more complex (Fig 1-5) (Shen, Zhu et al. 2011, Ryotokuji, Yamaguchi et al. 2016). Furthermore, some mutations strongly segregate with specific chromosomal abnormalities such as mutation of *KIT* in inv(16) and t(8;21) in complex karyotype AML (Beghini, Magnani et al. 2002, Cairoli, Beghini et al. 2006).

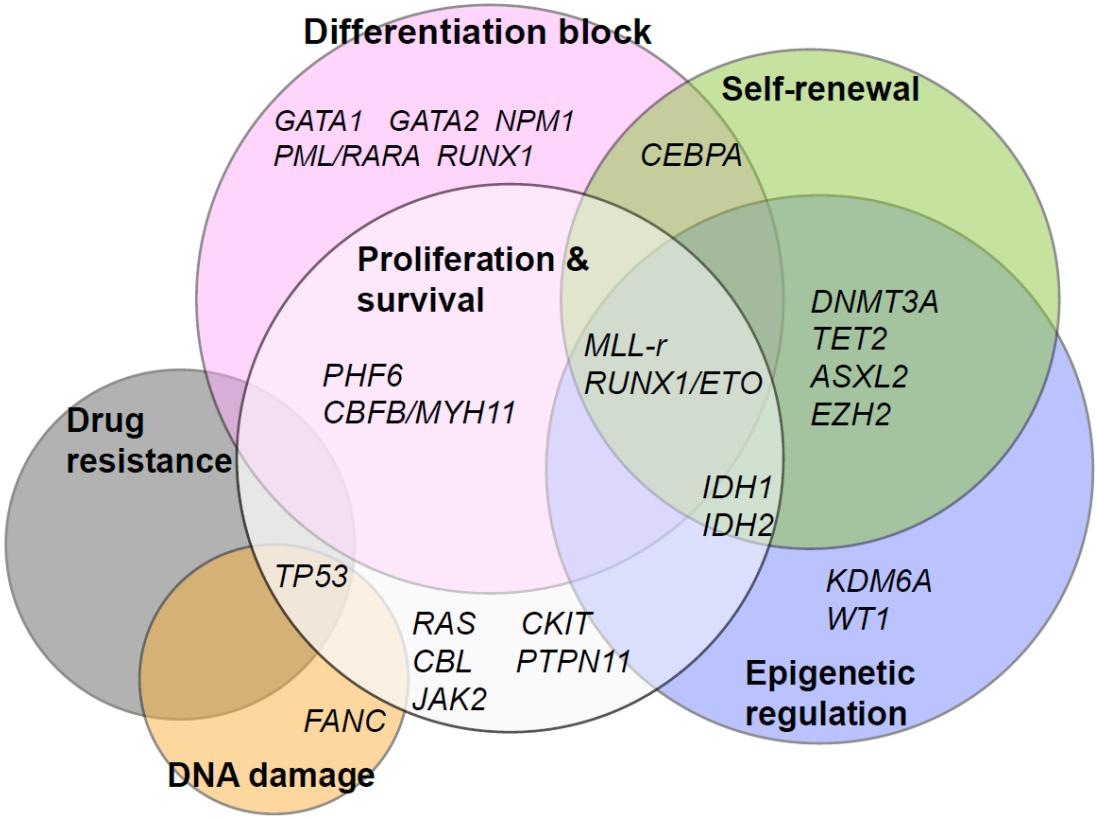

Fig1-5: AML mutated genes. Summary of AML mutated genes and their prognostic factors. Adapted from (Itzykson, Gardin et al. 2011, Shen, Zhu et al. 2011, Vaskova, Dubayova et al. 2015, Ryotokuji, Yamaguchi et al. 2016)

1.2 t(8;21) positive AML

1.2.1 RUNX1, a master regulator of haematopoiesis

RUNX1 (also known as AML1, CBFα2 or PEBP2aB) belongs to the Runt-related transcription factors (RUNXs), which are required in Drosophila embryogenesis for sex determination, segmentation, and neurogenesis. The *RUNX1* gene is located on chromosome 21 (21q22.12), spans 260 kb and contains 12 exons. *RUNX1* has complex transcription and translation variants due to its distinctive 5'-UTRs and differential 3'-polyA sites. There are several alternative splice variants of *RUNX1* coding a range of protein products spanning from 20 to 52 kDa (Lorsbach, Moore et al. 2004, Lam and Zhang 2012).

RUNX1 is tightly regulated during haematopoiesis and HSCs homeostasis by two tissue-specific enhancers (regulatory elements 1 and 2) and two promotors, distal promotor P1 and proximal promoter P2, both sequentially activated and linked to different 5'-UTRs (Fig 1-6). The transcript of P1 promotor controls RUNX1c expression that is required for the initiation but not the maintenance of definitive haematopoiesis. The P2 promotor strictly controls the dosage of RUNX1b and RUNX1a expression levels that are required to initiate and complete the endothelial-to-hematopoietic transition and subsequent generation of haematopoietic cells from the haemogenic endothelium (HE). *RUNX1* knockout mice die in early embryogenesis with deficient foetal haematopoiesis emphasising the pivotal role of RUNX1 as a master regulator of haematopoiesis. Even though RUNX1 expression is not essential for adult HSCs production and survival, disruption of RUNX1 levels perturbs the differentiation of several blood lineages. In adults, RUNX1 is expressed in all tissues except the heart and brain (Barseguian, Lutterbach et al. 2002, Lam and Zhang 2012, Ichikawa, Yoshimi et al. 2013, Martinez, Hinojosa et al. 2016, Lie, Marinopoulou et al. 2018).

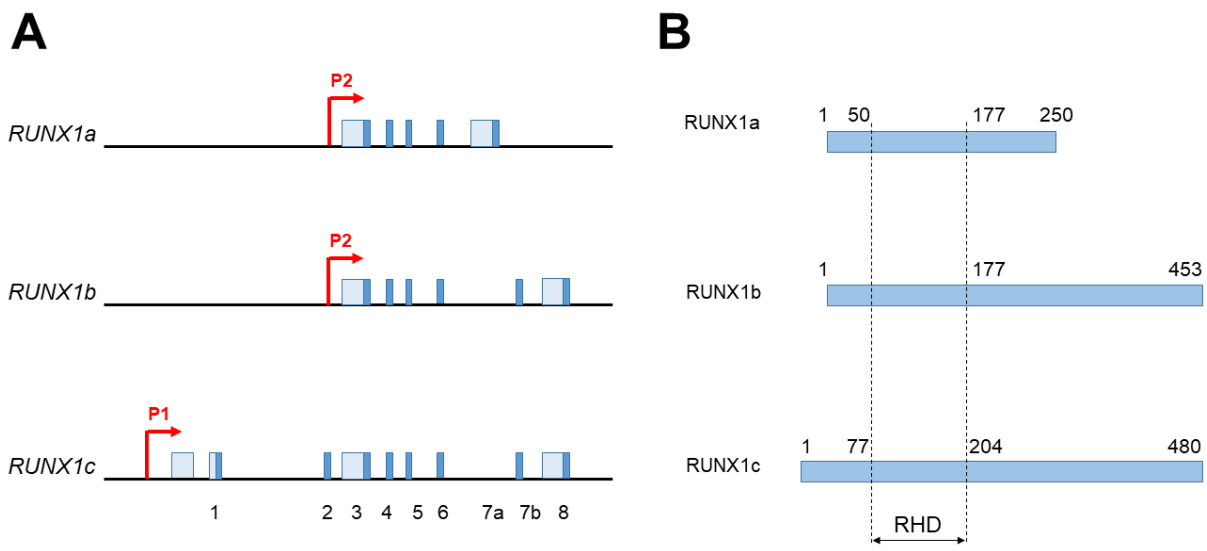

Fig 1-6: Schematic illustration of RUNX1 isoforms, locus and protein. (A) RUNX1 gene spliced variants and promotors localisation on *RUNX1* locus on chromosome 21. Both *RUNX1a* and *RUNX1b* are transcribed from the same P2 promotor and contains 5 and 6 exons, respectively. *RUNX1c* is transcribed from the P1 promotor and has 8 exons. (B) The runt homology domain (RHD) is conserved between all the three isoform products of *RUNX1. Adapted from (Sroczynska, Lancrin et al. 2009, Lam and Zhang 2012).*

RUNX1 has two main regulatory domains: the runt homology domain (RHD) encoded by exons 2-4, which is a DNA-binding domain and the transactivation domain (TAD) encoded by exon 6, which mediates protein-protein binding. RUNX1 binds to the DNA via the RHD domain (128 amino acids) as a monomer (Fig 1-7A). The TAD domain interacts with E-twenty-six (ETS) family transcription factors RID, GATA1, MLL, CDK6, PU.1 and others. Furthermore, the core binding factor CBFβ does not bind DNA directly, but its interaction with RHD domain and forming the CBF heterodimer increases the DNA binding affinity by 10-fold. The dimerisation between CBFβ and the RHD domain protects RUNX1 from proteasomal degradation and supports the activation or repression of downstream targets (Lam and Zhang 2012, Obenauer, van Strien et al. 2015).

RUNX1 does not only interact with other CBFs proteins but it also transcriptionally regulates co-regulators. RUNX1 requires cooperating factors to be able to bind the promoter and activates its target genes in tissue- and lineage-specific manner. For instance, RUNX1 binds ELF4 (ETS family member) to activate *IL3* promotor and

interacts with LEF1 (Lymphoid Enhancer Binding Factor 1) to bind the enhancer of *TCRβ*. RUNX1 synergises with LEF1 and CREB (CAMP Responsive Element Binding Protein 1) to activate *TCRα* expression. RUNX1 also binds transcription factors directly or indirectly to regulate several master regulators of haematopoiesis such as GATA1, PU.1, C/EBPα (CCAAT Enhancer Binding Protein Alpha), and P300 (E1A-associated cellular p300 transcriptional co-activator protein) (Graf 2002, Lorsbach, Moore et al. 2004).

RUNX1 is regulated by post-translational modifications (Fig 1-7B). In CD34+ progenitors, RUNX1 is found to be phosphorylated by ERK (extracellular signal-regulated kinases) on S266, T273, and S276. Phosphorylation at S397 via CDK1 or CDK6 alters its DNA binding affinity and mediates its degradation. Importantly, phosphorylation impairs interaction with histone deacetylases (HDACs) and contributes to RUNX1 capacity to activate transcription by reducing its interaction with transcriptional repressors. P300 can acetylate the N-terminus of RUNX1 on K24 and K43, which controls interaction with MLL. Moreover, RUNX1 methylation promotes transcription repression. For example, RUNX1 methylation on R223 by PRMT4 (Type-I arginine methyltransferase) downregulates miR-223 which is involved in myeloid differentiation. Other post-translational modifications of RUNX1 include ubiquitination that alters protein stability and activity (Jin, Jeon et al. 2004, Jongen-Lavrencic, Sun et al. 2008, Scholl, Gilliland et al. 2008).

Mutated *RUNX1* is frequently found in leukaemic chromosomal translocations and abnormal haematopoiesis (Fig 1-7C). Mutations in the RHD domain are often detected in familial platelet disorder with associated myeloid malignancy (FPD/AML) as a primary event that can progress to leukaemia. The most common chromosomal translocations affecting *RUNX1* are t(8;21), t(12;21) and t(3;21). *RUNX1* fusions that retain the RHD domain can bind DNA and dysregulate RUNX1 transcriptome (Zaidi, Dowdy et al. 2009, Gerritsen, Tijchon et al. 2016).

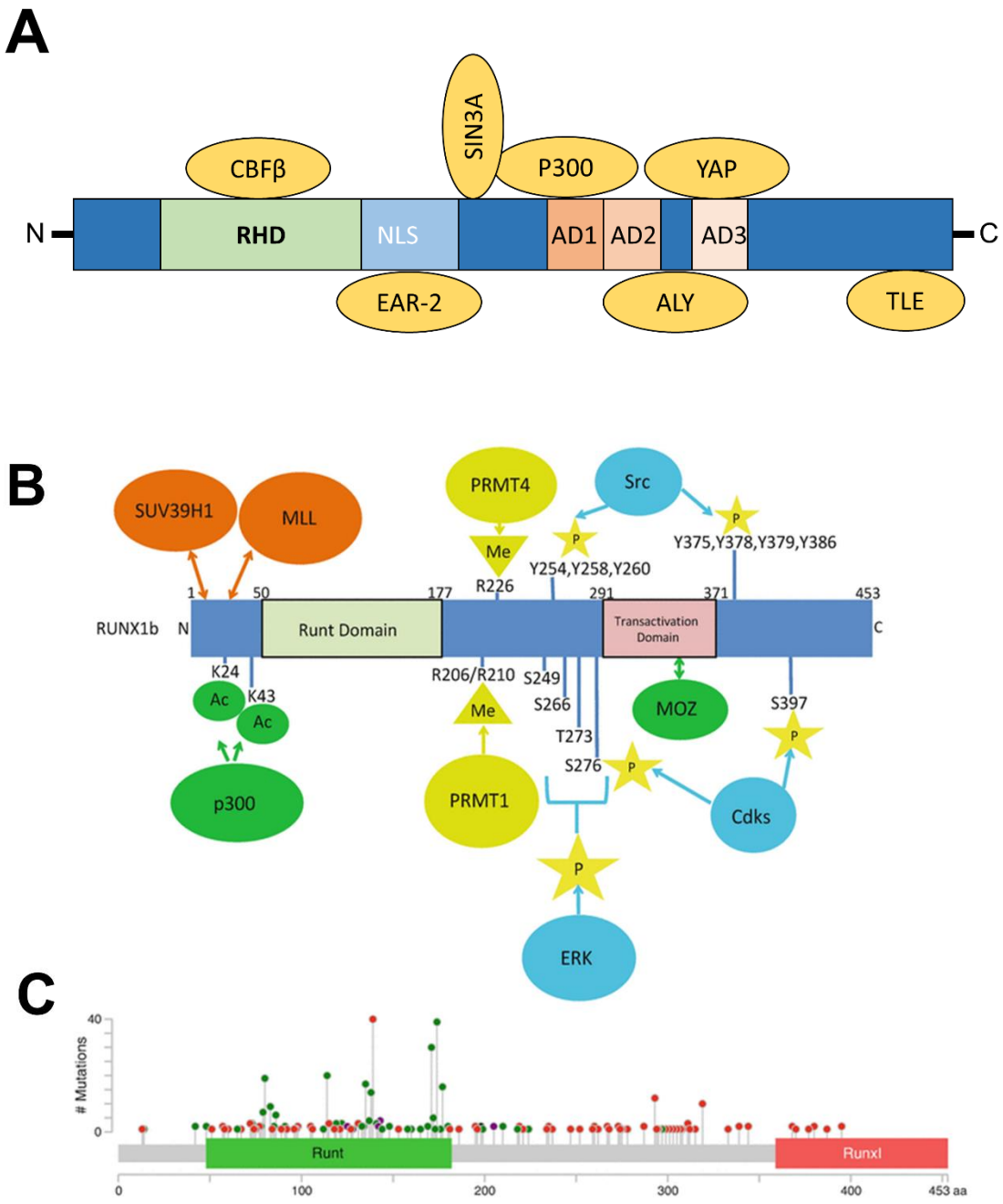

Fig 1-7: Schematic illustration of RUNX1 protein. (A) RUNX1 protein structure showing the main interacting proteins, the DNA-binding Runt domain is shown in green. (B) RUNX1 protein post-translational modifications and the resulting interactions (C). Somatic point mutations found in the *RUNX1* transcript variant 2 in AML patients. The nonsense and frameshift changes are shown in red, the missense variants are shown in green. Adapted from (Blumenthal, Greenblatt et al. 2017, Metzeler and Bloomfield 2017).

1.2.2 ETO, a co-repressor partner

The eight twenty-one (*ETO*) genes belong to one evolutionarily conserved gene family and represent a homologue of the Drosophila *nervy* gene. In human, *ETO* locus is located in chromosome 8 and spans over 87 kb and 13 exons. The gene family gives rise to three main genes; *MTG8* (also known as *RUNX1T1, CBFA2T1, CDR* or *ETO*), *MTG16* (*CBFA2T3*, *MTGR2 or ETO2*), and *MTGR (EHT or ETOR1).* The molecular function of the *ETO* family is largely unexplored and the majority of *ETO* properties have been derived from studies of its fusion *RUNX1/ETO*. Nevertheless, *ETO* is widely viewed as a transcriptional corepressor upon dimerisation with histone deacetylases (Barseguian, Lutterbach et al. 2002).

ETO produces two distinct protein isoforms consisting of 577 and 604 amino acids. ETO proteins do not bind DNA but can acquire this capacity when *ETO* fuses with genes encoding transcription factors where the DNA binding regions are present on the fusion gene such as *RUNX1/ETO* in t(8;21). ETO has four characteristic domains named NHR1-4 (Nervy Homology Regions) as shown in Fig 1-8. NHR1 is a homologue of the TATA-box binding protein of Drosophila and is responsible for protein-protein interactions. This domain is essential for ETO interactions with E-proteins and nuclear localisation. NHR2 has a hydrophobic region with an α-helix structure responsible for homo- and hetero-dimerisation with other NHR domains. There is a binding site of SIN3 in NHR2, making this domain an essential factor for transcriptional repression. Both NHR3 and NHR4 are involved in the activation of some corepressors such as SMRT. NHR4, also known as MYND, contains two zinc finger motifs, but it does not bind the DNA. However, NHR4 mediates protein-protein interactions such as recruiting the corepressors NCOR and SMRT to the promotor of *RUNX1* in *RUNX1/ETO* fusion. ETO also interacts with HDAC1-3 indirectly via NCOR and SIN3A through various regions inside and outside the NHR1-4 domains. ETO protein is expressed in the heart, brain, pancreas and lung tissues. Despite being detected in the CD34+ progenitors, ETO is globally downregulated in the haematopoietic system (Jakubowiak, Pouponnot et al. 2000, Amann, Nip et al. 2001, Barseguian, Lutterbach et al. 2002).

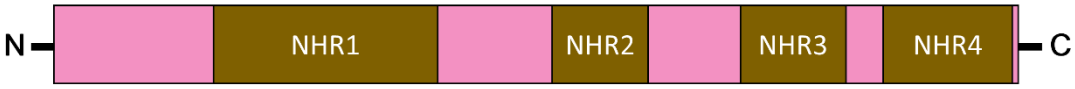

Fig 1-8. ETO protein structure. ETO consists of four Nervy Homology Regions NHR1-4. (Rulina et al., 2010).

1.2.3 t(8;21)(q22;q22) a novel chromosomal abnormality

The specific molecular mechanisms underlying chromosomal translocation are still vague. However, it has been suggested that a long non-coding RNA (lncRNA) named *RUNXOR* might be involved in the translocation process. *RUNXOR* is a 216 kb un-spliced sense RNA transcribed from a 5 kb upstream the distal promotor (P1), overlaps all *RUNX1* exons and introns, and interacts with the 3'-UTR of *RUNX1* promotors and enhancers. It has been found that *RUNXOR* lncRNA interacts with the chromatin at the exact intragenic site involved in *RUNX1* chromosomal translocations with *ETO* leading to the formation of intrachromosomal loop, which may imply that *RUNXOR* regulates the translocation process (Wang, Li et al. 2014, Bracht, Wang et al. 2017).

As aforementioned, the translocation t(8;21) is highly prevalent in AML, and leads to the creation of the fusion gene *RUNX1/ETO* (also known as *AML1/ETO, RUNX1/RUNX1T1 or AML1/MTG8*) and expression of the resulting RUNX1/ETO protein. In fact, RUNX1/ETO contributes to 12% - 15% of AML cases and 40% of the M2 subtype of AML, which associates with granulocytic differentiation. This genetic rearrangement can also be found in 6% of M1 (AML without maturation) cases but is far less common in M4 (AML with myelomonocytic differentiation) and M5 (AML with monocytic differentiation) cases. Both t(8;21) and inv(16) chromosomal changes are

grouped under the CBFβ leukaemia, and they indicate a favourable prognosis (Peterson and Zhang 2004, Burnett, Hills et al. 2010).

RUNX1/ETO results from the fusion of the intron 5 of *RUNX1* on chromosome 21 to either intron 1 or 1b of *ETO* on chromosome 8 when the t(8;21) takes place (Fig 1-9A). When expressed, the fusion gene produces a transcript containing the *RUNX1* N-terminus DNA-binding domain and the repressor domains that are located towards the C-terminus of *ETO*. The resulting transcripts share a conserved and unique breakpoint, and since t(8;21) is an initiating event, all leukaemic cells will contain the same transcript. Thus, the chimaeric oncoprotein RUNX1/ETO is leukaemia-specific and is responsible for driving and maintaining key hallmarks of AML. RUNX1/ETO competes with RUNX1 binding to the DNA and disrupts the CBF complex leading to enhanced self-renewal and impaired myeloid differentiation (Heidenreich, Krauter et al. 2003, Gu, Hu et al. 2014). Despite being an early event that interrupts normal haematopoiesis, *RUNX1/ETO* and its fusion protein are not sufficient to start leukaemia, and secondary mutations must be required to generate the leukaemic phenotype (Burnett, Hills et al. 2010, Harada, Inoue et al. 2013).

1.2.4 RUNX1/ETO protein characterisations and variants

RUNX1/ETO has 752 amino acids, including nearly all ETO sequence at the C-terminus, while the N-terminus of RUNX1 contains the Runt homology domain and regulates the interaction with DNA and transcription factors (Fig 1-9B). There are multiple isoforms of *RUNX1/ETO* transcripts, but most of the activity is coming from the full-length RUNX1/ETO protein. It was shown that one amino acid deletion or mutation in the NHR4 domain disturbs RUNX1/ETO structure and changes its ability to cause leukaemia (Peterson and Zhang 2004, Wang, Huang et al. 2009, Zaidi, Dowdy et al. 2009, Lam and Zhang 2012).

A splice variant coding a shorter RUNX1/ETO protein has been described where an additional exon (exon 9a) is added to the *ETO* domain in the C-terminus. The truncated RUNX1/ETO9a has 575 amino acids and lacks the NHR4 and NHR3 domains, which are essential for interaction with transcription repressors (Yan, Kanbe et al. 2006). In addition to *RUNX1/ETO9a*, another truncated splice variants

RUNX1/ETO11a is detected in t(8,21) AML cell lines. The expression of *RUNX1/ETO11a* in patients is insignificant, and the presence of this variant correlates with the expression of a truncated ETO11a protein in the testis tissue only. The spliced 11a exon at the C-terminus of *ETO* encodes 27 amino acids and does not correlate to any known functional motif (Kozu, Fukuyama et al. 2005).

Post-translational modifications of RUNX1/ETO are poorly described in comparison to RUNX1 counterparts. The RHD domain post-translational modifications are preserved in both RUNX1 and RUNX1/ETO. However, the fusion lacks the regulatory parts of RUNX1 at the C-terminus, and thus several phosphorylation sites are lost in the fusion protein. RUNX1/ETO interactions with E3-ligases such as STUB1, SIAH1, and E2-conjugase UBCH8 lead to its ubiquitin-mediated degradation (Wang, Huang et al. 2009).

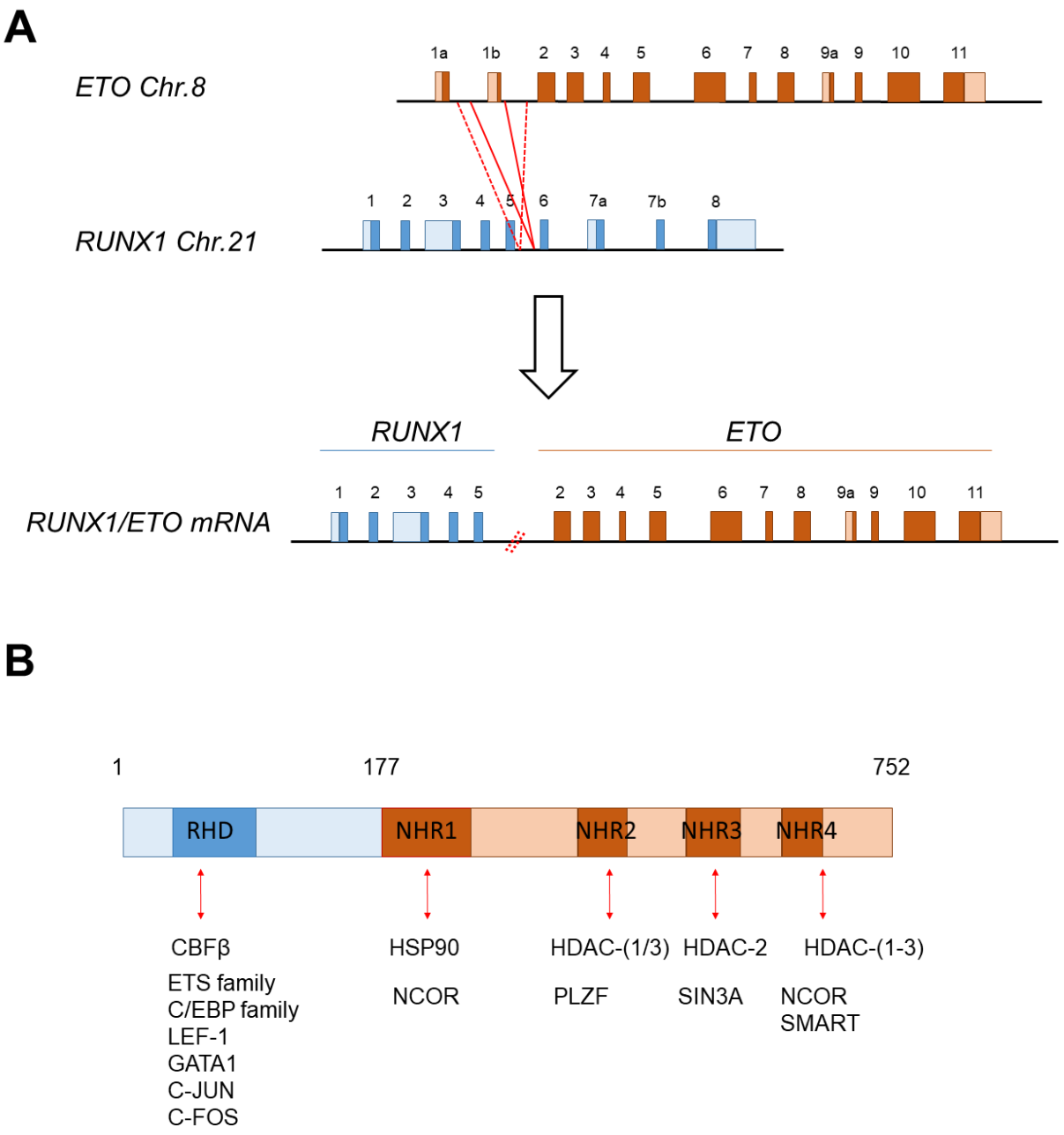

Fig 1-9: Schematic illustration of the translocation (8;21)(q22;q22). (A) The translocation chr.8 and chr.21 occurs between one breakpoint in *RUNX1* gene in intron 5 and two possible breakpoints in *ETO* gene; either 1a or 1b intron. There is no splice acceptor in exon 1b in the *ETO* gene, thus the translocation leads to one fusion site. The dark-coloured boxes refer to the translated regions. In the *RUNX1/ETO* mRNA, the underlined numbers refer to *ETO* exons and the non-underlined numbers refer to *RUNX1* exons (B) Schematic illustration of RUNX1/ETO functional domains and its partners. Interacting proteins are located at their binding/interaction site along RUNX1/ETO regions. Vertical arrows refer to the region mediating the interaction. Adapted from (Wang, Huang et al. 2009, Lam and Zhang 2012).

1.2.5 The molecular mechanism of RUNX1/ETO leukaemogenesis

The t(8;21) leads to expression of the oncogenic RUNX1/ETO fusion protein which initiates, drives and maintains leukaemia by interfering with RUNX1-dependant transcriptional networks. In t(8;21) AML, the reservoir of the leukaemic blast is guarded by RUNX1/ETO that transforms the CD34+ haematopoietic stem and progenitors cells into clonogenic, self-renewing and hyperproliferative leukaemic cells. The translocation also associates with cooperating mutations that further enhance the proliferation and promote survival. For instance, almost 50% of t(8;21) patients carry non-overlapping mutations in *C-KIT*. Activating mutations in the *RAS* gene including *KRAS* and *NRAS*, and mutations in the FMS-like tyrosine kinase 3 (*FLT3*) such as *FLT3-ITD and FLT3-TKD,* are detected in around 30% of t(8;21) AML patients. These mutations accelerate disease progression and reduce drug sensitivity. In general, the co-expression of *RUNX1/ETO* and activating mutations in the tyrosine kinase pathways leads to an aggressive leukaemic phenotype with a high incidence of relapse and poor prognosis (Wichmann, Chen et al. 2007, Nick, Kim et al. 2012).

RUNX1/ETO enhances leukaemic cell clonogenicity by directly regulating several stem cell markers and self-renewal genes. (Martinez, Drescher et al. 2004, Ptasinska, Assi et al. 2012). Chromatin immunoprecipitation assays (Chip-Seq) show direct binding sites of RUNX1/ETO on the promotor of telomerase (*TERT*) leading to its constitutive expression. Moreover, RNAi-mediated depletion of *RUNX1/ETO* decreases *TERT* expression, triggers senescence and reduces clonogenicity of t(8;21) AML cell lines. Furthermore, RUNX1/ETO maintains high expression of the stem cell marker *CD34* via direct binding to its transcription start site (TSS). Collectively, RUNX1/ETO is essential for the maintenance of the malignant phenotype by sustaining high expression of *TERT* and *CD34 (Loke, Assi et al. 2017)*.

RUNX1/ETO can act as an activator and/or repressor of its direct target genes (Fig 1-10). The RHD domain (N-terminus) regulates its binding to the DNA and drives it transcriptional activating activity, while ETO recruits class-I histone deacetylases leading to a closed chromatin structure and transcriptional repression (Loke, Assi et al. 2017). For example, ETO interacts with the NCOR/SMART complex leading to

histone deacetylation and repression of the granulocyte-macrophage colony-stimulating factor (*GM-CSF*) promoter (Matsuura, Yan et al. 2012). Moreover, RUNX1/ETO recruits DNA (cytosine-5)-methyltransferase 1 (DNMT1) leading to DNA methylation and subsequent repression of its downstream genes. Generally, t(8;21) leukaemia is associated with epigenetic changes where RUNX1/ETO differentially alters chromatin accessibility and blocks differentiation of myeloid lineages (Gu, Hu et al. 2014).

RUNX1/ETO can upregulate some of the RUNX1 target genes and it is not fully understood how the fusion changes DNA binding regions and shifts RUNX1 original transcriptome in the fusion protein. It is suggested that RUNX1/ETO may dissociate the corepressor SIN3A from RUNX1 leading to enhanced binding and thus transcription activation. For example, RUNX1/ETO differentially activates the granulocyte colony-stimulating factor (*G-CSF*) via enhanced RUNX1 binding following the previously explained mechanism (Matsuura, Yan et al. 2012).

Although the main transcriptional activity of RUNX1/ETO is a consequent of its competitive binding to the RUNX1 heterodimeric partner CBFβ, the fusion protein can indirectly regulate transcription and independently from RUNX1. For instance, RUNX1/ETO binds PU.1 and displaces JUN resulting in transcriptional repression of *PU.1.* Moreover, RUNX1/ETO ceases transcriptional repression of several genes by competitive binding to their activators and thus significantly reducing promotor activation. For example, *IgA* and *NP3* expression are reduced in the presence of RUNX1/ETO which prevents their activators TGF-β and C/EBPα to bind the promoters, respectively (Zaidi, Dowdy et al. 2009, Gu, Hu et al. 2014, Loke, Assi et al. 2017).

AML propagation is driven by inhibition of the myeloid differentiation programmes by the RUNX1/ETO transcriptome. For instance, RUNX1/ETO represses *CEBPA* via direct binding, and RNAi-mediated depletion of the fusion gene triggers global chromatin changes towards the activation of C/EBPα network of myeloid differentiation. RUNX1/ETO blocks erythropoiesis through the inhibitory domain NHR4 of ETO, which prevents P300 acetylation of GATA1 resulting in a block of the erythroid lineage. Moreover, RUNX1/ETO activates the transcriptional repressor *PLZF* resulting in reduced myeloid differentiation. Collectively, RUNX1/ETO alters

the transcriptional network of several myeloid lineages to sustain the immature phenotype of the leukaemic blast (Heidenreich, Krauter et al. 2003, Lam and Zhang 2012, Gu, Hu et al. 2014).

Moreover, RUNX1/ETO cooperates with the Activation protein 1 (AP-1) to promote and maintain the progression of the cell cycle via a CCND-CDK complex. RUNX1/ETO directly binds *CCND2* in a -30 kb element and interacts with the TSS inducing high expression of the cell cycle gene *CCND2*. Depletion of *RUNX1/ETO* by RNAi reduces *CCND2* expression, inhibits proliferation and causes cell cycle arrest. Moreover, repression of *CCND2* via RNAi or pharmacological inhibition of the CDK4/6 complex leads to G1 cell cycle arrest and induces cellular senescence (Martinez-Soria 2018). Cyclin D2 is involved in the phosphorylation of the tumour suppressor protein RB1, and its complex with CDK4/6 regulate the G1 to S phase transition. *CCND2* is commonly mutated and overexpressed in AML, including t(8;21) (Buschges, Weber et al. 1999, Helsten, Kato et al. 2016).

AML is characterised by downregulation of the retinoic acid signalling pathway (RA) which is involved in myeloid differentiation (Fazi, Zardo et al. 2007). RUNX1/ETO has a dominant negative effect on RA pathway by recruiting HDACs to *RA* promotor (Ferrara, Fazi et al. 2001). The retinoic acid receptor beta2 (*RARβ2*) has a tumour suppressor activity, but RUNX1/ETO downregulation of *RA* results in increased methylation on *RARβ2* promotor and hinders transcription (Tabe, Konopleva et al. 2006).

The depletion of RUNX1/ETO leads to downregulation of Angiopoietin-1(*ANGPT1*), which regulates vascular development and angiogenesis. ANGPT1 is a secreted glycoprotein that binds the endothelial tyrosine-protein kinase receptors TIE-1 and TIE-2. The angiopoietin protein family (ANGPT1-4) are growth factors contribute to blood vessels maturation and stability (Patan 1998, Teichert-Kuliszewska, Maisonpierre et al. 2001, Parikh 2017). RUNX1/ETO induces high expression level of *ANGPT1,* which regulates to the leukaemic stem cell proliferation and interaction with the microenvironment by adhesion, migration and cell-cell interaction (Takakura, Watanabe et al. 2000, Loke, Assi et al. 2017).

RUNX1/ETO deregulates genes involved in leukaemic cell survival, such as the lysosomal-associated protein transmembrane 5 gene (LAPTM5) (Trombly, Whitfield et al. 2015, Nuylan, Kawano et al. 2016). While *LAPTM5* is globally overexpressed in the haematopoietic system, RUNX1/ETO hypermethylates *LAPTM5* promotor leading to transcriptional repression. LAPTM5 regulates the pH of the lysosome and consequently controls the lysosomal degradation pathway (autophagy) (Inoue, Misawa et al. 2009, Chen, Wang et al. 2017). Overexpression of *LAPTM5* in AML cell lines decreases autophagy activity and increases sensitivity to chemotherapies (Jun, Kim et al. 2017, Loke, Assi et al. 2017).

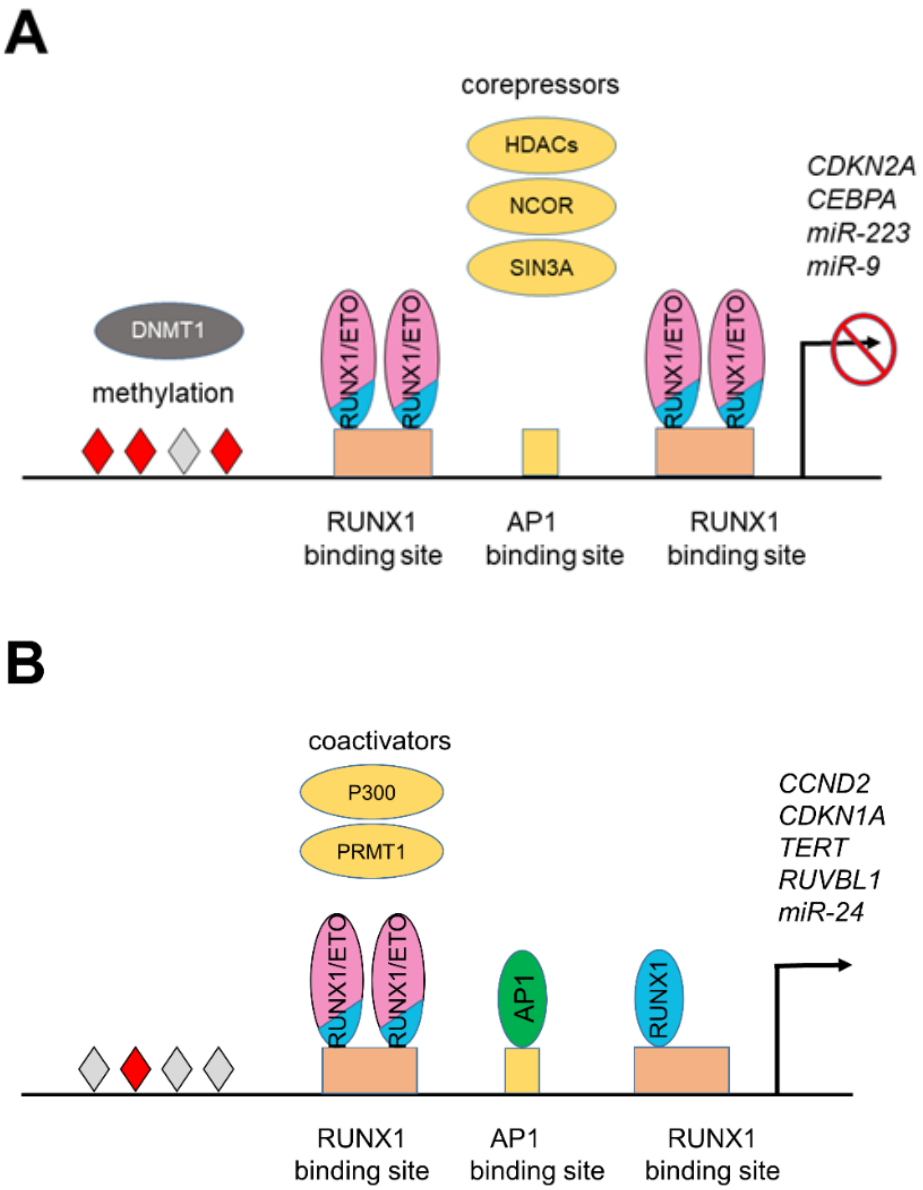

Fig 1-10: Schematic illustration of RUNX1/ETO transcriptional network. (A) Transcription repression, RUNX1/ETO displaces RUNX1 from its binding sites. RUNX1/ETO recruits transcription corepressor such as HDACs, NCOR, and SIN3A. RUNX1/ETO also coordinates with DNMT1 for chromatin methylation and transcription repression. (B) Transcription activation, RUNX1/ETO, and RUNX1, along with CBFβ partners, bind to RUNX1 binding elements. RUNX1/ETO and RUNX1 complex then recruits AP-1. RUNX1/ETO also recruits the transcription coactivators such as P300 and PRMT1 to activate direct target genes. Adapted from (Gessner, Thomas et al. 2010, Gu, Hu et al. 2014, Loke, Assi et al. 2017, Martinez-Soria 2018).

1.2.6 t(8;21) AML animal models

Several animal models were developed to study the effect of *RUNX1/ETO* on haematopoiesis. In Drosophila, *RUNX1/ETO* leads the expansion of immature haematopoietic progenitors, and this model helped to explain the role of calpain B (a Ca^{2+}-dependent protease) as a mediator of *RUNX1/ETO (Peterson and Zhang 2004)*. The expression of *RUNX1/ETO* in zebrafish mirrors the human phenotype in terms of disruption of haematopoiesis and accumulation of immature blasts. Given that zebrafish haematopoiesis is very similar to its mammalian counterpart, this model is often used to screen chemical modulators of RUNX1/ETO. Despite quickly and inexpensively providing large numbers due to their short lifespans and high reproductive rate, zebrafish and Drosophila models are not commonly used and most recent *in vivo* studies have been performed on murine models (Peterson and Zhang 2004).

The generation of a murine model of AML, and more specifically t(8;21) leukaemia, has always been a challenge and an optimal mouse model for *RUNX1/ETO* is yet to be created. The first attempt aimed to generate a *RUNX1/ETO* transgenic mouse by inserting the *RUNX1/ETO* gene into the *RUNX1* locus and producing a *RUNX1/ETO* heterozygous mouse. Of interest, homozygous mice from this model died during the embryonic stage (E12.5) mimicking the phenotype of *RUNX1* or *CBFβ* deletion. In those models, mice foetus failed to establish definitive liver haematopoiesis. Indeed, CD45+ cells isolated from heterozygous embryos could differentiate into dysplastic myeloid colonies and macrophages, while those taken from *RUNX1* and *CBFβ* mutant mice could not develop any haematopoietic progenitors. In conclusion, early attempts to establish transgenic *RUNX1/ETO* mice revealed that *RUNX1/ETO* acts as a negative regulator of *RUNX1* with other functions may stimulate leukaemogenesis (Yan, Kanbe et al. 2006, Hyde, Zhao et al. 2015).

A second mouse model was generated by inserting controlled *RUNX1/ETO* promotors such as, tetracycline response element (Tet), Ca^{2+}-binding proteins calgranulin B (*Mrp8*) which is expressed in the myeloid lineage, Cre recombinase-mediated (*Cre*), and hematopoietic stem cell *Sca-1* locus (*Sca1*) transgenic mice (Yuan, Zhou et al. 2001).

A xenograft mouse model was successfully generated by retroviral transduction of human CD34+ progenitors with the truncated fusion *RUNX1/ETO9a* and then transplanting them into immunodeficient mice. The 9*a* exon of *ETO* provides a stop codon at the end of exon 8 leading to the expression of a truncated version of the fusion protein. The expression of *RUNX1/ETO9a* in CD34+ cells leads to early onset of immature blast and AML in the xenograft model (Yan, Kanbe et al. 2006). Clinically, the co-expression of *RUNX1/ETO9α* with *RUNX1/ETO* is present in over 50% of the M2 subtype of AML and often correlates with a lower count of aberrant myelocytes in the bone marrow with downregulated CD19 and upregulated CD56 expressions. Although patients with t(8;21) have a favourable prognosis, the occurrence of *RUNX1/ETO9α* with an elevated level of *C-KIT* mutation indicates poor prognosis. The *RUNX1/ETO9a* xenograft model makes a clinically relevant model of AML in a murine background (Li, Chen et al. 2012, DeKelver, Lewin et al. 2013).

1.2.7 CBF AML treatment and clinical outcomes

The standard AML treatment consists of two stages: induction and post-remission. Induction usually includes DNA damaging agents such as cytarabine (AraC) and anthracyclines, which cause cell death and reduce the bulk of leukaemic blasts. Post-remission treatments are usually selected according to the leukaemia karyotype and age of the patient. The most common combinational therapy is a high dose of AraC with mitoxantrone (Burnett, Hills et al. 2010, Grimwade, Hills et al. 2010).

Generally, CBF leukaemias, including t(8;21) AML, share a good prognosis and a high response rate to chemotherapy, especially to AraC, with complete remission achieved in around 90% after standard treatment. Some patients benefit from a combination of high a dose of AraC and HDACs inhibitors (Grimwade, Hills et al. 2010). Although the treatment protocol is standardised for CBF AML, the t(8;21) patients have the worst response in comparison to those with in(16) AML. The overall survival is 4.4 years with 14% relapse incidents compared to 7.1 years for t(8;21) and inv(16), respectively (Cairoli, Beghini et al. 2006, Burnett, Hills et al. 2010, Vaskova, Dubayova et al. 2015).

In some cases, when chemotherapies fail to restore normal haematopoiesis, stem cell transplantation can be a third option, but bone marrow transplantation is not widely common in t(8;21) leukaemia. The MRC clinical data showed a subtle difference in the survival between standard chemotherapy and stem cells transplantation while other trials in Europe suggested that transplantation might lead to a worse prognosis. In summary, there is a need for better treatment for t(8;21) AML and new treatments should increase the survival rate, reduce relapse and lessen the burden of the side effects (Burnett, Hills et al. 2010, Vaskova, Dubayova et al. 2015).

1.3 Gene Silencing via RNAi

1.3.1 Small RNAs biogenesis

Genome scales up with developmental complexity, but the number of protein-coding genes does not correlate with this organismal complexity. For example, the single-celled eukaryote *T. vaginalis* has 160 million base pair (bp) of genomic DNA coding over 60,000 protein-coding genes while human DNA (2.9 billion bp) compasses just around 20,000. The so-called ‘’ junk DNA’’ is believed to be differentially transcribed to generate non-coding RNAs that regulate the architecture of gene expression during development and differentiation (Cech and Steitz 2014, Deniz and Erman 2017, Liu, Liu et al. 2017, Belair, Sim et al. 2018).

The first evidence for small non-coding RNA (sRNA) gene-mediated silencing was found in plants and fungi, yet those silencing pathways are believed to be dominant in almost all eukaryotic cells including humans (Davis, Zuckerman et al. 2010). To date, research led to the identification of over twenty distinct sRNA classes. Some sRNA subtypes have been extensively studied while others remain poorly understood (Diederichs 2014).

The discovery of double-stranded RNA (dsRNA) as a putative regulator of post-transcriptional gene expression has elucidated several puzzling observations of gene regulation in plants and yeast. This phenomenon was termed as RNA interference (RNAi). RNA interference depends on dsRNA to inhibit protein synthesis by targeting specific messenger RNA (mRNA) for degradation or translational inhibition. RNAi-mediated gene silencing became a ubiquitous research tool for understanding biology and gene regulation in eukaryotes (Davis, Zuckerman et al. 2010, Schuck, Gursinsky et al. 2013, Liu, Liu et al. 2017).

It is estimated that over 60% of human mature mRNAs undergo several RNAi-mediated pathways, mostly promoting mRNA decay. Several genes regulate RNA interference biogenesis and pathways such as *AGO2, R2D2, DICER2, TRBP, GW182* and others. The best two understood classes of RNA interference are microRNA (miRNA) and short interference RNA (siRNA). Both miRNA and siRNA assemble into a protein complex named the RNA Induced Silencing Complex (RISC) (Diederichs 2014, Schirle, Sheu-Gruttadauria et al. 2014).

The canonical biogenesis of endogenous siRNAs and miRNAs involves several steps of endonucleolytic processing of nuclear dsRNA precursors by RNase III family enzymes (Fig 1-11). In the nucleus, dsRNAs are transcribed by RNA polymerase II from the vast majority of the DNA, and these precursors are called pri-miRNA, which encode one or several precursor miRNAs and/or siRNAs. The cytoplasmic fully complement dsRNAs precursors follow endonucleolytic cleavage by DICER producing a duplex of 21 - 25 nucleotide-long known as siRNA. On the other hand, the nuclear pri-miRNAs are processed by DROSHA (RNase III family enzyme) resulting in hairpin per-miRNA transcripts. The pre-miRNAs are then exported to the cytoplasm where DICER performs a second cleavage producing the miRNA-miRNA* duplex in which miRNA is the antisense (also known as mature or guide strand) and the miRNA* is the sense (star or passenger strand) (Carthew and Sontheimer 2009, Chiang, Schoenfeld et al. 2010, Wei, Jones et al. 2011, Ryotokuji, Yamaguchi et al. 2016).

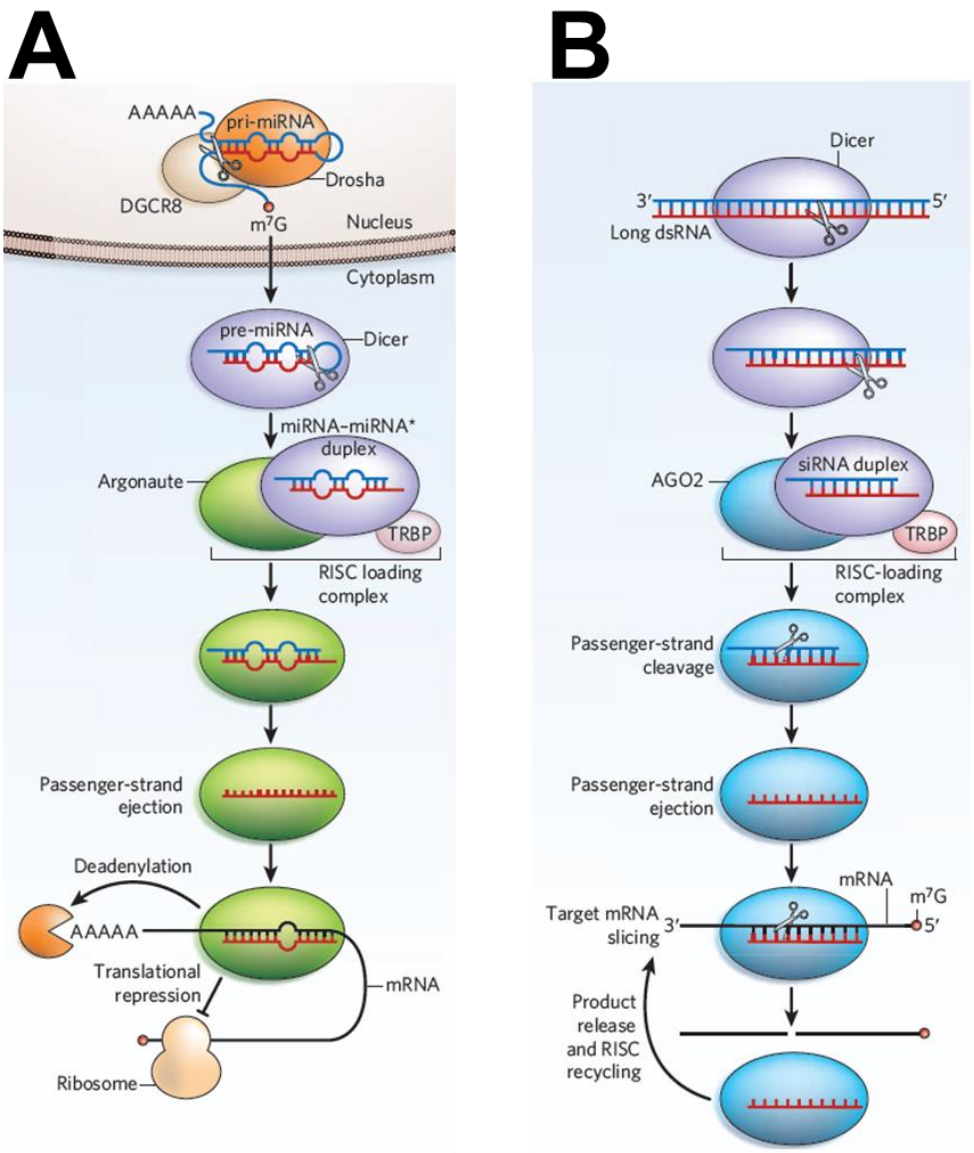

Fig 1-11. Small regulatory RNAs biogenesis and mechanisms. (A) pri-miRNA is processed by DROSHA/DHCR8 complex to produce pre-miRNA which are exported to the cytoplasm. DICER processes pre-miRNA by removing the hairpin to generate miRNA-miRNA* duplex which is loaded into the RISC complex. After loading into RISC, the antisense strand is selected by AGO2, and the sense strand is released. The antisense strand directs the RISC complex to a complementary mRNA. (B) Long dsRNA are exported to the cytoplasm where DICER generates 21 - 25 nucleic acid short siRNA which is loaded into the RISC complex. The selection of the antisense strand and recognition of the mRNA are performed by the RISC complex in the same mechanism of miRNA. RNA interference by siRNA and miRNA lead to transcript repression by several mechanisms, including miRNA degradation and translation inhibition. Adapted from (Carthew and Sontheimer 2009, Chiang, Schoenfeld et al. 2010).

1.3.2 Short interference RNA (siRNA)

Synthetic siRNA is a double-stranded oligonucleotide where the antisense strand is complementary to a specific mRNA. However, the sense strand is not supposed to perform any RNAi-mediated gene regulation. In the cytoplasm, siRNA incorporates into the RISC complex and targets specifically the complementary mRNA resulting in either mRNA cleavage or inhibition of ribosomal translation. RISC assembly requires both siRNA and miRNA to be at least 14 nucleotides long and carry a 5'-monophosphate and a 3'-dinucleotide overhang (Pham and Sontheimer 2005, Tomari and Zamore 2005, Maiti, Nauwelaerts et al. 2011).

1.3.3 Structural insights into AGO functions

The Argonaute proteins family (AGOs) is found in almost every living organism. While there is only one AGO protein in the fission yeast (*Schizosaccharomyces pombe*), there are up to 27 AGO family members in *C. elegans.* In humans, there are eight subfamilies of AGO proteins involved in several silencing pathways, which are divided into four clades (AGO1-4) and four PIWI clades (PIWI1-4). The catalytic activity of RISC is believed to be solely controlled by AGO2, although AGO1-3-4 can bind dsRNA (Pham and Sontheimer 2005, Vasselon, Bouttier et al. 2013, Yi 2018).

AGO2 hosts the siRNA in which it plays two roles in RISC functions. First, the recognition of the siRNA termini and second facilitating the slicing activity. Within RISC, the full complementary base pairing between the siRNA and mRNA requires conformational changes in AGO2 structure. One AGO2 protein can catalyse many silencing cycles where the siRNA guide strand remains bound to the protein, and the cleaved mRNA fragments are released (Kawamata and Tomari 2011, Nakanishi 2016, Sasaki, Tadakuma et al. 2018).

1.3.4 AGO2 functional domains

AGO2 consists of four domains, PIWI in the C-terminus, PAZ, middle domain (MID), and an N-terminus domain. AGO2 has a bilobate architecture where the first lobe is made of the MID and PIWI domains, whereas the N-terminus and PAZ domains make the second lobe (Fig 1-12). The PAZ domain recognises and binds the 3'-ends of the siRNA. The PIWI domain acts as RNase H endoribonuclease and performs the mRNA cleavage. The MID domain adopts the ribose binding domain of the lactose repressor (DNA-binding protein) and binds to the 5'-phosphate of the guide strand (Kawamata and Tomari 2011, Naruse, Matsuura-Suzuki et al. 2018).

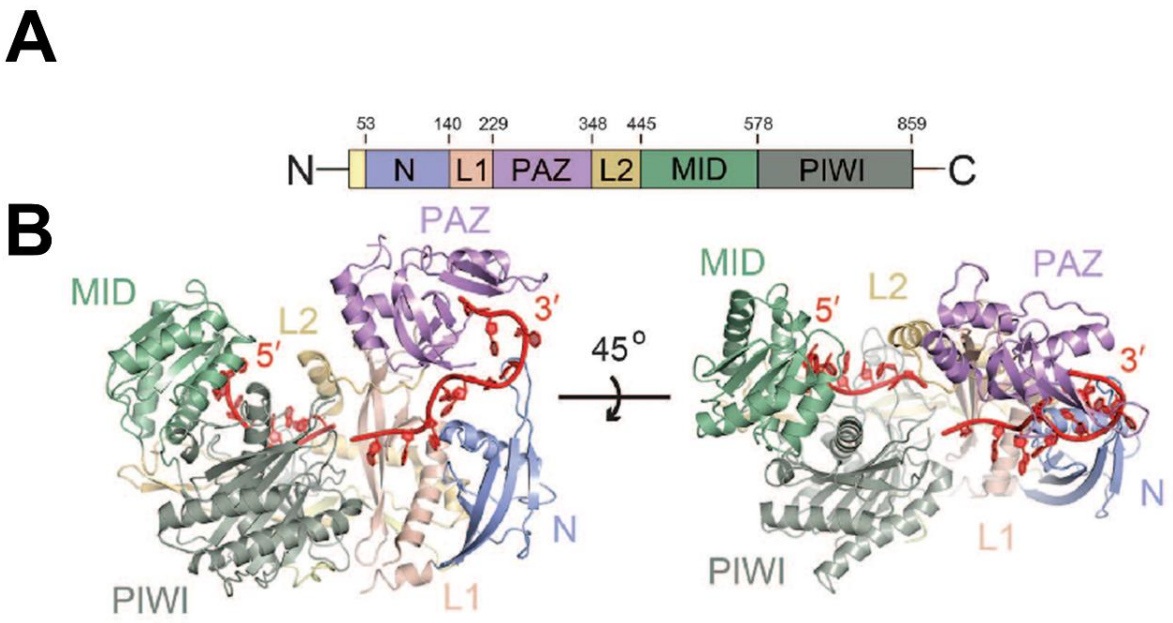

Fig 1-12. **Structure of human Argonaute protein AGO2.** (A) Schematic illustration of AGO2 protein domains. AGO2 contains four functional domains connected by two linker domains. N-terminus and PAZ domains are connected by L1 domain, MID and PIWI domains are connected by L2 domain. (B) Crystal structure of AGO2 domains hosting a guide RNA in red. The 3'-terminus of the RNA is hosted in the PAZ domain while the 5'-end is hidden in the MID domain. (Schirle, Sheu-Gruttadauria et al. 2014).

1.3.5 Recognition of siRNA termini

The PAZ domain is responsible for initiating RISC assembly as well as determining which strand of the siRNA is the antisense. PAZ differentially interacts with the thermodynamically stable end that is characterised by strong Watson−Crick base pairings. PAZ domain hosts the first two 3'-end overhang nucleotides of the antisense in a sequence-nonspecific recognition and makes less interaction with the 5'-end (Gu, Jin et al. 2012, Kwak and Tomari 2012).

The two terminal bases at 3'-end of the antisense stay exposed to the solvent where their phosphodiester backbone interacts with the PAZ side chain. Additionally, a hydrophobic pocket in PAZ domain partly hosts the terminal 3'-end nucleobase of the antisense (Pham and Sontheimer 2005).

The 5'-end of the siRNA antisense strand is hosted in a deep pocket between the PIWI and MID domains. The 5'-end phosphate group is crucial for RISC assembly as it twists and does not base pair with the mRNA. The 5'-end is also recognised by two invariant lysines in the MID domain. However, the 5'-end does not play any role in recognition of the antisense (Frank and Nagar 2017, Schlundt, Tants et al. 2017, Sasaki, Tadakuma et al. 2018).

1.2.6 RISC slicer activity

In eukaryotic cells, AGO2 functions similarly to RNase H as an RNA-guided endonuclease. The seed region (5 nucleotides between the 2^{nd} and 7^{th} base of the antisense at the 5'-end) makes the first interaction with the target mRNA, but a full complementarity between the antisense and mRNA and is required for efficient RISC-mediated cleavage. The endonucleolytic attach occurs at the mRNA scissile phosphate group located opposite to the phosphodiester bridge between the 10^{th} and 11^{th} nucleotides of the antisense 5'-end (Martinez and Tuschl 2004, Schwarz, Tomari et al. 2004, Sontheimer 2005).

Similarly, to RNase H, the catalytic cleavage performed by the PIWI domain requires a divalent metal cation such as Mg^{2+}. Given that RISC mechanism is endonuclease

analogue, the 5’-end products carry a 3’-OH group, and the 3’-end products carry a 5’-phosphate group (Fig 1-13). RNase H enzymes are characterised by a catalytic tetrad motif (Asp-Glu-Asp-Asp), but the catalytically active PIWI domain in AGO2 carriers an (Asp-Asp-His) motif which coordinates two Mg^{+2} between the antisense and mRNA (Martinez and Tuschl 2004, Schwarz, Tomari et al. 2004, Sontheimer 2005, Nakanishi 2016).

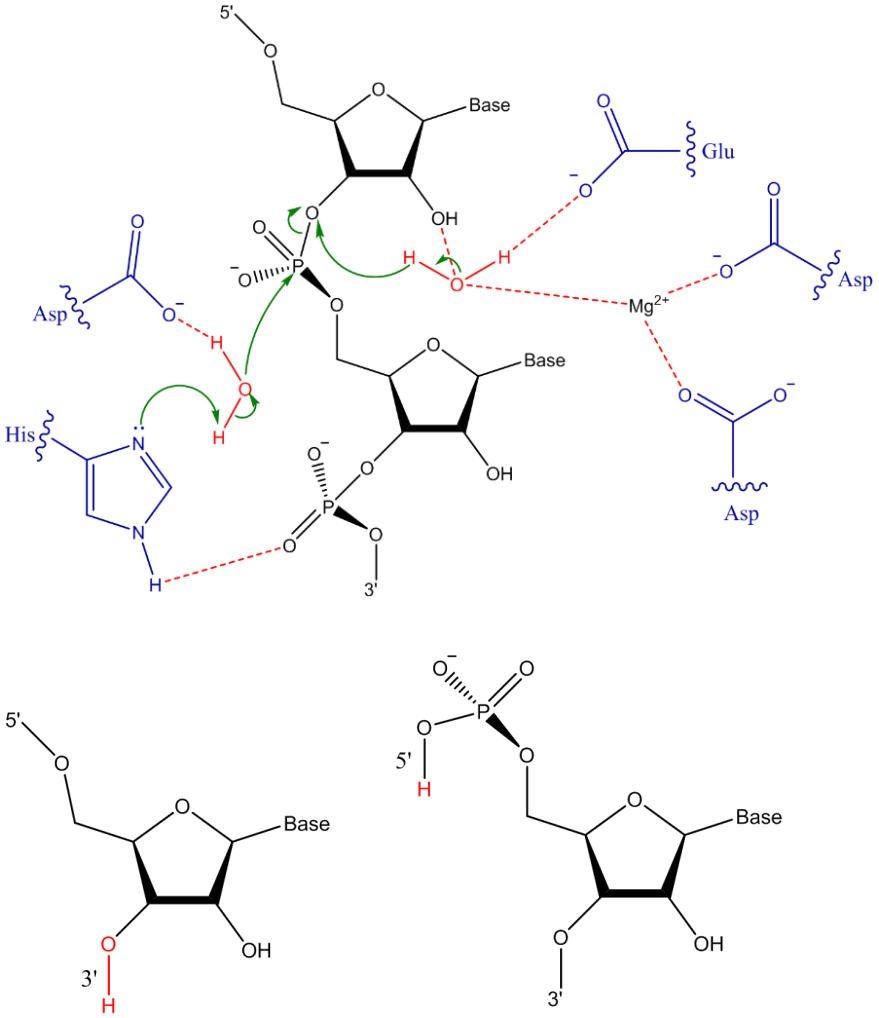

Fig 1-13. mRNA cleavage mechanism and products mediated by RISC. The mRNA nucleotides pair to the 10th and 11th antisense nucleotides (counting from the 5’-end). AGO2 provides the catalytic motifs where one or more Mg2+ cations directly coordinate the oxygen atoms of the water molecules. The cleavage products are 3′-hydroxyl and 5′-phosphate. Adapted from (Martinez and Tuschl 2004, Schwarz, Tomari et al. 2004, Sontheimer 2005).

The RNA duplex formed from the base pairing between the antisense and mRNA is about 2 rounds of α-helix given that every 10 nucleotides make one RNA turn. For this reason, in order for RISC to perform its endonucleolytic activity, AGO2 first undergoes structural rearrangement to accommodate the full-length RNA duplex by shifting the two lobs apart to allow mRNA full hybridisation with the antisense. The new conformation of AGO2 leads to the release of the antisense 3'-end from the PAZ domain. (Lingel, Simon et al. 2003, Schlundt, Tants et al. 2017, Yi 2018).

Mismatches are not highly tolerated in siRNA in comparison with miRNA. The full complementarity between the target mRNA and antisense is crucial for efficient endonucleolytic cleavage. For this reason, introducing a mismatch in the seed region may reduce target recognition, and the presence of several mismatches in the antisense impairs the efficacy of the cleavage (Tomari and Zamore 2005). The introduction of mismatches is a universal tool for the design of reference and control oligonucleotides (Haley and Zamore 2004).

1.4 siRNA chemical modification

To utilise the RNAi pathway as a therapeutic agent, siRNA should overcome several pharmacokinetic (PK) and pharmacodynamic (PD) challenges. Oligonucleotides, and siRNA specifically, are susceptible to enzymatic degradation and have a poor pharmacokinetic profile in the systemic circulation. The siRNA pharmacodynamics challenges are target specificity, off-target binding and immunostimulation. For these reasons, chemical modifications have been investigated to control the nucleases stability, bioavailability, binding affinity and specificity (Kobayashi and Tomari 2016, Shen and Corey 2018). In general, chemical modifications are classified into three main categories;

1- Phosphodiester linkage modifications.
2- Sugar modifications.
3- Nucleobase modifications.

The potency of siRNA is driven by its target specificity. Introducing chemical modifications to siRNA changes both siRNA-mRNA and siRNA-protein interactions, which may improve the silencing efficiency. Given that the human genome encodes homologous regions, it is difficult to silence these transcripts efficiently by siRNA. That is because a full complementarity of mRNA to siRNA in the seed region is the major determent of siRNA specificity. It is not always feasible to eliminate the off-target binding of siRNA by sequence adjustments making it challenging to discriminate between the on-target and off-target silencing. However, chemical modifications that weaken the (siRNA/RISC)-mRNA interactions might reduce the off-target silencing (Lee, Seok et al. 2015, Jiang, Zhu et al. 2017) .

Since riboendonucleases such as RNase A, as well as, exonucleases exist in almost every intra and extracellular environment or body fluid, it is crucial to increase siRNA enzymatic stability. Several RNases catalyse the hydrolysis of oligonucleotides into shorter fragments. For example, RNase H2, which requires divalent cations such as Mg^{+2}, targets oligonucleotides at the 3'-phosphodiester and gives 3'-OH and 5'-phosphate products. Moreover, exonucleases attack the 3'-end, and hydrolysis progress toward the 5'-end (Martinez and Tuschl 2004, Schwarz, Tomari et al. 2004, Sontheimer 2005).

The first chemical modification of oligonucleotides is phosphorothioate linkage (PS) at the 3'-end of the siRNA. This modification enhances the siRNA serum stability. Among the earliest potent modifications is the substitution of 2'-OH of the ribose in pyrimidine bases with either fluoro (2'-F) or O-methyl (2'-O-Me) moieties. Those modifications improve siRNA PK and PD *in vivo*. Combinations of PS with 2'-F and/or 2'-O-Me result in much more stable siRNA in comparison with each modification alone (Watts, Martin-Pintado et al. 2010, Wei, Jones et al. 2011, Lee, Seok et al. 2015).

Food and Drug Administration (FDA) approved in 2010 an antisense-based drug called ''Kynamro'', carries PS and 2'-O-Me modifications. Kynamro have been proven a potent inhibitor of apolipoprotein B synthesis, and shown to be effective in reducing the LDL cholesterol level in hypercholesterolaemia patients (Shen and Corey 2018).

The activity of 2'-sugar modifications depends on the charge and size of the introduced group. Replacement of 2'-OH with a more electronegative element such as F leads to sugar conformation and alters the geometry of the oligonucleotide α-helix. This structural change reduces the efficiency of nucleases attack and improves siRNA stability. On the other hand, introducing a neutral group such as O-Me does not significantly interfere with the sugar puckering and thus does not improve siRNA stability against metal-dependent endonucleases. However, 2'-O-Me enhances siRNA stability by lessening the efficacy of water molecule nucleophilic attack on the phosphodiester backbone (Watts, Martin-Pintado et al. 2010, Wei, Jones et al. 2011).

The sugar ribose exists in two different forms, either C2'-endo (South) as in DNA or C3'-endo (*North*) in RNA (Fig 1-14). The favourable gauche confirmation for 2'-F is C3'-endo because the fluorine atom will be in the same orientation with the ring 4O' in a stable α-helix confirmation. In unmodified RNA, 2'-OH makes hydrogen bonds with water molecules in the solvent around the phosphodiester group in the minor groves, but 2'- F hinders the formation of these hydrogen bonds. On the contrary, since 2'-F is antiperiplanar, the nucleobases are more polar, which lead to stronger Watson−Crick interactions. For this reason, 2'-F modification shifts the balance towards C3'-endo, which improves RNA duplex stability via enhancing W-C base pairing in α-helix. The North confirmation can also be generated by 2'-O-Me modification (Watts, Martin-Pintado et al. 2010, Deleavey and Damha 2012).

2'-F modifications are well tolerated in both siRNA strands. In general, 2'-F modification enhances the stability of pyrimidine-rich sequences toward endonucleases, but it does not provide significant resistance in comparison with 2'-O-Me modification (Eder, DeVine et al. 1991, Beigelman, Karpeisky et al. 1995).

Importantly, 2'-modifications influence the melting temperature of the siRNA. In fact, the master role in siRNA design is to create thermodynamic asymmetry in the duplex that favours the retention of the antisense in the RISC complex. For instance, 2'-F modification at the siRNA 5'-end stabilises the siRNA by creating two types of hydrogen bonds (Fig 1-15). The first type is pseudo hydrogen bonds in purine bases between the 2'-F and H8 of the same base. The second type of hydrogen bonds is

formed between 2'-F and H8 of the 3′-complementary neighbouring base (Watts, Martin-Pintado et al. 2010, Anzahaee, Watts et al. 2011).

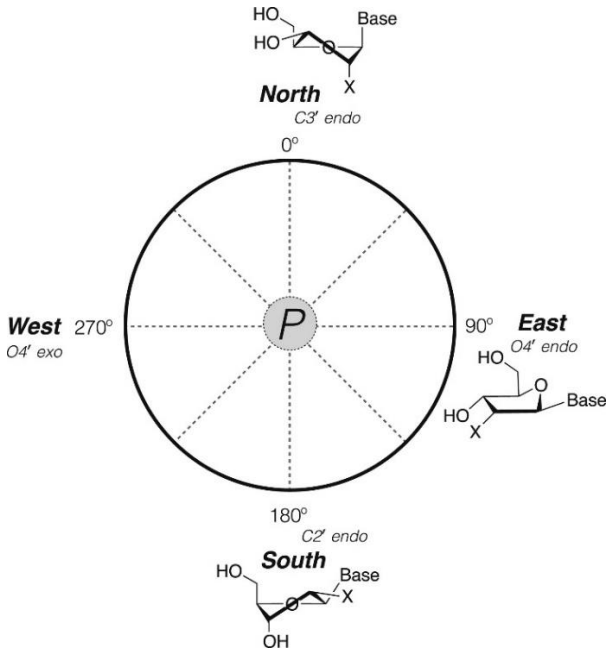

Fig 1-14. Pseudorotational wheel of furanose interactions. The α-form of RNA sugar is C3'-endo (*North*), and the β-form of DNA sugar is C2'-endo (*South*). X= OH in RNA, X= H in DNA. Adapted from (Deleavey and Damha 2012).

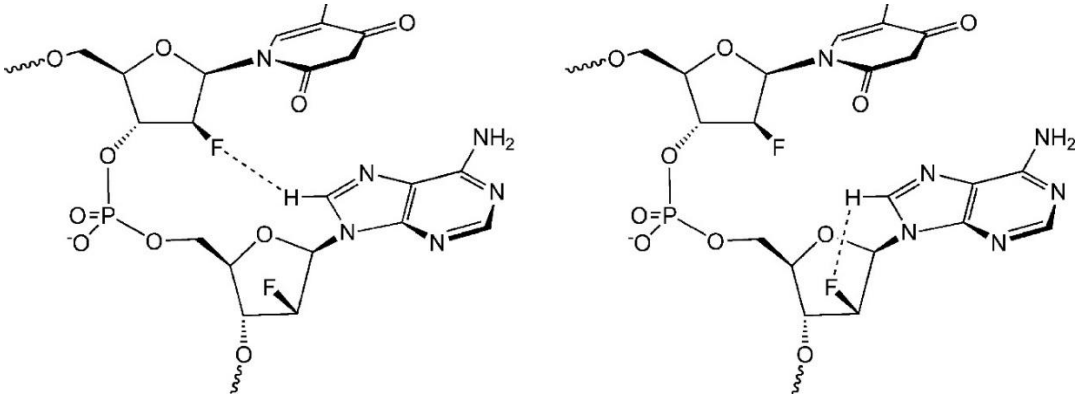

Fig 1-15. Pseudohydrogen interactions between 2'-F and H8 in purine. Introducing 2'-F to the sugar prefers the North confirmation where the 2'-F is antiperiplanar and can form interaction with the H8 of it is won purine base (right) or with the H8 of the 3'-proximal purine base (left). Adapted from (Anzahaee, Watts et al. 2011).

Since the 70s, phosphorothioate (PS) modification is a proven approach to increase siRNA stability against endonucleases. The modification is achieved by replacing one of the non-bridging oxygen atoms of the phosphate group with a sulphur atom. Phosphodiester linkage is negatively charged under physiological conditions (pKa = 2). The synthesis of PS oligonucleotides via standard phosphoramidite synthesis methods yields diastereomeric products, which may contribute to variable activities. The *Rp* isomer is more susceptible to RNase H degradation while the *Sp* configuration exhibits stronger nuclease resistance. The stereo-random PS isomer is more stable in comparison with the *Sp* and *Rp* isomers. For this reason, controlling PS chirality is vital for predicting the therapeutic activity of the siRNA (Cook, Holman et al. 1969, Zon and Geiser 1991, Jaroszewski, Clausen et al. 1996, Iannitti, Morales-Medina et al. 2014).

Nevertheless, elimination of the chiral phosphor centre by substituting both oxygen atoms of the phosphate group with two sulphur atoms (PS2) results in only non-isomeric products (Bailey, Shen et al. 2017). Combination of 2'-O-Me and PS2 modifications enhance the siRNA activity and improve stability. Of notice, when 2'-O-Me and PS modification increases siRNA duplex stability, the combination of PS2 with 2'-O-Me not elevate the melting point of the siRNA duplex but it increases siRNA loading into RISC (Incarnato, Anselmi et al. 2017).

Phosphorothioate and 2'-sugar modifications are position dependent. In general, modifications at the 3'-end of the antisense strand are more effective than 5'-end modifications. In fact, body fluids contain more 3'-end exonucleases than 5'-end nucleases. Moreover, modifications at the 5'-end might impair the affinity of the seed region to the targeted mRNA. The most well-tolerated modifications on the antisense strand are those 2'-F as they are feasible almost along the whole stand. On the contrary, 2'-O-Me modifications on the antisense strand are strictly sequence-dependent. The 2'-O-Me is more effective at the 3'-end and in the centre of the siRNA sense strand (Eder, DeVine et al. 1991, Heemskerk, de Winter et al. 2009, Iannitti, Morales-Medina et al. 2014).

1.5 Oligonucleotide delivery

1.5.1 siRNA delivery challenges

Oligonucleotide delivery to their target by systemic administration is a major challenge facing the development of siRNA therapeutics. Oligonucleotides are negatively charged under physiological conditions and cannot maintain their effective dose in the targeted site for a prolonged period. That is because oligonucleotides are not stable in the bloodstream and undergo rapid elimination by the kidney via tubular secretion. Beside renal secretion, siRNA is also retained and accumulated in the liver. Due to the siRNA large molecular weight (about 13 kDa) and its hydrophilic properties and negative charge, naked siRNA cannot pass the cellular membrane by passive diffusions. For these reasons, introducing chemical modifications and developing delivery vehicles are essential for the development of siRNA-based drugs (Juliano 2016, Kaczmarek, Kowalski et al. 2017, Khvorova and Watts 2017).

siRNA has immunogenic properties when they are administered systemically. The immune stimulation by siRNA is either sequence dependant controlled by the stimulation of the pattern recognition receptors (PRRs) or sequence independent driven by the status of the 5'-phosphate terminus. The innate immune system recognises siRNA and induces the production of pro-inflammatory cytokines such as IL-1, IL-6, IL-12, and TNF-α (Whitehead, Dahlman et al. 2011, Lim and Staudt 2013, Meng and Lu 2017).

Moreover, siRNA activates different members of the toll-like receptor family (TLR). For instance, siRNA activates TLR-3 pathway resulting in release of interferons IFN-α and IFN-β, which lead to enhanced proliferation of the natural killer (NK) cells and memory T cells. Single-stranded RNA also can activate TLR-8, which is enriched in the myeloid lineage, leading to hyperproliferation of NK cells. Furthermore, siRNA activates, in a sequence-independent manner, the RNA helicase protein retinoic acid-inducible gene 1 (RIG-1) and triggers a strong interferon response. The dsRNA-dependent protein kinase (PKR) can also be activated by siRNA resulting in translational inhibition and increased interferons secretion (Clemens and Elia 1997, Pang, Keeble et al. 2000, Hiratsuka, Watanabe et al. 2008, Dalpke and Helm 2012).

Chemical modification and the avoidance of specific motifs during siRNA design can reduce the immunostimulatory potential. The cytoplasmic receptors RIG-1 and PKR also bind bunt ended oligonucleotides and 5'-triphosphate. The TLR-7 and TLR-8 receptors recognise AU- and GU-rich motifs, but 2'-O-Me modifications reduce the activation of these TLR pathways (Forsbach, Nemorin et al. 2008, Zhang, Ohto et al. 2017).

With the exception of the liver, systemic delivery to haematopoietic tissues and organs has proved to be challenging. Leukaemic cells are circulating in the body fluids, and malignant HSCPs are hidden in the protective bone marrow niche. Moreover, siRNA has slow penetration through the capillary endothelium emphasising the need for a delivery system. Nanoparticles can cope with some of the delivery challenges. For instance, encapsulating siRNA into a nanoparticle protects the siRNA from serum nucleases, provides improved biodistribution and enhances the pharmacodynamic and pharmacokinetic properties. Nanoparticles can be functionalised with surface ligands that improve the accumulation of siRNA in the relevant leukaemic compartments (Juliano 2016, Kaczmarek, Kowalski et al. 2017).

The efficiency of the delivery vehicle depends on the size and charge of the nanoparticle. The diameter of a nanoparticle between 20 - 70 nm is desirable for targeting leukaemic cells because it allows cellular uptake by receptor-mediated endocytosis. The reticuloendothelial system usually recognises nanoparticles larger than 100 nm and shortens their half-life. Moreover, nanoparticles carrying high positive or negative charge coagulate rapidly with serum proteins and have short circulation time. Typically, the nanoparticle circulation time can be enhanced by the addition of polyethylene glycol (PEG) which stabilises the surfaces and provides a stealth effect. However, PEGylation reduces the efficacy of the siRNA endosomal escape and triggers an immune response. For these reasons, the development of nontoxic nanoparticle for siRNA delivery is an arduous task that requires multi-disciplinary skills (Hoarau, Delmas et al. 2004, Akinc, Goldberg et al. 2009, Semple, Akinc et al. 2010, Chen, Tam et al. 2016).

1.5.2 Polymer nanoparticle

Micellar delivery systems are intensively investigated drug nanocarriers. Micelles are formed from synthetic copolymers bearing at least two polymer blocks that provide amphiphilic properties. The physical phenomena behind the self-assembly of micelles is the hydrophilic and hydrophobic interactions between the polymer chains and the solvent. When the concentration of amphiphilic molecules reaches a specific concentration, known as the critical micelles concentration (CMC), these molecules assemble in symmetric structures. These self-assembled structures vary from spherical vesicles, cylinders, tubes and bilayer or lamellar. The formed micellar structure depends on the critical packing parameter of the amphiphilic molecule, which is determined by the ratio between the volume of the hydrophobic chain and the length of the hydrophilic chains (Jones and Leroux 1999, Zhang, Huang et al. 2014, Braunova, Kostka et al. 2017, Keskin and Tezcaner 2017). Synthetic polymers allow for the addition of conjugates to the surface of the micelles. Functionalised micelles with ligands specific for leukaemic cells such as single-chain variable fragment (scFv) (Jhaveri and Torchilin 2014), aptamers or short peptides against specific surface markers enhance the association of the micelles with the leukaemic cells and increase the bioavailability of the siRNA (Bolu, Sanyal et al. 2018).

Despite a large amount of research on synthetic polymers for drug delivery, very few are showing promising clinical perspectives mainly due to cytotoxicity. Water-soluble polymers, especially cationic polymers such as polyethyleneimine (PEI), efficiently encapsulate siRNA due to the electrostatic interaction between the protonated polymer chains and the negatively charged siRNA (Shi, Chou et al. 2013, Navarro, Pan et al. 2015). These particles are called polyplexes, and they have fast cellular uptake and easy endosomal release by the so-called proton sponge mechanism. Following endocytosis, polyamines absorb protons in the endosomes leading to an increase the endosomal membrane potential. Consequently, chloride molecules are diffused into the endosome to restore the equilibrium leading to rapid raise of osmotic pressure and further swelling of the endosome followed by rupture and release of the endosome contents onto the cytoplasm (Benjaminsen, Mattebjerg et al. 2013, Jhaveri and Torchilin 2014).

Under physiological conditions, polyplexes interact and aggregate with negatively charged serum proteins. For this reason, shielding polyplexes with PEG is required to improve circulation time. Moreover, cationic polymers usually have high cytotoxicity. Shortening the length of the polymer may reduce the toxicity but also destabilise the polyplexes. The chemical addition of PEG to copolymers generates triblock copolymers which are less toxic and have prolonged circulation time (Werfel, Jackson et al. 2017).

1.5.3 Cell-penetrating peptides (CPP)

Cell-penetrating peptides (CPPs) consist of 5 - 40 amino acids, typically positively charged or have amphipathic properties. Polycationic CPPs complex siRNA by electrostatic interactions. Moreover, some CPPs covalently couple siRNA via linkers capable of releasing siRNA upon cellular uptake. The most common CPPs are arginine-rich such as the HIV-TAT peptide which has high cell penetrating properties. Furthermore, some peptides have tissue-specific homing properties such as the LSD peptide (CLSDGKRKC) which target melanoma and osteocarcinoma cells, and 293P-1 peptide (SNNNVRPIHIWP) is specific for hepatocytes. Cell-penetrating peptides can target leukaemic surface markers such as TLR-2 receptor and integrins. The mechanism by which CPPs entre the cell is not well defined and mostly contributed to surface binding followed by active endocytosis, membrane internalisation or membrane flip-flop mechanism (Ishihara, Goto et al. 2009, Li, Lv et al. 2014).

1.5.4 Lipid-based delivery systems

Lipid-based delivery systems are attractive nanocarriers for oligonucleotides due to their high encapsulation efficiency and reduced immunogenicity. The most two intensively studies lipid nanocarriers of siRNA are liposomes and lipid nanoparticles (LNPs) (Fontana, Liu et al. 2017, Shajari, Mansoori et al. 2017).

A liposome is closed phospholipid bilayers with aqueous core and spherical structure. Alec Bangham in 1965 described membrane-like vesicles as swollen phospholipid systems and called them bangosomes which are later named liposomes (Bangham, Standish et al. 1965). Liposomes are promising drug carriers with improved biodistribution and minimal toxicity. Unilamellar liposomes are typically generated under low pressure via simple techniques involving extrusion through polycarbonate filters. Liposomes with diameters less than a 100 nm can be produced by sonication and extrusion of lipid films. It is feasible today to produce liposomes, and LNPs with size ranges between 20 to 200 nm via microfluidics mixing techniques (Al-Jamal and Kostarelos 2011, Abu Lila and Ishida 2017, Yue and Dai 2018).

Liposomes have been widely used in drug delivery due to their chemical and structural properties. A typical liposome can encapsulate both hydrophobic molecules within its lipid shell, and hydrophilic molecules in the aqueous core. The size and surface charge of liposomes influence their stability and pharmacokinetic properties *in vivo*. Research in the late 80s led to the development of the first clinical liposome encapsulating doxorubicin. There are several clinically approved lipid-based vehicles encapsulating different drugs, mostly cancer therapeutics (Table 1-4). The size of these liposomes is less than 100 nm, which provides enhanced penetration retention (EPR) in the targeted site after intravenous administration. Besides the hydrodynamic diameter, several factors influence the EPR, such as surface charge and vascularity of the targeted site (Cullis and Hope 2017, Yue and Dai 2018) (Barata, Sood et al. 2016, Bobo, Robinson et al. 2016).

Name	**Drug**	**Disease**	**Year approved**
AmBisome	amphotericin B	Fungal infections Leishmaniasis	1990 (Europe), 1997 (USA)
Doxil/Caelyx	doxorubicin	Kaposi’s sarcoma Ovarian cancer	1995 (USA) 1999 (USA)

		Breast cancer	2003 (Europe, Canada)
DaunoXome	daunorubicin	Kaposi's sarcoma	1996 (Europe), 1996 (USA)
Myocet	doxorubicin	Breast cancer	2000 (Europe)
Abelcet	amphotericin B	Aspergillosis	1995 (USA)
Amphotec	amphotericin B	Aspergillosis	1996 (USA)
Visudyne	verteporphin	Macular degeneration	2000 (USA), 2003 (Japan)
Lipo-Dox	doxorubicin	Kaposi's sarcoma, breast and ovarian cancer	2001 (Taiwan)
Marqibo	vincristine	Acute lymphoblastic leukaemia	2012 (USA)

Table 1-4: Lipid-based drugs in the clinic. Adapted from **(Barata, Sood et al. 2016, Bobo, Robinson et al. 2016)**

Formulations of lipid with the siRNA-loaded solid core, such as metal-based nanoparticles can improve siRNA delivery. It is also possible to shield polyplexes and micelles with a lipid mono or bilayer. This strategy stabilises the nanoparticle structure by eliminating the effect of the critical micelle concentration (Braunova, Kostka et al. 2017, Keskin and Tezcaner 2017).

Lipids are versatile materials to design unique siRNA nanocarriers, such as LNPs. Lipid nanoparticles do not contain large aqueous core. Instead, they have packed core with several islands encapsulating hydrophilic materials. LNPs consist of ionisable cationic lipids, helper lipid, cholesterol and stabilising agent such as polyethylene glycol or dextran. The flexibility of lipid formulations allows for control over the LNPs size and charge. For example, the rigidity and permeability of the LNP membrane can be modulated by changing the cholesterol concentration. The

addition of helper lipid can alter the lipid membrane structure. Typically, helper lipids are added to LNPs formulations to improve stability and bioavailability. For example, addition of cationic lipid, such as dipalmitoylphosphatidylcholine (DOPC) leads to laminar bilayer structure. Another class of helper lipids are thehosphorylethanolamines which promote active endocytosis such as 1,2-distearoyl-sn-glycerol-3-phosphoethanolamine (DSPE). Sphingomyelin and phosphocholine lipids are commonly used in formulations of stable liposomes and LNPs. Furthermore, LNPs stability is achieved by the addition of PEG that provides a shielding effect. Helper lipids should be added to LNPs formulations with caution because they slowdown siRNA endosomal release as well as trigger immunogenic responses (Bao, Jin et al. 2013, Chen, Tam et al. 2014, Leung, Tam et al. 2014, Cheng and Lee 2016, Hashiba, Sato et al. 2017).

Immunoliposomes are generated from the coupling of ligands such as antibodies, antibody fragments (scFv), CPPs or small molecules. Targeting ligands are usually chemically bound to hydrophobic anchors. The anchors are either added to the lipid formulation or added to liposomes by postinsertion. Among the most commonly used anchors, PEGylated helper lipids terminating with functional groups, such as maleimide or azide, which allow thiol-maleimide Michael additions or azide-alkyne cycloaddition, respectively. Functionalised immunoliposomes and LNPs accumulate in the targeted site and have improved pharmacodynamics (Leung, Tam et al. 2014, Fisher, Mattern-Schain et al. 2017, Hashiba, Sato et al. 2017, Kuang, Ku et al. 2017).

Ionisable cationic amino-lipids (Fig 1-16) such as dilinoleylmethyl 4-dimethylaminobutyrate (Dlin-MC3-DMA) and 2,2-dilinoleyl 4-dimethylaminoethyl-[1,3]-dioxolane (Dlin-KC2-DMA) are used for potent LNPs formulations. These LNPs have demonstrated high *in vivo* efficacy with low doses in several animal models (Semple, Akinc et al. 2010, Maier, Jayaraman et al. 2013). Ionisable lipid-based LNPs have provided improved tolerable preclinical vehicles for siRNA delivery. The Food and Drug Administration (FDA) approved LNP/siRNA drug called ONPATTRO or Patisiran for patients with transthyretin-related hereditary amyloidosis (ATTR) (Rizk and Tuzmen 2017, Hoy 2018). Other similar LNPs encapsulating

oligonucleotides are in clinical trials for liver cancer, hypercholesterolemia and others (Table 1-5).

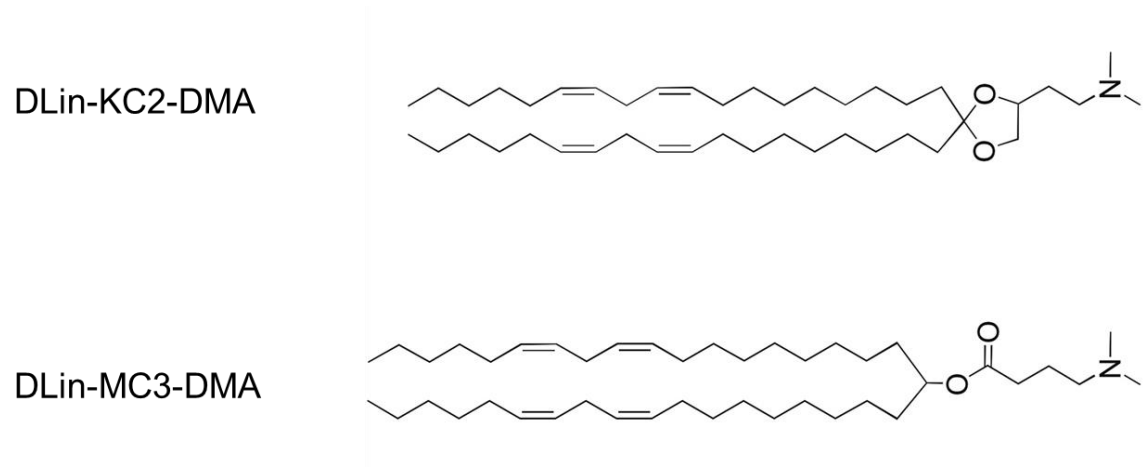

Fig 1-16: Chemical structure of ionisable cationic lipids. Adapted from (Semple, Akinc et al. 2010)

Name	siRNA target	Disease	Phase
Patisiran	*TTR*	Transthyretin induced amyloidosis	Approved
ARB 1467	*PLK1*	Hepatocellular carcinoma	Phase 2
	HBV	Hepatitis B	Phase 2
	KSP and *VEGF*	Liver cancer	Phase 1
	PCSK9	Atherosclerosis	Phase 1

Table 1-5: LNP/siRNA drugs in clinical trials. Adapted from (Rizk and Tuzmen 2017)

Ionisable cationic lipid nanoparticles have high encapsulation efficiency of siRNA because the formulation is performed with the so-called ‘’ethanol loading procedure’’. The amino lipids have pKa < 7 and siRNA packaging is carried out at acidic pH, where the lipids are positively charged, and siRNA carry a negative charge. The technique (Fig 1-17) in brief includes vigorous mixing of ethanol-dissolved lipid mixture with the siRNA solution in sodium acetate buffer (pH = 4), which allows high loading efficiency of the negatively charged siRNA into the positively charged lipids. The second step involves rapid controlled mixing in a microfluidic system to formulate LNP/siRNA particles. Finally, pH then increases to physiological values. Molecular modelling and structural studies on LNP/siRNA have shown that microfluidic systems produce nanoparticles with hydrophobic core containing multiple inverted lipid micelles encapsulating the siRNA (Fig 1-18) (Leung, Hafez et al. 2012, Gilleron, Querbes et al. 2013, Leung, Tam et al. 2015, Cullis and Hope 2017). The ONPATTRO drug is formulated following these parameters (Fig 1-19).

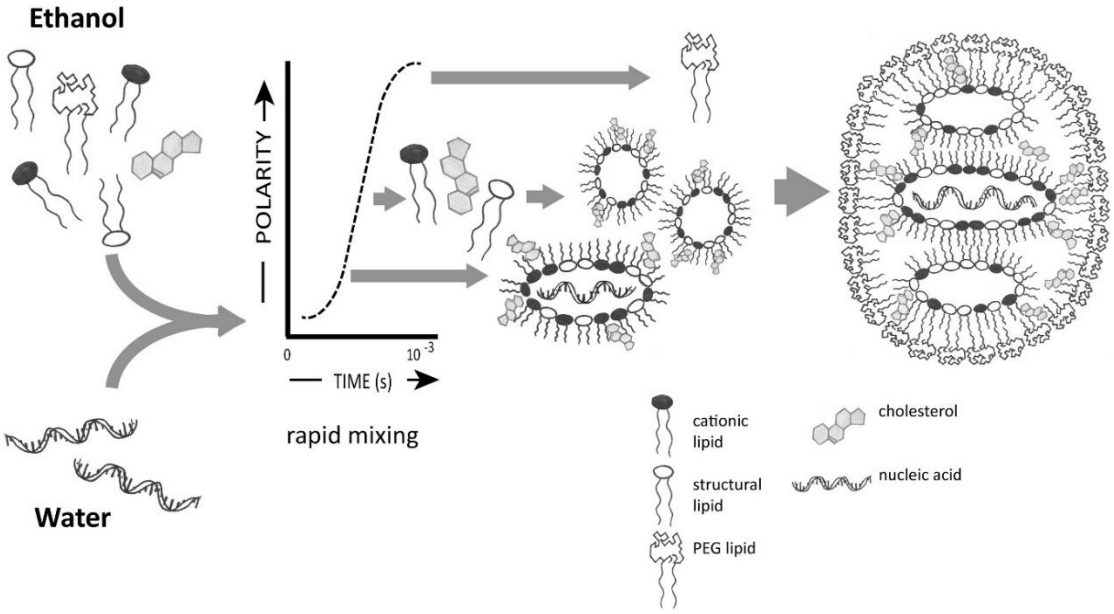

Fig 1-17: Ethanol loading technique of LNP/siRNA. Lipids are dissolved in ethanol and mixed with siRNA in aqueous solution at pH = 4. The electrostatic interactions between the positively charged lipid and negatively charged siRNA drive the inverted micelles formation. If the mixing is vigorous and rapid enough then the aggregation of these micelles is eliminated as PEGylated lipid shields these micelles and stabilises the structure (Cullis and Hope 2017).

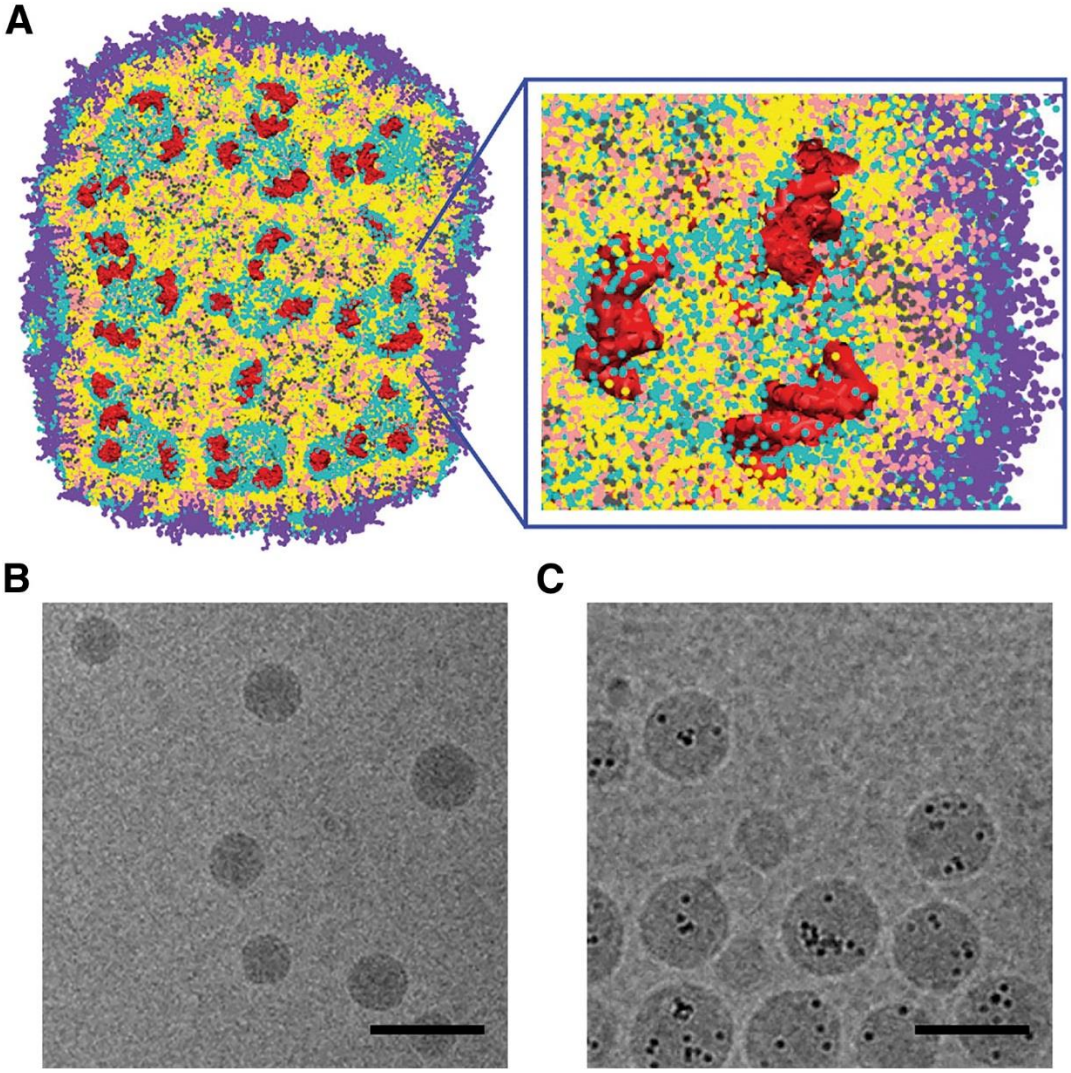

Fig 1-18: LNPs structure. (A) Molecular modelling of a cross section of LNP/DNA produced in the microfluidic system. The composition of the LNP/DNA is Dlin-KC2-DMA (yellow), cholesterol (pink), DSPC (grey), charged polar lipid moiety (cyan), PEG (violet), DNA (red). The ratios of mixing is lipid/DSPC/cholesterol/PEG-lipid (4:1:4:1; mol/mol) and DNA-to-lipid ratio is 0.05 wt/wt. (B). Cryo-TEM microscopy image of LNP/siRNA. The composition of the LNP/siRNA is Dlin-KC2-DMA/ DSPC/ Chol/ PEG-lipid (40/11.5/47.5/1; mol/mol) and siRNA/lipid ratio is 0.06 wt/wt, scale bar 100 nm. (C). Cryo-TEM microscopy image of LNP containing 5 nm diameter of negatively charged gold nanoparticles. The LNP/Au-NP composition is Dlin-KC2-DMA /DOPE/ Chol/ PEG-lipid (40/11.5/47.5/1; % mol) and Au-NP to lipid ratio is 2.2×10^{13} particles/µmol lipid, scale bar 100 nm. (Leung, Hafez et al. 2012, Leung, Tam et al. 2015).

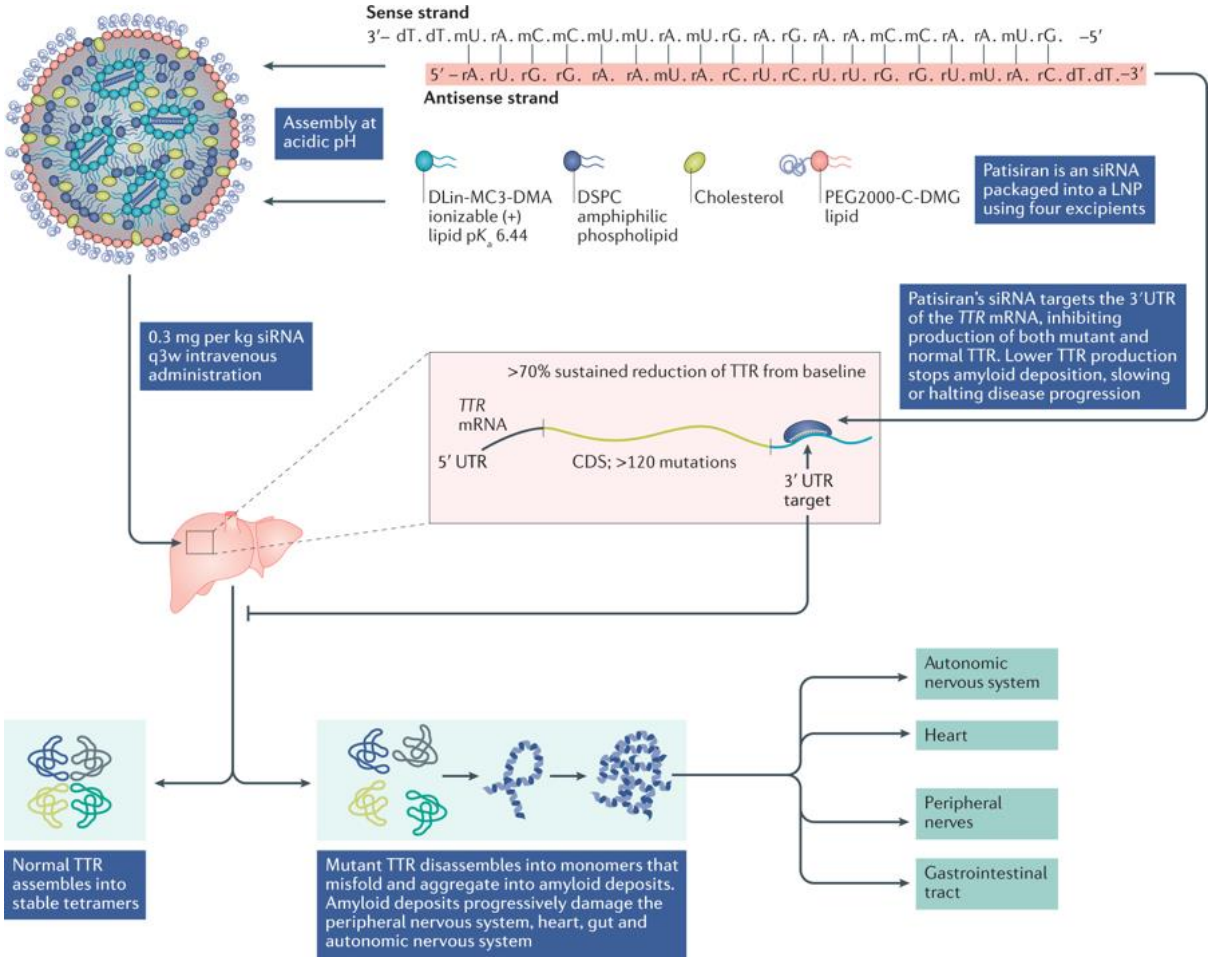

Fig 1-19: Schematic illustration of ONPATTRO composition and mode of action. ONPATTRO consists of chemically modified siRNA, targeting 3'-UTR of *TTR* mRNA, encapsulated into Dlin-MC3-DMA lipid nanoparticle. The drug is formulated under acidic pH using microfluidic system. The nanoparticles are injected intravenously at 0.3 mg/kg every three weeks (q3w). Where for the siRNA, r: RNA bases, D: DNA bases and m: 2'-O-Me modified bases. Adapted from (Setten, Rossi et al. 2019).

1.6 Aims of the project

The main goal of the project was to establish a delivery system for siRNA, which has the potential for clinical use. The aims are as follow;

1. Enhancing the siRNA potency by introducing chemical modifications.

2. Establishing a lipid nanoparticle (LNP) system for siRNA delivery, and validating the gene knockdown *in vitro* in cell lines, and in co-culture in t(8;21) primary and PDX cells.

3. Establishing a gene knockdown *in vivo* and exploiting the therapeutic potential of novel drug combinations.

Chapter 2.

Materials and Methods

2.1 Materials

2.1.1 Lab equipment

Instrument	Manufacturer
Allegra X-12R centrifuge	Beckman Coulter
Allegra X-22R centrifuge	Beckman Coulter
5415 R microfuge	Eppendorf
GeneAmp PCR System 2700	Applied Biosystems
FACS Calibur	Beckton Dickinson
FACS Canto II	Beckton Dickinson
ND-1000 spectrophotometer	Nanodrop Technologies
FLUOstar Omega Microplate Reader	BMG labtech
Elektroporations-Impulsgenerator EPI 2500	Dr. L Fischer, Heidelberg
Zetasizer Nano ZS	Marvern Panalytical
Viia7 PCR System	Applied Biosystems

Table 2-1: Equipment.

2.1.2 Softwares

Software	Software developer
GraphPad Prism 7	GraphPad Software lnc
Image Lab	Bio-Rad Laboratories
SDS 2.0	Applied Biosystems
Primer express 2.0	Applied Biosystems
FunRich 3.1.3	Mathivanan and colleagues
FlowJo -V10	FlowJo
RStudio	R
QuantStudio Real Time PCR	Applied Biosystems

Table 2-2: Software.

2.1.3 General Chemicals

Chemicals were purchased at analytical grade from Sigma-Aldrich Ltd, Bio-Rad, VWR, Thermo Fisher Scientific, R&D Systems, EMC microcollections GmbH.

Chemical	**Supplier**
2-mercaptoethanol	Sigma
Acetone	Thermo Fisher Scientific
Ammonium persulphate	Chem Cruz
Acrylamide 40% (1:29)	Sigma
Acrylamide 30% (1:37.5)	Sigma
CHAPS	Sigma
Dimethylsulphoxide	Sigma
Dithiothreitol	BioRad
Dried skimmed milk	Marvel
Ethanol	Thermo Fisher Scientific
Ethylenediaminetetraacetic acide	Sigma
HEPES	Sigma
Hydrochloride acid	Sigma
Immobilon membrane	Millipore
Luciferin	Roche
Methanol	Thermo Fisher Scientific
Paraformaldehyde	Sigma
PEG_{400}	Sigma
Phosal 50 PG	Fisher Scientific
Phosphate buffered saline	Gibco
Propidium Iodide	Sigma
Protein Assay Reagent	BioRad
RNase A	QIAGEN
Sodium chloride	Sigma
Sodium dodecyl sulfate	Sigma
Sodium hydroxide	Sigma
SulfoCyanaine7.5 alkyne	Lumiprobe GmbH

Sybr Green	Lifetech
Tetramethylethylenediamine	Sigma
Tris	Sigma
Trypan blue	Sigma
Triton 100	Sigma
Tween 20	Sigma
XenoLight™ D-Luciferin	Caliper Life Sciences

Table 2-3: Reagents and chemicals.

2.1.4 Experimental kits

Kit	**Supplier**
Qiashredder	QIAGEN
RNeasy Mini Kit	QIAGEN
RNeasy Micro kit	QIAGEN
RevertAid™ H Minus cDNA Synthesis Kit	Thermofisher

Table 2-4: Experimental kits.

2.1.5 Cell culture media and supplements

Item	Supplier
Fetal calf serum	Gibco
RPMI1640	Sigma
DMEM	Sigma
GM-CSF	R&D Systems
IL-3	R&D Systems
IL-6	R&D Systems
FLT-3L	STEMCELL Technologies
Trypsin	R&D Systems
L-Glutamine	R&D Systems
SFEM	STEMCELL Technologies
FGF-1	STEMCELL Technologies
100X Myeloid Expansion	STEMCELL Technologies
SR1	STEMCELL Technologies

Table 2-5: Cell culture media and supplements.

2.1.6 RT-PCR primers (Sigma-Aldrich Ltd)

Gene	5’ → 3’
GAPDH	Fw: 5’- TGG CAT GGC CTT CCG T -3’ Rev: 5’- TCT CCA GGC GGC ACGT T -3’
hGAPDH	Fw: 5’- GAA GGT GAA GGT CGG AGT C -3’ Rev: 5’- GAA GAT GGT GAT GGG ATT TC -3’
TBP	Fw: 5’- CCT AAA GAC CAT TGC ACT TCG T -3’ Rev: 5’- GTT CGT GGC TCT CTT ATC CTC A -3’
RNUX1/ETO	Fw: 5’- AAT CAC AGT GGA TGG GCC C -3’ Rev: 5’- TGC GTC TTC ACA TCC ACA GG -3’
ANGPT1	Fw: 5’- TCT CTT CCC AGA AAC TTC AAC ATC T -3’

	Rev: 5’- TCA TGT TTT CCA CAA TGT AAT TCT CA-3’
TERT	Fw: 5’- GGA GAA CAA GCT GTT TGC GG -3’ Rev: 5’- AGG TTT TCG CGT GGG TGA G -3’
CCND2	Fw: 5’- CTG TGT GCC ACC GAC TTT AAG TT -3’ Rev: 5’- TGC TCC CAC ACT TCC AGT TG -3’
LAPTM5	Fw: 5’- CTC CCC AGC CAG GAG GAT AT -3’ Rev: 5’- CCA CCG AGT TCA TGC ACT TG -3’
CEBPA	Fw: 5’- GAG GGA CCG GAG TTA TGA CA -3’ Rev: 5’- AGA GGC GCA CAT TCA CAT T -3’
CD34	Fw: 5’- AAA GCA CCA ATC TGA CCT GAA AA -3’ Re: 5’- CGA GGT GAC CAG TGC AAT CA -3’
RUNX1	Fw: 5’- TCC ACA AAC CCA CCG CAA GT -3’ Rev: 5’- CGC TCG GAA AAG GAC AAG C -3’
CCND2	Fw: 5’- CTG TGT GCC ACC GAC TTT AAG TT -3’ Rev: 5’- TGC TCC CAC ACT TCC AGT TG -3’

Table 2-6: PCR primers.

2.1.7 siRNA oligonucleotides

Name	**5’ → 3’**	**Supplier**
siRE	5’- CCUCGAAAUCGUACUGAGAAG -3’ 3’- UUGGAGCUUUAGCAUGACUCU -5’	Axolabs GmbH
siRE-mod	5’- CFCFUFCFGAAAU$_{OMe}$C$_{OMe}$GU$_{OMe}$AC$_{OMe}$U$_{OMe}$GdAdGdAd T$_{PS}$dT -3’ 3’- dT$_{PS}$dTGGAGCUUUAGCAUGACUCU -5’	Axolabs GmbH
siMM	5’- CCUCGAAUUCGUUCUGAGATT -3’ 3’- TTGGAGCUUAAGCAAGACUCU -5’	Axolabs GmbH

siMM-mod	5'- CFCFUFCFGAAU$_{OMe}$U$_{OMe}$CGU$_{OMe}$U$_{OMe}$C$_{OMe}$UGAGAdT$_{PS}$ dT -3' 3'- dT$_{PS}$dTGGAGCUUAAGCAAGACUCU -5'	Axolabs GmbH
SiCCND2_2	Unknown	QIAGEN
SiCCND2_4	Unknown	QIAGEN

Table 2-7: siRNA sequences. F and OMe refer to 2'-modified ribose with fluoro and methoxy, respectively. d refers to 2'-deoxyribose and PS refers to phosphorothioate modified backbone.

2.1.8 Immunoblot antibodies

Epitope	Dilution	Company
mouse α-GAPDH	1:300,000 (5% milk in T-BST)	HyTest, Turku, Finland
rabbit α-hGAPDH	1:1000 (5% milk in T-BST)	Abcam
rabbit α-hTERT	1:1000 (5% milk in T-BST)	Cell Signalling
rabbit α-RUNX1/RHD	1:40 – 1:60 (5% milk in T-BST)	Merc Millipore
rabbit α-RUNX1/RHD	1:250 (5% milk in T-BST)	Santa Cruz Biotechnology
rabbit α-CCND2	1:250 (5% milk in T-BST)	Proteintech
rabbit α-BCL2	1:1000 (5% BSA in T-BST)	Cell Signalling
rabbit α-BCLXL	1:1000 (5% BSA in T-BST)	Cell Signalling
rabbit α-MCL1	1:1000 (5% BSA in T-BST	Cell Signalling

rabbit α-BIM	1:1000 (5% BSA in T-BST	Cell Signalling
Mouse α-Clathrin Heavy Chain	1:1000 (5% milk in T-BST)	BD Biosciences
Mouse α-βActin (HRP conjugated)	1:1000 1:250 (5% milk in T-BST)	Abcam
α-rabbit IgG-HRP	1:2,500 – 1:10,000 1:250 (5% milk in T-BST)	Amersham
α-mouse IgG-HRP	1:2,500 – 1:10,000 1:250 (5% milk in T-BST)	Amersham

Table 2-8: Western blotting primary and secondary antibodies.

2.1.9 FACS antibodies

Epitope	Company
Mouse CD45 PE-Cy7	BD Pharmingen
human CD45 APC	BD Pharmingen
human CD45 FITC	BD Pharmingen
human CD33 APC	R&D Systems
human CD33 BV 420	BD Pharmingen
human CD34 PE	BD Pharmingen
human CD34 APC-Cy7	BD Pharmingen
human CD14 APC	BD Pharmingen
human CD11b BV 420	BD Pharmingen

Table 2-9: Flow cytometry antibodies.

2.1.10 Cell culture media

Cells	Medium	Supplemented
Kasumi-1	RPMI 1640	10% FCS
SKNO-1	RPMI 1640	15% FCS, 5 ng/ml GM-CSF
MSCs	DMEM	20% FCS 1% L-Glutamine 8 ng/ml FGF-1 1% Penicillin/Streptomycin
Patient t(8;21) primary , t(8;21) PDX	SFEM	20% FCS 1 mM L-Glutamine 1X myeloid expansion 10 ng/ml IL3 20 ng/ml FLT3-L 1% Penicillin/Streptomycin

Table 2-10: Cell culture full media.

2.1.11 Cell Lines

Cell line	Origin	Cytogenetics	Identifier
Kasumi-1	Relapsed childhood (7 years) AML	t(8;21)(q22;q22) RUNX1/RUNX1T1	DSMZ RRID: CVCL_0589 Cat#ACC 220
SKNO-1	Relapsed young adult (22 years) AML	t(8;21)(q22;q22) RUNX1/RUNX1T1	DSMZ RRID: CVCL_2196 Cat#ACC 690

Table 2-11: Cell clines origins and genetic features.

2.1.12 Primary and PDX samples

Cells	Origin	Cytogenetics
LK19	6 year old – male	45,X,-Y,t(8;21)(q22;q22)[10]; No FISH; FLT3 and NPM1 wild type
LK111	16 year old – male	46,XY,t(8;21;8)(p21;q22;q22)[8]/47,idem,+4[4]; FISH: RUNX1-RUNX1T1 fusion positive[99/100]; cKIT c.2446G>T, p.Asp816Tyr (D816V) mutation detected.
PDX1 (RL048)/ NSG mice	72 year old - Relapse	t(8;21)(q22;q22) Homozygous TET2 mutation c.4179delA:p.T1393fs Heterozygous KIT mutation exon17:c.2435A>T:p.D812V
PDX2 (CC209)/ MSTRG mice	Relapse	t(8;21)(q22;q22) Heterozygous ETV6 insertion: c.313_314insGG:p.R105fs Heterozygous GATA1 mutation: c.158C>A:p.A53D Heterozygous KIT deletion: c.1253_1255del:p.418_419del Heterozygous NOTCH mutation: c.4898G>A:p.R1633H Heterozygous NOTCH mutation: c.6980G>A:p.R2327Q Heterozygous WT1 insertion: exon6:c.420_421insGTGTGCGA:p.R141fs
MSCs	N.A	(Pal, Blair et al. 2016)

Table 2-12: Patient primary cells and patient derived xenograft cells (PDX).

2.2 Methods

2.2.1 Freezing and thawing cell lines

Cells were centrifuged at 350 g for 5 min, then the cell pellet was resuspended in chilled freezing media (10% DMSO + 90% FCS) at concentration between 0.5 x 10^7 - 1.0 x 10^7 cells/ml. Then up to 1 ml of the cell suspension was transferred into cryovials and frozen at -80˚C for 24 hours then moved to liquid nitrogen tank for prolonged storage.

Frozen cells were thawed quickly and tenfold diluted in pre-warmed media then centrifuged at 350 g for 5 min. The supernatant containing DMSO was removed and cell pellet was resuspended in fresh media to a final cell density 0.5 x 10^6 -1.0 x 10^6 cells/ml and transferred into an appropriate plate or flask.

2.2.2 Cell counting using dye exclusion method

Cells were counted using trypan blue which selectively stains the dead cells with dark blue colour. The negatively charged trypan blue molecules pass only through the membrane of damaged and dead cells while viable cells do not absorb the dye. Patient primary and PDX cells taken from spleen were counted using methylene blue to lyse the red blood cells.

For suspension cell lines, equal volumes from cell suspension and trypan blue were mixed, giving a dilution factor of 2. For adherent cell lines, after tryptic digest of the adherent monolayer cells and stopping the enzymatic activating of trypsin, appropriate dilution factor using fresh media applied (1:10 or 1:20) and then 1 volume of trypan blue added. Finally, 10 µl of the cell suspension/dye solution was loaded into one side of haemocytometer and the live/dead cells were counted under 10X microscope magnification.

The haemocytometer consists of two chambers, and each chamber has four squares. Each square is divided into 16 (4×4) smaller squares. Determination of the cells concentration in 1 ml using haemocytometer is made using the following equation;

$$C = n \times F \times D$$

Where D is the dilution factor and F is the chamber factor.

$$F = \frac{final\ volume}{counted\ volume} = \frac{1\ ml}{surface\ x\ depth\ of\ the\ champer} = \frac{1000\ ml}{1mm^2\ x\ 0.1\ mm} = 10{,}000$$

In the proliferation assays, cells were counted twice using two different aliquots of the cells suspension, and then the average of the two counts was applied to calculate cells density. If the difference between the two counts was more than 10%, a third independent aliquot of cell suspension was counted.

2.2.3 Routine cell line culture – suspension cells

Leukaemic cell lines Kasumi-1 and SKNO-1 were cultured at 0.5 x 10^6 - 1.5 x 10^6 cells/ml cell density. Cells were cultured in 25 cm^2 or 75 cm^2 flasks in a fully humidified incubator at 37^{o}C and 5% CO2. Cells were counted every 2 - 3 days and splitted 1:2 or 1:3. Cells were routinely checked for mycoplasma contamination. The authentication certificates for Kasumi-1 and SKNO-1 cells are provided in the supplementary tables (s-Table-1 & sTable-2).

2.2.4 Mesenchymal stem cells culture

Mesenchymal stem cells (MSCs) were cultured in 6-well plates in a fully humidified incubator at 37^{o}C and 5% CO_2. Cells were split when they reached 60% confluency. To split the cells, the medium was aspirated, and adherent cells were washed once with PBS, then an appropriate volume of 1X trypsin was added for 1 - 5 minutes. Following incubation with trypsin, a twofold volume of complete culture medium containing FCS was added to inhibit the enzymatic activity of trypsin. Finally, cells were counted and seeded at the desired density. MSCs were kept in culture for 5 - 7 passages only or until they showed differentiation or slow proliferation.

2.2.5 t(8;21) primary and PDX co-culture

AML t(8;21) patient primary and patient-derived xenograft (PDX) cells were cultured on 50% confluent MSCs feeder layer. Directly after harvesting PDX cells from the mice or thawing frozen vials, cells were washed twice with 5%FCS in PBS, then cell pellet was suspended in fully supplemented SFEM media and seeded on MSCs after removing the MSCs media. Depending on the viability of the cells, cells were seeded at densities ranging from $0.2 \times 10^6 – 0.5 \times 10^6$ cells/ml.

2.2.6 siRNA hybridisation

siRNAs were provided lyophilised as separate single strands. In order to rehydrate the oligonucleotides, the required volume of hybridisation buffer was added to each tube to make 200 µM final concentration. The tube was then vortexed and centrifuged for 1 min at maximum speed and stored at -80ºC.

In order to make the double-stranded siRNA, equal molar quantities of each strand were added into RNase free Eppendorf tube, vortexed and centrifuged for 1 minute at maximum speed. The tube was then placed at 95ºC in a pre-heated heat block for 5 minutes. Finally, the heat block was switched off allowing the hybridisation mixture to gradually reach room temperature. Placing the single stands at 95ºC excludes any secondary structures and ensures complete annealing of the complementary strands.

The original siRNA single strands were kept at -80ºC and working solutions at -20ºC.

The siRNA rehydration and hybridisation were performed in a sterile environment using RNase free equipment.

Hybridisation buffer	
HEPES	25 mM
NaCl	100 mM
pH	7.5

Table 2-13: Hybridisation buffer recipe.

2.2.7 LNP/siRNA formulation – Hannover (Germany)

Dr. Nidhi Jyostana performed the packaging of siRNA into the Dlin-MC3-DMA lipid nanoparticle at Hannover Medical School in the laboratory of Prof. Michael Heuser's lab (Germany).

In brief, siRNA were hydrated in sodium acetate buffer (25 mM NaAc, pH = 4) and quantified using a NanoDrop A_{260} assay then equal molar amounts of siRNA were hybridised. Formulation of LNP/siRNA was performed in NanoAssemblr (Precision Nanosystems) where the lipid organic solution (Table 2-14) and the siRNA aqueous solution were pumped through a microfluidic mixer at a combined 12 ml/min flow rate. The final LNP/siRNA solution was then dialysed against PBS overnight at 4°C to remove ethanol and raise the LNPs pH to physiological condition values (pH = 7.4). Finally, the nanoparticles were sterile filtered by passing through a 0.2 µm cellulose acetate filter.

Composition	**Molar ratio** %
Dlin-MC3-DMA	50
DSPC	10
Cholesterol	38.5
PEG-DMG	1.5

Table 2-14: LNP/siRNA formulation composition. All components were dissolved in Ethanol.

The encapsulation efficiency of siRNA was determined by Quant-iT Ribogreen RNA assay (Life Technology). First, the LNP/siRNA solution was lysed by incubating with 1% Triton X-100 for 10 - 15 minutes at 37°C. Second, the Quant-iT Ribogreen assay was perfumed according to the manufacturer protocol, and the absorbance intensity was measured at 480 nm.

2.2.8 LNP/siRNA physical parameters measurements

The physical parameters of LNP/siRNA were measured using Malvern Zetasizer. Determination of the hydrodynamic diameter of the nanoparticles was performed after diluting the mixture 1:100 in PBS. The charge of the particles was quantified after applying 1:1000 dilution in deionised water.

2.2.9 LNP/siRNA particles labelling

In order to label the nanoparticles with ligands, DSPE-PEG-N3 was added to the lipid mixture at 0.3% molar ratio. After LNP/siRNA formation, free azide groups were supposed to be covering the surface of the particles (LNP/siRNA)N3. These azide groups were utilised in a click chemistry reaction.

A Cyanine7.5 derived dye (SulfoCyanine7.5 alkyne) was chosen for fluorescence imaging *in vivo*. The dye carries an alkyne group that can react with the free azide molecules in the presence of a catalyst such as copper. Decorating the LNPs with SulfoCyanine7.5 was achieved by click chemistry reaction. The table below (Table 4-2) shows the composition of the reaction. In brief, copper was dissolved in 55% DMSO/water solution at 500 mM concentration, and Ascorbic acid stock solution was prepared at 500 mM. To start the reaction, 10 µl of the copper was added to 10 µl of ascorbic acid in 1.5 ml Eppendorf tube and heated for 20 minutes at 40°C in a heat block, then 890 µl of (LNP/siRNA)N3 and 100 µl of SulfoCyanine7.5 alkyne were added. Finally, the heat block temperature was adjusted to 25°C and the reaction was kept overnight. After completion of the reaction, the nanoparticle solution was purified by dialysed against PBS for 10 - 12 hours at 4°C. The ascorbic acid and SulfoCyanine7.5 solutions, as well as the click chemistry reaction, are photosensitive, so all procedures were carried in the dark and tubes were warped with aluminium foil.

Composition/reagent	Final concentration
(LNP/siRNA)N3	50 - 300 µM
SulfoCyanine7.5 alkyne	100 µM
DMSO	55% vol
$CuCl_2$	0.5 mM
Ascorbic Acid	0.5 mM

Table 2-15: Click reaction composition.

2.2.10 Lipid quantification in the LNP/siRNA

The total lipid concentration in the LNP/siRNA mixture was determined indirectly using a calorimetric measurement of the phospholipid (DSPC) which makes 10% of total LNPs mixture. The amount of DSPC was measured by recording the absorbance of the complex formed between ammonium ferrothiocyanate [$(NH4)Fe(SCN)_4$] and the phosphorus in DSPC.

In brief, 100 mM and 400 mM of ferric chloride hexahydrate $FeCl_3.6H_2O$ and ammonium thiocyanate NH4SCN solutions were prepared in deionised water, respectively. Then 0.5 M ammonium ferrothiocyanate [$(NH4)Fe(SCN)_4$] solution was generated by mixing the ferric chloride and ammonium thiocyanate at 1:1 volume ratio. A serial dilution (0 - 50 µM) of DSPC lipid was prepared in ethanol, and the LNPs mixture was diluted 1:10 with ethanol. In a glass test tube, 500 µl of the lipid/ethanol solution was combined with 500 µl of ammonium ferrothiocyanate and vortexed for few second then 2 ml of chloroform was added to the mixture. Ammonium ferrothiocyanate is not soluble in organic solvents, but its complex with phospholipids is soluble in chloroform. The deep red-coloured chloroform layer was then removed using a glass Pasteur pipette, and 100 µl was transferred into a 96-well plate and absorbance was recorded at 488 nm in microplate reader.

The recorded absorbances were plotted against the corresponding DSPC concentrations in µM. Absorbances of three independent dilutions of 250 µg/ml LNP/siMM-mod stock solutions were recorded and the final DSPC concentration was then calculated from the linear regression plot.

2.2.11 Electroporation

One day before electroporation, cells were supplemented with 1:3 volume of fresh media. On the day of electroporation, cells were counted and desired cell number was taken. Cells were centrifuged at 300 g for 5 minutes then cell pellet was resuspended in fresh media at 1 x 10^7 – 1 x 10^8 cells/ml density. Next, 100 - 700 µl of cell suspension was moved into 4 mm gap-width cuvettes followed by addition of siRNA solution. After 10 - 15 minutes of performing electroporation, cells were transferred into plates or flasks, and the cells density was adjusted to 0.5 x 10^6 cells/ml in the appropriate media then placed onto fully humidified incubator at 37^{o}C and 5% CO_2.

Cell lines were electroporated using different voltages to obtain the optimal transfection rate. The electroporation parameters were 330 V (for Kasumi-1) or 350 V (for SKNO-1) delivered with a single square wave pulse during 10 ms. Primary t(8;21) cells were electroporated three times with three pulses of 80 V during 5 ms each in 1 mm gap electroporation cuvette.

In the serial electroporation experiments, cells were electroporated every three days following the same procedures as mentioned earlier.

2.2.12 LNP/siRNA treatment of cell lines

siRNA transfection of cell lines using lipid nanoparticles was performed at 1 x 10^6 cells/ml density. The desired volume of LNP/siRNA was added to the cell suspension and mixed well. After 24 hours of treatment, cells were washed three times with PBS and resuspended in fresh media at 0.5 x 10^6 cells/ml density. Only one single treatment of LNP/siRNA was applied. In the proliferation assays, cells were counted every 2 - 3 days and the density was readjusted to 0.5 x 10^6 cells/ml.

2.2.13 LNP/siRNA treatment of t(8;21) primary and PDX cells

t(8;21) primary and PDX cells were treated with LNP/siRNA in co-culture system in 96- or 48-well plates. At first, leukaemic cells were added on top of MSCs feeders at 1 x 10^6 cells/ml density. After 24 hours, the LNP/siRNA solution was added to a final concentration of 4 µg/ml. In order to maintain the viability of leukaemic cells and due to the limited number of primary and PDX cells, there was no further washing with PBS to remove the access amount of LNP/siRNA. After 24 h of treatment, leukaemic cells were moved onto a new 50% confluent MSCs and seeded at 0.2 x 10^6 cells/ml density.

2.2.14 Cell proliferation analysis

In the proliferation assay, cells were counted every 2 - 3 days and the desired cell number was taken after adjusting the cell density to 0.5 x 10^6 cells/ml. The following equation was used to calculate the corrected cell number:

$$N(i2)cor = \mathrm{N(i2)X}\ \frac{N(i1)}{N(cont)}$$

Where: N(i2)cor = corrected cell number at time point i2

N(i2) = determined cell number at time point i2

N(i1) = determined cell number at time point i1

N(cont) = cell number of the taken cells for the next time point

The previous equation was utilised to calculate the doubling time. The Ln(Ni2)cor values were plotted against the corresponding time points to generate a linear regression plot. The doubling time was then calculated from the linear regression equation using the following formula:

$$t_D = \frac{Ln(2)}{\mu}$$

Where, t_D: doubling time in days.

µ: slope of the linear regression line

2.2.15 Cellular senescence staining

The induction of cellular senescence was assessed using X-Gal staining at pH = 6.0 to detect the β-Galactosidase presence in the lysosome. Cellular senescence β-galactosidase staining kit from Sell Signalling was used after slight modifications in the kit protocol. In brief, 0.1 x 10^6 - 0.5 x 10^6 cells were harvested and washed once with PBS in 1.5 ml Eppendorf tube. Cells were fixed with 1X fixation solution for 15 minutes at room temperature then washed three times with PBS. The staining solution was prepared according to the manufacturers protocol and pH was precisely adjusted to 6.0 at 37°C. Finally, cell pellet was resuspended in 500 µl of staining solution and transferred onto a 24-well plate. The plate was tightly sealed with parafilm and placed at 37°C incubator (without CO_2) overnight at 37° C.

2.2.16 Cell cycle analysis

Cell cycle analysis was performed in flow cytometry after staining DNA with either propidium iodide (PI) or Hoechst-33342.

Cells have different DNA content at each phase of the cell cycle. SKNO-1 and Kasumi-1 cell lines are diploid. This means that cells in the G0/G1 phase have 2n DNA content and cells in the tetraploid phase G2/M have 4n DNA content. Cells that are in the S phase occupy the area between G0/G1 and G2/M. Quantification of each phase was performed after eliminating the doublets and plotting the histogram between the single cell events and the area occupied by each population. The apoptotic cells in subG1 phase occupy the areas before the G0/G1 peak. The following histogram in Fig 2-1A represents the corresponding DNA content for each cell cycle phase. The gating strategy for cell cycle profiling and quantification of the population in each phase was performed according to the representative scheme Fig 2-1B.

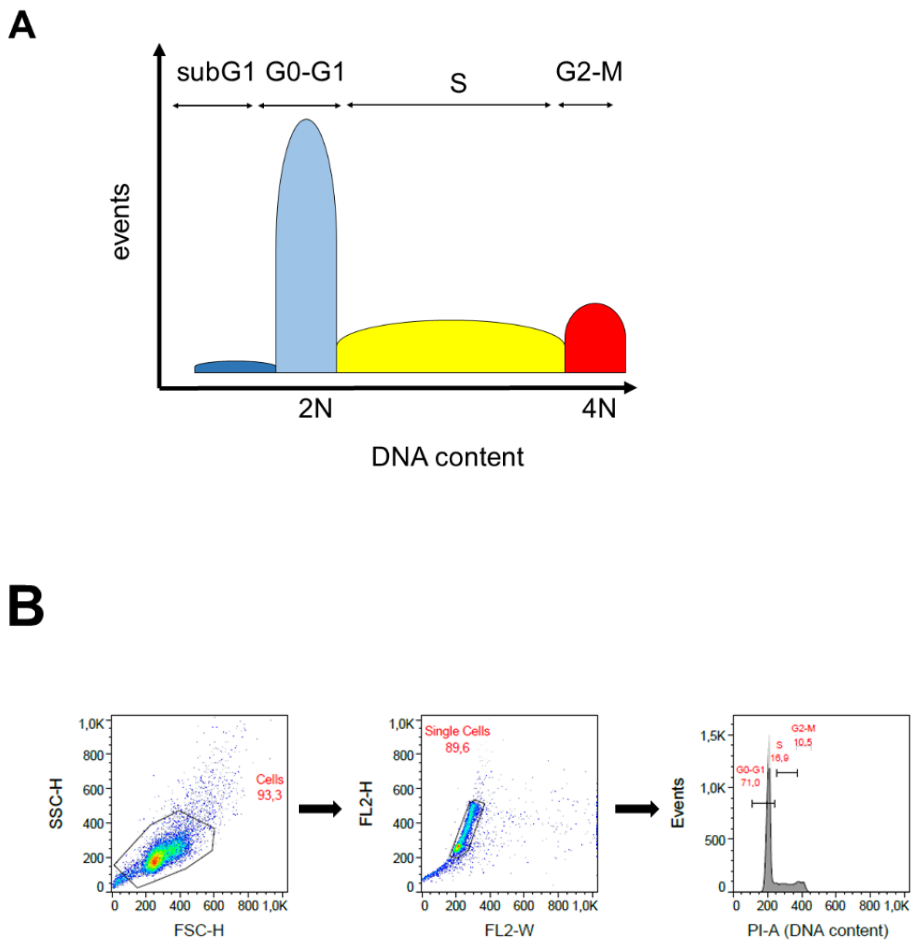

Fig 2-1. Cell Cycle analysis. (A) Schematic illustration of cell cycle profile. (B) The gating strategy in Kasumi-1 and SKNO-1 cell lines.

PI staining buffer	**Citrate buffer**	**Hoechst -33342 staining buffer**
Propidium iodide 20 µg/ml	Sucrose 250 mM	Hoechst 33258 2 µg/ml
NP40 0.5%	Sodium citrate 40 mM	NaCl 150 mM
EDTA 0.5 mM		KCl 30 mM
PBS pH= 7.2		Na_2HPO_4 10 mM pH= 7.0

Table 2-16: Cell cycle buffers recipes.

PI cell cycle stain

In brief, 0.2 x 10^6 - 0.5 x 10^6 cells were taken for cell cycle staining. At first, cells were washed once with PBS and resuspended in 200 µl of cold citrate buffer after addition of 1 ng/ml of RNase A. Second, cells were incubated for 5 minutes at 4°C then 800 µl of PI staining solution was added. Stained cells were incubated with the stain for 10 minutes in the dark and then taken for analysis by flow cytometry.

Hoechst -33342 cell cycle stain

Hoechst-33342 fluorescent stain was used to measure the cell cycle when the cells were expressing GFP, such as Kasumi-1 p.SLIEW and SKNO-1 p.SLIEW. That is because GFP fluorescence overlaps with PI excitation wavelength. Similarly, in the case of LNP/siRNA treatment, the Dil dye fluorescence overlaps with PI excitation.

In brief, 0.2 x 10^6 - 0.5 x 10^6 cells were harvested and washed once with PBS then 500 µl of Hoechst stain was added. Stained cells were kept in the dark until flow cytometry analysis. Hoechst staining was performed on live cells without prior fixation.

2.2.17 RNA extraction using RNeasy Kit

Cells were harvested and washed once with PBS then RNA extraction was carried out according to the manufacturer protocol. In brief, 0.5 x 10^6 - 5 x 10^6 cells were lysed with 350 µl (600 µl for cell number > 5 x 10^6 cells) RLT lysis buffer. Cell lysate was transferred into a QIAshredder column and centrifuged for 1 minute at maximum speed. An equal volume of 70% ethanol was added then the total volume was transferred into RNeasy spin column and centrifuged for 30 seconds at 8000 g. The flow-through containing protein was transferred into 2 ml Eppendorf tube and 1 ml of chilled acetone was added. Protein samples were stored at -20°C for at least 24 hours and protein extraction was processed as described under 2.2.22.

The RNeasy column was then moved to a new tube and membrane washed once with 700 µl RW1 buffer (8000 g for 30 seconds). RNA was precipitated by two

washing steps of 500 µl of RPE buffer (8000 g for 30 seconds then 8000 g for 2 minutes). The column was moved into a new tube and the membrane dried out by centrifugation for 1 minute at full speed. Finally, the column was moved into nuclease free collection Eppendorf tube and RNA was eluted (8000 g for 30 second) in 30 - 50 µl nuclease free water. RNA quantity and purity were measured by Nanodrop.

2.2.18 RNA extraction using RNeasy Micro Kit

RNeasy micro kit was used to isolate RNA from samples containing less than 0.5 x 10^6 cells. In brief, cells were washed once with PBS and cell pellet was lysed with 350 µl of RLT Plus buffer, then the lysate was loaded onto a QIAshredder column. The homogenised lysate was generated in the same way as described previously in 2.2.17. Then, 350 µl of 70% ethanol was added and the total volume transferred into RNeasy micro-column following by centrifugation at 8000 g for 30 seconds. Flow-through containing protein was collected as described in 2.2.22.The RNeasy micro-column was washed with 700 µl of RW1 buffer (8000 g for 30 seconds), then RNA was precipitated by 500 µl of RPE buffer (8000 g for 30 seconds) followed by 500 µl of 80% ethanol (8000 g for 2 minutes). The membrane was dried out by centrifugation for 5 minutes at full speed. Finally, RNA was eluted in 12 - 14 µl of nuclease free water. The quantity and purity of RNA were determined by Nanodrop.

2.2.19 cDNA synthesis by reverse transcription

Revert Aid H Minus 1st strand cDNA kit (Thermo Fisher K1632) was used for cDNA synthesis. In brief, up to 1000 ng of RNA was diluted in 11 µl of nuclease free water and 1 µl of random hexamers was added. The mixture was then incubated at 70°C for 5 minutes to disrupt the RNA secondary structures, followed by rapid cooling to 4˚C and 8 µl of the master mix (Table 2-16) was added. The final 20 µl PCR reaction was then heated to 25°C for 10 minutes, followed by 42°C for 60 minutes. Finally,

the enzymes were denatured by heating for 10 minutes at 70°C and the cDNA was cooled down to 4°C after completion for the cDNA synthesis.

Composition/reagent	Volume (µl)
5X reaction buffer	4
dNTP mix (10 mM)	2
Riboblock RNase inhibitor	1
RevertAid H minus reverse transcriptase	1

Table 2-17: cDNA synthesises master mix composition.

2.2.20 mRNA real time quantification by RT-PCR

Real time quantitative reverse transcription polymerase chain reaction qRT-PCR was performed in 384-well plates using Applied Biosciences ABI Prism- 7900HT Sequence Detection System or Viia7 system. Samples were measured in triplicates where in each well 2 µl of diluted cDNA was added to 8 µl of PCR master mix (Table 2-17). The 384-well plate was then sealed with adhesive cover and spun to collect the PCR mixture in the bottom of the wells. The PCR thermal cycles consisted of heating for 2 minutes at 50°C followed by 10 minutes at 95°C to denature the cDNA, inactivate the Uracil-DNA Glycosylate (UDG) and activate the polymerase. The extension step was carried out for 15 seconds at 60°C. The amplification continued for 40 cycles consisted of 95°C for 15 seconds and at 60°C for 1 minute. The final step was one cycle of 15 seconds at 95°C, 15 seconds at 60°C and finally 15 seconds at 95°C.

Composition/reagent	Volume (µl)
SybrGreen (2X) *	5
Primer mix (10 mM)	0.3
RNase free water	2.7

Table 2-18: Real Time RT PCR master mix composition. * SybrGreen (2X) is a mixture of SYBR Green 1 Dye, AmpliTaq Gold DNA Polymerase, dNTPs with dUTP, Passive Reference 1 (ROX), and buffer (unknown).

2.2.21 Gene expression analysis by qRT-PCR

Analysis of qRT PCR data was performed in SDS2.3 software and QuantStudio Real-Time PCR software. Starting from the cycle threshold (Ct) of each replicate, the mean of the Ct was calculated. The ΔCt for each gene was calculated by subtracting the Ct of the gene from the Ct of the housekeeping gene. Then the ΔCt values were used to calculate the ΔΔCt Ct for each sample after subtracting the ΔCt of the experimental sample from the ΔCt of the control. Given that in each cycle the DNA content was doubled, then the fold change is $2^{-\Delta\Delta Ct}$.

$$Ct_{\text{sample}} - Ct_{\text{housekeeping gene}} = -\Delta Ct_{\text{sample}}$$

$$-\Delta Ct_{\text{sample}} - (-\Delta Ct_{\text{control}}) = -\Delta\Delta Ct_{\text{sample}}$$

$2^{-(-\Delta\Delta Ct_{sample})}$ = fold change of gene expression (relative mRNA expression)

2.2.22 Protein isolation

Protein collected during RNA extraction (see 2.2.17) was precipitated after storing the sample at -20°C for 24 hours in order to increase the precipitation yield. The protein/acetone mixture was centrifugation at maximum speed for 20 minutes at 4°C then the supernatant was removed. Finally, protein pellet was dissolved in 50 - 150 µl of urea buffer and stored at -20°C.

RIPA buffer was used to isolate the protein directly from cell pellet. In brief, cells were collected and washed twice with PBS then cell pellet was lysed with 50 - 200 µl RIPA buffer (50 µl for 1 x 10^6 cells). Cells were lysed on ice for 30 minutes including vortexing for 30 seconds every 5 - 10 minutes. Cell lysate was then centrifuged at maximum speed for 15 minutes at 4°C to precipitate the debris. Finally, the supernatant containing the protein was moved into a new Eppendorf tube and protein samples were stored at -20°C.

Lysis buffer	Recipe
Urea buffer	9 M urea 4% CHAPS 1% DTT
RIPA	50 mM Tris 1 mM EDTA 1 mM EGTA 150 mM NaCl 0.5% Sodium deoxycholate 0.1% SDS 1% Triton X-100 5 mM NaF pH = 7.5

Table 2-19: Protein lysis buffers.

2.2.23 Protein quantification

Bradford assay (Bio-Rad) or BCA assay (Pierce, Thermo Fisher) were used to quantify the protein concentration. Bradford assay was used to quantify protein dissolved in urea buffer. That is because urea buffer contained 9 M urea, which is beyond the BCA assay compatibility (maximum 3 M urea). The presence of SDS in RIPA buffer was also not compatible with the Bradford assay.

BCA assay was performed according to the manufacturer protocol. In brief, BSA standard (0.1 - 2 mg/ml) was prepared and 10 µl of the standard solution was pipetted in triplicate into a 96-well plate. Protein samples were prepared with relevant dilutions (e.g. 1:10 dilution for 5 million cells) then 10 µl was pipetted in triplicates. Finally, 50 parts of reagent A were mixed with 1 part of reagent B and 190 µl from the working solution were transferred into a 96-well plate. After 2 hours incubation at 37°C, absorbance was recorded at 562 nm in microplate reader.

Bradford assay was performed following the manufacturer protocol. In brief, BSA standard (0.1 - 2 mg/ml) was prepared in urea buffer. Protein samples were diluted

in urea buffer with relevant dilution (1:10 for 2 million cells). Then 5 µl from the standard or the sample was pipetted in triplicate into a 96-well plate. Bradford dye was diluted from stock solution at 1:5 in water and 195 µl was added to each well. After 10 minutes incubation at room temperature, absorbance was measured at 570 nm in microplate reader.

Protein concentration was calculated after generating the BSA standard curve. Then the concentration of sample in mg/ml was calculated from the linear regression equation of the standard followed by applying the dilution factor.

2.2.24 Gel electrophoresis

High molecular weight proteins > 200 kDa were separated using Bis-Tris gel system. Low to medium molecular weight proteins were separated in SDS-PAGE system.

In general, SDS-PAGE (SDS polyacrylamide gel electrophoresis) separates proteins according to their molecular weight as the presence of SDS in the sample buffer and the gel itself uniforms the negative charges of the proteins. Thus, the movement of the proteins under an electric field is proportional to the log10 of the protein molecular weight. When the protein sample was prepared in RIPA buffer, the disulphide bonds in the protein was reduced by addition of 2-mercaptoethanol in the sampling buffer (5%) and boiling at 95°C for 10 minutes before loading the samples onto the gel. On the other hand, if the protein sample was prepared in urea buffer, the boiling step was skipped.

SDS-polyacrylamide gel consists of two layers; a top layer (stacking) which is 4% polyacrylamide, and a resolving (separating) layer that ranges between 7 - 20% polyacrylamide. The gel mixture was prepared by adding 25% v/v of 4X gel buffer to deionised water followed by addition of to 40% acrylamide-bis-acrylamide (1:29) or 30% acrylamide-bis-acrylamide (1:37.5). The mixture was then homogenised by mixing followed by addition of 0.1% w/v ammonium persulphate (APS) and 0.01% w/v TEMED. Finally, the gel mixture was poured into 1mm or 1.5 mm casting chamber followed by few hundred microliters of 70% ethanol to degas the gel. Ones the separating gel was set (about 15 minutes), ethanol was removed and the stacking gel mixture was poured on the top of the separating gel. Finally, the desired

compatible comb was added. After 15 minutes, the gel was ready to use or to storage at 4°C up to two weeks.

Gels were placed in the electrophorese tanks and filled with electrophoresis buffer. Before loading the samples, wells were cleaned using a fine syringe needle. Protein samples and ladder were loaded onto the wells and electrophoresis started at 50 V until the sample buffer dye passed into the separating gel, then the voltage was increased to 100 - 150 V to resolve the proteins.

In the standard SDS-PAGE, proteins were already denatured in the sampling buffer pH = 7 - 7.4 which contains detergents and 2-mercaptoethanol as a reducing agent, the basic pH (pH = 8.8) facilitates protein alkylation, de-amination and re-oxidisation of the reduced cysteines which were occurred during the electrophoresis. Thus, proteins reform disulphide bonds in the stacking gel (pH = 6.8) as they move away from the reducing agents (2-mercaptoethanol) in the sample buffer. However, in Bis-Tris polyacrylamide gel, the re-oxidation of cysteine is prevented in the weak acidic gel pH = 6.8 as the cysteine will be completely protonated pKa = 8.18. Moreover, the presence of $NaHSO_3$ as a reducing agent in the electrophoresis buffer maintains the reducing integrity in the whole gel. Bis-Tris and MOPS electrophoresis system was used to resolve only the high molecular weight proteins.

The following table includes the two types of polyacrylamide gels and electrophoresis buffers used.

	SDS-PAGE	**Bis-Tris**
% polyacrylamide	8 – 10	4 – 8
pH	8.8	6.8
Electrophoresis buffer	Tris-Glycine	MOPS
% SDS	0.1	0
kDa of resolved protein	10 – 160	50 – 450
U(V)/ t(hour)	100 V / 1 hour	25 V / 10 – 16 hours

Table 2-20: Gel electrophoresis conditions.

2.2.25 Immunoblotting

Immunoblotting followed the gel electrophoresis to detect specific proteins using the relevant blotting system and antibodies. In brief, gel was removed from the glass plates and a methanol-activated PVDF membrane (0.4 µm) was placed next to the gel and the blotting sandwich was assembled. Blotting was performed at 4°C to prevent heating the buffer. Two different blotting systems were used depending on the gel type as shown in the following table.

	SDS-PAGE	**Bis-Tris**
Blotting buffer	Tris-Glycine	CAPS
% Methanol	10	15
pH	6.8	11
U(V)/ t(hour)	100 V / 1 hour	25 V/ 16 hours or 50 V/ 4 hours

Table 2-21: Protein transfer conditions.

Ponceau-S red staining was used to assess the loading and blotting efficiency. The stain also helps to denature the proteins in the membrane and increases binding affinity of the antibodies. Membrane was then blocked with 10% milk or 5% BSA for 30 minutes followed by overnight incubation with the relevant primary antibody at 4°C. Membrane was washed several times (10 minutes each) with T-BST to remove the unbound and weakly bound primary antibody then incubated with the secondary antibody for 1 hour at room temperature. Then membrane was washed serval times for 10 minutes each with T-BST followed by addition of ECL solutions and detecting the chemiluminescence. The chemiluminescence signal was either recorded by automated Bio-Rad system or captured on X-Ray film in a darkroom.

Membrane stripping was performed for sequential detection of proteins. In brief, membrane was washed once with T-BST followed by three washes with mild stripping buffer for 10 minutes each. After 30 minutes of stripping, membrane was washed twice with PBS for 10 minutes followed by blocking with milk or BSA and incubation with new primary antibody. The following table includes the buffers recipes.

Buffer	Component
4X stacking buffer	0.5 M Tris 0.4% SDS pH = 6.8
4X separating buffer	1.5 M Tris 0.4% SDS pH = 8.8
10X Tris-Glycine	250 mM Tris, 1.92 M Glycine
SDS-PAGE electrophoresis buffer	1X Tris-Glycine 0.1% SDS
SDS-PAGE blotting buffer	1X Tris-Glycine 10% methanol
10X TBS	100 mM Tris.Cl 1.5 M NaCl pH = 8
Ponceau-S red staining	0.1% Ponceau-S red 5% acetic acid
6X SDS-PAGE loading buffer	50% 4X stacking buffer 0.1% bromophenol blue 36% SDS 30% Glycerol 15% 2-mercaptoethanol
20X MOPS electrophoresis buffer	250 mM MOPS 250 mM Tris 5 mM EDTA pH = 11
Bis-Tris electrophoresis buffer	1X MOPS 5 mM $NaHSO_3$ 0.5% SDS
10X CAPS	50 mM CAPS pH = 11

2X Bis-Tris gel sampling buffer	25% 4X stacking buffer 25% 1.25 M Bis-Tris buffer 0.1% bromophenol blue 0.5% 1 M NaHSPO3 35% Glycerol
Mild stripping buffer	200 mM Glycine 10% Tween-20 1% SDS pH = 2.2

Table 2-22: Gel electrophoresis conditions.

2.2.26 Colony formation assay

Colony formation assay (CFA) was performed using methylcellulose semi-solid media. The media was prepared by dissolving 0.56 g of methylcellulose in 5 ml PBS followed by autoclaving. Under sterile conditions, 85 ml of RPMI and 10 ml of FCS was added to the methylcellulose and stirred overnight at 4°C. The media was then filtered through a 0.2 µm syringe filter and stored at 4°C. In the case of SKNO-1 cell lines, GM-CSF was added to the methylcellulose media at 5 ng/ml concentration.

In order to perform the routine CFA, cells were centrifuged at 300 x g for 5 minutes then resuspended in fresh media at 0.5 x 10^6 cells/ml in fresh media. 25 µl of cell suspension was then added to 2.5 ml of the methylcellulose media and pipetted gently without air bubbles. Into a 24-well plate, 0.5 ml of the suspension was added to three wells and incubated at 37°C and 5% CO2 for approximately one week, or until the formation of colonies. Colonies number was determined by counting under microscope using 4X magnification, and the selection criteria were that each colony > 25 cells.

For the colony replating experiments, colonies were collected into a 50 ml falcon tube and washed twice with PBS. The harvested cells were then resuspended in fresh media at 0.5 x 10^6 cells/ml density and plated following the previously mentioned procedures.

2.2.27 Determination of cell viability

To administer the drug dose, cells were collected and centrifuged at 300 x g for 5 minutes then resuspended in fresh media at 0.1 x 10^6 cells/ml. The cell suspension was then transferred into a 96-well plate (90 µl per well). Stock solutions of the drugs were prepared in their appropriate solvent and stored in aliquots at -20°C. The working solutions were prepared at 10X concentrations prior to use by diluting the stock in the culture medium. For each condition, 10 µl of the working solution was added in triplicates. Finally, the cells were incubated at 37°C and 5% CO2 for 2 - 3 days.

Two different assays, luciferase and resazurin, were used to assess the drug response in cell lines.

Luciferase assay performed using (Promega Luciferase Assay System) in Kasumi-1 p.SLIEW and SKNO-1 p.SLIEW cells, which express the firefly luciferase gene. In order to perform the assay, the luciferin working solution was prepared according to the manufactural protocol by adding 10 ml of the luciferase assay buffer to one vial of lyophilised luciferin. To perform the assay, 20 µl of luciferin working solution was pipetted into 50 µl of cell suspension in a 96-well plate followed immediately by recording the bioluminescence in a microplate photometer.

The fluorescence-based assay, resazurin, was used in Kasumi-1 and SKNO-1 cells. Under oxidation-reduction conditions, resazurin can be reduced to resorufin and shift its weak fluorescence into highly red- florescence. Resazurin stock solution was prepared by dissolving 1 g resazurin in 50 ml PBS to make a100X stock solution. The stock solutions were aliquoted and stored at -20°C. Before performing the assay, the 100X stocks were thawed and diluted 1:10 in PBS, followed by addition of 10 µl of the 10X working solution to each well. Finally, the 96-well plate was covered with aluminium foil and incubated at 37°C and 5% CO2 for 4 hours. In a microplate photometer, the fluorescence of resorufin was recorded at 590 nm.

2.3 Animal work

2.3.1 Animal husbandry

Three immunodeficient mice strains were used in the *in vivo* studies as shown in Table 2-23. Mice weighing and checking were carried out at least twice per week. Mice were checked every day when they showed high leukaemic burden and during the dosing period. Mice general health condition assessment included mentoring of movement, anaemia, coat quality, piloerection, and the colour of the eyes, paws, feet and ears.

Mice were humanely culled by cervical dislocation when they reached the protocols endpoints as they were defined by the project license PPL60/4552 and Home Office regulations. The endpoints are:

1. Body weight loss of 20% or more, (30% if mouse is under treatment).
2. Body weight loss of 10% – 20% and maintained low for three days.
3. Tumour size is 1 cm in any dimension, (1.5 cm if mouse is under treatment).
4. Tumours are affecting the mice movement.
5. Any sign of sickness that is severely affecting the health of the mouse.

Abbreviation	Strain name	Source
NSG	*NOD.Cg-Prkdc^{scid}Il2rg^{tm1Wjl}/SzJ*	Jackson Laboratory
Rag2$^{-/-}$ γC$^{-/-}$ (RG)	*Rag2$^{-/-}$Il2rg$^{-/-}$129×Balb/c*	Jackson Laboratory
MISTRG	*Rag2$^{-/-}$Il2rg$^{-/-}$ Csf1$^{tm1.1(CSF1)Vlcg}$Csf2Il3$^{tm1.1(CSF2,IL3)Flv}$ Thpo$^{tm1.1(TPO)Flv}$Il2rg$^{tm1.1Flv}$*	Markus G. Manz

Table 2-23: Mice strain and genetic background.

2.3.2 Intrahepatic transplantation

Intrahepatic (IH) injection method was used to transplant Kasumi-1 p.SLIEW and t(8;21) PDX cells. The injection was performed using a fine flexible Hamilton needle under a sterile environment in a category II hood. Newborn mouse (2 - 4 days old) was held firmly by the end of the thumb and the index finger then the needle was inserted in the top of the chest under the skin. When the needle reached the end of the ribs, the needle was pushed toward the right side of the mouse chest in 45° wherein it simultaneously bent and reached the liver. Finally, 25 µl of cell suspension was released slowly and the needle was withdrawn smoothly. After injection, the mouse was placed back into the nest and monitored.

2.3.3 Intrafemoral transplantation

Primary and primograft t(8;21) AML patient cells were injected with intrafemoral (IF) route in NSG female mice. The injections were performed under a sterile environment in a category II hood. Mice were anaesthetised with 5% isoflurane then anaesthesia was marinated with 2 - 3% isoflurane. Before transplantation, mice were weighed and injected with 5 mg/kg Carprofen for analgesia. The injected leg was shaved and sterilised with skin disinfection spray. A hole was made in the injected femur by inserting 29G insulin needle in the kneecap and through the femur then the needle was removed and A new needle containing the sample was inserted and 20 µl of cell suspension was injected. After injection, the mouse was placed back into the cage and monitored for anaesthesia recovery.

2.3.4 Intraperitoneal dosing route

Intraperitoneal (IP) injection route was used to inject luciferin, Carprofen, and LNP/siRNA. The injection was performed using 29G insulin needle.

For injection of adult mice, the mouse was restrained firmly by tightly scruffing the skin back the body then the needle was inserted at 45° into the peritoneal area. The injection site of male mice is located in the upper peritoneal area in order to avoid the

testicles. The injection site of the females is located in the lower abdomen below the nipples.

For injection of pups (5 - 16 days), the mouse was held on its back and placed above the middle finger where the index and the middle fingers gripped the tail. The needle was inserted at 45° in the lower abdominal avoiding the stomach. The injection site was switched every time in order to avoid bruising.

2.3.5 Intravenous dosing route

Intravenous (IV) injection route was used to inject the LNP/siRNA. In brief, the mouse was restrained under category II hood. In order to reveal the vain, the tail was either massaged or placed in warm water. Finally, the tail was stretched straight tightly and the needle inserted at around 180° and the drug released steadily. Once the injection was completed, pressure was applied on the injection site for 30 seconds to prevent any bleeding, then the mouse was placed back in the cage and monitored.

2.3.6 Oral gavage dosing route

Oral gavage was used to dose mice with ABT-199 and its control vehicle (CV). The gavage was performed using a round-tipped gavage needle. The mouse was tightly scuffed and held in a vertical angle. Then the needle was inserted into the mouse mouth while pushing the head back, allowing the needle to go through the oesophagus into the stomach. When the needle stopped in the stomach, the volume was released slowly, and then the needle was smoothly removed to prevent any injuries.

ABT-199	CV
ABT-199 20 mg/ml Phosal 50 PG 60% PEG400 30% Ethanol 10%	Phosal 50 PG 60% PEG400 30% Ethanol 10%

Table 2-24: ABT-199 and control vehicle recipe for oral gave.

2.3.7 In vivo imaging

Bioluminescence imaging was performed using an *in vivo* imaging system (IVIS). In brief, the mouse was injected with 5 mg/kg luciferin by IP route. After 5 minutes, the mouse was anaesthetised with 5% isoflurane in anaesthesia induction box. Anaesthesia was then maintained with 2 - 3% isoflurane. The mouse was then placed on a 37°C heat mat inside the IVIS machine where the head was placed into a face mask to maintain the anaesthesia. Ten minutes after the luciferin injection, imaging was performed then the mouse was placed back in the cage and monitored for recovery.

2.3.8 Mice dissection and cells isolation

Leukaemic cells were collected from several sites such as tumours, spleen, bone marrow. The spleens and tumours were weighed first then homogenised, and cells passed through a cell strainer using PBS under sterile conditions. Leukaemic cells engrafted in the bone marrow were extracted from the femur, tibia, desk, and spine. In brief, bones were cleaned from muscles crushed in mortar and pestle and passed through a cell strainer using PBS under sterile conditions.

Harvested cells were washed once with PBS and counted using trypan blue and methylene blue to lyse the murine red blood cells. Viable cells were either cultured *ex vivo*, reinjected into mice or frozen at -80°C.

Chapter 3

Establishment of *in vitro RUNX1/ETO* knockdown utilising modified siRNA encapsulated into a lipid nanoparticle

3.1 Introduction

Successful *RUNX1/ETO* knockdown using unmodified siRNA has long been established in our group. The si*RUNX1/ETO* (siRE) specifically targets the fusion site of *RUNX1/ETO* transcript, and a mismatch control siRNA (siMM) has also been generated by swapping two nucleotides in the antisense strand. The group has also optimised electroporation protocols to deliver 100 - 500 nM siRNA sequentially. Using t(8;21) AML cell lines, a single electroporation of 200 nM siRE can reduce *RUNX1/ETO* expression by twofold after 48 hours, followed by a maximal reduction in the protein level after 72 hours. The disruption of RUNX1/ETO transcriptional network has been observed within 24 hours post electroporation. We have defined a set of early responding RUNX1/ETO direct target genes including *CD34* and *CEBPA.* Furthermore, we have shown that the clonogenic potential of leukaemic cell lines is also affected after a single transfection. However, transcriptional modulation of late responding RUNX1/ETO direct and indirect target genes such as *TERT* and *CCND2* requires sequential transfections with siRE. Moreover, serial administration of siRE is needed to resolutely reduce proliferation, cause G1 cell cycle arrest and induce senescence (Martinez, Drescher et al. 2004, Soria, Tussiwand et al. 2009, Ptasinska, Assi et al. 2012).

Therapeutic siRNAs are designed to exhibit maximal activity after parenteral administration (Cullis and Hope 2017). Chemical modifications of oligonucleotides are routinely used to improve the siRNA resistance to nucleases and produce favourable pharmacodynamics and pharmacokinetic profiles (Haley and Zamore 2004, Ameres, Martinez et al. 2007, Huang, Cheng et al. 2016). Several functional studies have been conducted by our group relying on achieving *RUNX1/ETO* depletion by siRE. Considering that the PhD project aims to exploit RUNX1/ETO knockdown therapeutic potential, I have introduced several chemical modifications to the siRNA. The chemically modified si*RUNX1/ETO* (siRE-mod) harbours modifications on the 2'-OH of the ribose and 3'-phosphodiester backbone.

Oligonucleotides administration by systemic route activates the innate immunity by the toll-like receptors (TLRs). Moreover, naked siRNA has very poor pharmacokinetics when administered intravenously. To diminish the siRNA immunogenicity and enhance the therapeutic index, many studies have developed

novel lipid nanoparticle formulations *(Semple, Akinc et al. 2010, Maier, Jayaraman et al. 2013)*. Based on previous reports of successful siRNA-mediated gene silencing *in vivo (Leung, Tam et al. 2014)*, we have chosen the Dlin-MC3-DMA lipid nanoparticle (LNP) to encapsulate the siRNA targeting RUNX1/ETO. We assessed the depletion of RUNX1/ETO by lipid nanoparticles encapsulating chemically modified si*RUNX1/ETO* (LNP/siRE-mod) in t(8;12) cell lines as well as in primary and patient derived xenograft (PDX) cells.

3.2 Aims

The aims of the project include:

1. To enhance the overall *RUNX1/ETO* knockdown by introducing chemical modifications, which stabilise the siRNA and reduce the off-target effect.
2. To encapsulate the modified siRNA into LNP and determine the physical parameters of the LNP/siRNA system.
3. To establish a robust depletion of *RUNX1/ETO* using LNP/siRNA in t(8;21) AML cell lines.
4. To investigate the efficacy of LNP/siRNA in t(8;21) primary and t(8;21) PDX cells in a co-culture system using MSCs as feeder cells.

3.3 Experimental design

3.3.1 Establishment of modified siRNA

The effect of single chemical modification on the siRNA activity was already known from the literature. In order to obtain an enhanced *RUNX1/ETO* knockdown, a combination of several modified nucleotides was introduced in the same time. These modifications were already established and validated by pharmaceutical companies such as Alnylam and IONIS (Davis, Zuckerman et al. 2010, Adams, Gonzalez-Duarte et al. 2018). The chemical modification were as follow,

a. The 2'-OH substituted with 2'-F at the first 4 nucleotides of the sense strand at the 5'-end.
b. The 2'-OH substituted with 2'-H at the last 5 nucleotides of the sense strands at the 3-'end. The same substitution but placed at the 3'-end of the antisense stand by having two deoxyribose thymidine moieties.
c. All the ribose of the pyrimidine nucleotides in the middle of the sense strand modified with 2'-OMe.
d. The phosphodiester backbone between the first and the second nucleotide at the 3'-end of each strand replaced with phosphorothioate 3'-PS.

Sequences of the unmodified si*RUNX1/ETO* (siRE), modified si*RUNX1/ETO* (siRE-mod), mismatch siRNA (siMM) and modified mismatch siRNA (siMM-mod) are shown in Table 3-1. The chemical structures of modified ribose units and phosphodiester backbone are shown in Fig 3-1.

siRNA	Sequences
siMM	5'-CCUCGAAUUCGUUCUGAGAAG-3' 3'-UUGGAGCUUAAGCAAGACUCU-5'
siMM-mod	5'-C$_F$C$_F$U$_F$C$_F$GAAU$_{OMe}$U$_{OMe}$CGU$_{OMe}$U$_{OMe}$C$_{OMe}$UGAGAdT$_{PS}$dT-3' 3'-dT$_{PS}$dTGGAGCUUAAGCAAGACUCU-5'
siRE	5'-CCUCGAAAUCGUACUGAGAAG-3' 3'-UUGGAGCUUUAGCAUGACUCU-5'

siRE-mod	5’-C$_F$C$_F$U$_F$C$_F$GAAAU$_{OMe}$C$_{OMe}$GU$_{OMe}$AC$_{OMe}$U$_{OMe}$G**d**A**d**G**d**A**d**T$_{PS}$**d**T-3’ 3’-**d**T$_{PS}$**d**TGGAGCUUUAGCAUGACUCU-5’

Table 3-1: siRNA sequence and the chemical modifications. The 2’-modified ribose with fluoro and methoxy are indicated as **F** and **OMe**, respectively. The 2’-deoxyribose was annotated as **d**. The **PS** refers to the phosphorothioate-modified backbone.

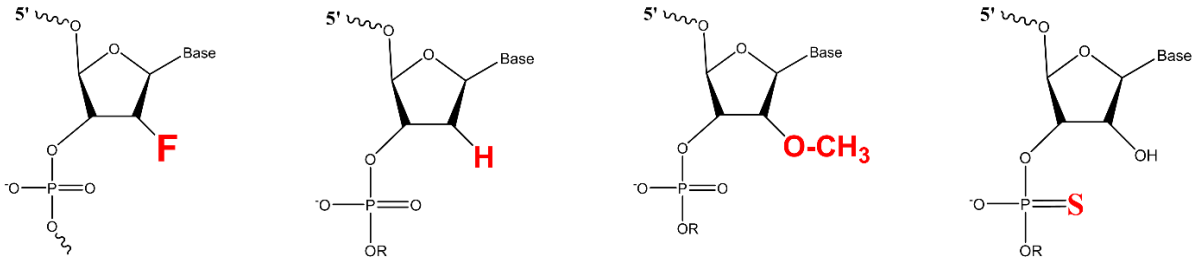

Fig 3-1: siRNA chemical modifications. From left to right, the 2’-hydroxyl of the sugar ribose was replaced with either fluoro, hydrogen or methoxy group. The 3’-phosphodiester was substituted with phosphorothioate.

3.3.2 siRNA modifications efficiency in vitro.

The efficiency of modified siRNA in depleting RUNX1/ETO was assessed in t(8;21) AML cell lines Kasumi-1 and SKNO-1. siRNAs were transfected by electroporation using two settings, either single or sequential electroporation.

Sequential electroporation of Kasumi-1 and SKNO-1 cell lines were performed every 3 days as described in 2.2.11. During the experiments, cells were collected for functional analysis including cell count (see 2.2.14), cell cycle profiling (2.2.16), colony formation assay (2.2.26), senescence-associated β-Galactosidase staining

(2.2.15), and assessment of RNA and protein expression (2.2.17 to 2.2.25) as shown in (Fig 3-2).

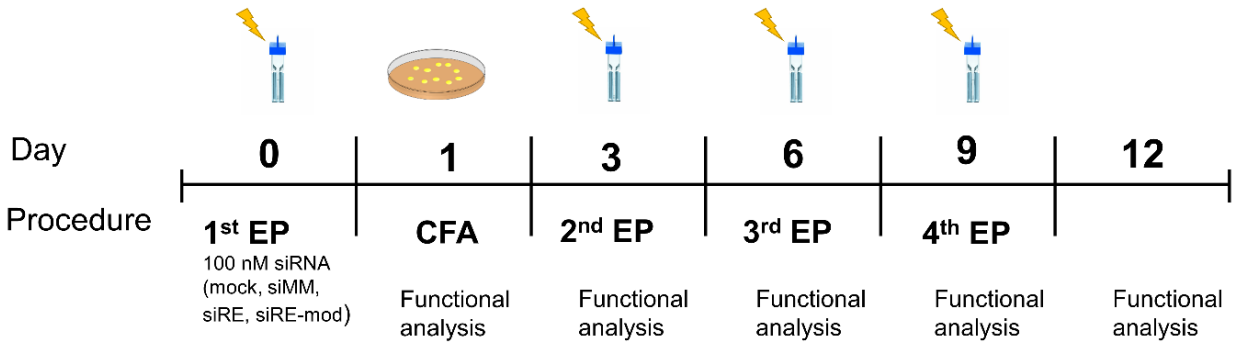

Fig 3-2: Schematic illustration of the serial electroporation experiments.

In order to determine the prolonged siRNA activity, a single electroporation with escalating concentrations of the siRNA was performed. Cells were collected on days 3 and 7, RNA extracted for qRT-PCR and cell lysate prepared and measured for Western blotting.

3.3.5 Treatment with LNP/siRNA in AML cell lines

The *RUNX1/ETO* knockdown efficiency of lipid nanoparticles LNP/siRNA *in vitro* was explored in Kasumi-1 and SKNO-1 cell lines. Treatment of cell lines using LNP/siRNA was performed at a cell density of 1 x 10^6 cells/ml as described in 2.2.12. At the end of each treatment period, cells were washed twice with PBS and resuspended in the relevant culture media at 0.5 x 10^6 cells/ml density. Cell count was performed every 2- 3 days throughout the experiments, and cell densities were maintained between 0.5 x 10^6 to 1 x 10^6 cells/ml. Cells were taken at several time points for functional analysis.

3.3.6 Primary and PDX treatment with LNP/siRNA

AML t(8;21) patient primary and t(8;21) PDX cells were co-cultured on MSCs feeder layer as described in 2.2.13. One day prior to treatment, primary cells were cultured on MSCs at a density of 1 x 10^6 cells/ml (approximately 50% confluence). Co-cultures were treated with 4 µg/ml of LNP/siRE-mod and LNP/siMM-mod for 24 hours, then AML primary cells were moved onto new MSCs feeders and kept at 0.2 x 10^6 – 0.5 x10^6 cells/ml density. Analysis of gene expression and protein level were performed after 3 and 6 days post treatment.

PDX cells were thawed and cultured overnight on matrigel. On the next day, PDX cells were counted and seeded on MSCs feeder at 1 x 10^6 cells/ml density. After 24 hours, 4 µg/ml LNP/siRNA was added to the co-cultures. Next day, PDX cells were moved onto new MSCs feeder and kept at 0.2 x 10^6 - 0.5 x 10^6 cells/ml density. Cells were taken after 3 and 6 days post treatment.

3.4 Results

3.4.1 Efficacy of chemically modified siRNA in vitro

3.4.1.1 RUNX1/ETO knockdown effect on proliferation

The efficacy of siRNA modification was tested in Kasumi-1 and SKNO-1 cell lines by assessing the proliferation after *RUNX1/ETO* knockdown. Previous work performed by our group has led to routine conditions for sequential electroporation by applying either 200 or 500 nM siRE for an effective *RUNX1/ETO* knockdown. In my experiments, I have used a reduced concentration of 100 nM siRNA in order to compare the potency of siRE-mod and siRE.

Serial electroporation with siRNAs targeting *RUNX1/ETO* led to reduced cell proliferation. The doubling time of Kasumi-1 and SKNO-1 increased by two-fold. Moreover, siRE-mod and siRE robustly inhibited proliferation in both cell lines when 100 nM siRNA was electroporated four times (Fig 3-3A, C). Notably, two sequential electroporations of siRE-mod were sufficient to significantly reduce proliferation for a prolonged period compared to siRE treated cells (Fig 3-3B, D).

3.4.1.2 RUNX1/ETO knockdown at mRNA level

The potency of modified siRE-mod was also assessed by observing its ability to induce robust changes at the mRNA level. *RUNX1/ETO* expression was measured after 48 hours of electroporation. In Kasumi-1 and SKNO-1 cell lines, *RUNX1/ETO* expression decreased by 60% in the siRE and siRE-mod treated cells in comparison to the control siMM treated cells (Fig 3-4A, B).

The reduction of *RUNX1/ETO* mRNA was consistent in the siRE or siRE-mod transfected cells. However, *CEBPA* expression, a direct target gene of RUNX1/ETO, greatly increased in the siRE-mod transfected cells in comparison with the siRE. The enhanced upregulation in *CEBPA* transcript was observed in both cell lines (Fig 3-4C, D). Upon *RUNX1/ETO* knockdown in Kasumi-1, *CEBPA* mRNA increased by 2- and 2.5-fold when cells transfected with siRE and siRE-mod, respectively. The siRE-

mod did not provide significant upregulation of *CEBPA* in Kasumi-1. However, the difference in SKNO-1 cell line was statistically significant (p= 0.023).

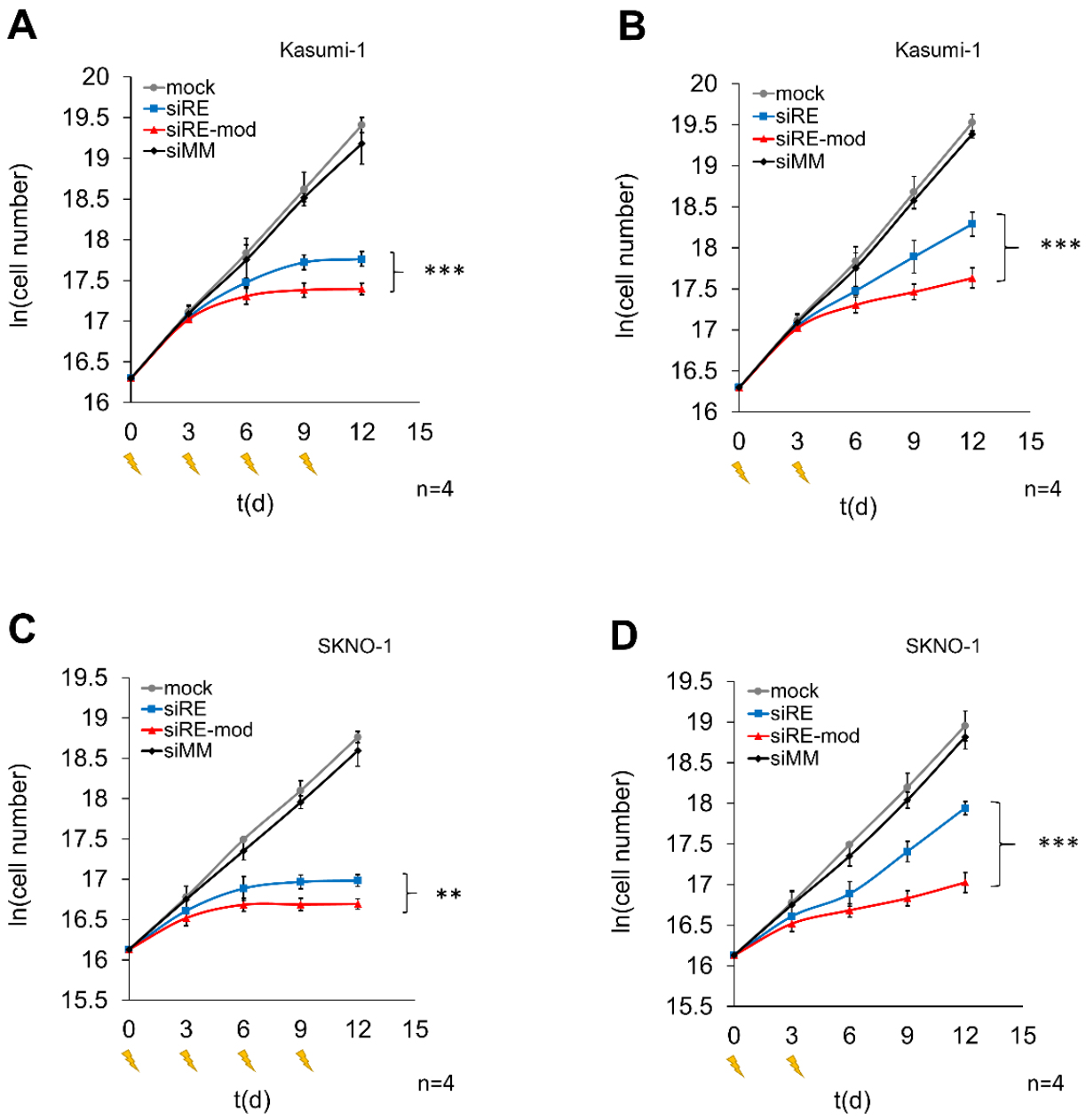

Fig 3-3: RNAi mediated *RUNX1/ETO* knockdown effect on proliferation. Cell lines were electroporated sequentially at 1 x 10^7 cells/ml density with 100 nM of siRE, siRE-mod or siMM and untreated mock control. The electroporation was performed either four times on days 0, 3, 6 and 9 (A & C), or twice on days 0 and 3 (B and D). Error bars represent the Standard Error of the Mean (SEM) of four independent experiment at each time point. For the last time point (day 12) **P*<0.05, ***P*<0.01, ****P*<0.001, two-tailed Student's *t*-test.

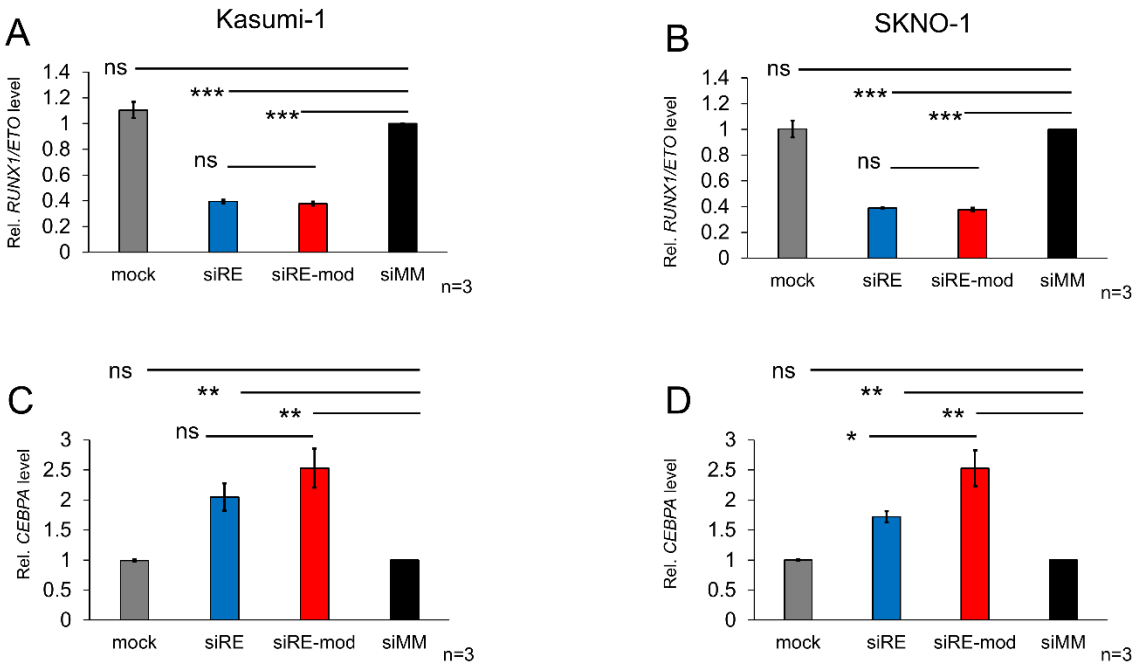

Fig 3-4: RNAi mediated knockdown of *RUNX1/ETO* in Kasumi-1 and SKNO-1. Cell lines were electroporated at 1 x 10^7 cells/ml density with 100 nM of siRE, siRE-mod, siMM or untreated mock control. After 48 hours of electroporation, *RUNX1/ETO* mRNA level (A and B) was measured against the siMM treated control and *GAPDH* served as a housekeeping gene. The expression level of *CEBPA* was measured after 48 hours of electroporation (C & D). Error bars represent SEM of three independent experiments, **P*<0.05, ***P*<0.01, ****P*<0.001, two-tailed Student's *t*-test.

The reduction of *RUNX1/ETO* mRNA was maintained during the course of four serial electroporations in both Kasumi-1 and SKNO-1 (Fig 3-5). Sequential electroporations with 100 nM were not sufficient to further reduce *RUNX1/ETO* mRNA level. It was evident, throughout the electroporation experiments, that there was a basal level of *RUNX1/ETO* transcript which could not be depleted by the siRNA.

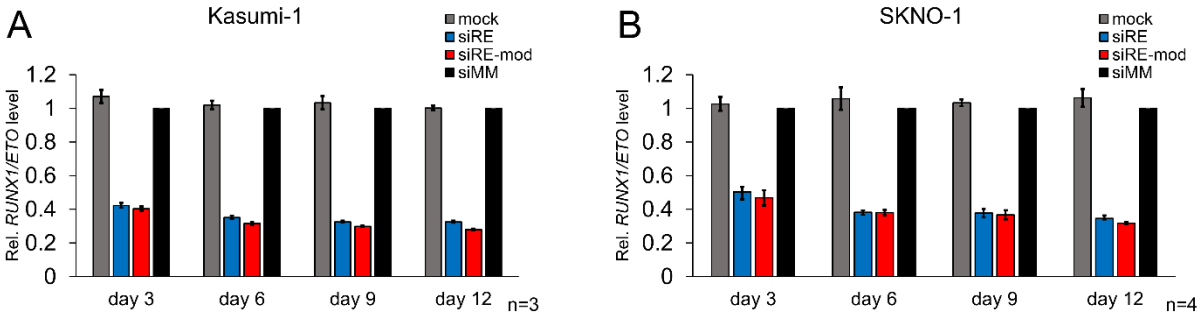

Fig 3-5: RNAi mediated knockdown of *RUNX1/ETO* in Kasumi-1 (A) and SKNO-1 (B). Cell lines were serially electroporated at1 x 10^7 cells/ml density on days 0, 3, 6, and 9 with 100 nM of siRE, siRE-mod, siMM or untreated mock control. RNA expression was measured against siMM treated cells and *GAPDH* served as a housekeeping gene. Error bars represent SEM of three and four independent experiments for Kasumi-1 and SKNO-1, respectively.

3.4.1.3 RUNX1/ETO knockdown at protein level

In order to confirm RUNX1/ETO knockdown on the protein level, samples were collected at several time points for Western blotting. To detect RUNX1/ETO and RUNX1 simultaneously an antibody recognises the N-terminus of RUNX1 protein was used.

The knockdown of RUNX1/ETO was stronger in siRE-mod treated cells in comparison with siRE (Fig 3-6). The siRE-mod was able to reduce RUNX1/ETO level more effectively throughout the serial electroporation experiments consistent in both Kasumi-1 and SKNO-1 cell lines.

In line with previous observations by our group, the robust depletion of RUNX1/ETO led to a reduction in RUNX1 level. The serial electroporation experiments showed that cells transfected with siRE-mod had an enhanced reduction in RUNX1 protein expression, especially in the SKNO-1 cell line (Fig 3-6). This finding indicated robust RUNX1/ETO knockdown in siRE-mod cells.

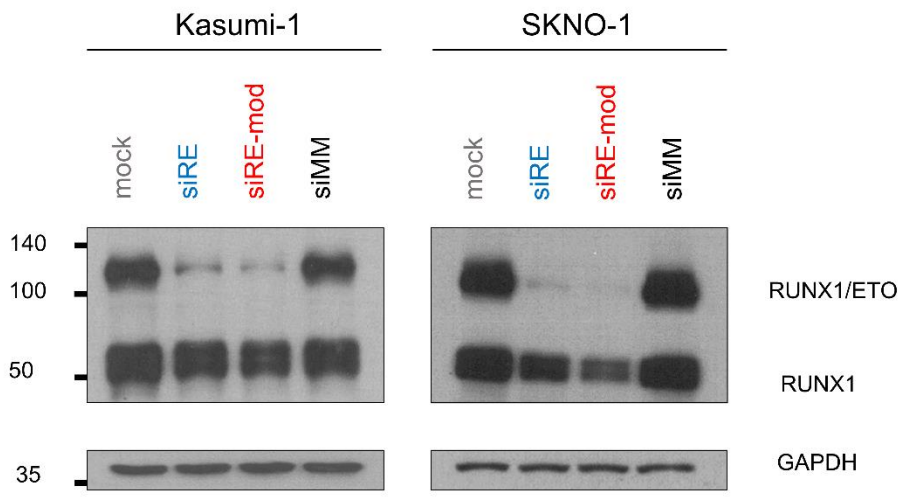

Fig 3-6: RUNX1/ETO protein level in Kasumi-1 (left) and SKNO-1 (right) on day 6. Cell lines were serially electroporated on days 0 and 3 with 100 nM of siRE, siRE-mod, siMM or untreated control. Cell lysates were collected on day 6. Membranes were blotted against α-RUNX1 antibody and α-GAPDH loading control. Marker size in kDa was presented on the left of the blots.

The serial electroporation experiments did not provide evidence that siRE-mod was substantially more potent than siRE in reducing *RUNX1/ETO* mRNA expression. Moreover, both siRE and siRE-mod robustly reduced RUNX1/ETO protein level after two sequential electroporations as shown in Fig 3-6. In order to confirm whether siRE-mode outperforms siRE, the effect of one single transfection was investigated.

Single electroporation showed that siRE-mod provided a stronger and prolonged reduction in RUNX1/ETO protein level in comparison with siRE transfected cells. When electroporating SKNO-1 cells once with a serial dilution of siRNAs, RUNX/ETO protein level remained low in the siRE-mod treated cells, while siRE treated cells recovered from the knockdown one week after transfection (Fig 3-7).

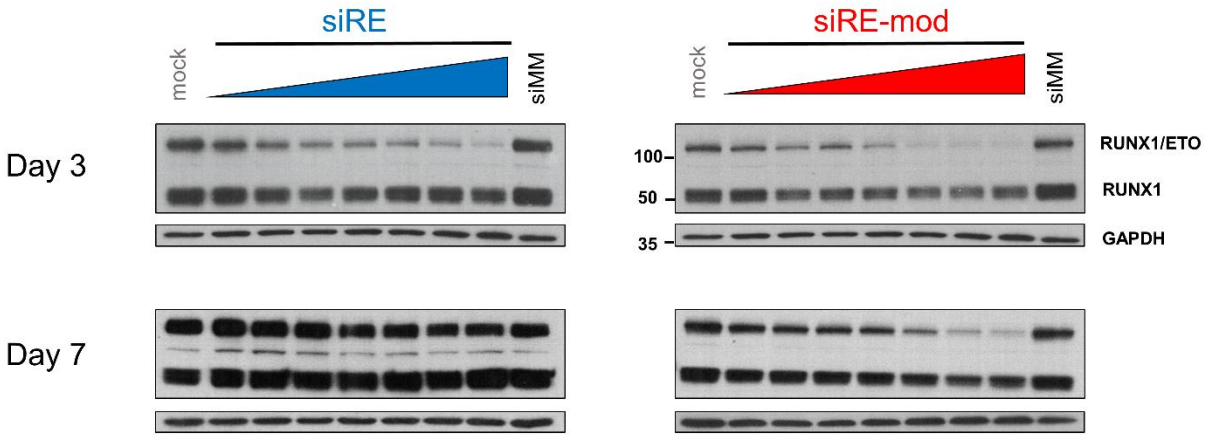

Fig 3-7: RUNX1/ETO protein level in SKNO-1 on days 3 and 7. Cells were electroporated ones with 1, 10, 20, 50, 100, 200, 500 nM of either siRE or siRE-mod, and with 500 nM of siMM or untreated mock control. Cell lysates were collected on days 3 and 7 for Western blotting analysis. Membranes were blotted against α-RUNX1 antibody and α-GAPDH loading control. Marker size in kDa was presented on the left of siRE-mod of the day 3 blot.

The serial electroporation experiments showed downregulation in RUNX1/ETO direct target genes. When Kasumi-1 cells were serially electroporated with 100 nM siRNA, RUNX1/ETO was virtually absent on day 9 (Fig 3-8). The knockdown led to a reduction in CCND2, a direct target gene of RUNX1/ETO, protein level. Moreover, Western blotting showed that RUNX1/ETO knockdown reduced RB1 phosphorylation at T-821 and the total RB1 protein level. These findings led us to investigate the cell cycle profile after RUNX1/ETO repression because RB1 phosphorylation status and CCND2 expression regulate the cell cycle (Bertoli, Skotheim et al. 2013, Indovina, Pentimalli et al. 2015, Thwaites, Cecchini et al. 2017).

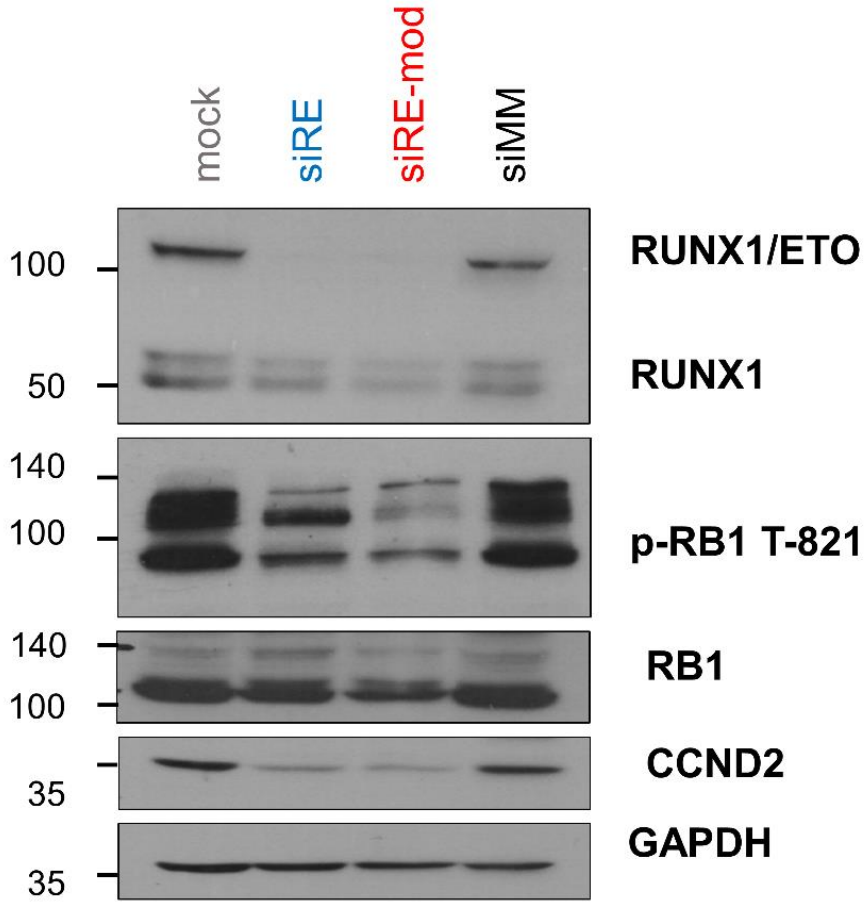

Fig 3-8: RUNX1/ETO knockdown in Kasumi-1 on day 9. Kasumi-1 cells were serially electroporated on days 0, 3 and 6 with 100 nM of siRE, siRE-mod, siMM or untreated mock control. Cell lysates were collected on day 9. Membranes were blotted against α-RUNX1, α-CCND2, α-RB1, α-p-RB1-T-821 and α-GAPDH loading control. Marker size in kDa was presented on the left of the blots.

3.4.1.4 RUNX1/ETO knockdown effects on the cell cycle

The depletion of RUNX1/ETO in Kasumi-1 and SKNO-1 did not only reduce proliferation, but it also led to G1 cell cycle arrest. Single transfection with siRNA did not lead to an apparent cell cycle arrest, although subtle changes in the cell cycle profile were detectable 24 hours after transfection. However, serial electroporation resulted in prolonged G1 cell cycle arrest upon RUNX1/ETO knockdown.

Observing the morphological changes in cells upon knockdown was consistent with the results of the cell cycle profiling. The knockdown of *RUNX1/ETO* reduced the cell diameter. These observations were confirmed in flow cytometry, which showed a significant reduction in the forward scatter of RUNX1/ETO knockdown cells (Fig 3-9A, B). After two serial electroporations on days 0 and 3, the side scatters on day 6 for the untreated cells and mismatch transfected Kasumi-1 cells were 270 and 268 K, respectively, while siRE and siRE-mod transfected cells had 191 and 182 K side scatter. The knockdown of *RUNX1/ETO* in SKNO-1 cells reduced the side scatters of the cells in a similar manner as shown in Fig (3-9B).

Moreover, *RUNX1/ETO* knockdown predominantly led to cell cycle arrest without any increase in cell death as shown through the absence of cell debris and apoptotic nuclei in Fig 3-9A. After serial electroporations, the sub-G1 population was equal in both RUNX1/ETO knockdown cells and the controls as shown in Fig (3-9A). For this reason, the sub-G1 population was neglected during cell cycle profiling.

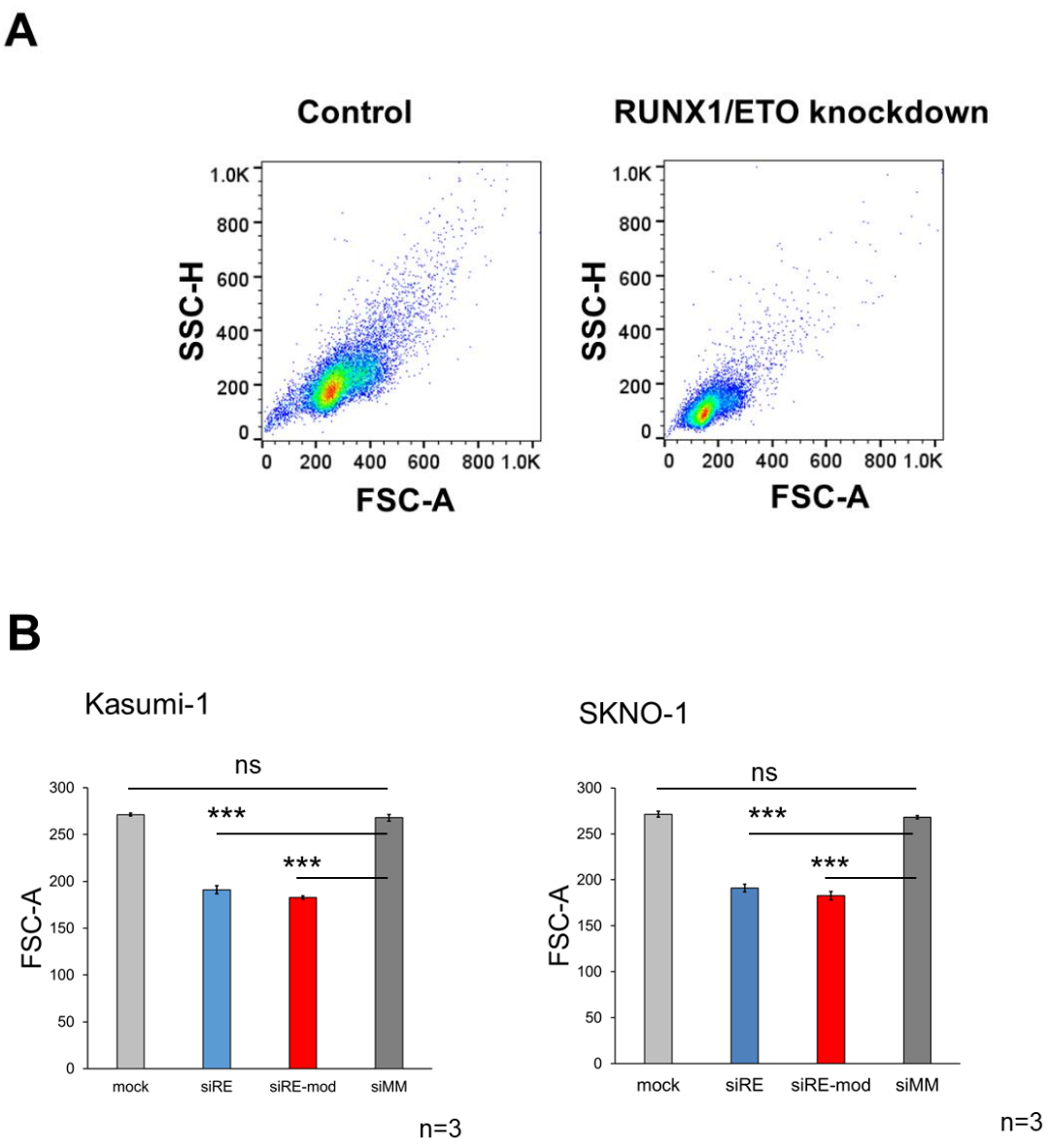

Fig 3-9: Forward and side scatter of *RUNX1/ETO* depleted cells. Cell lines were electroporated twice with 100 nM siRNA on days 0 and 3, followed by flow analysis on day 6. (A) Flow cytometry profile showing the forward and side scatters of Kasumi-1 cells on day 6 after transfection with siMM (control) and siRE-mod (*RUNX1/ETO* knockdown). (B) The geometric mean of the side scatter of Kasumi-1 (left) and SKNO-1 (right) on day 6. Error bars represent SEM of three independent experiments. **P*<0.05, ***P*<0.01, ****P*<0.001, two-tailed Student's *t*-test.

Propidium iodide (PI) staining showed that *RUNX1/ETO* knockdown by siRE and siRE-mod led to more than 50% reduction in the S phase of Kasumi-1 (Fig 3-10A) and 25% reduction in the S phase of SKNO-1 (Fig 3-10B). The siRE-mod did not induce any stronger cell cycle arrest compared to the siRE on day 6 when siRNAs were serially electroporated on days 0 and 3. Moreover, when siRE and siRE-mod were serially electroporated three or four times, the level of G1 cell cycle arrest was similar in both siRE and siRE-mod treated cells.

Even though both siRE and siRE-mod caused comparable G1 cell cycle arrest on day 6 after two serial electroporations compared to the siMM (Fig 3-10A, B), the cell cycle arrest was maintained until day 12 in siRE-mod treated cells in Kasumi-1 cell line (Fig 3-10C). In Kasumi-1 cells, *RUNX1/ETO* knockdown on day 12 elevated the G1 phase to 72% and 78% in siRE and siRE-mod transfected samples ($p= 0.016$) compared to 65% in control treated cells. Additionally, siRE-mod transfected cells had also significantly ($p= 0.032$) fewer cells in the S phase on day 12 in comparison with siRE treated cells. Cell cycle profiling of Kasumi-1 showed 19% and 14% in the S phase of siRE and siRE-mod transfected cells, respectively. Nevertheless, two sequential electroporations led to liminal changes in the cell cycle profile of SKNO-1 on day 12 (Fig 3-10D).

SKNO-1 cell line culturing medium contains 7 ng/ml GM-CSF and 20% FCS. Under these conditions, it was not feasible to obtain a strong growth inhibition or clear changes in the cell cycle profile after RUNX1/ETO knockdown. For this reason, the GM-CSF concentration and FCS content were reduced to 5 ng/ml and 15%, respectively. The reduction in GM-CSF and FCS did not affect SKNO-1 proliferation or change RUNX1/ETO knockdown level. This optimised condition of SKNO-1 culture was used throughout the whole PhD project.

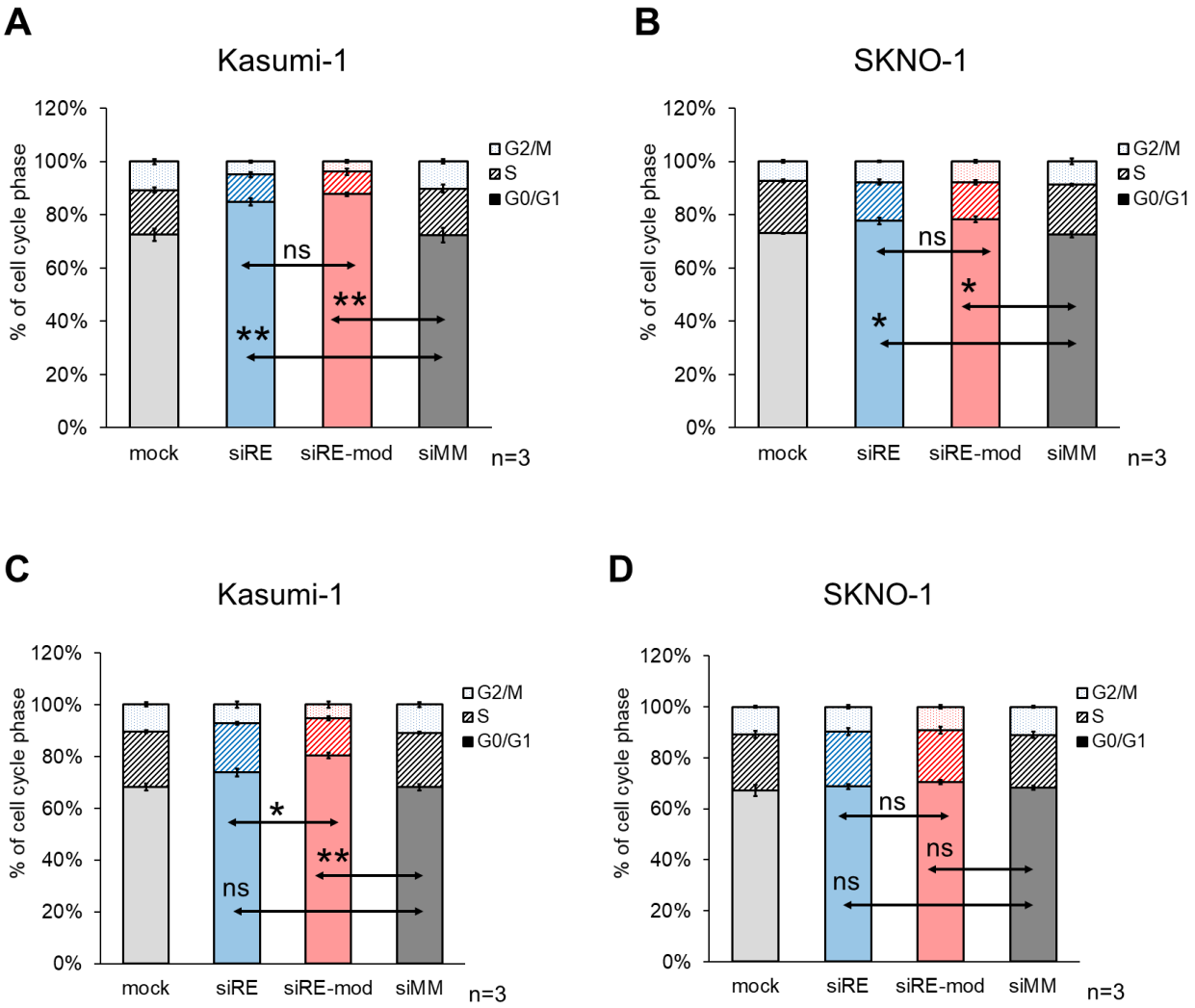

Fig 3-10: Cell cycle profile after *RUNX1/ETO* depletion in Kasumi-1 and SKNO-1. Cell lines were electroporated twice with 100 nM siRNA on days 0 and 3. Cell cycle profiling by PI staining was performed on days 6 (A & B) and 12 (C & D). Error bars represent SEM of three independent experiments. **P*<0.05, ***P*<0.01, ****P*<0.001, two-tailed Student's *t*-test.

3.4.1.5 RUNX1/ETO knockdown effects on senescence

The knockdown of *RUNX1/ETO* led to induction of cellular senescence. The number of senescent cells was determined after staining with senescence-associated β-galactosidase activity assay. Upon staining, senescent cells appeared dark green under a bright-field microscope while the proliferative cells remained unstained. The inclusion criteria used to count senescent cells was that their shape was unchanged, and over 50% of the cell surface appeared as dark green.

RUNX1/ETO knockdown with single transfection did not lead to senescence. Four sequential electroporations with siRE and siRE-mod resulted in 40% and 60% senescence, respectively, in Kasumi-1 cells (Fig 3-11A). Notably, when siRE-mod was serially electroporated twice, it induced the same level of senescence obtained with four transfections using siRE under the same conditions.

Similarly, the modified siRE-mod induced significantly higher senescence levels in SKNO-1 in comparison with siRE (Fig 3-11B).

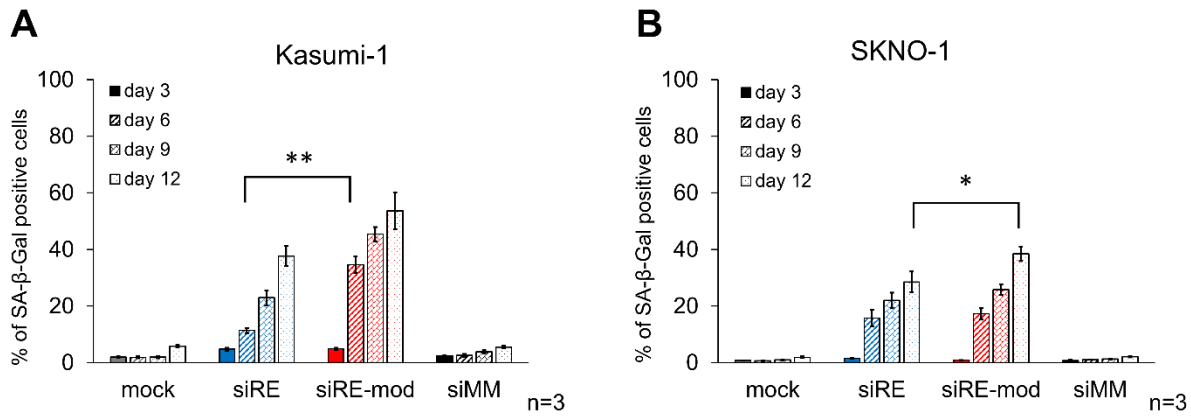

Fig 3-11: Induction of senescence after *RUNX1/ETO* knockdown in Kasumi-1 (A) and SKNO-1 (B). Serial electroporations of Kasumi-1 and SKNO-1 with 100 nM of siRNA were performed on days 0, 3, 6 and 9. Staining with X-Gal was performed every three days. Cell count was carried under a bright-field microscope. Error bars represent SEM of three independent experiments, **P*<0.05, ***P*<0.01, ****P*<0.001, two-tailed Student's *t*-test.

3.4.1.6 RUNX1/ETO knockdown effects on clonogenicity

To investigate the effect of *RUNX1/ETO* knockdown on self-renewal, and to evaluate the level of *RUNX1/ETO* knockdown in a more stringent assay, colony formation assay (CFA) was performed. Our group optimised a protocol for colony formation in t(8,21) AML cell lines using methylcellulose semi-solid media. The plating of naïve untreated cells at 5 x 10^3 cells/ml resulted in up to 30% and 20% colonies in Kasumi-1 and SKNO-1, respectively.

Multiple CFA replating is commonly used to test the long-term self-renewal capacity. The effect of the cell density on colony formation was tested. When the CFA was performed using different cell numbers (0.5, 1, 2, 5, and 10 x 10^3 cell/well), the CFA recovery was constant (Fig 3-12). Regardless of the starting seeding density, Kasumi-1 cells yielded in about 30% colonies of the seeded cells, and 20-25% of SKNO-1 cells. The inclusion criteria used to count colonies was the presence of more than 25 cells in a single colony.

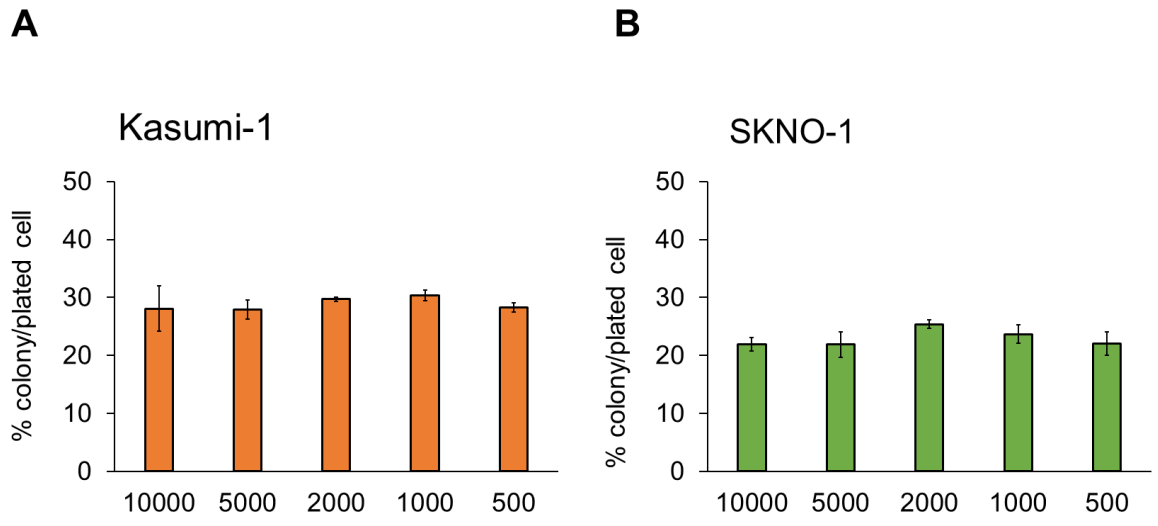

Fig 3-12: Colony formation assay of Kasumi-1 (A) and SKNO-1 (B). Cells lines were seeded for colony formation at 0.5, 1, 2, 5, and 10 x 10^3 cells/well in 0.5 ml methylcellulose media. After approximately one week, (A) Kasumi-1 and (B) SKNO-1 colonies were counted. Data represent the percentage of counted colonies divided by the seeded cell number. Four wells were counted per sample. Error bars represent the standard deviation of the percentage of counted colonies in four wells per condition (technical replicates, n=1).

RUNX1/ETO knockdown resulted in significant reduction of clonogenicity of Kasumi-1 and SKNO-1 cell line (Fig 3-13). The siRE-mod outperformed siRE and led to over 80% reduction in clonogenicity of Kasumi-1 compared to a 65% reduction in siRE by comparison with the siMM control (Fig 3-13A). Replating Kasumi-1 colonies did not significantly differ between siRE and siRE-mod transfected cells and siRE-mod provided a more substantial decrease in clonogenicity.

In SKNO-1 cells, siRE-mod transfected cells formed significantly fewer colonies in comparison with siRE (Fig 3-13B). RUNX1/ETO knockdown by siRE resulted in a 40% reduction in CFA, while siRE-mod yielded in 50% reduction in clonogenicity. Similar to Kasumi-1, replating of SKNO-1 colonies also proved that RUNX1/ETO knockdown achieved with siRE-mod was more potent in impairing clonogenicity (Fig 3-13B).

Remarkably, *RUNX1/ETO* knockdown by single electroporation impaired Kasumi-1 and SKNO-1 self-renewal up to 5 replatings (Fig 3-14). The siRE-mod significantly outperformed siRE in impairing clonogenicity in the first and second platings in both cell lines. In SKNO-1 cell line, siRE-mod substantially reduced the colony formation potential until the last replating, while in Kasumi-1 both siRNAs had showed similar potency (Fig 3-14).

Notably, the first and second generations of CFA took about 8-10 days to form large round backed colonies. However, the replated cells were able to form colonies faster, seven days in the third CFA and five days only for the fourth and fifth generations.

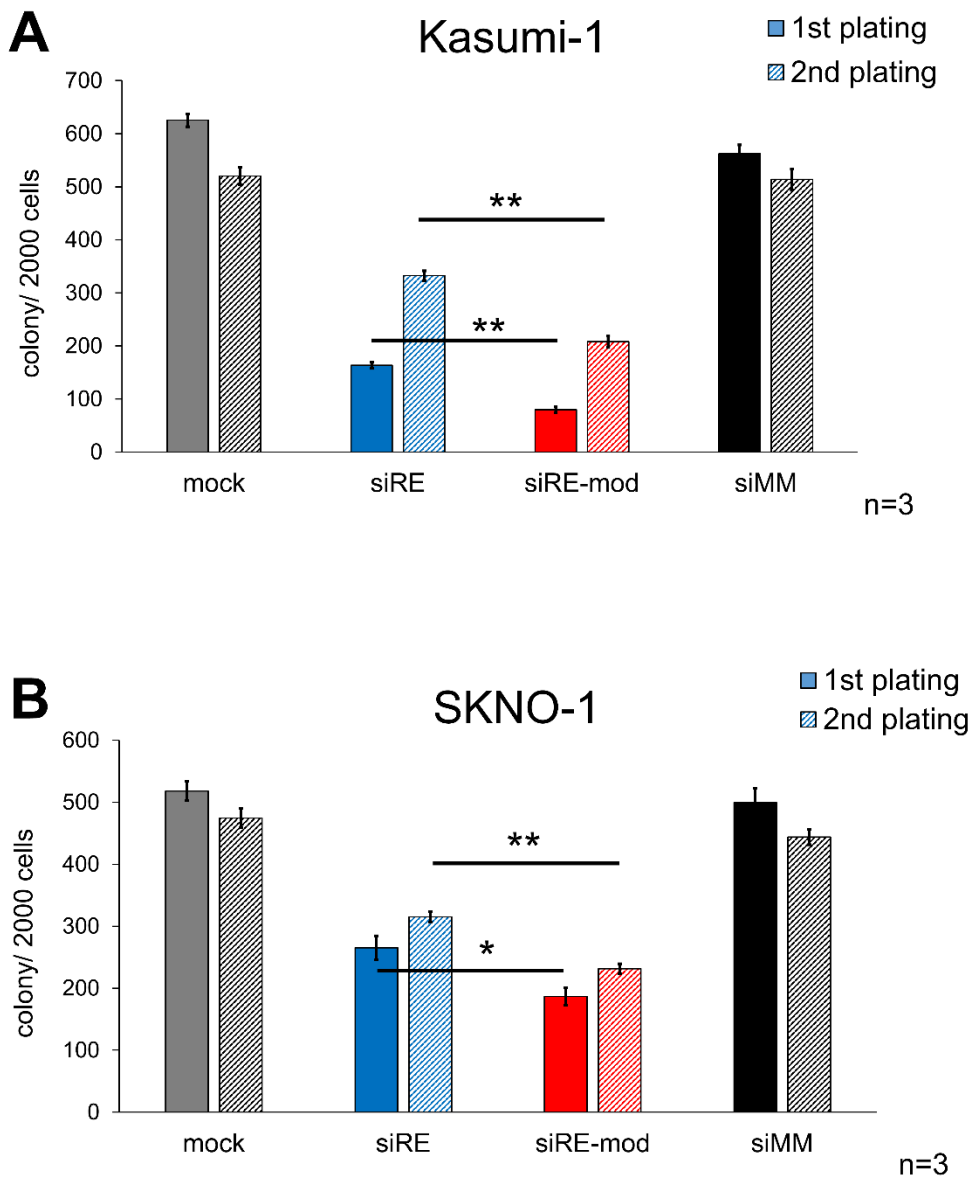

Fig 3-13: Colony formation assay of Kasumi-1 (A) and SKNO-1 (B) after *RUNX1/ETO* knockdown. Cell lines were electroporated with 100 nM siRNA and 2000 cells per well were seeded after 24 hours of the knockdown in methylcellulose semi-solid media. The solid-filled column represents the total colonies number after 9 days, the pattern-filled column represents the re-plated (2000 cells per well) colonies number after 7 days. Error bars represent SEM of three independent experiments (four wells were counted per experiment), **P*<0.05, ***P*<0.01, ****P*<0.001, two-tailed Student's *t*-test.

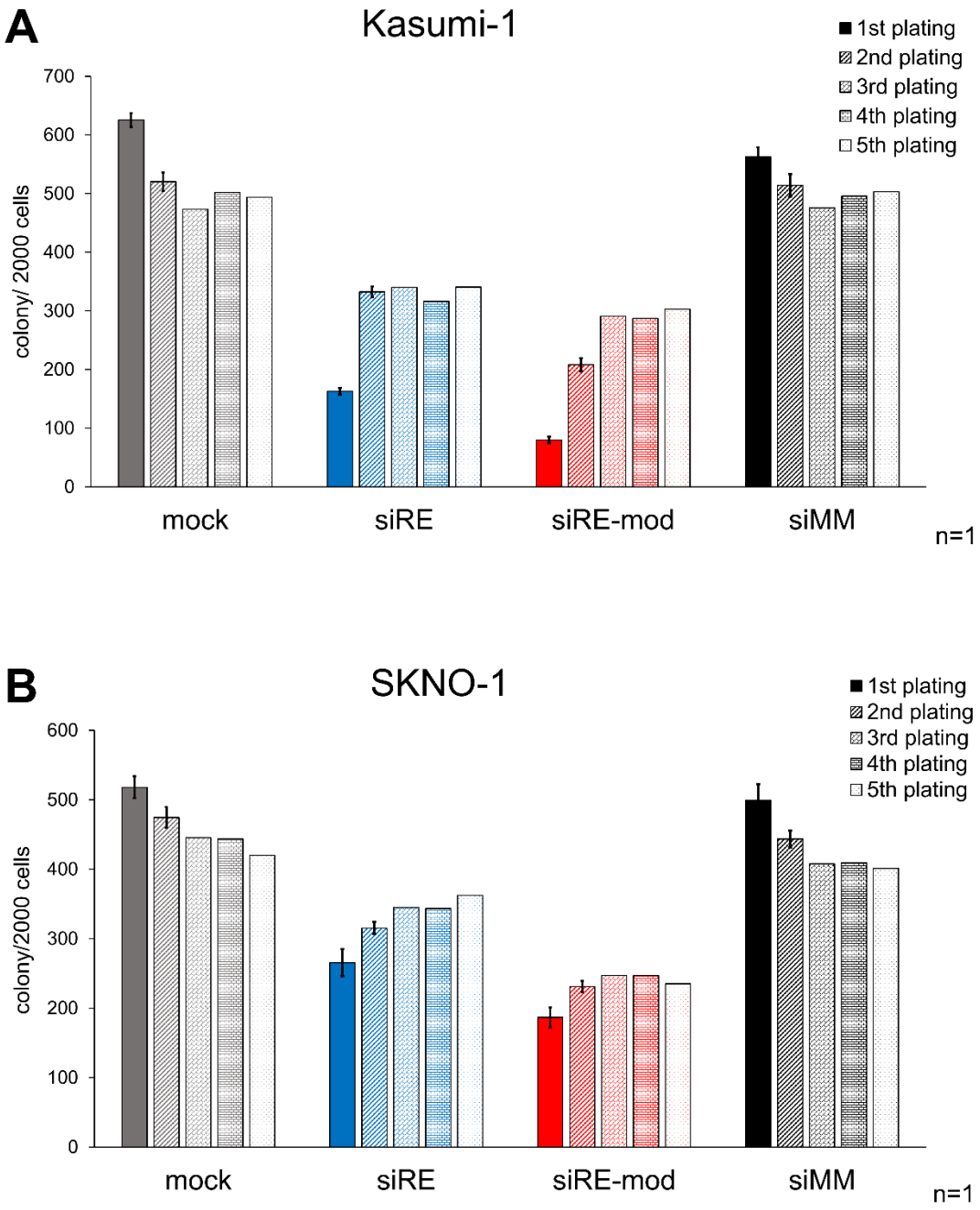

Fig 3-14: Replating experiment for colony formation of Kasumi-1 (A) and SKNO-1 (B) after *RUNX1/ETO* knockdown. Cell lines were electroporated with 100 nM siRNA and seeded after 24 hours of transfection in methylcellulose semi-solid media at 4 x 10^3 cells/ml density. After counting, colonies were collected and washed twice with PBS, then cells were resuspended in methylcellulose at 4x10^3cell/ml density. Colonies were counted when large (more than 25 cells) backed colonies were formed. For the first and second platings, error bars represent SEM of three independent experiments (four wells were counted per experiment), *P<0.05, **P<0.01, ***P<0.001, two-tailed Student's t-test.

3.4.2 LNP/siRNA efficacy in vitro

3.4.2.1 LNP/siRNA characterisation

In vitro experiments in Kasumi-1 and SKNO-1 cell lines showed that the siRE-mod outperformed the siRE. The next pursued step was to encapsulate the siRNA into a lipid nanoparticle. Throughout the PhD project, five different batches of LNP/siRNA were generated using independently synthesised siRNA batches. For this reason, where applicable, statistical analyses were performed on independent biological replicates using independent LNP/siRNA formulations.

Quality control measurements for each LNP/siRNA batch were performed in Zetasizer to ensure its suitability for the *in vitro* and *in vivo* experiments. These measurements included the particles' size, charge and polydispersity. The dynamic light scattering measurement reflected the hydrodynamic size of the LNP/siRNA particles, the polydispersity index (PDI) reflected the homogeneity of the LNP/siRNA solution, and the zeta potential indicated the surface charge of the particles. Throughout the *in vitro* and *in vivo* experiments, the size of LNP/siRE-mod, LNP/siMM, and LNP/siMM-mod were in the range between 65 to 85 nm, as shown in Table 3-2. The PDI numbers were below 0.25, indicating that the LNP/siRNA mixtures had a uniform distribution of the particles size.

LNP/siRNA solution was stable for over one year stored at 4°C. There were no significant changes in the size, PDI or charge of LNP/siRE-mod, LNP/siMM or LNP/siMM-mod in either concentrated or 1:100 diluted solutions (Fig 3-15A, B & C). The lipid nanoparticles had a small negative charge between -4 to -7 mV after packaging, and the surface charge increased to become more neutral over time. The LNP/siRNA charge did not exceed the 1 mV after 76 weeks of storage at 4°C (Fig 3-15D). There was not any significant difference between the particles encapsulating either siMM, siMM-mod or siRE-mod.

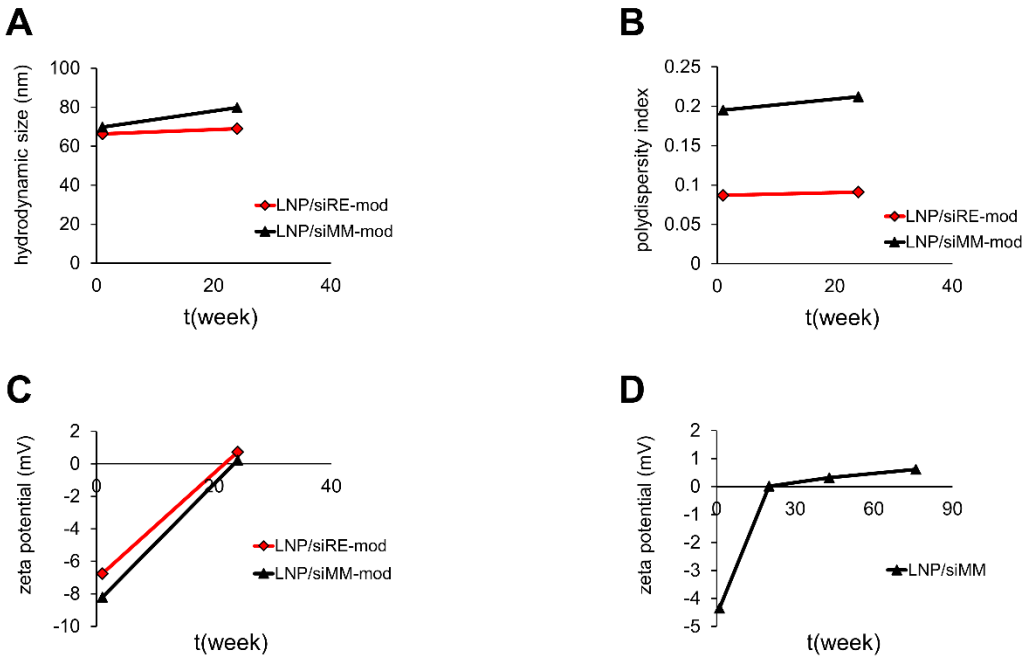

Fig 3-15: LNP/siRNA physical parameters as assessed by the Zetasiser. LNP/siRNA solution was diluted 1:100 in PBS for size and PDI measurements, and diluted1:1000 in deionised water for the zeta potential measurement. (A) Changes in the LNP/siRNA particle size after 24 weeks. (B) changes in the polydispersity of the LNP/siRNA mixture after 24 weeks. (C) Changes in the LNP/siRNA charge over 24 weeks. (D) Changes in 1:1000 diluted LNP/siMM particles zeta potential over 18 months. All measurements were performed after calibrating the measurement cuvettes at 25°C for one minute.

Batch.No /date	LNP/siRNAs	Size (nm)	PDI	Zeta potential (mV)	siRNA encapsulation efficiency (%)
Batch.1 Sep.2015	LNP/siRE-mod	84.6	0.22	-5	54.5
	LNP/siMM	76.1	0.19	-4.19	43
Batch.2 Feb.2016	LNP/siRE-mod	76.3	0.16	-6.3	87
	LNP/siMM	77.9	0.18	-4.9	83
Batch.3 May.2017	LNP/siRE-mod	65.6	0.08	-6.6	93
	LNP/siMM	68.4	0.1	-8.15	94
Batch.4	LNP/siRE-mod	69.1	0.09	-6.1	95

Nov.2017	LNP/siMM-mod	73.0	0.11	-4.2	96

Table 3-2: LNP/siRNA formulations and physical parameters. Measurement of the particles size, PDI and zeta potential were performed in Zetasizer within one week of the particles formulations. The packaging efficiency was determined after quantifying the siRNA content by by Quant-iT RiboGreen assay

3.4.2.2 Lipid quantification in the LNP/siRNA

The therapeutic action of the LNP/siRNA particles is due to the siRNA molecules. Thus, *in vitro* and *in vivo* doses were calculated based on the siRNA content. Although the lipid molecules in the vehicle were not relevant for gene knockdown, it was crucial to determine the siRNA to lipid ratio in order to rule out the side effects and cytotoxicity of the vehicle component.

The total lipid content was measured in a colourimetric assay that quantified the total amount of phospholipids in the particles. The lipid mixture contained 10% molar ratio of DSPC. The absorbance of the complex between ammonium ferrothiocyanate [$(NH4)Fe(SCN)_4$] and the phosphorus in the DSPC showed that the LNP/siRNA mixture contained around 1.1 mM DSPC. The methods of quantifying DSPC was adapted (Stewart 1980) and as described in 2.2.10.

For 250 µg/ml LNP/siMM-mod, the final total lipid concentration was estimated to be 11 mM. The aforementioned calorimetric assay determined only the organic phosphorus in the mixture. The presence of lipid-like compounds in the lipid mixture might have influenced or interfered with the absorbance. Nevertheless, the method provided a sensible measurement of the siRNA: lipid ratio in the lipid nanoparticles.

3.4.2.3 LNP/siRNA cytotoxicity

The first step in establishing *RUNX1/ETO* knockdown *in vitro* was determining the optimal LNP/siRNA concentration and exposure time. The criteria for the effective LNP/siRNA dose were minimal cytotoxicity, robust repression of RUNX1/ETO and dysregulation of its target genes in both t(8;21) cell lines.

During the PhD project, four LNP/siRNA batches were made. Dr Nidhi Jyotsana in Hannover Medical School (Germany) performed the LNP/siRNA formation and quantified the siRNA content by Quant-iT RiboGreen as briefly described in 2.2.7. The encapsulation efficiency of siRNA was above 80% apart from the first batch (Table 3-2).

The encapsulation efficiencies varied between the LNP/siRNA batches. However, the difference in the cytotoxicity of different LNP/siRNA batches was minimal. In the Kasumi-1 cell line, both 5 µg/ml and 0.125 µg/ml LNP/siRNA doses had minimal cytotoxicity after 24 hours of continuous exposure (Fig 3-16A). Moreover, there was no substantial or statistically significant differences in the cytotoxicity between lipid nanoparticles encapsulating either siMM or siRE-mod (Fig 3-16B).

The Lipid mixture contained DiI dye that prevented the use of available absorbance or fluorescence-based toxicity assays. Cytotoxicity assays such as WST-1, WST-8, and resazurin were not successful in providing meaningful readings using a plate reader due to the interference of DiI spectra. Consequently, cell viability was determined by trypan blue exclusion counting.

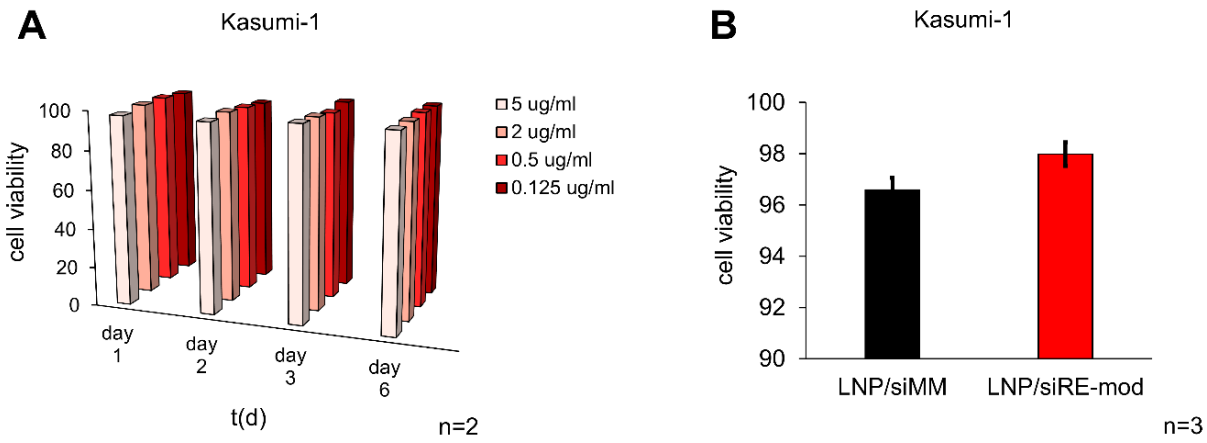

Fig 3-16: Cytotoxicity of LNP/siRNA in Kasumi-1. (A) Kasumi-1 cells were treated with 0.125, 0.5, 2 and 5 µg/ml of LNP/siMM for 24 hours. After 24 hours, cells were washed twice with PBS and resuspended in media and counted on days 2, 3 and 6. Columns represent the average of two independent experiments. (B) Kasumi-1 cells were treated with 2 µg/ml of either LNP/siMM or LNP/siRE-mod for 24 hours. After 24 hours, cells were washed twice with PBS and resuspended in fresh media and counted after 48 hours. Cell viability was determined with trypan blue. Error bars represent the SEM of three independent experiments.

3.4.2.4 LNP/siRNA dose and exposure time optimisation

The first experiment in SKNO-1 cell line showed that 24 hours continues exposure to 0.2 µg/ml LNP/siRNA resulted in a 40% reduction in *RUNX1/ETO* mRNA on day 2 (Fig 3-17A). However, RUNX1/ETO direct target genes such as *CCND2*, *ANGPT1* or *LAPTM5* did not change greatly (Fig 3-17B, C, D). Treatment with 2 µg/ml LNP/siRNA for 24 hours led to a 60% knockdown of *RUNX1/ETO*. Moreover, RUNX1/ETO transcriptional network was significantly dysregulated with 2 µg/ml LNP/siRNA treatment in comparison with the 0.2 µg/ml dose. For example, *RUNX1/ETO* repression led to about 40% downregulation of *CCND2* mRNAs. (Fig 3-16B). RUNX1/ETO late responding target genes were substantially dysregulated after six days of treatment. For instance, *ANGPT1* was reduced two-fold, and *LAPTM5* was increased 2.5-fold upon *RUNX1/ETO* knockdown (Fig 3-17C, D).

Similarly, Kasumi-1 cells treated with 2 µg/ml LNP/siRNA for 24 hours had 70% reduction in *RUNX1/ETO* transcript while 0.2 µg/ml dose resulted in a mild reduction

(Fig 3-18A). Furthermore, Kasumi-1 treated with 2 µg/ml LNP/siRNA for 24 hours showed robust regulation of RUNX1/ETO target genes. For instance, RUNX1/ETO repression led to a reduction in *CCND2*, *ANGPT1* and *TERT* mRNAs, and an increase in *LAPTM5* on day 8 (Fig 3-18B).

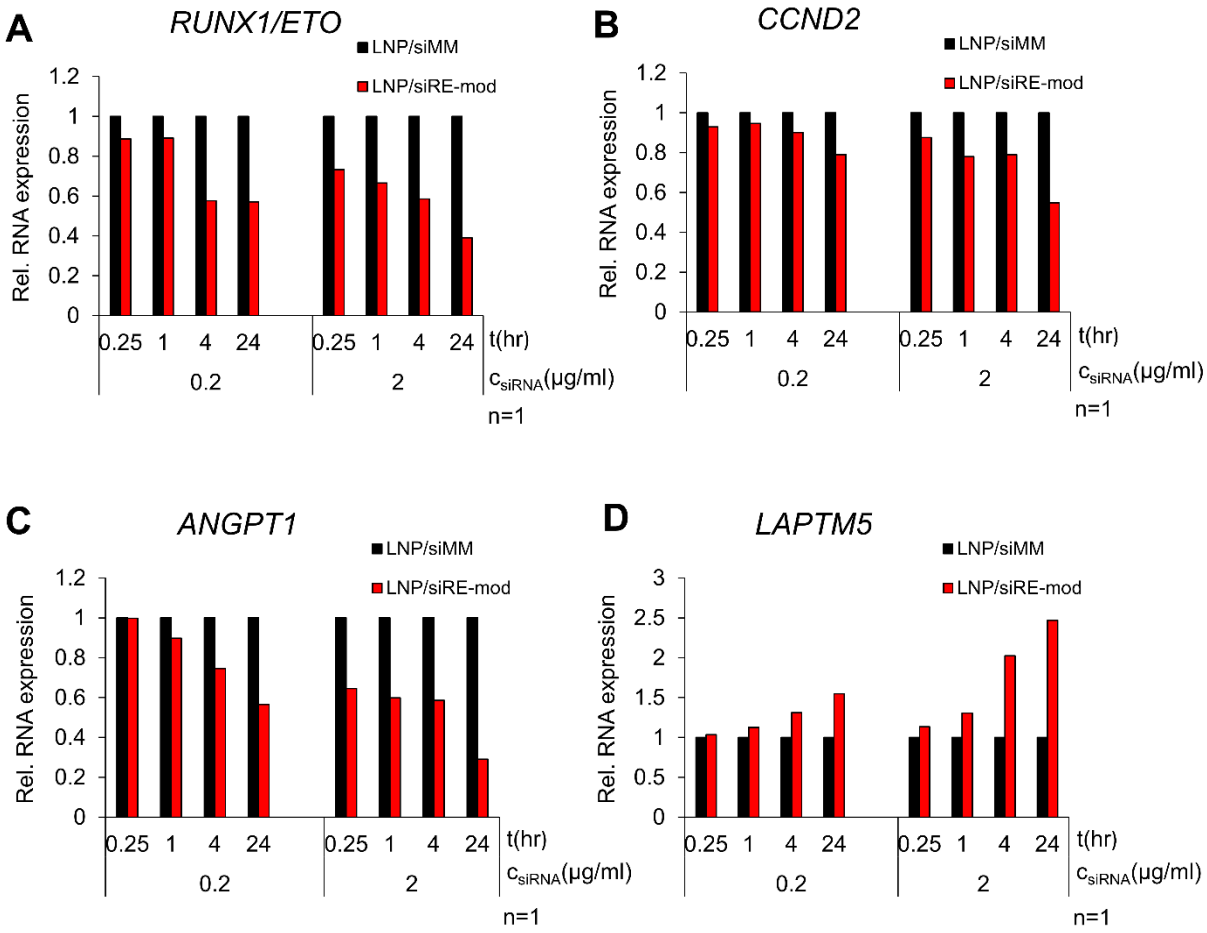

Fig 3-17: qPCR analysis in SKNO-1 after LNP/siRNA treatment. SKNO-1 cells were incubated at 1 x 10^6 cells/ml density with either 0.2 or 2 µg/ml of LNP/siMM or LNP/siRE-mod for 15 minutes, 1, 4 and 24 hours. Treated cells were washed twice with PBS and resuspended in SKNO-1 media at 0.5 x 10^6 cells/ml density. On day 3, cell lysates were taken for the analysis of *RUNX1/ETO* and *CCND2* expressions as shown in A and B, respectively. On day 6, the mRNA levels of *ANGPT1* and *LAPTM5* were measured as shown in C and D, respectively. The analysis of the expression data of LNP/siRE-mod treated samples were normalised against LNP/siMM treated cells and *GAPDH* served as a housekeeping gene.

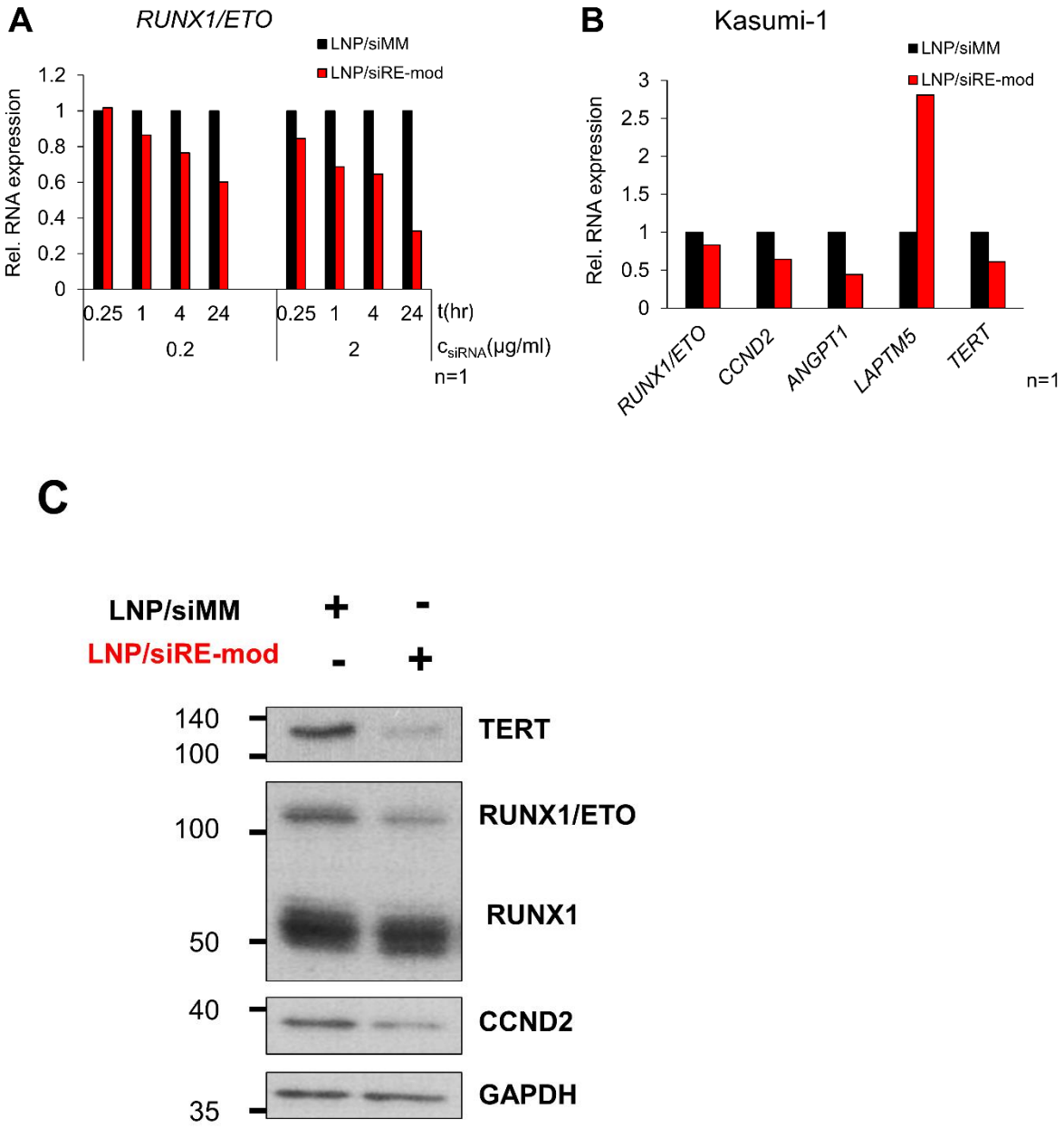

Fig 3-18: LNP/siRNA treatment in Kasumi-1. Kasumi-1 cells were incubated at 1 x 10^6 cells/ml density with either 0.2 or 2 µg/ml of LNP/siMM or LNP/siRE-mod for 15 minutes, 1, 4 and 24 hours. Treated cells were washed twice with PBS and resuspended in Kasumi-1 media at 0.5x10^6 cells/ml density. (A) On day 3, cell lysates were taken for the analysis of *RUNX1/ETO* mRNA. (B) On day 8, the mRNA level of *RUNX1/ETO*, *CCND2*, *ANGPT1*, *LAPTM5,* and *TERT* of the 2 µg/ml of treated cells. The analysis of the gene expression level of LNP/siRE-mod treated cells was normalised against LNP/siMM treated cells and *GAPDH* served as a housekeeping gene. (C) Western blotting on day 10 for 2 µg/ml treated cells. Membranes were blotted against α-RHD, α-TERT, α-CCND2 and α-GAPDH loading control. Marker size in kDa are presented on the left side of the blots.

Treatment with low LNP/siRNA concentrations and for short periods was not sufficient to induce robust *RUNX1/ETO* knockdown or changes in the fusion protein target genes. For this reason, 24 hours treatment with 2 µg/ml LNP/siRNA was considered the optimal dose for the *in vitro* functional studies. A dose of 2 µg/ml of LNP/siRNA corresponds to 150 nM siRNA given that siRNA MW ≈ 13.3 kg/mol. The LNP/siRNA dose was comparable with the siRNA molarity used in the electroporation experiments (100 nM). Nevertheless, LNP/siRNA treatment was applied once rather than repetitive administrations.

3.4.2.5 LNP/siRNA treatment effects on proliferation

The phenotype of *RUNX1/ETO* knockdown cells by LNP/siRNA was investigated in Kasumi-1 and SKNO-1 cell lines. Cells at 1 x 10^6 cells/ml density were treated with 2 µg/ml LNP/siRE-mod or LNP/siMM for 24 hours as described in 2.2.12.

LNP/siRNA-mediated *RUNX1/ETO* knockdown significantly reduced Kasumi-1 proliferation (Fig 3-19A). However, the reduction in Kasumi-1 proliferation was less pronounced compared to what the serial electroporation achieved. On the other hand, LNP/siRNA did not provide a significant impact on SKNO-1 proliferation, but a subtle trend of reduced proliferation was observed (Fig 3-19B).

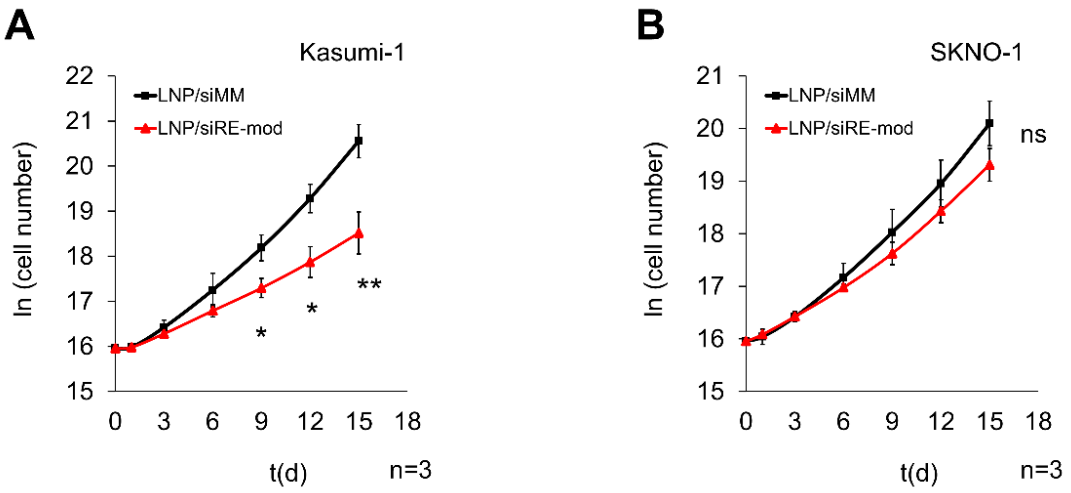

Fig 3-19: LNP/siRNA mediated *RUNX1/ETO* knockdown effect on Kasumi-1 and SKNO-1 proliferation. Kasumi-1 cell line (A) and SKNO-1 cell line (B) were treated at 1 x1 0^6 cells/ml density with 2 µg/ml of LNP/siRE-mod or LNP/siMM. After 24 hours, cells were washed twice with PBS and cultured at 0.5 x 10^6 cells/ml density and counted every three days. Error bars represent SEM of three independent experiments, **P*<0.05, ***P*<0.01, ****P*<0.001, two-tailed Student's *t*-test.

3.4.2.6 The dynamics of RUNX1/ETO knockdown by LNP/siRNA

Quantitative RT-PCR showed that LNP/siRNA treatment resulted in a rapid *RUNX1/ETO* knockdown and a robust dysregulation of the fusion transcriptional network in t(8;21) AML cell lines.

In Kasumi-1 cell lines, *RUNX1/ETO* expression was quickly reduced by 80% after 24 hours while and 60% - 70% knockdown was maintained over a week (Fig 3-20, A). The mRNA level of *RUNX1/ETO* had gradually recovered after 9 days of LNP/siRNA treatment. The robust knockdown of *RUNX1/ETO* resulted in a substantial modulation of its direct target genes. For instance, *CCND2* expression level was decreased by 40% after 24 hours, while the maximal reduction was observed on day 6 (Fig 3-19, B). Other RUNX1/ETO activated genes such as *CD34* and *ANGPT1* were also downregulated in the mRNA level, 70% and 90% reductions were observed in *CD34* and *ANGPT1* on days 6 and 3, respectively (Fig 3-20, E & F).

Moreover, RUNX1/ETO-repressed genes such as *CEBPA* and *LAPTM5* were strongly upregulated after the knockdown. *CEBPA* transcript level was increased 4-fold and 5-fold after 24 hours and 48 hours of treatment, respectively (Fig 3-20D). After 9 days of treatment, *LAPTM5* expression exceeded the 5-fold increase in the LNP/siRE-mod treated Kasumi-1 in comparison with the control treatment LNP/siMM (Fig 3-20G).

Similarly to Kasumi-1, LNP/siRNA treatment achieved robust knockdown of *RUNX1/ETO* in SKNO-1 cells. *RUNX1/ETO* transcript level was reduced by 60% until day 9, and 40% knockdown was detected on day 12 (Fig 3-21A). *CCND2* was downregulated after the knockdown, and 40% reduction was observed on day 6 (Fig 3-20B). Genes that are repressed by RUNX1/ETO were also upregulated after the knockdown. There was a 2.5-fold increase in *CEBPA* after 24 hours of the treatment (Fig 3-21D), and over 8-fold increase in *LAPTM5* on day 6 (Fig 3-21E).

Telomerase, a direct target gene of RUNX1/ETO, belongs to the late responding genes. It has been observed that *RUNX1/ETO* knockdown led to an increase in *TERT* expression for the first two days of treatment in Kasumi-1 and SKNO-1 cells. However, one week upon the knockdown, *TERT* expression was reduced by 50% in Kasumi-1 (Fig 3-19D) and 20% in SKNO-1 (Fig 3-21C).

Western blotting confirmed RUNX1/ETO knockdown at protein level. A single dose of 2 µg/ml LNP/siRNA provided a potent knockdown up to two weeks in Kasumi-1 and SKNO-1 cell lines (Fig 3-22). In Kasumi-1, RUNX1/ETO protein level was decreased more than 90% after 24 hours of treatment. The reduction in RUNX1/ETO remained potent for the first week and 32% knockdown was observed on day 15 (Fig 3-22,A). Similarly, in SKNO-1 cells, the LNP/siRNA treatment led to strong knockdown ar protein level (Fig 3-22,A). The knockdown of *RUNX1/ETO* resulted in approximately 40% reduction at protein level in CCND2 on day 3 (Fig 3-22,B).

Two different loading controls were used in Kasumi-1 Western blot due to technical issues while cutting the membrane prior to incubation with the primary antibody.

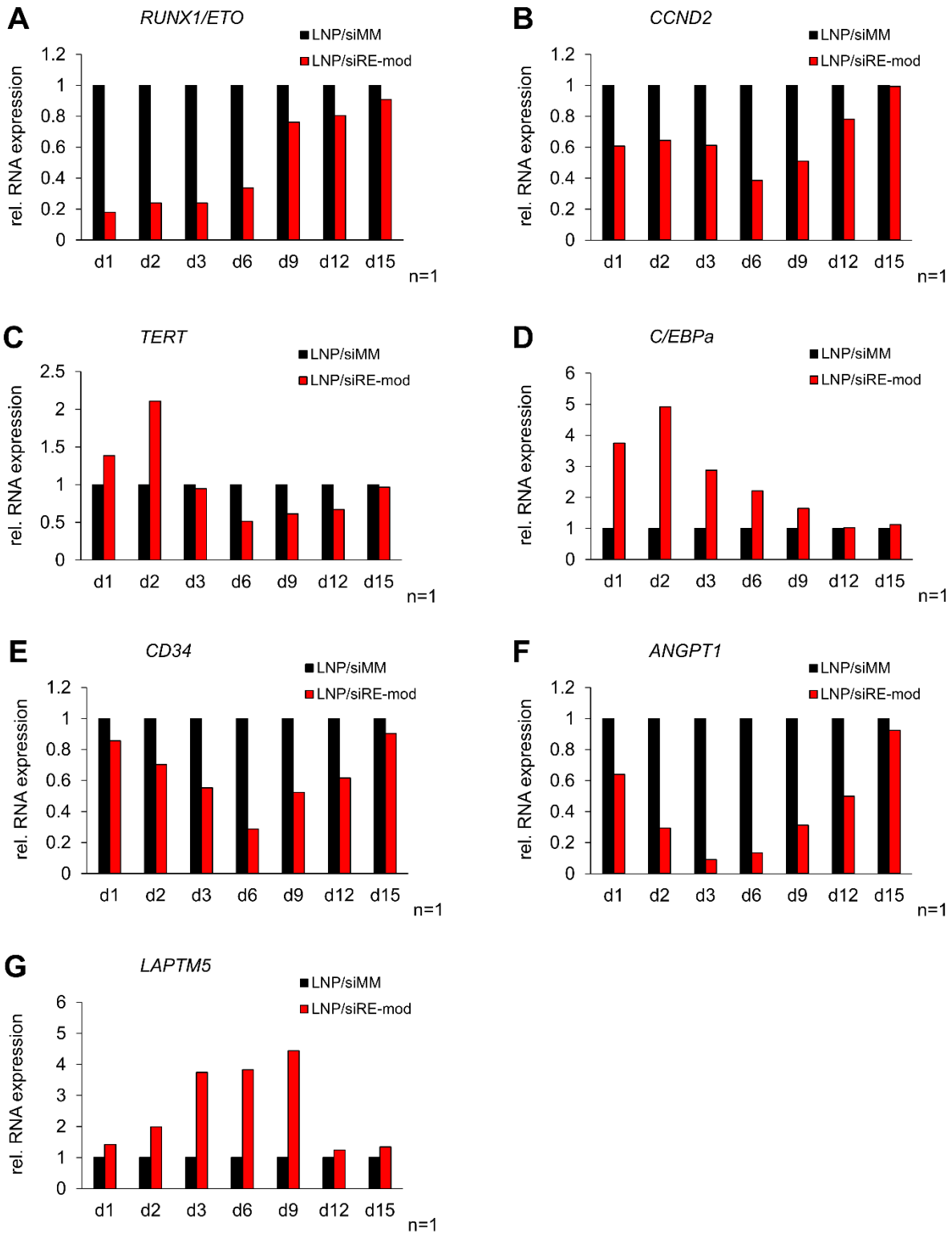

Fig 3-20: mRNA level of *RUNX1/ETO* and its direct target genes in Kasumi-1 after LNP/siRNA treatment. Kasumi-1 cells were treated at 1 x 10^6 cells/ml density with 2 µg/ml of LNP/siRE-mod or LNP/siMM. After 24 hours, cells were washed twice with PBS and resuspended in media at 0.5 x 10^6 cells/ml. Cell lysates were taken at days 1, 2, 3, 6, 9, 12 and 15. The expression of LNP/siRE-mod treated samples was normalised against LNP/siMM treated cells and *GAPDH* served as a housekeeping gene.

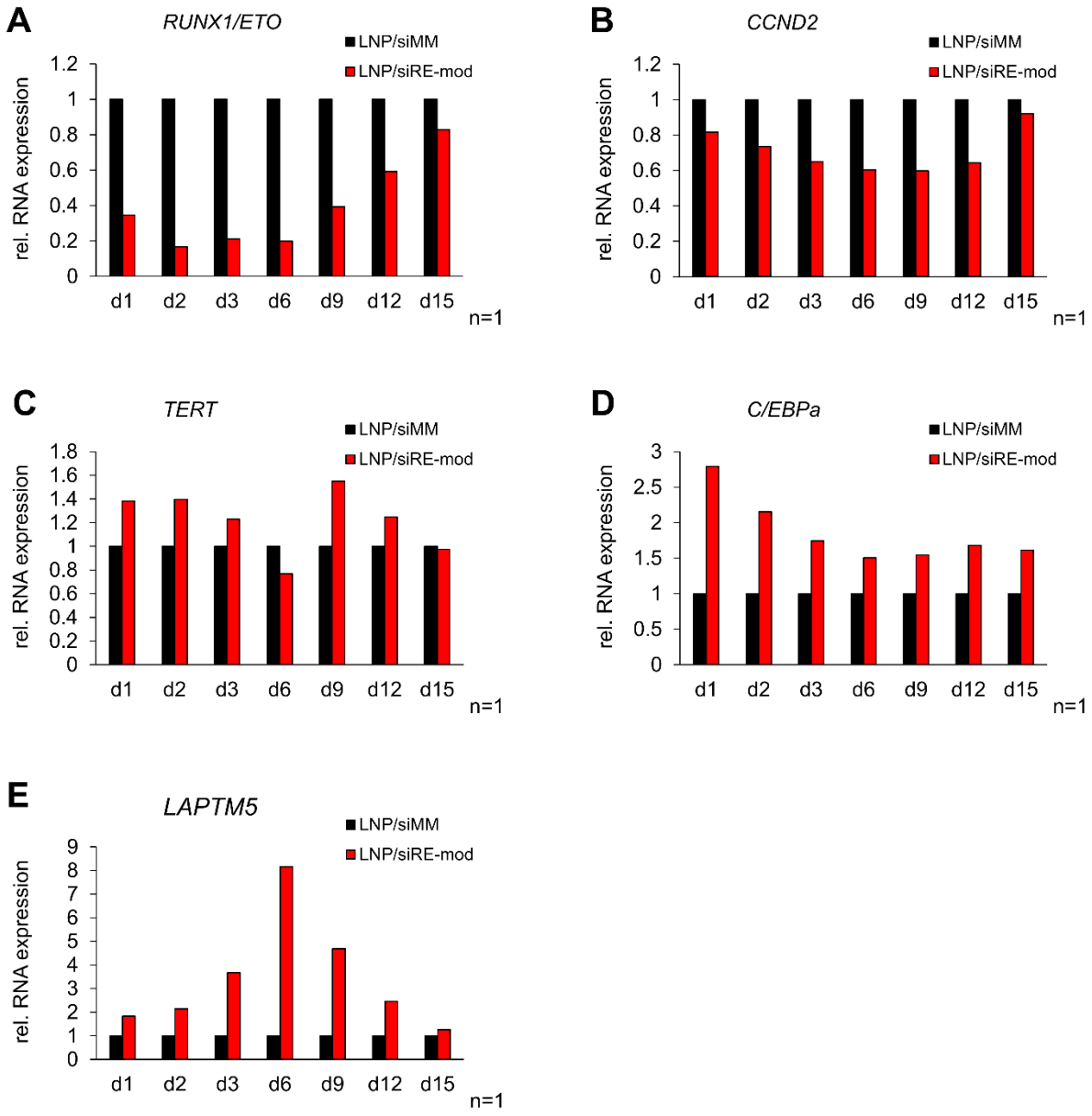

Fig 3-21: mRNA level of *RUNX1/ETO* and its direct target genes in SKNO-1 after LNP/siRNA treatment. SKNO-1 cells were treated at 1 x 10^6 cells/ml density with 2 µg/ml of LNP/siRE-mod or LNP/siMM. After 24 hours, cells were washed twice with PBS and resuspended in media at 0.5sx 10^6 cells/ml. Cell lysate was taken at days 1, 2, 3, 6, 9, 12 and 15. The expression of LNP/siRE-mod treated samples was normalised against LNP/siMM treated cells and *GAPDH* served as a housekeeping gene.

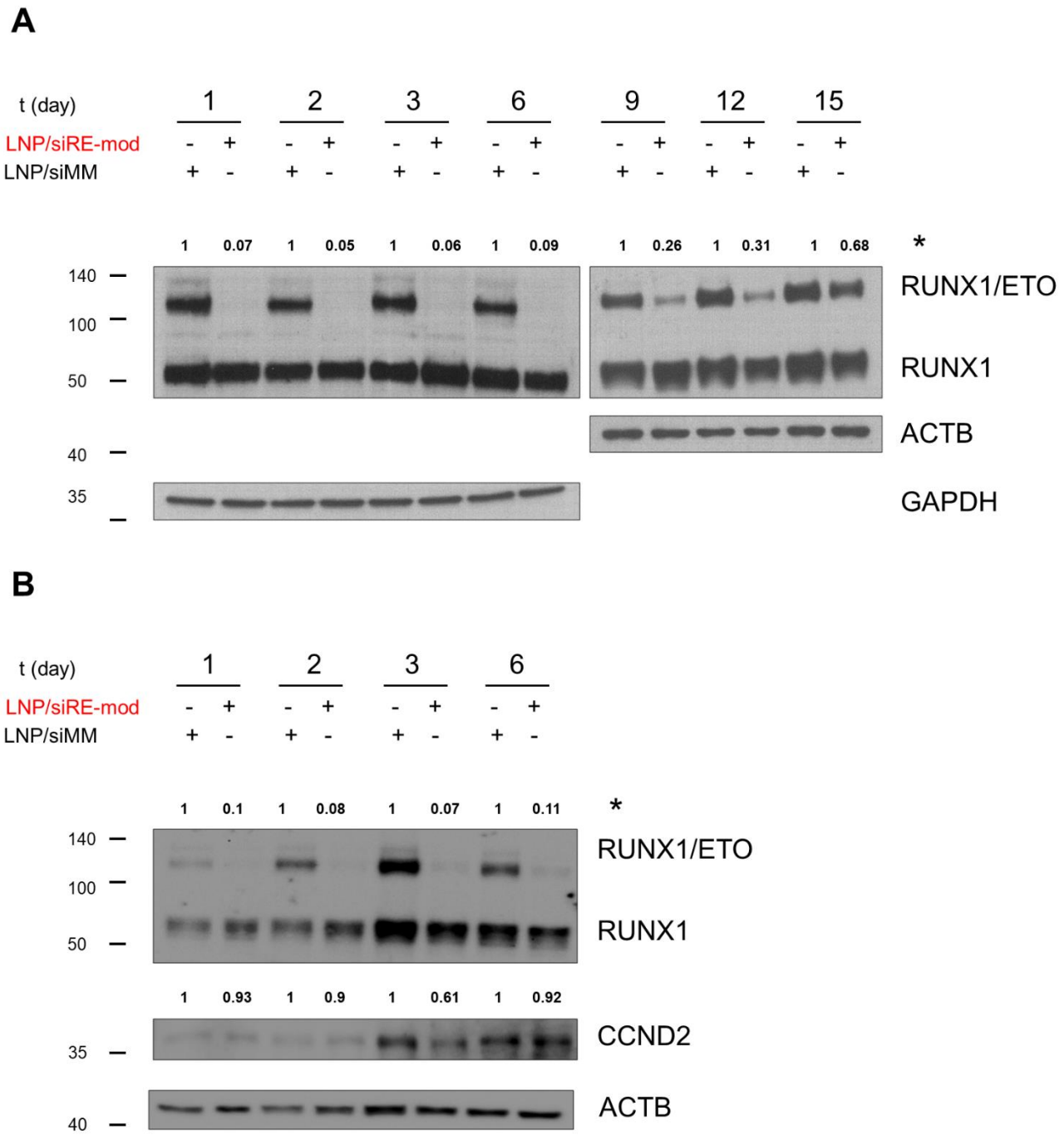

Fig 3-22: RUNX1/ETO knockdown upon LNP/siRNA treatment. Kasumi-1 and SKNO-1 cells were treated at 1 x 10^6 cells/ml density with 2µg/ml of LNP/siRNA. After 24 hours, cells were washed twice with PBS and resuspended in media at 0.5 x 10^6 cells/ml density. Cell lysates were taken at days 1, 2, 3, 6, 9, 12 and 15 for western botting. Membranes were blotted against α-RUNX1, α-CCND2 antibodies and α-GAPDH and α-ACTB served as loading controls. Marker size in kDa is presented on the left side of the blot.

3.4.2.7 LNP/siRNA effects on the cell cycle

Given that LNP/siRNA contained DiI dye, it was not possible to use PI for cell cycle staining. Hoechst 33342 live cell staining was used to quantify the DNA content and generate the cell cycle profile as described in 2.2.16.

LNP/siRNA-mediated *RUNX1/ETO* knockdown resulted in G1 cell cycle arrest in line with the electroporation experiments. On day 8, LNP/siRNA treatment in Kasumi-1 led to a 14% increase in the G0/G1 phase, together with a 50% reduction in the S phase (Fig 3-23A). The same effect was observed in the SKNO-1 cell cycle. *RUNX1/ETO* knockdown by LNP/siRNA resulted in an increase in the G0/G1 phase from 58% to 67% in the LNP/siMM and LNP/siRE-mod, respectively (Fig 3-23B).

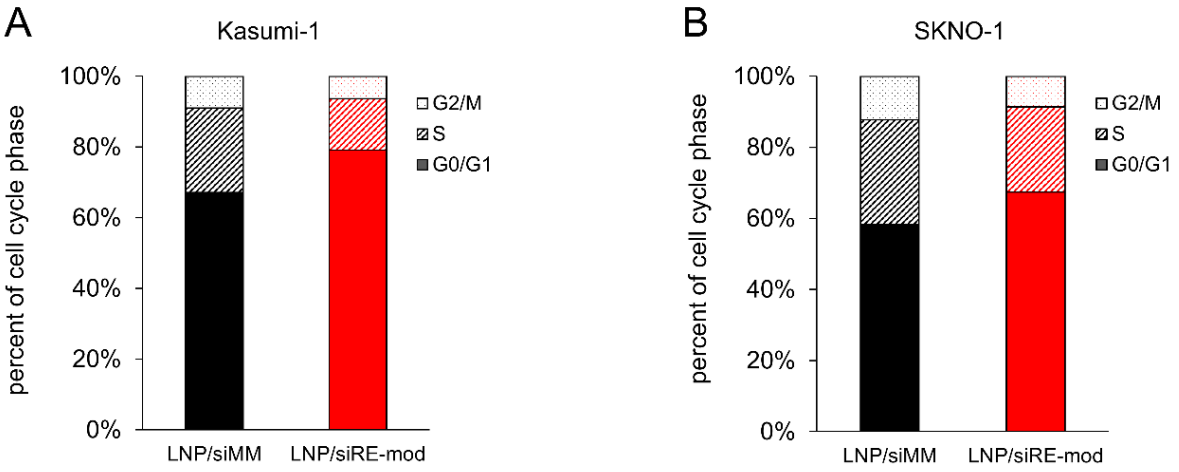

Fig 3-23: Cell cycle profile on day 8 after LNP/siRNA treatment in Kasumi-1 (A) and SKNO-1 (B). Cells were treated at 1 x 10^6 cells/ml density with 2µg/ml of LNP/siRNA. After 24 hours, cells were washed twice with PBS and resuspended in media at 0.5 x 10^6 cells/ml density. On day 8, cells were washed once with PBS, stained with Hoechst and analysed by flow cytometry (n=1).

3.4.2.8 LNP/siRNA effects on senescence

The senescence-associated beta-galactosidase assay showed that *RUNX1/ETO* knockdown by LNP/siRNA led to cellular senescence. Twelve days upon LNP/siRNA treatment, 40% of LNP/siRE-mod treated Kasumi-1 cells were positive for X-Gal staining while less than 8% were positive in the LNP/siMM treated control and the untreated control cells (Fig 3-24A, C). The knockdown of *RUNX1/ETO* with LNP/siRNA in SKNO-1 also led to 20% senescence in comparison with 6% in the LNP/siMM treated control (Fig 3-24B, D).

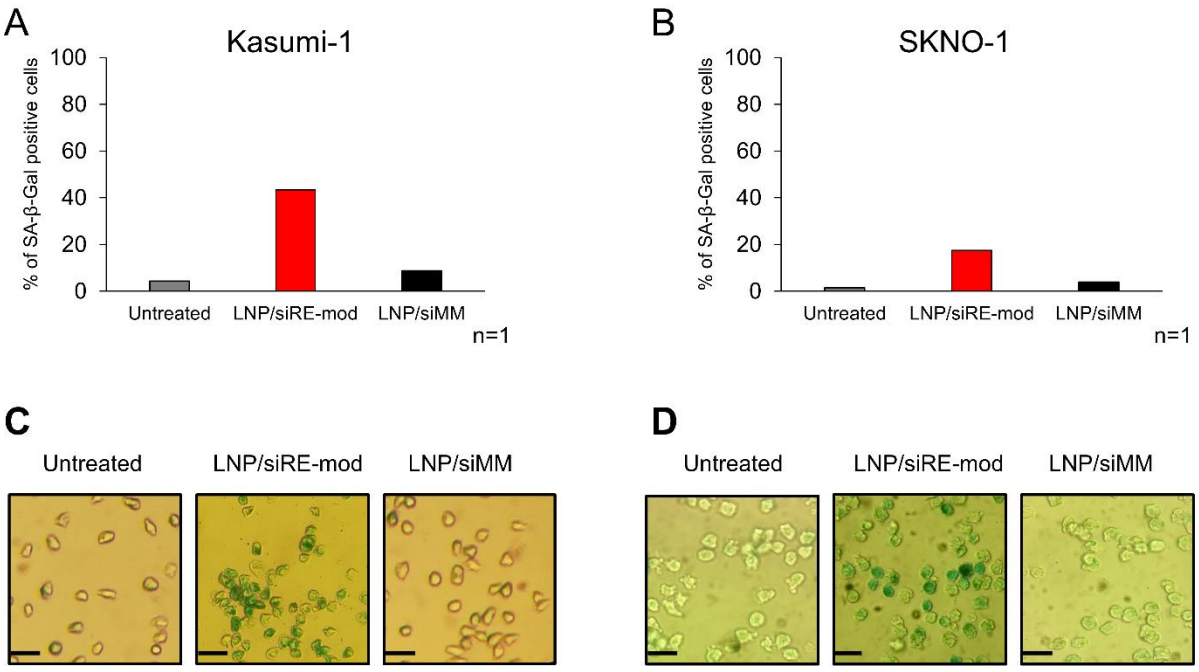

Fig 3-24: Induction of senescence after LNP/siRNA treatment in Kasumi-1 (A& C) and SKNO-1 (B& D). Cells were treated at 1 x 10^6 cells/ml density with 2 µg/ml of LNP/siRNA. After 24 hours, cells were washed twice with PBS and resuspended in media at 0.5 x 10^6 cells/ml density. On day 12, cells were washed with PBS, fixed at room temperature and stained overnight at 37^{o}C with X-Gal as described in 2.2.15. Positively stained cells were counted under a bright-field microscope. Scale bar= 20 µm, (n=1)**.**

3.4.2.9 LNP/siRNA effects on clonogenicity

RUNX1/ETO knockdown by LNP/siRNA remarkably reduced the clonogenic potential of AML t(8;21) cell lines (Fig 3-25). Treatment with LNP/siRE-mod resulted in over fivefold reduction in clonogenicity in Kasumi-1 and SKNO-1 cells. Furthermore, replating of the colonies showed that the clonogenicity was greatly impaired in the *RUNX1/ETO* knockdown cells. The LNP/siMM did not provide any significant effect on clonogenicity of Kasumi-1 or SKNO-1, although a slight reduction in colonies number was observed in the first plating. However, upon re-plating, LNP/siMM treated cells formed as many colonies as the untreated cells, which may indicate a low degree of cytotoxicity.

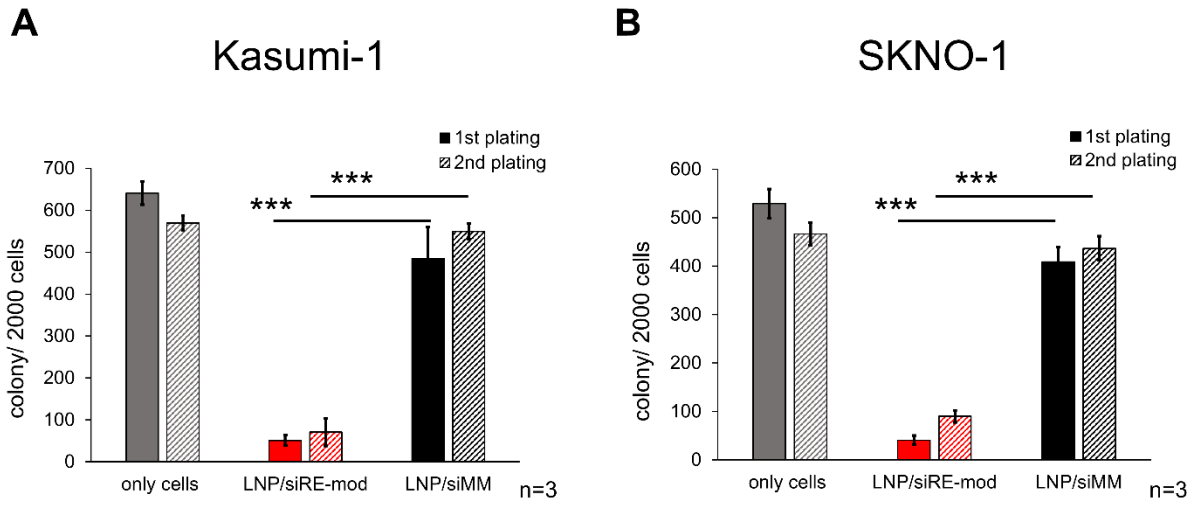

Fig 3-25: Colony Formation Assay of Kasumi-1 (A) and SKNO-1(B) treated with LNP/siRNA. Cells were treated at 1 x 10^6 cells/ml density with 2 µg/ml LNP/siRNA. After 24 hours, cells were washed twice with PBS and suspended in methylcellulose media at 4000 cells/ml density. After 7 days, colonies were counted and cells washed in PBS and replated at 4000 cell/ml density. The solid-filled columns represent the total colonies number after 7 days, and the pattern-filled column represents the replated colonies number after 8 days. Error bars represent SEM of three independent experiments (four wells were counted per experiment), **P*<0.05, ***P*<0.01, ****P*<0.001, two-tailed Student's *t*-test.

RUNX1/ETO knockdown at the mRNA level was stable even after seeding the cells in colony formation. In SKNO-1 harvested colonies, there was a significant reduction (~30%) in *RUNX1/ETO* (Fig 3-26A). Moreover, SKNO-1 colonies also presented a significant increase (~50%) in *LAPTM5* expression (Fig 3-26, B) and over 40% reduction in *RUNX1* (Fig 3-26C). Kasumi-1 colonies also showed a reduced *RUNX1/ETO* expression by 22% (Fig 3-26A). There was reduction in *ANGPT1* (~50%) and *RUNX1* (~20%), respectively (Fig 3-27C, D) and increase in *LAPTM5* (~50%) (Fig 3-27B).

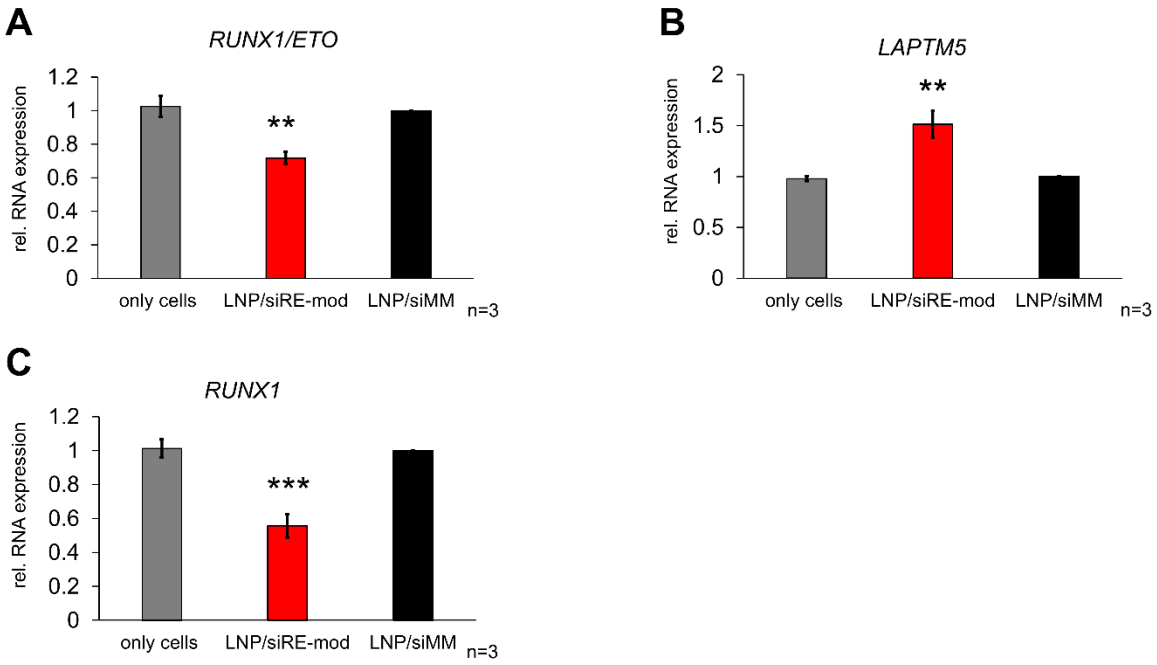

Fig 3-26: qPCR analysis in SKNO-1 harvested colonies after the first round of plating. SKNO-1 cells were incubated at 1 x 10^6 cells/ml with 2 µg/ml LNP/siRNA. After 24 hours, cells were washed twice with PBS and resuspended in SKNO-1 colony formation media at 4000 cells/ml density and seeded. After 7 days, colonies were washed twice with PBS and cell lysates were taken for RNA extraction. Quantitative RT-PCR of *RUNX1/ETO*, *LAPTM5,* and *RUNX1* expressions are shown in A, B and C respectively. The gene expression of LNP/siRE-mod treated cells was normalised against LNP/siMM treated cells and *GAPDH* served as a housekeeping gene. Error bars represent SEM of three independent experiments, **P*<0.05, ***P*<0.01, ****P*<0.001, two-tailed Student's *t*-test.

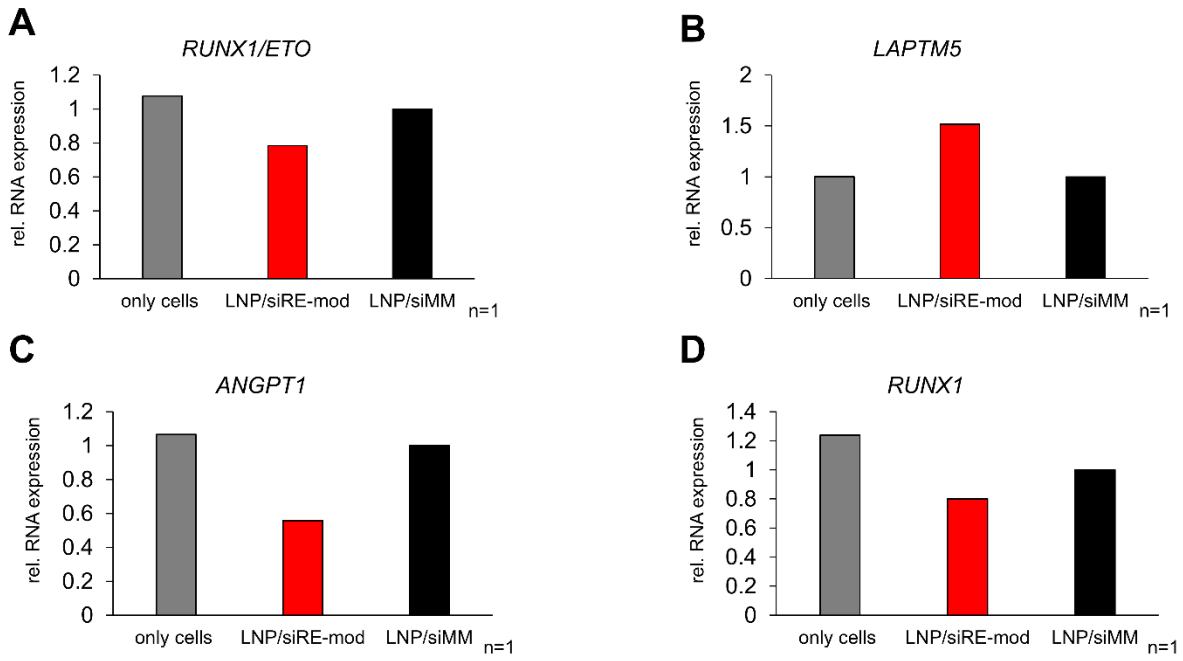

Fig 3-27: qPCR analysis in Kasumi-1 harvested colonies after the first round of plating. Kasumi-1 cells were incubated at 1 x 10^6 cells/ml with 2 µg/ml LNP/siRNA. After 24 hours, cells were washed twice with PBS and resuspended in Kasumi-1 colony formation media at 4000 cells/ml density and seeded. After 7 days, colonies were washed twice with PBS and cell lysates were taken for RNA extraction. Quantitative RT-PCR of *RUNX1/ETO*, *LAPTM5*, *ANGPT1,* and *RUNX1* expressions are shown in A, B, C and D respectively. The gene expression of LNP/siRE-mod treated cells was normalised against LNP/siMM treated cells and *GAPDH* served as a housekeeping gene (n=1).

3.4.3 LNP/siRNA efficacy in t(8;21) primary cells

LNP/siRNA-mediated *RUNX1/ETO* knockdown in t(8;21) primary cells was investigated in two primary patient cells. Before applying any LNP/siRNA treatment, cells were seeded on MSCs feeders for 24 hours then treated with 4 µg/ml LNP/siRNA as described in 2.2.13.

In the LK19 primary sample, treatment with LNP/siRE-mod resulted in a 62% reduction in *RUNX1/ETO* mRNA after three days of treatment and *CEBPA* was upregulated onefold (Fig 3-28). The knockdown of *RUNX1/ETO* in LK19 also led to a 40% reduction in *CCND2* level and 60% reduction in *ANGPT1* (Fig 3-28).

LK111 primary sample showed 56% knockdown of RUNX1/ETO after 4 days of LNP/siRNA treatment. The knockdown resulted in twofold upregulation in *CEBPA* expression.

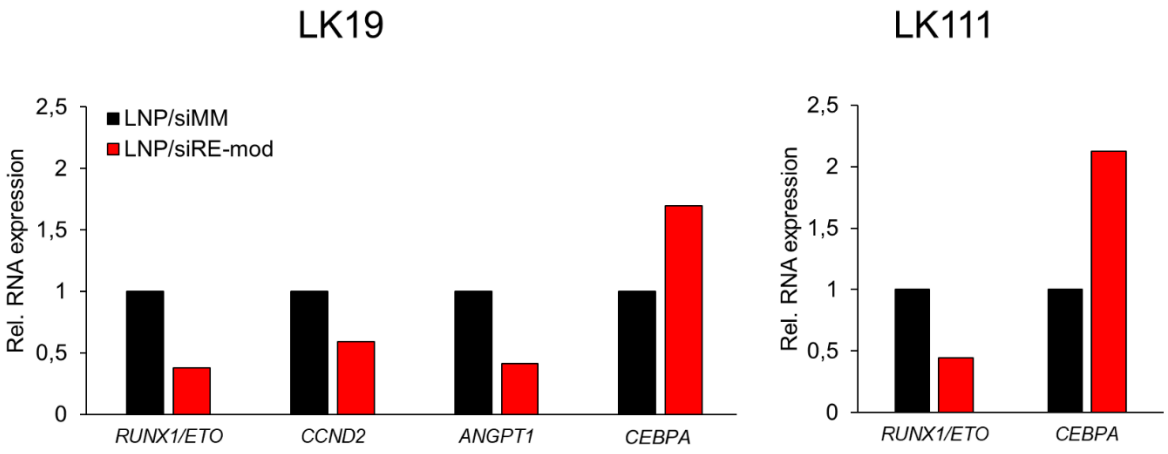

Fig 3-28: qPCR analysis of AML t(8;21) primary patient cells. Primary cells were seeded on top of MSCs feeder layer. On the next day, 2 µg/ml of LNP/siRNA was applied. AML cells were separated from the feeders and harvested on day 3 for LK19 and day 4 for LK111. The gene expression of LNP/siRE-mod treated cells was normalised against LNP/siMM treated cells, and *GAPDH* served as a housekeeping gene (n=1).

3.4.4 LNP/siRNA efficacy in t(8;21) PDXs

Two AML t(8;21) PDX models (PDX1 and PDX2) were tested *RUNX1/ETO* knockdown *ex vivo*. PDXs cells were seeded on MSCs feeders for 24 hours then treated with 4 µg/ml LNP/siRNA. Leukaemic cells were harvested at days 3 and 6 for analysis.

RUNX1/ETO knockdown level after 3 days of treatment in PDX1 and PDX2 was 40% (Fig 3-29A). However, the knockdown on the protein level was greater in PDX2. PDX1 had 25% reduction in RUNX1/ETO protein level and PDX2 has 80% reduction (Fig 3-29B). RUNX1/ETO direct target genes were also affected after the knockdown, for example, CCND2 protein was reduced to 43% in PDX1 and completely depleted in PDX2 (Fig 3-29B).

RUNX1/ETO knockdown in PDX1 caused changes in RUNX1/ETO target genes. The mRNA level of *RUNX1/ETO* recovered partially 6 days after treatment where only 25% of knockdown was detected by qRT-PCR (Fig 3-29C). However, the fusion downstream targets were greatly changed at day 6 in comparison with day 3. The knockdown led to over 90% reduction in *ANGPT1* transcript level 6 days after treatment. Moreover, RUNX1/ETO-repressed genes were upregulated with LNP/siRNA treatment, for instance, *CEBPA* and *LAPTM5* increased 150 % and 130%, respectively on day 6 (Fig 3-29C).

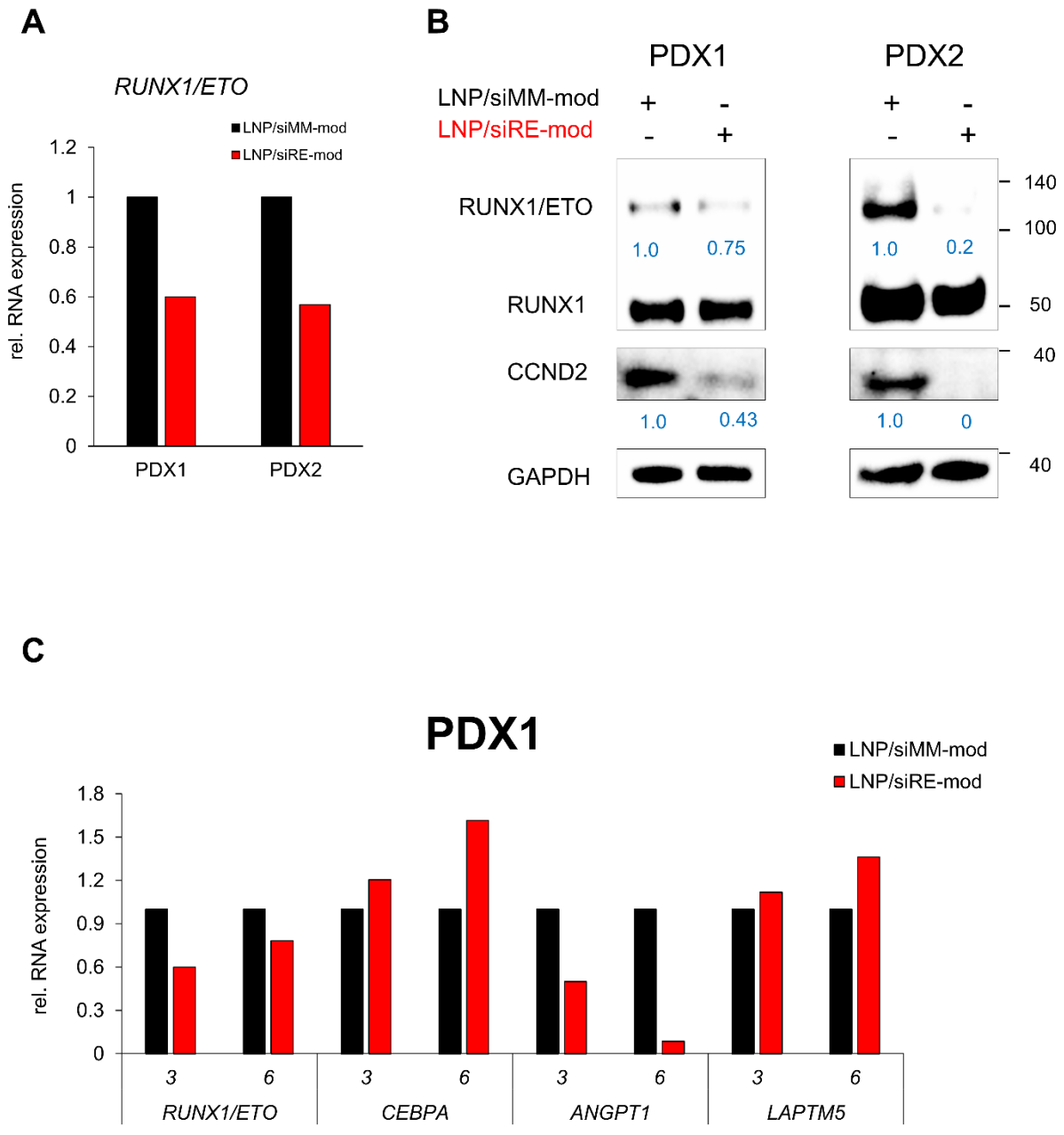

Fig 3-29: *RUNX1/ETO* knockdown in t(8;21) PDXs. AML t(8;21) PDXs cells were seeded on MSCs feeders. On the next day, 2 µg/ml LNP/siRNA were added, and AML cells were harvested on days 3 and 6. (A) *RUNX1/ETO* mRNA expression on day 3 was normalised to the LNP/siMM-mod control and *GAPDH* served as a housekeeping gene. (B) Western blotting showing the protein level on day 3 for RUNX1/ETO and CCND2, membrane was incubated with α-RUNX1 antibody, α-CCND2, and α-GAPDH loading control. (C) The mRNA level of *RUNX1/ETO* and its target genes in PDX1 on days 3 and 6. The expression level was normalised to the LNP/siMM-mod control and *GAPDH* served as a housekeeping gene (n=1).

3.5 Results summary and analysis

RNAi-mediated gene knockdown using transient siRNA transfection is efficient in AML cell lines *in vitro*, however, gene knockdown in primary or PDX cells as well as *in vivo* is typically more challenging. Implementation of siRNA in the clinic faces several challenges such as; low intracellular and extracellular stability, poor pharmacokinetics, TLR immuno-stimulation, and the off-target silencing (Zimmermann, Lee et al. 2006, Shimizu, Kida et al. 2008, Hernandez, Stockdale et al. 2012, Huang, Cheng et al. 2016). This PhD project was designed to overcome the siRNA associated pharmacological challenges, and explore the therapeutic benefits of interfering with the fusion gene *RUNX1/ETO.*

The PhD project was designed to follow sequentially three main steps. The first part of the project was introducing chemical modifications to maximise the siRNA knockdown efficiency. The second step was to encapsulate the siRNA into a non-toxic delivery vehicle that allows *in vivo* systemic administration. The vehicle should also protect the siRNA from degradation, improve the circulation time, provide a window for targeted tissue accumulation and uptake, and stimulate the endosomal escape. The final step was to study the effect of the knockdown on a xenotransplantation model of AML.

Combination of several well-established chemical modifications on both strands of *RUNX1/ETO* siRNA led to a robust depletion of the RUNX1/ETO fusion in the mRNA and protein levels. The modified siRNA also demonstrated a stronger effect on modulating RUNX1/ETO transcriptional network in comparison with the unmodified siRNA. Modulation of *RUNX1/ETO* expression by modified siRNA yielded stronger effects on inhibiting proliferation, induction of G0/G1 cell cycle arrest, initiating cellular senescence, and reducing clonogenicity. Colony formation replating experiments showed that depletion of *RUNX1/ETO* has a long-lasting effect, which proves the importance of RUNX1/ETO on self-renewal.

Following the validation of the siRNA modifications, the modified siRNA and the mismatch control were encapsulated into a Dlin-MC3-DMA lipid nanoparticle. That work was carried out at Dr. Heuser lab in Hannover (Germany) using a microfluidic packaging system (NanoAssemblr, Precision NanoSystems) (Leung, Hafez et al.

2012, Jyotsana, Sharma et al. 2018). The encapsulation efficiency of the siRNA was high and the LNP/siRNAs parameters were reproducible. Long storage did not affect the nanoparticles' parameters or compromise the siRNA efficacy. The size and charge of LNP/siRNAs were optimal for *in vitro* gene knockdown and allowed rapid and robust modulations of *RUNX1/ETO* expression and its target genes with minimal toxicity.

A co-culture system has already been established in our lab for primary and primograft ALL cells expansion *ex vivo (Pal, Blair et al. 2016)*. Due to the limited number of cells in the t(8;21) primaries and PDXs experiments, there was no proper characterisation of cell proliferation. Nevertheless, the MSCs feeders were able to support the expansion of PDXs and did not impair the gene knockdown.

The lipid nanoparticle demonstrated the ability to a achieve strong gene knockdown in two t(8;12) patient primary cells in the co-culture system. LNP/siRNA was also potent in reducing *RUNX1/ETO* expression and modulating its transcriptional network in t(8;12) PDXs in the mRNA and protein levels.

Confirming a robust knockdown of *RUNX1/ETO* with the modified siRNA and LNP/siRNA *in vitro* and in *ex vivo* in co-culture, made the targeting of *RUNX1/ETO in vivo* feasible. LNP/siRNA was taken forward for the *in vivo* studies in a xenotransplantation model of t(8;21) AML.

Chapter 4.

In vivo knockdown of *RUNX1/ETO* in t(8;21) xenotransplantation model

4.1 Introduction

Previous studies in our group proved the role of the oncoprotein RUNX1/ETO in initiating and maintaining the propagation of leukaemia in t(8;21) AML cell lines *in vitro.* The transcription factor RUNX1/ETO interferes with RUNX1 transcriptome leading to activation of self-renewal genes and repression of myeloid differentiation programmes (Ptasinska, Assi et al. 2012, Loke, Assi et al. 2017). It was also found that RNAi-depletion of *RUNX1/ETO in vitro* upregulates *CEBPA* expression, alleviating the myeloid differentiation block (Martinez, Drescher et al. 2004). Furthermore, *in vitro* studies demonstrated that transient depletion of *RUNX1/ETO* by siRNA (siRE), administered by electroporation, in Kasumi-1 cells significantly increased the median survival of transplanted mice, and enhanced the median survival by 50% from 64 to 90 days (Soria, Tussiwand et al. 2009).

The knockdown experiments utilising chemically modified siRNA encapsulated into nanoparticles proved robust RUNX1/ETO repression *in vitro*. The next step of this project was to assess the potency of LNP/siRNA *in vivo* and investigate the therapeutic benefits of the knockdown using the modified version of siRNA. *In vivo* experiments were carried out in a xenotransplantation model for Kasumi-1 cells in the immunodeficient $Rag2^{-/-}$ $\gamma C^{-/-}$mice. In order to assess leukaemic burden and engraftment *in vivo*, transplanted Kasumi-1 cells were stably transduced with the p.SLIEW vector allowing for a continuous expression of firefly luciferase (*Luc*) and green fluorescent protein (*eGFP*) genes. Kasumi-1 p.SLIEW cells were previously generated and validated (Bomken, Buechler et al. 2013). In the mouse transplantation model, Kasumi-1 cells usually do not engraft in the bone marrow, and occasionally the spleen is 3 to 10-fold enlarged. The usual engraftment of Kasumi-1 cells, however, results in forming extra-medullary tumours in the abdominal. Harvested cells from these tumours mainly express the human markers CD45, CD33, and CD34. For these reasons, the *in vivo* model is suitable to investigate the LNP/siRNA treatment effect on Kasumi-1 cells.

4.2 Aim

The second aim of the PhD was silencing *RUNX1/ETO* expression *in vivo* in xenotransplantation model of t(8; 21) AML to:

1. Study the pharmacodynamics of LNP/siRNA in Rag2$^{-/-}$ γC$^{-/-}$ mice upon systemic administration.
2. Prove the on-target RUNX1/ETO knockdown in leukaemic cells.
3. Determine the survival benefits after *RUNX1/ETO* depletion.
4. Investigate the effect of repressing RUNX1/ETO *in vivo* on self-renewal and differentiation.

4.3 Experimental design

4.3.1 t(8,21) AML murine models

Three different t(8;21) leukaemia murine models were used during the project. The xenotransplantation model for Kasumi-1 cell line was performed in Rag2$^{-/-}$ γC$^{-/-}$ mice. The RL048 and CC209 t(8;21) PDXs were generated in NSG and MISTRG mice, respectively.

Rag2$^{-/-}$ γC$^{-/-}$ immunodeficient mice are suitable to host human haematopoietic cells because they do not exhibit B and T cells due to the loss of *Rag2* gene. The IL-2 receptor gamma chain knockout (γC$^{-/-}$) also ensures the profound T cell defect by eliminating the cytokines receptors IL-2, IL-4, IL-7, IL-9 and IL-15 and consequently rendering NK cells activation (Sugamura, Asao et al. 1996). Moreover, Rag2$^{-/-}$ γC$^{-/-}$ mice have normal haematopoietic parameters such as red blood cells, white blood cells, haemoglobin and platelets (Ohbo, Suda et al. 1996, Mazurier, Fontanellas et al. 1999). We performed intrahepatic transplantation of Kuasmi-1 cells in newborn Rag2$^{-/-}$ γC$^{-/-}$ mice because the liver in young mice resembles a suitable niche for leukaemia engraftment (Cheung, Fung et al. 2010).

NSG mice are immunodeficient with mutation in the DNA repair complex protein (*Prkdc)* gene, which impairs B and T cells development and leads to a severe combined immunodeficiency genotype (SCID). The mice also have a complete knockout of the IL-2 receptor gamma chain. The immunodeficient NSG mice support the engraftment of CD34+ haematopoietic stem cells as well as leukaemic cells taken directly from the patients (Ito, Hiramatsu et al. 2002, Andre, Erbacher et al. 2010).

The humanised MISTRG mice carry the Rag2$^{-/-}$ γC$^{-/-}$ immunodeficiency, and they express the human version of several cytokines necessary for development of the innate immune system. MISTRG mice express M-CSF, IL-3, GM-CSF, and THPO. Moreover, these mice also have the human SIRPα-encoding BAC transgene, in which the binding of SIRPα to CD47 enables the murine phagocytes to accept the engrafted human cells. MISTRG mice are highly permissive for human haematopoiesis and were reported to support the engraftment of AML patient-

derived xenografts (Rongvaux, Willinger et al. 2014, Saito, Ellegast et al. 2016, Wunderlich and Mulloy 2016).

4.3.2 Pharmacokinetics of LNP/siRNA in Rag2$^{-/-}$γC$^{-/-}$ mice

In order to monitor the biodistribution of the lipid nanoparticles *in vivo*, we have labelled the nanoparticles with a near-infrared (NIR) fluorescent dye called SulfoCyanine7.5 as described in 2.2.9. The labelled nanoparticles, hereinafter, LNP/siRNA-SulfoCyanine7.5 were formulated twice and tested in two independent pharmacokinetics (PK) studies.

The first PK experiment (Fig 4-1) consisted of four Rag2$^{-/-}$ γC$^{-/-}$ mice transplanted with Kasumi-1 p.SLIEW. The targeted group contained three mice and one mouse served as a control. Upon confirmation of engraftment by IVIS, mice were intravenously (IV) injected with 0.5 mg/ml (~ 50 µl) LNP/siRNA-SulfoCynanine7.5. The control mouse received 50 µl of the control vehicle (10% SulfoCyanine7.5/PBS) by tail injection. *In vivo* imaging by IVIS was performed 2, 4, 6, 24, 48, and 120 hours post injection. At day 5, mice were culled and IVIS imaging was performed on harvested tumours and organs.

For the second PK experiment (Fig 4-2) four mice were used. All mice were transplanted with Kasumi-1 p.SLIEW cells followed by IVIS to assess to assess the engraftment. Mice were then injected by intraperitoneal (IP) route with unlabelled LNP/siRNA (not carrying the SulfoCyanine7.5 dye). Each mouse received 1 mg/ml of LNP/siRNA per day for three consecutive days. On day 4, three mice were given one IV injection of 0.5 mg/ml (~ 50 µl) LNP/siRNA-SulfoCyanine7.5. The control mouse was injected with 50 µl 10% SulfoCyanine7.5/PBS. IVIS was performed 1, 4, 24, and 72 hours post injection. On DAY 3, mice were culled, tumours and organs were imaged by IVIS.

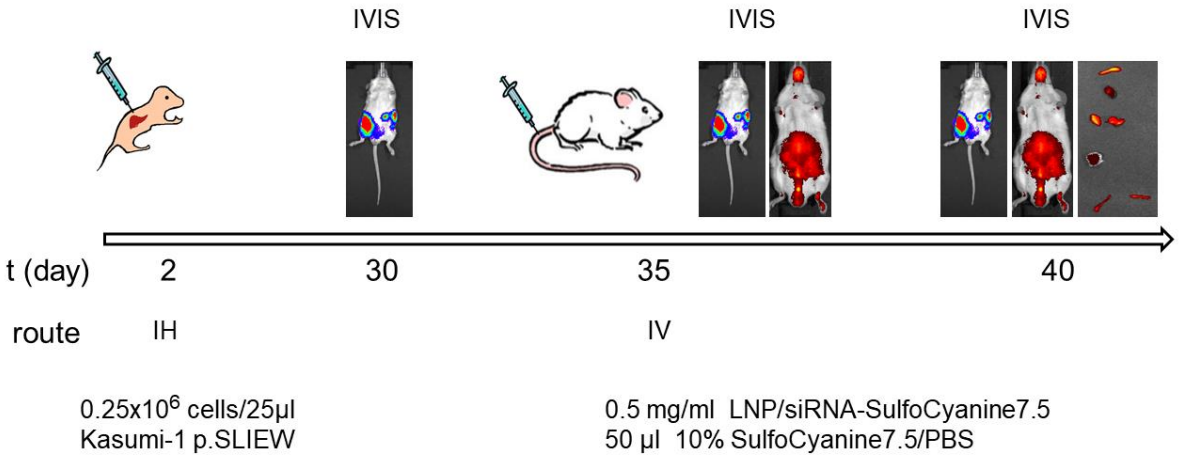

Fig 4-1: Experimental set up: Lipid nanoparticles pharmacokinetics in *vivo*, first PK study. Newborn Rag2$^{-/-}$ γC$^{-/-}$ mice were transplanted with Kasumi-1 p.SLIEW cells and engraftment was assessed by IVIS. Three mice were injected with 0.5 mg/ml of LNP/siRNA-SulfoCyanine7.5. The control mouse was injected with 50 µl of 10% SulfoCyanine7.5/PBS. Fluorescent and bioluminescence imaging were performed after 2, 4, 6, 24, 48, and 120 hours. Five days after LNP/siRNA-SulfoCyanine7.5 injection, mice were culled and harvested tumours and organs were imaged by IVIS.

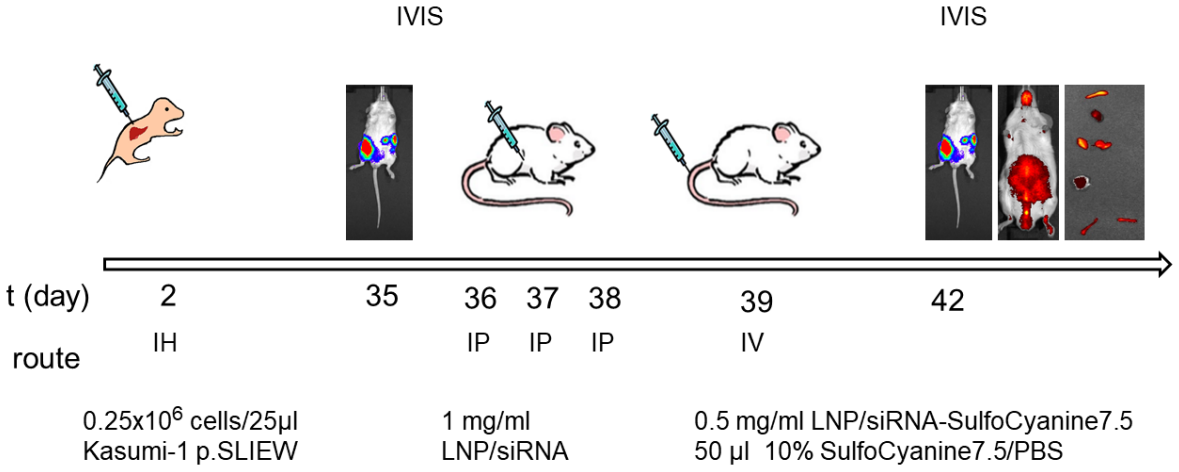

Fig 4-2: Experimental set up: Lipid nanoparticles pharmacokinetics in *vivo*, second PK study. Newborn Rag2$^{-/-}$ γC$^{-/-}$ mice were transplanted with Kasumi-1 p.SLIEW cells and engraftment was assessed by IVIS. Mice were treated with 3 consecutive doses of 1 mg/ml of LNP/siRNA every 24 hours. On the fourth day, mice were injected with 0.5 mg/ml of LNP/siRNA-SulfoCyanine7.5 or 50 µl of 10% SulfoCyanine7.5/PBS. Fluorescent and bioluminescence imaging were performed after 1, 4, 24, and 72 hours. After 3 days of injection, mice were culled and harvested tumours and organs were imaged by IVIS.

4.3.3 In vivo knockdown experiments

Gene knockdown *in vivo* was performed in a xenotransplantation model of Kasumi-1 cells in Rag2$^{-/-}$ γC$^{-/-}$ mice. In brief, Kasumi-1 p.SLIEW cells stably expressing luciferase (*Luc*) and *eGFP* were injected intrahepatically in newborn mice as described in 2.3.1. After waning, IVIS imaging was performed to confirm the engraftment of leukaemic cells by biochemiluminescence assay as described in 2.3.6.

During the project, four independent LNP/siRNA formulations were used in four *in vivo* experiments. Each *in vivo* experiment consisted of two arms,

I. Control arm, nanoparticles encapsulating mismatch siRNA.
II. *RUNX1/ETO* targeted treatment arm, nanoparticles encapsulating the modified si*RUNX1/ETO*.

In the first three experiments, after confirming the engraftment by IVIS, mice were treated with LNP/siRNA by IV route. In the fourth experiment, mice were treated by IP route three days after transplantation. The doses and treatment schedules are shown in figures Fig 4-3, Fig 4-4, Fig 4-5, and Fig 4-6.

Leukaemic burden was assessed by IVIS and mice were culled when they reached any of the protocol endpoints stated in 2.3.1. The endpoints for mice under treatment were:

1. Body weight loss of 30% or more.
2. Body weight loss of 10 – 20% and maintained low for three consecutive days.
3. Tumour size is 1.5 cm or more in any dimension.
4. The tumour is affecting the movement or feeding.
5. Any sign of sickness that is severely affecting the health of the mouse.

The numbers of mice required during the animal studies were determined using two different approaches. The resource equation approach was followed in the first three *in vivo* experiments. That is because there was no prior information about the predicted level of *RUNX1/ETO* knockdown or the effectiveness of nanoparticles treatment. The power calculation was used to determine the size of the cohort needed for the survival experiments.

Based on the resource equation method, the acceptable degree of freedom (DF) for the error when using ANOVA analysis is 10 to 20. The *in vivo* experiments consisted of two treatment groups and the predicted readout were quantitative variables, such as IVIS signals or gene expression. Given that these experiments aimed to compare the effect of the treatment between the two groups, the collected data can be analysed by one-way ANOVA or independent student *t*-test (Festing and Altman 2002, Charan and Kantharia 2013). Thus, animal numbers were calculated as follow:

$$n = \frac{DF}{k} + 1$$

Where; n = number of animals per group, DF = 10 or 20 to calculate the minimum or maximum number of animals, and K = number of groups.

The maximum $n = \frac{20}{2} + 1 = 11$

The minimum $n = \frac{10}{2} + 1 = 6$

The total number of animals needed for the knockdown experiments should be between 12 to 22 mice, with at least 6 mice per group.

The survival experiment consisted of four treatment arms. The power calculation was performed using the following formulas,

$$n = \frac{1}{pA*pB*pC*pD*pE}\left(\frac{Z_{1-a}+ Z_{1-\beta/2}}{\delta-|ln(\theta)|}\right)^2$$

$$1 - \beta = 2\Phi(z - z_{1-a}) - 1$$

$$z = (\delta - |\ln(\theta)|)\sqrt{n * pA * pB * pC * pC}$$

Where; θ is the hazard ratio. We have considered θ = 0.24 based on former work in our group showed that *in vitro* knockdown of *RUNX1/ETO* reduced the hazard of death of transplanted mice by 76% (Soria, Tussiwand et al. 2008).

pA,pB,pC and pD are the proportions of the group size allocated to the four groups.

We have considered pA = pB = pC = pD = 0.25

pE is the overall probability of the event. The readout was survival, thus the probability is pE = 0.5 where at each time point the mouse is either live or dead.

Φ is the standard normal distribution function.

1 – β is the power and we have considered 1 – β = 0.8

δ is the testing margin. In our experiment we have considered δ = -2.

The power and testing margin values were considered from the literature and former work in our lab (Charan and Kantharia 2013, Martinez-Soria 2018).

After applying the aforementioned equations and values in RStudio, the minimum number of animals per group was found to be 7. Thus, the survival experiment consisted of 28 mice.

The xenotransplantation model was generated by injecting leukaemic cells in newborn mice. The first *in vivo* experiment consisted of 9 mice instead of 12 because the allocated letters for the experiment did not provide the needed number of animals. The following table (Table 4-1) shows the number and gender of mice used throughout the four experiments.

Experiment	**Control group**	***RUNX1/ETO* targeted group**	**Total number**
1st *in vivo*	3 females & 1 male	3 females & 2 males	9
2nd *in vivo*	5 females & 1 male	4 females & 2 males	12
3rd *in vivo*	2 females & 5 males	3 females & 5 males	15
4th *in vivo*	8 females & 6 males	8 females & 6 males	28

Table 4-1: Animal number and gender distribution throughout the *in vivo* experiments.

At the end of each experiment, Kasumi-1 p.SLIEW cells from treated mice were harvested and frozen as viable cells as described in 2.3.7 and 2.2.1. During the *ex vivo* proliferation assay and colony formation, 1% penicillin/streptomycin (P/S) antibiotic was added to the media. The RNA and protein expression of RUNX1/ETO and its target genes were quantified in qRT-PCR and Western blotting.

4.3.4 Self-renewal assays

In order to investigate the effect of *RUNX1/ETO* depletion *in vivo* on the self-renewal, harvested cells where either seeded for *ex vivo* colony formation assay or retransplanted into new recipients mice.

Two independent secondary retransplantation experiments were conducted using harvested cells from the third *in vivo* experiment as shown in Table 4-2. In the secondary retransplantations, Kasumi-1 p.SLIEW cells were injected into newborn $Rag2^{-/-}$ $\gamma C^{-/-}$ mice as described in 2.3.1 (Fig 4-5).

Mice were dosed with LNP/siRNA as shown in (Fig 4-5). The first secondary retransplantation experiment was carried out three days after finishing the LNP/siRNA treatment. During this experiment, two mice were used from each treatment group, and harvested Kasumi-1 p.SLIEW cells from treated mice were transplanted into two litters (2 and 5 days old). The second retransplantation experiment was performed at a later time point using frozen cells from treated mice. Kasumi-1 p.SLIEW cells were thawed, two from each treatment arm, and transplanted into one litter (2 days old).

	Primary treated mice (third *in vivo* experiment)			**Recipient mice**		
Experiment date	**Treatment arm**	**No. mice**	**Gender**	**No. litters**	**No. mice**	**Gender**
05.07.17	LNP/siMM	2	1 Male 1 Female	2	4	2 Males 2 Females
	LNP/siRE-mod	2	2 Males		4	2 Males 2 Females
20.02.18	LNP/siMM	2	2 Males	1	4	1 Male 3 Female
	LNP/siRE-mod	2	1 Male 1 Female		4	2 males 1 Female

Table 4-2. Secondary transplantation experiment.

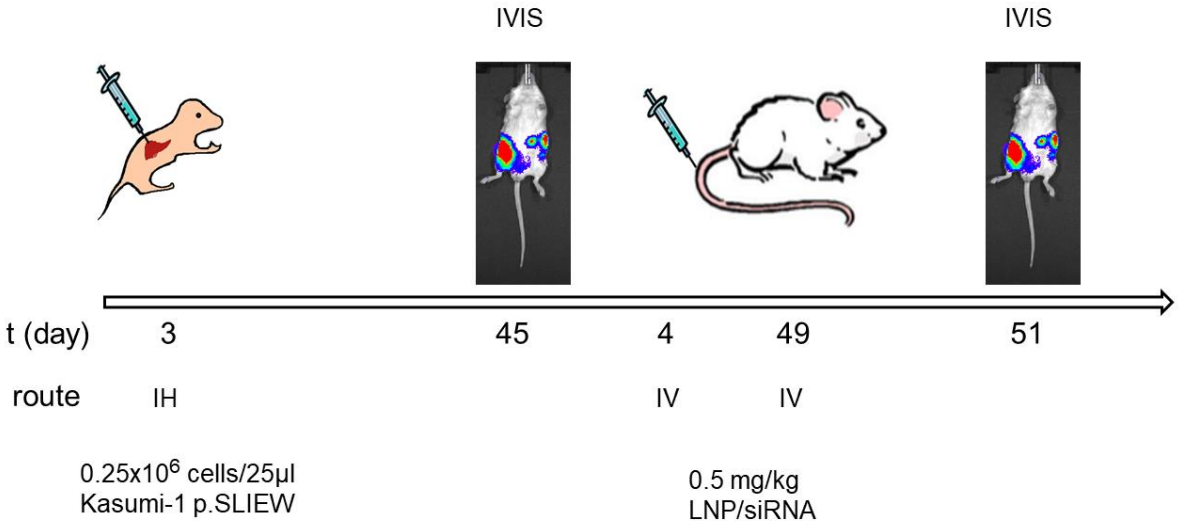

Fig 4-3: Experimental set up of the first *in vivo* experiment. Nine newborn Rag2$^{-/-}$ γC$^{-/-}$ mice were transplanted intrahepatically with Kasumi-1 p.SLIEW cells. After 6 weeks, engraftment was assessed by IVIS and mice were randomised into two groups, *RUNX1/ETO* targeted group received LNP/siRE-mod treatment and control group received LNP/siMM treatment. Mice were IV dosed with 0.5 mg/kg of LNP/siRNA twice. Leukaemia burden was assessed by IVIS throughout the experiment and mice were culled when they reached any of the protocol endpoints described in 4.3.3.

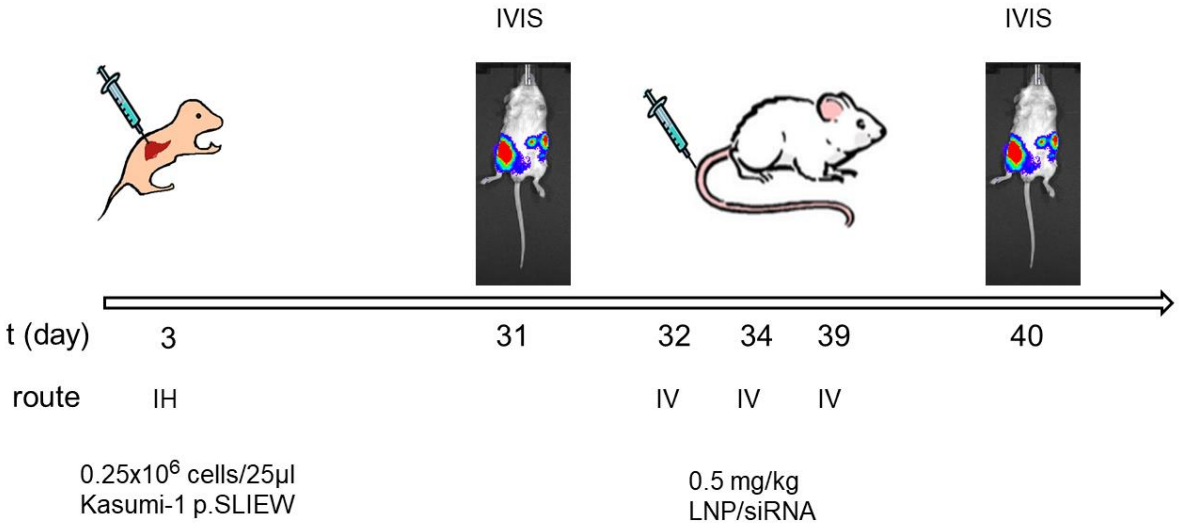

Fig 4-4: Experimental set up of the second *in vivo* experiment. Twelve newborn Rag2$^{-/-}$ γC$^{-/-}$ mice were transplanted, randomised and treated as described in Fig 4-3. Mice were dosed by three IV inactions of 0.5 mg/kg of LNP/siRNA, and leukaemia burden was assessed by IVIS and mice were culled when they reached any of the protocol endpoints.

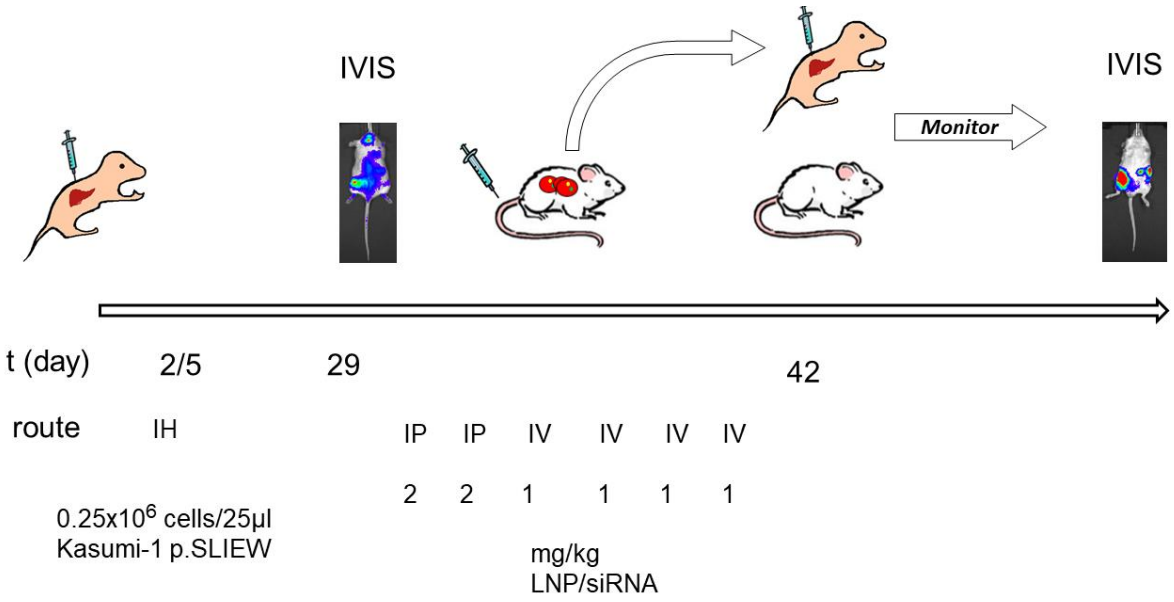

Fig 4-5: Experimental set up of the third *in vivo* experiment. Fifteen newborn Rag2$^{-/-}$ γC$^{-/-}$ mice were used for the experiment following the same setting as described in Fig 4-3. LNP/siRNA was administered by two routes as shown in the scheme. Mice received 2 x IP doses of 2 mg/kg followed by 3 x IV doses of 1 mg/kg of LNP/siRNA. Three days after finishing the treatment, two mice from each group were culled and harvested cells were retransplanted into new recipients as described in 4.3.4. Mice were imaged by IVIS to assess leukaemia burden and culled when they reached any of the protocol endpoints.

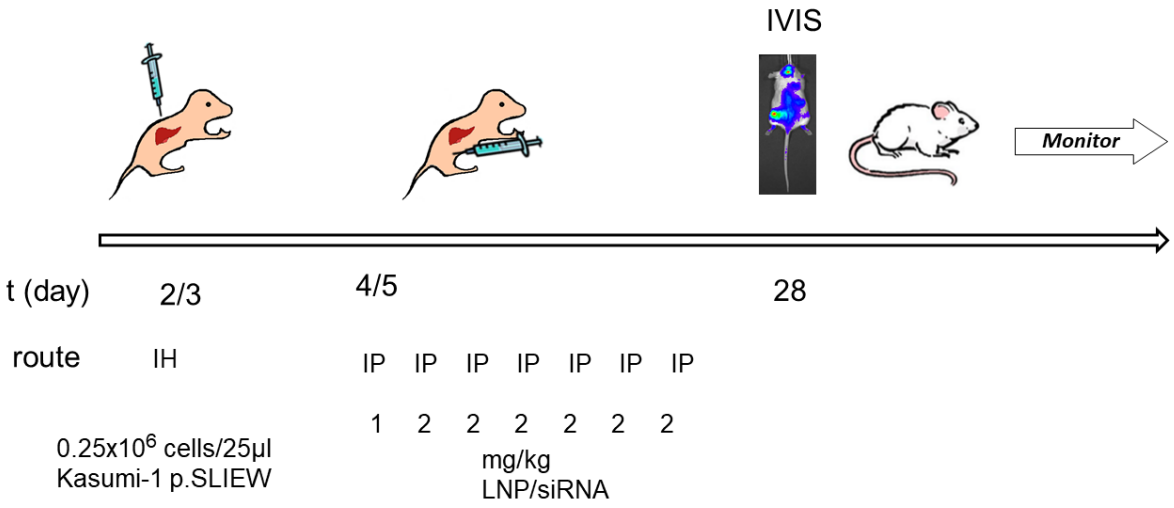

Fig 4-6: Experimental set up of the fourth *in vivo* experiment. Twenty-eight newborn Rag2$^{-/-}$ γC$^{-/-}$ mice were intrahepatically transplanted with Kasumi-1 p.SLIEW cells followed by lipid nanoparticles treatment by IP route as indicated in the scheme above. The *RUNX1/ETO* targeted group (14 mice) was treated with LNP/siRE-mod and the control group (14 mice) was treated with LNP/siMM-mod. Mice were monitored and leukaemia expansion was assessed by IVIS imaging. Mice were culled when they reached any of the protocol endpoints.

4.4 Results

4.4.1. Pharmacokinetics of LNP/siRNA in Rag2$^{-/-}$ γC$^{-/-}$

The lipid mixture contained a fluorescent dye, DiI, which is not suitable for *in vivo* imaging. That is because the fluorescence spectrum of DiI overlaps with the autofluorescence of mice tissue preventing accurate quantification of the emitted signal. For this reason, the lipid nanoparticles were labelled with SulfoCyanine7.5, a NIR dye, which is compatible with *in vivo* imaging.

There is not any published protocol for click chemistry reaction on the surface of lipid nanoparticles. For this reason we have optimised a protocol for labelling the lipid nanoparticles as described in 2.2.9. First, the click reaction components were assigned to the lipid mixture and the dye. The NIR dye was obtained as a SulfoCyanine7.5 alkyne, and a new molecule (DSPE-PEG2000-N3) was introduced to the lipid mixture before performing the LNP/siRNA formulation. DSPE-PEG2000-N3 contains a phospholipid part, the DSPE, and a polyethylene glycol bearing a terminus azide group (PEG2000-N3). The azide group can readily react with alkyne to form a stable triazole.

Given the amphiphilic properties of DSPE-PEG2000-N3, during the siRNA packaging in the lipid nanoparticles, the DSPE is entrapped in the hydrophobic layer, and the PEG2000-N3 is oriented either towards the surface or the hydrophilic centre. The DSPE-PEG2000-N3 was added at 0.3% mol ratio to the lipid mixture, which means its theoretical concentration in the LNP/siRNA solution is 300 µM. The lipid nanoparticle has a solid core of tightly packed hydrophilic pocket encapsulating the siRNA. For this reason, some of the PEG2000-N3 might be present in those pockets rather than on the surface. Taken together, the concentration of free azide groups on the LNP/siRNA surface was speculated to be around 50 µM.

Following the procedures described in 2.2.9, the click reaction was performed by dissolving $CuCl_2$ to a 0.5 mM in a solution of 50% DMSO in H_2O. A final mixture of ascorbic acid, LNP/siRNA and SulfoCyanine7.5 alkyne was mixed in a 1.5 Eppendorf tube and heated for 20 minutes at 40°C then the $CuCl_2$ solution was added to the mixture and left in the Eppendorf tube overnight at 25°C in the dark. Next day, the labelled LNP/siRNA was dialysed using 3,500 MWCO dialysis tubes

against PBS at 4°C. The dialysis was performed in the dark overnight, and the PBS was changed three times. After completion of the dialysis, the size and charge of LNP/siRNA-SulfoCyanaine7.5 were determined by Zetasizer. The colour of the labelled nanoparticles became green/blue which is the same colour of SulfoCyanaine7.5 dye. Elimination of the copper or ascorbic acid form the click reaction served as negative controls. Under these conditions, we did not observe any changes in the colour of the nanoparticles after dialysis, meaning the click reaction did not happen. Addition of the NIR dye to the LNP/siRNA did not significantly affect the diameter of particles, but the polydispersity (PDI) of the practices increased by twofold (Fig 4-7A, B). Moreover, the zeta potential became slightly more negative (Fig 4-7C).

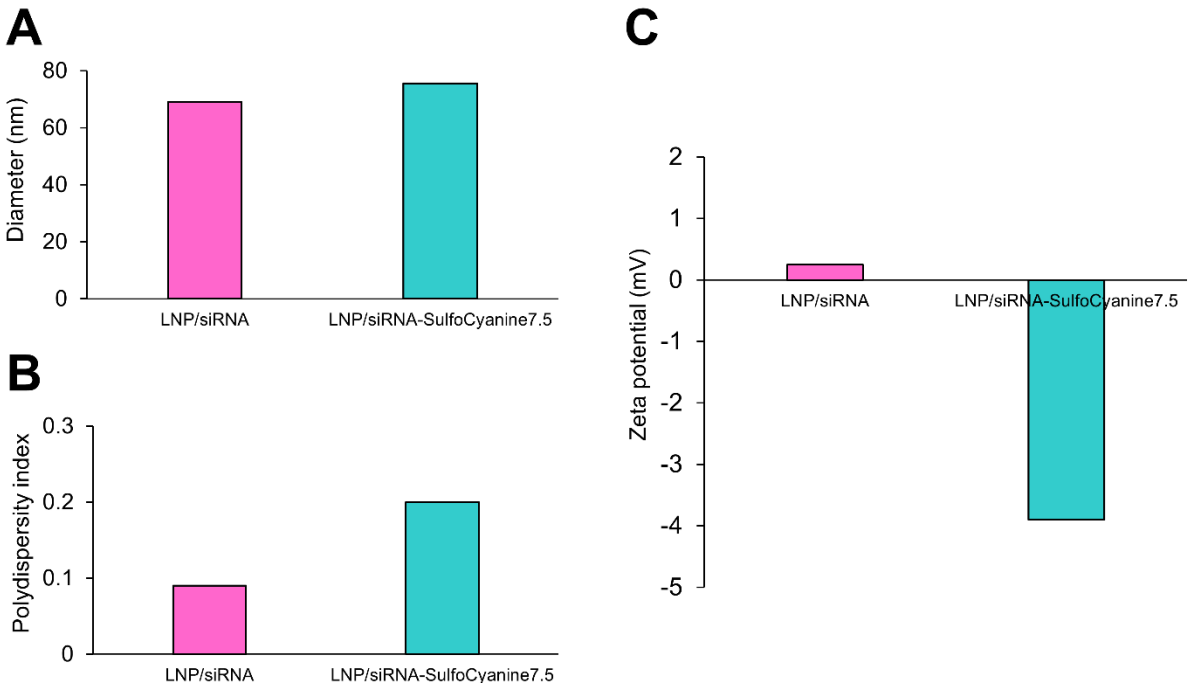

Fig 4-7: LNP/siRNA parameters before and after labelling with NIR dye. Measurements of the dynamic light scattering in Zetasizer of nanoparticles before and after performing the click reaction. (A) The diameter of the nanoparticles measured in nm scale in the Y-axis. (B) Changes in the polydispersity of the nanoparticle mixture after the click reaction. (C) Surface charge of the nanoparticles measured as a zeta potential in mV. All measurements were performed at 25°C after one-minute temperature calibration.

The Zetasizer measurements showed that the labelled nanoparticles (LNP/siRNA-SulfoCyanine7.5) have suitable diameter and charge for *in vivo* treatment. The first PK study showed that a single intravenous injection of the nanoparticles provided a global body distribution. The nanoparticles accumulated in the liver after 2 hours of the intravenous injection. The mean of the fluorescence of treated mice liver remained higher than the untreated control until day 3 (Fig 4-8A).

In the second PK study, pre-treatment with unlabelled LNP/siRNA was applied for continues three days to saturate the liver with the nanoparticles. Unexpectedly, upon intravenous injection of labelled nanoparticles, the liver fluorescence signal was twofold higher than the control. This means that the liver remained the first target of labelled nanoparticles despite the pre-treatment (Fig 4-8B).

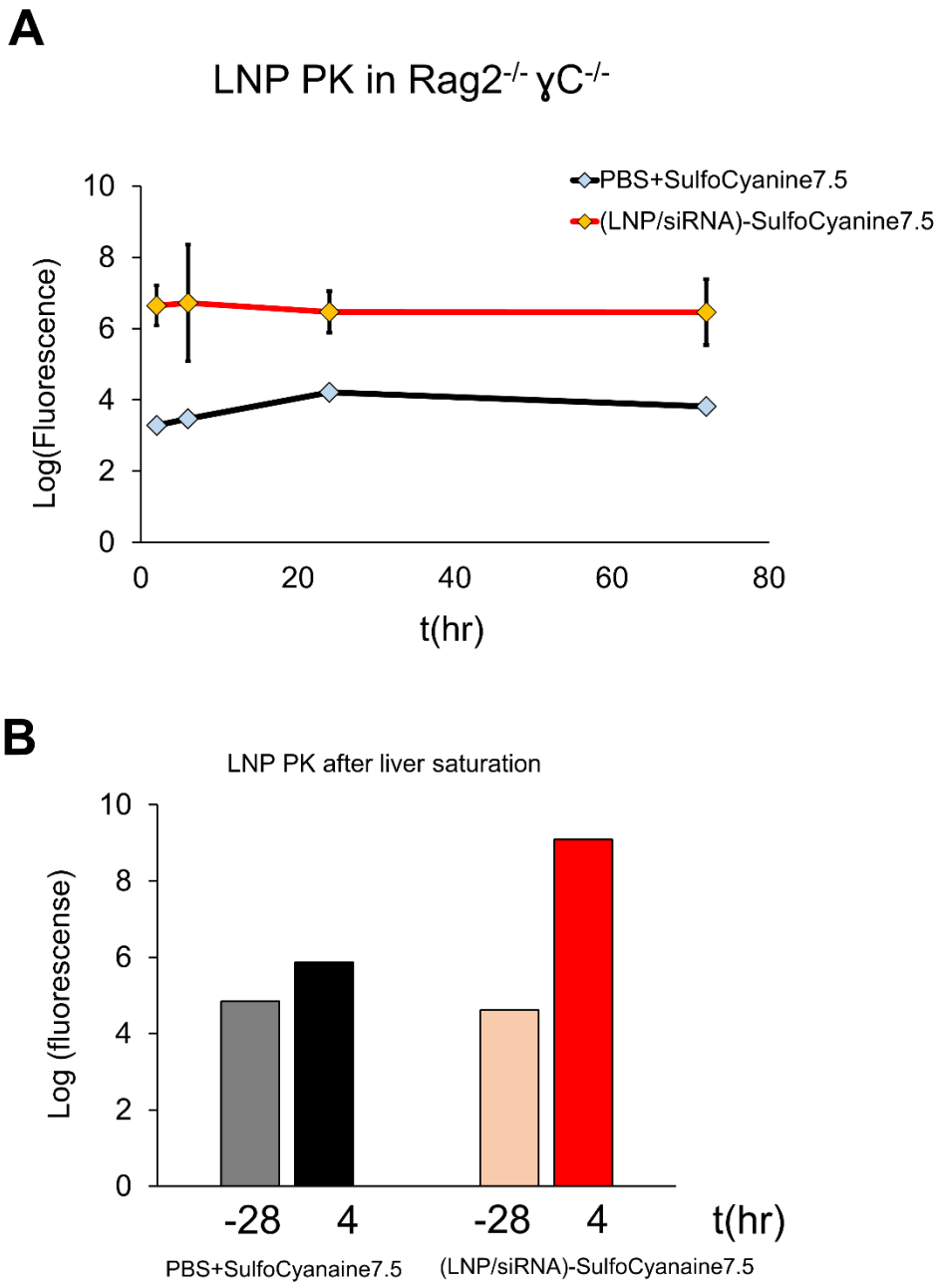

Fig 4-8: Liver uptake of the lipid nanoparticles. Analysis of fluorescence from Rag2$^{-/-}$ γC$^{-/-}$ mice treated with labelled nanoparticles. (A) Mice treated with labelled nanoparticles had threefold higher fluorescence signal than the control mouse. Data represent the mean of the NIR fluorescence of the liver of three mice in the targeted group and the fluorescence signal of the liver of the control mouse. Error bars represent the SEM of the fluorescence of three mice. (B) The liver remains the main target of the nanoparticles even after saturation with the nanoparticles. Mice were pre-treated with unlabelled nanoparticles to saturate the liver followed by IV injection of the labelled nanoparticles. Data represent the total fluorescence signal of the liver 4 hours after the IV injections showing higher uptake of the labelled nanoparticle in the targeted mouse. The baseline measurement was performed 24 hours before the IV injection and shows that both groups have a comparable fluorescence.

Furthermore, the labelled nanoparticles accumulated in the tumours after intravenous administration (Fig 4-9). Upon injection of luciferin, the bioluminescence signal overlapped with the fluorescence signal in the site of the tumours. In order to eliminate any emission from the luciferase activity into the NIR channel, the fluorescence image was acquired before injection of luciferin and recording the bioluminescence signal.

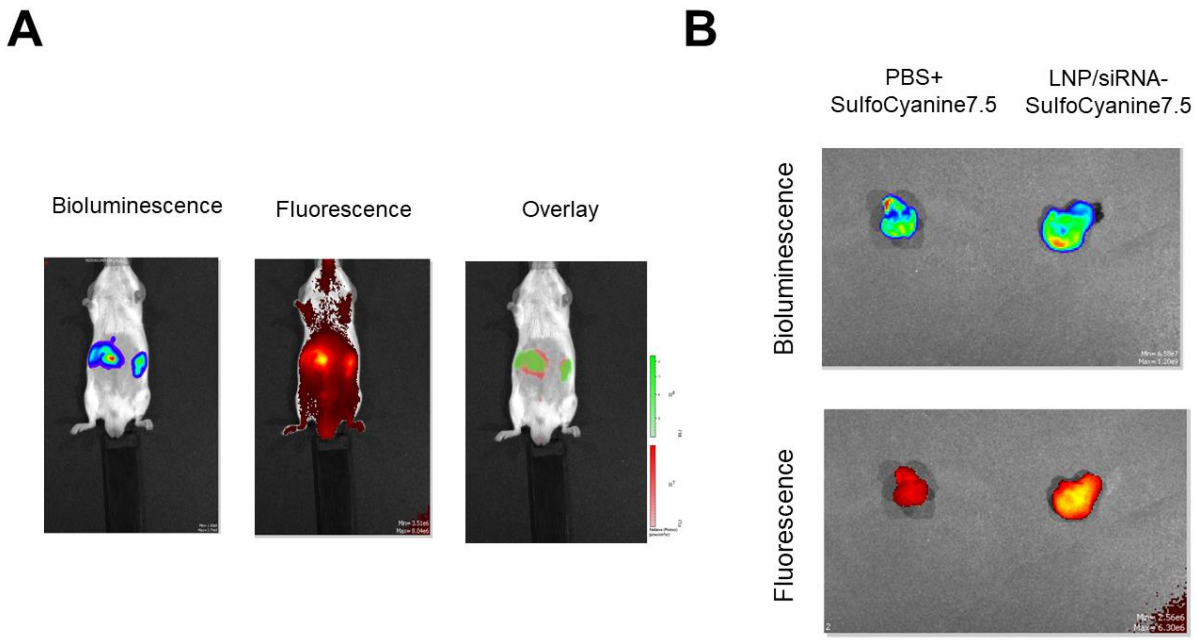

Fig 4-9: Accumulation of the LNP/siRNA in the tumour site. Mice were treated with the nanoparticles as described in scheme Fig 4-2. IVIS images show that the labelled nanoparticles reach the tumour site. (A) IVIS images demonstrate that the bioluminescence signal of the tumour colocalises with the fluorescence of the labelled nanoparticles. Scales are photons/second. (B) Harvested tumours confirmed the accumulation of the labelled nanoparticles on the tumour.

Even though the liver was mostly the main target of the nanoparticles, IVIS imagining showed that the nanoparticles were detectable in several organs. LNP/siRNA-SulfoCyanine7.5 were trapped in the spleen, kidneys, lungs, and heart. The IVIS imaging was able to detect the fluorescence signal in the spine, bones and the brain (Fig 4-10).

IVIS imagining cannot confirm that the fluorescence source is the bone marrow. The nanoparticles could be present in the periosteum membrane covering the bone surface. The excitation wavelength of SulfoCyanine7.5 dye is in the NIR channel. For this reason, it was not feasible to use flow cytometry or fluorescence microscopy to detect the labelled particles *ex vivo*.

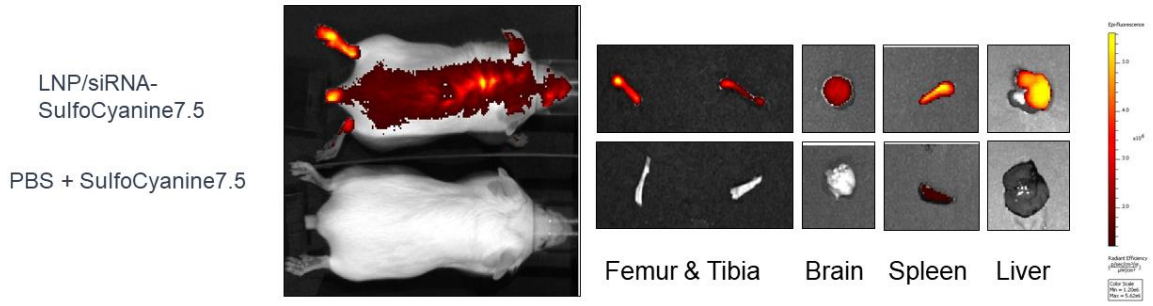

Fig 4-10: Pharmacokinetic of LNP/siRNA in Rag2$^{-/-}$ γC$^{-/-}$ mice. Mice were transplanted with Kasumi-1 p.SLIEW cells and treated with the nanoparticles as described in Fig 4-2. Fluorescence images show that the nanoparticles can be detected in several haematological compartments such as the liver, spleen, bones, and the brain.

4.4.2. LNP/siRNA mediated RUNX1/ETO knockdown in vivo

The pharmacokinetic experiments confirmed that the nanoparticles have global body distribution *in vivo,* and they can potentially reach the tumour site, bones, and CNS upon systemic administration. The gene knockdown was investigated after LNP/siRNA IV treatment in the Kasumi-1 p.SLIEW transplantation model.

LNP/siRNA was well tolerated in adult $Rag2^{-/-}\gamma C^{-/-}$ mice bearing leukaemic tumours. Mice received two or three doses of 0.5 mg/kg in the first and second *in vivo* experiments, respectively. The treatment did not decrease the body weight. Nevertheless, in the third *in vivo* experiment, mice showed a 10% - 15% drop in the body weight. That could be due to the treatment regimen as mice received two IV of 2 mg/kg every 24 hours, followed by one IV of 1 mg/kg on the third day. The body weight recovered over the weekend after the addition of soaked diet.

Harvested Kasumi-1 p.SLIEW cells showed a 28% reduction in *RUNX1/ETO* expression (Fig 4-11A) suggesting an on-target effect of LNP/siRNA treatment. Although the decrease in *RUNX1/ETO* mRNA was not statistically significant, several direct target genes were significantly changed. For example, LNP/siRE-mod treatment led to a significant 56% and 30% reduction in *ANGPT1* and *CD34* transcripts, respectively. Moreover, *LAPTM5* expression significantly increased after the treatment Fig (4-11A).

When LNP/siRNA treatment was given in the same dose and injection route in the second experiment, *RUNX1/ETO* knockdown was 40% and statistically significant ($p<0.05$) (Fig 4-11B). The differences between the first and second *in vivo* experiments were that the mice were two weeks younger and received an additional dose of the nanoparticles in the second experiment. These may have contributed to the knockdown efficiency.

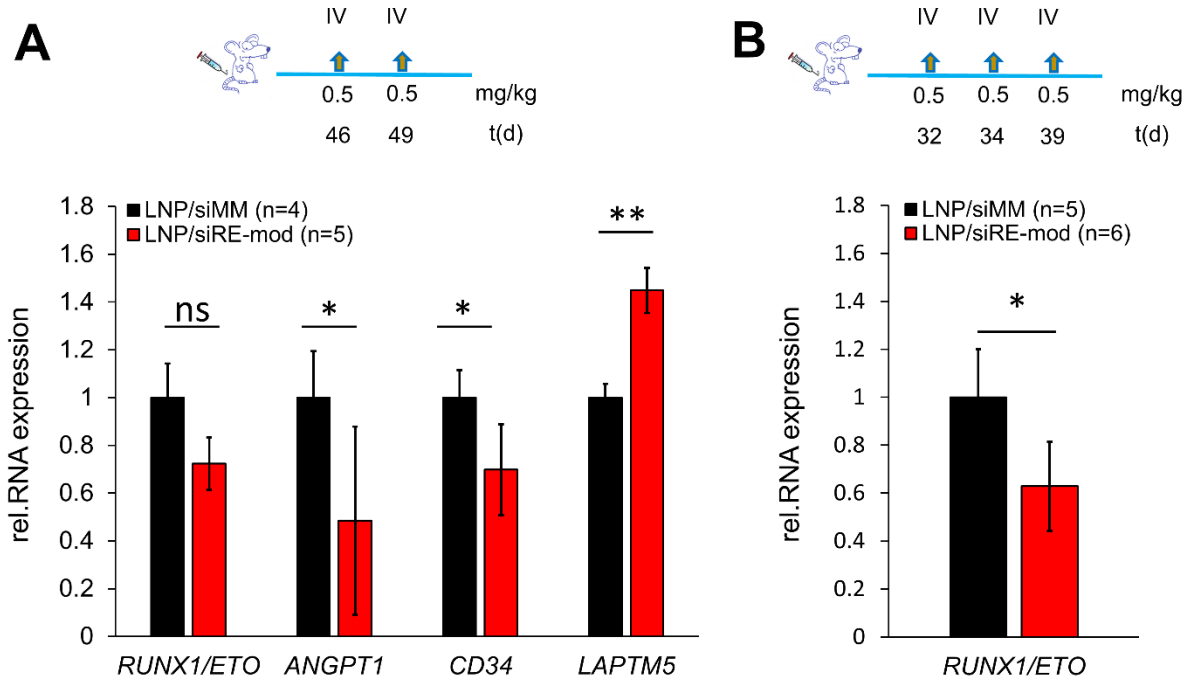

Fig 4-11: LNP/siRNA treatment effect on Kasumi-1 p.SLIEW cells *in vivo*. Lipid nanoparticles have on-target effect on leukaemic cells *in vivo* as proved by RT-qPCR analysis. Mice were treated as described previously and shown in the schemes above. (A) The expression level of *RUNX1/ETO*, *ANGPT1*, *CD34,* and *LAPTM5* in Kasumi-1 p.SLIEW cells harvested in the first *in vivo* experiment. (B) The knockdown of *RUNX1/ETO* mRNA in Kasumi-1 p.SLIEW in the second *in vivo* experiment. Gene expression in the LNP/siRE-mod treated arm was normalised to the control LNP/siMM treatment, and *GAPDH* served as a housekeeping gene. Error bars represent the SEM of Δct values in each treated group. **P*<0.05, ***P*<0.01, ****P*<0.001, two-tailed Student's *t*-test.

RUNX1/ETO knockdown *in vivo* was more prominent at the protein level. Western blotting analysis of two harvested samples in the first *in vivo* experiment showed a reduction in RUNX1/ETO protein level upon LNP/siRE-mod treatment in comparison with the control (Fig 4-12A). It was not feasible to calculate the fold change for RUNX1/ETO protein expression because the control antibodies were not human-specific. The control antibodies included GAPDH, Tubulin, and Actin. Nevertheless, considering RUNX1 a control, the reduction in RUNX1/ETO was apparent.

Western blotting analysis of the second *in vivo* experiment showed that RUNX1/ETO protein was significantly reduced (up to 50%) using three doses of 0.5 mg/kg LNP/siRNA (Fig 4-12B, C). The fold change calculations were confidently carried out after obtaining human-specific GAPDH and Clathrin heavy chain 1 (CLTA) antibodies. The knockdown of RUNX1/ETO resulted in ~ 90% downregulation of CCND2 protein level ($p<10^{-5}$) and over 50% reduction in TERT ($p<10^{-4}$) (Fig 4-12B, C).

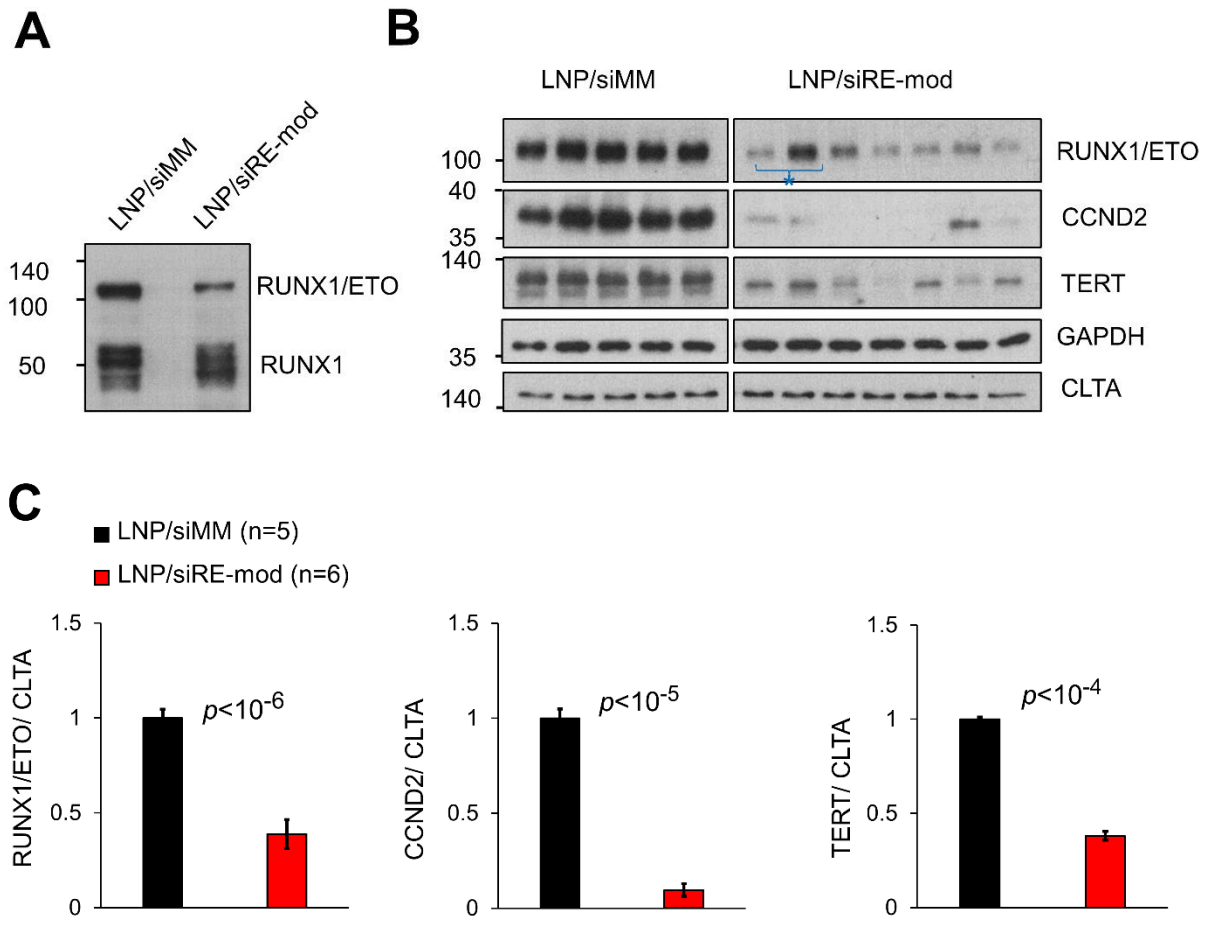

Fig 4-12: *In vivo* RUNX1/ETO knockdown at the protein level. End-point analysis of protein expression in harvested Kasumi-1 p.SLIEW cells cells. Mice were treated as indicated in Fig 4-11 schemes. (A) Immunoblot shows RUNX1/ETO protein level in one representative mouse from each treatment group for the first *in vivo* experiment. (B) Western blotting showing RUNX1/ETO, CCND2, TERT, GAPHD, and CLTA proteins in harvested cells in the second *in vivo* experiment. (C) Densitometric quantification of RUNX1/ETO, CCND2, and TERT bands normalised to CLTA loading control. Error bars represent the SEM of the relative protein expression in each group, two-tailed Student's *t*-test. The blue star represents two different lysates collected from the same mouse, and each lane was given a weight of 0.5 for the statistical analysis.

4.4.3. RUNX1/ETO depletion reduces leukaemia burden and ex vivo expansion

Protein and RNA analysis confirmed that LNP/siRNA systemic treatment provided on-target effect on Kasumi-1 p.SLIEW cells *in vivo*. However, the knockdown of *RUNX1/ETO* did not reduce the luciferase signal (Fig 4-13A, B, C). The first *in vivo* experiment started when all transplanted mice had high quantitative bioluminescence signal ($1x10^9$ p/s) in order to monitor any changes upon treatments. During the week of LNP/siRNA treatment, the bioluminescence signal of LNP/siRE-mod treated arm remained stable while the bioluminescence of the control group increased. However, three days after treatment, the IVIS signal of LNP/siRE-mod treated arm increased to the level control treated group. (Fig 4-13A).

The leukaemic burden was high in the first *in vivo* experiment due to rapid increase in the bioluminescence signal. Thus, LNP/siRNA treatment started two weeks earlier in the second *in vivo* experiment but this did not make a difference (Fig 4-13B). In the third *in vivo* experiment, mice received a total of 8 mg/kg of siRNA through IP and IV injections during ten days, yet the bioluminescence increased when the treatment stopped (Fig 4-13C).

The engraftment of Kasumi-1 p.SLIEW cells in $Rag2^{-/-}\gamma C^{-/-}$ led to the formation of granulocytic sarcomas-like tumours with yellow, pale colour. RUNX1/ETO knockdown in the first three *in vivo* experiments did not rescue the mice from the leukaemic burden as shown by IVIS. However, harvested tumours from the RUNX1/ETO targeted arm had consistently a distinct phenotype in comparison with the control treated arm. *RUNX1/ETO* knockdown in the first and second *in vivo* experiments led to the formation of flattened abdominal tumours with leaky vessels. On the other hand, mice in the control treatment arm developed yellow and pale tumours similar to the naïve transplantation model (Fig 4-13D).

Furthermore, *RUNX1/ETO* knockdown in the third *in vivo* experiment with higher siRNA dose of 8 mg/kg LNP/siRNA, reduced the size of the tumours showing smaller tumours (< 0.25 g) in *RUNX1/ETO* targeted mice and consequently lower number of viable Kasumi-1 p.SLIEW cells were obtained (< $2x10^6$ cells per mouse). The control-treated group showed substantially larger tumours (>1 g) and ~ $30x10^6$ Kasumi-1 p.SLIEW cells were harvested from each mouse. Moreover, the

RUNX1/ETO targeted group had tumours with leaky vessels (Fig 4-13D) replicating the observed phenotype in the first two *in vivo* experiments.

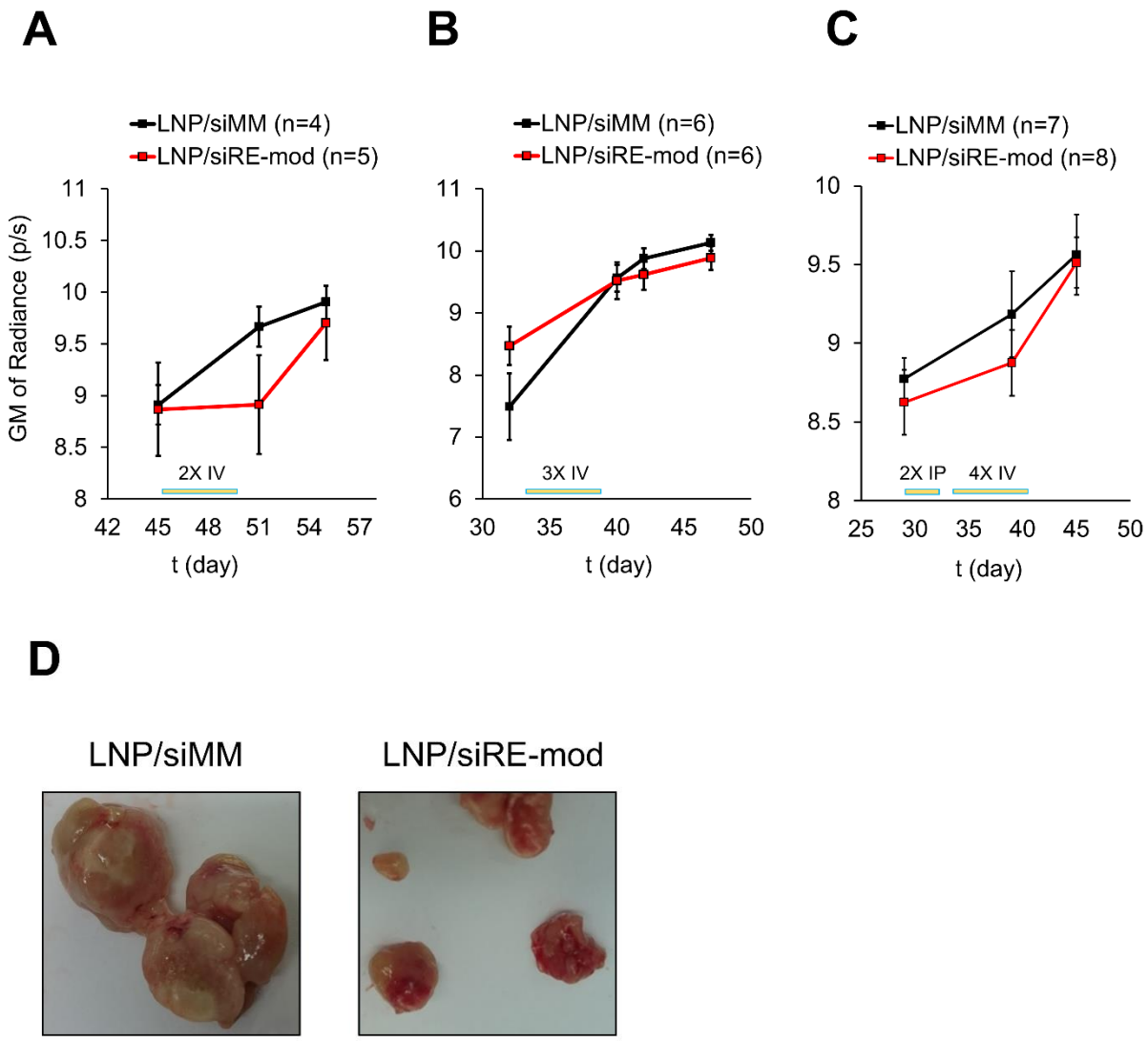

Fig 4-13: LNP/siRNA treatment effect on leukaemic tumours. Mice were transplanted with Kasumi-1 p.SLIEW cells and treated with LNP/siRNA as described previously and indicated in the schemes. IVIS imaging showed that LNP/siRNA treatment did not reduce leukaemia burden. Data represent the geometric mean (GM) of the bioluminescence signal of treated mice in the first (A), second (B) and third (C) *in vivo* experiments. Error bars represent SEM of the bioluminescence geometric mean. (D) Representative tumour images were taken after LNP/siRNA treatment in the first *in vivo* experiment.

Despite on-target effect of systemic LNP/siRNA treatments on leukaemic cells and reduction in RUNX1/ETO expression in the first three *in vivo* experiments, the knockdown was not sufficient to increase the survival (Fig 4-14).

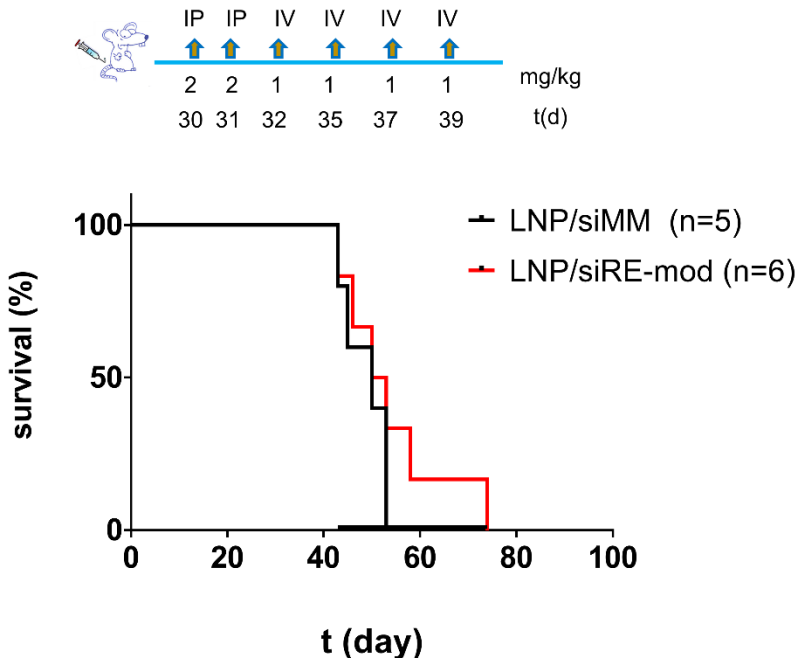

Fig 4-14: Kaplan-Meier survival graph of treated mice with LNP/siRNA. LNP/siRNA treatment did not increase the survival of leukaemic mice. Mice were transplanted as described previously and treated as indicated in the scheme above. Mice were culled when they reached any of the protocol endpoints mentioned in 4.3.3.

Notably, *ex vivo* proliferation assay of harvested leukaemic cells from treated mice showed long-lasting anti-proliferative effect of RUNX1/ETO knockdown. In the first *in vivo* experiment, RUNX1/ETO knockdown impaired the proliferation of harvested Kasumi-1 p.SLIEW cells from LNP/siRE-mod-treated mouse. On the other hand, harvested cells from a control-treated mouse had a doubling time of 2.8 day, similar to the naïve Kasumi-1 cells doubling time (Fig 4-15A).

Furthermore, harvested cells from the second *in vivo* experiment confirmed that RUNX1/ETO knockdown *in vivo* significantly inhibits proliferation *ex vivo*. Kasumi-1

p.SLIEW cells taken from five control mice (LNP/siMM treatment) proliferated rapidly with a doubling time of 2.8±0.2 days. On the other hand, cells harvested from the *RUNX1/ETO* knockdown mice expanded in different manner. For instance, one sample did not grow well, and cells died within the first week, two samples proliferated with 5 days doubling time, and three samples showed slow proliferation with doubling time between 7-12 days. The overall *ex vivo* proliferation rate of the LNP/siRE-mod-treated arm was significantly ($p<10^{-3}$) lower than the LNP/siMM treated arm (Fig 4-15B).

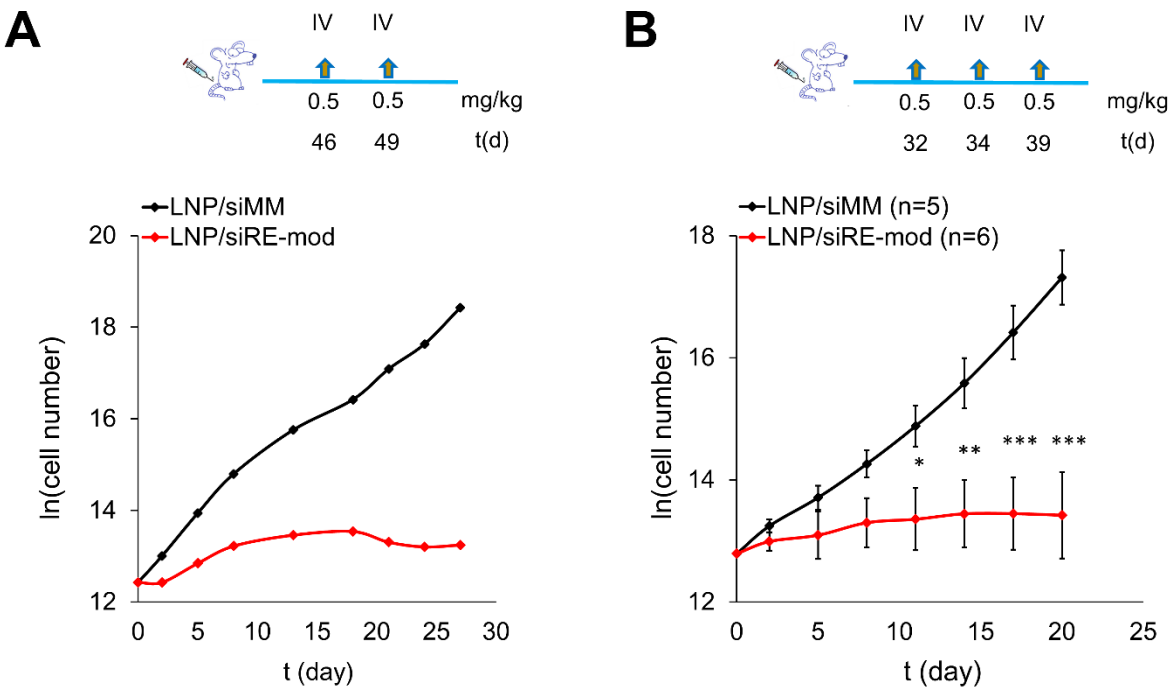

Fig 4-15: *Ex vivo* proliferation of harvested Kasumi-1 p.SLIEW cells after *RUNX1/ETO* knockdown *in vivo*. *RUNX1/ETO* knockdown inhibits the proliferation of harvested Kasumi-1 p.SLIEW ex vivo. Mice were treated with LNP/siRNA as indicated in the schemes showed above. (A) *Ex vivo* proliferation of harvested cells from one *RUNX1/ETO* targeted mouse and a control mouse from the first *in vivo* experiment. (B) *Ex vivo* proliferation of harvested cells of RUNX1/ETO targeted group and the control group from the second *in vivo* experiment. Proliferation lines represent the geometric mean of 5 and 6 samples. Error bars represent the SEM of the doubling time for each treated group. **P*<0.05, ***P*<0.01, ****P*<0.001, two-tailed Student's *t*-test.

4.4.4 In vivo knockdown of RUNX1/ETO triggers senescence

Beta galactosidase staining of harvested cells from the third *in vivo* experiment showed that *RUNX1/ETO* knockdown triggers senescence. Four samples from each treatment arm were subject to X-gal staining assay as described in 2.2.15. LNP/siRE-mod treatment led to higher level (~ 50%) of senescent cells in comparison with the LNP/siMM treatment group (15%) (Fig 4-16).

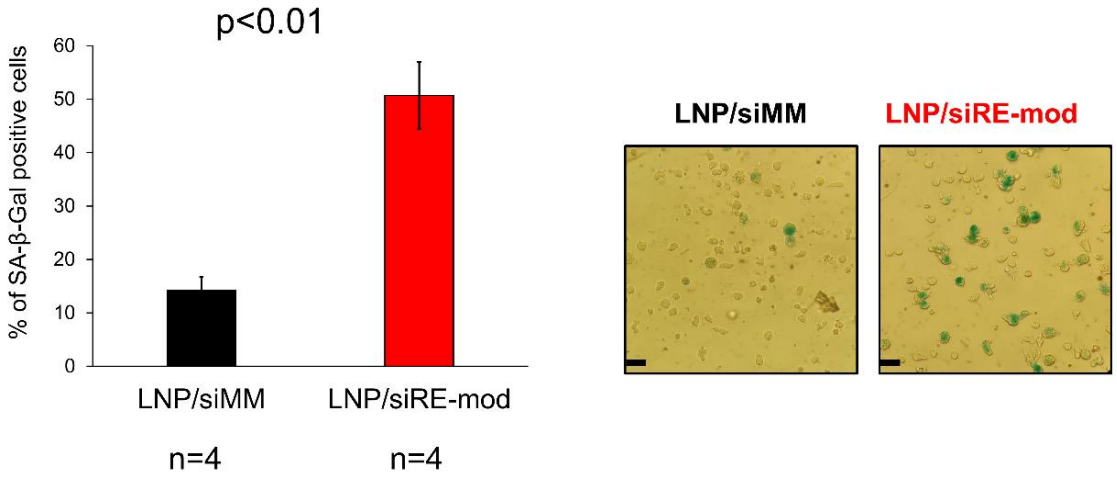

Fig 4-16: Induction of senescence after RUNX1/ETO knockdown *in vivo*. Newborn Rag2$^{-/-}$ γC$^{-/-}$ mice were transplanted with Kasumi-1 p.SLIEW cells, as described in 2.3.2.1. After one month, engraftment was assessed by IVIS. LNP/siRNA was administered as indicated in the scheme (4-5). Positive cells for the staining were counted under a bright-field microscope. Error bars represent the SEM of four mice from each treated group. **P*<0.05, ***P*<0.01, ****P*<0.001, two-tailed Student's t-test. Scale bar = 20 μm.

4.4.5 In vivo knockdown of RUNX1/ETO enhances the survival of leukaemic mice

The first three *in vivo* experiments confirmed the on-target effect of LNP/siRNA, however *RUNX1/ETO* knockdown did not enhance the survival of treated mice. For this reason, a fourth experiment was planned with two aims. First, to investigate whether *in vivo* depletion of RUNX1/ETO would enhance before the establishment of large leukaemic mass. Second, to explore the potential use of a clinically relevant chemotherapy compound alongside the *RUNX1/ETO* knockdown and exploit the combinational therapeutic benefits. The second part of the experiment will be addressed in Chapter 5.

Kasumi-1 p.SLIEW cells were transplanted in four litters, and pups were randomly marked by foot tattoo and divided into two treatment groups. Treatment started three days post-transplantation where each litter carried both treatment arms (LNP/siRE-mod and LNP/siMM-mod). Since the toxicity of the lipid nanoparticles in young mice was unknown. Therefore, the first dose consisted of 1 mg/kg LNP/siRNA by IP route. Treated pups did not show any obvious signs of toxicity after 24 hours. Thus, the dose was increased to 2 mg/kg. Treatment with 2 mg/kg of LNP/siMM-mod and LNP/siRE-mod continued throughout three weeks every 2 - 3 days.

Lipid nanoparticles treatment did not affect the main developmental milestones of the mice. At the end of the first week, the milk spot disappeared and light white fuzz appeared around the neck. Between days 8 and 10, the fuzz started to cover the whole body and skin became thicker. At day 10, the nipples were completely noticeable in the female mice, and it was feasible to distinguish the sex of the pups. The teeth fully erupted, and the eyes were open by day 12. By the end of the second week, the mice became very active, and the faeces became solid and darker, indicating that the mice had started feeding the solid diet. Daily handling of the pups and dosing 2-3 times per week might have affected the feedings by the mother, but there was no difference in the body weight of the treated mice and naïve untreated mice (Fig 4-17A, B). The body weight graph of the naïve mice was created from a separate litter consisting of four pups. LNP/siRNA treatment did not cause any significant changes in the body weight between the two treated arms or between the male and female mice.

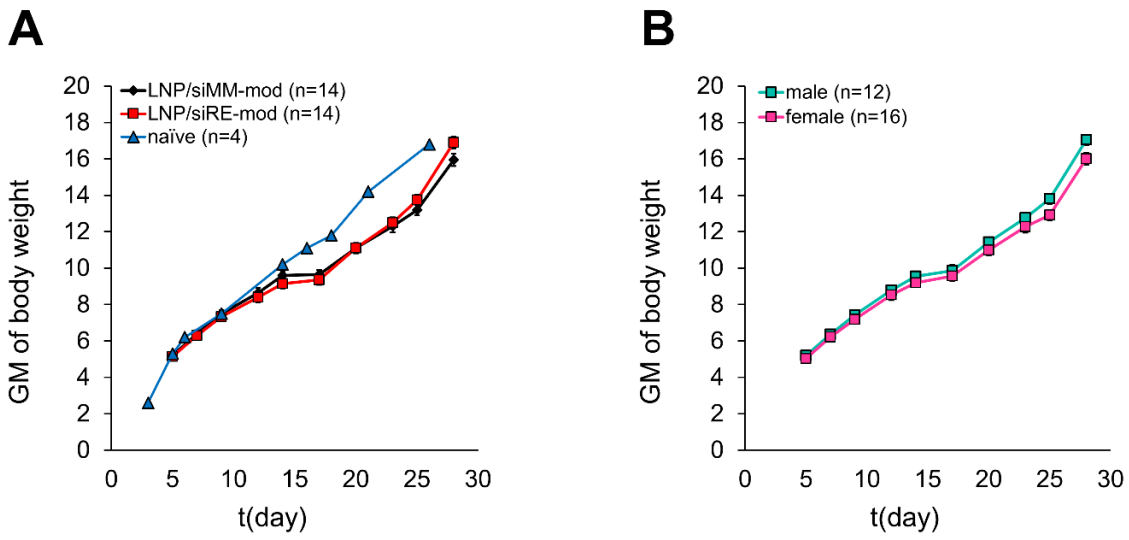

Fig 4-17: Body weight of treated Rag2$^{-/-}$γC-/- mice during LNP/siRNA treatment. Newborn Rag2$^{-/-}$ γC$^{-/-}$ mice were transplanted and treated as described in Fig 4-6. Monitoring of the mice body weight shows that young mice tolerate the lipid nanoparticle treatment. (A) Body weight graphs of LNP/siMM-mod and LNP/siMM-mod, and naïve untreated mice. (B) Body weight graph of the treated male and female mice. Error bars represent to the SEM of the mice body weight for each time point.

In vivo depletion of *RUNX1/ETO* significantly enhanced the survival of transplanted mice (p<0.0001). The median survival of mice was doubled from 44 days to 80 days (Fig 4-18).

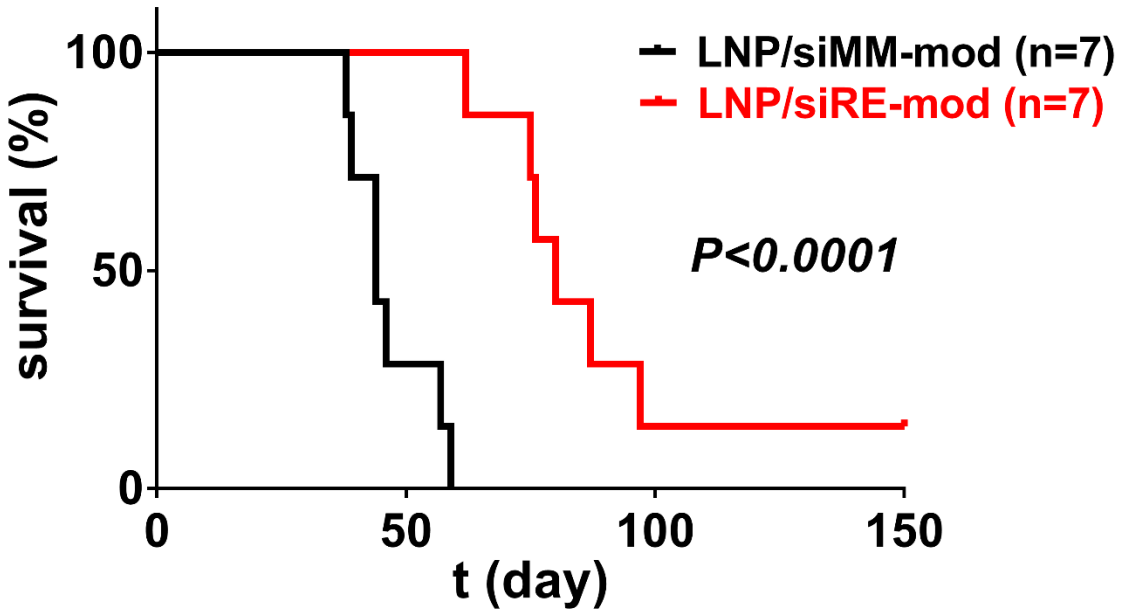

Fig 4-18: Survival of mice after *RUNX1/ETO* knockdown i*n vivo*. LNP/siRNA increased the survival of leukaemic mice. Mice were transplanted and treated with the nanoparticles as described in scheme 4-6. Kaplan–Meier graph of the treated mice. Mice were culled when they reached any of the protocol endpoints mentioned in 4.3.3.

After weaning the mice, IVIS imaging showed that the control group had significantly high bioluminescence signal (Log_{10} = 8.2). On the other hand, 11 out of 14 mice from the *RUNX1/ETO* targeted group had almost undetectable (<10^7 p/s) signal (Fig 4-19A, C). Two weeks after weaning, the bioluminescence of the control group increased 1.5-fold. The bioluminescence of *RUNX1/ETO* targeted group remained under the quantitative level (<10^7 p/s) until week eight, where all control mice were culled (Fig 4-19B).

Interestingly, the first IVIS imaging after weaning showed that leukaemic cells were engrafted in the abdominal or in the legs the control group. This engraftment behaviour is frequently observed in Kasumi-1 p.SLIEW in Rag2$^{-/-}$ γC$^{-/-}$ transplantation model. However, IVIS showed low bioluminescence emitted from the liver of LNP/siRE-mod treated mice (Fig 3-19C).

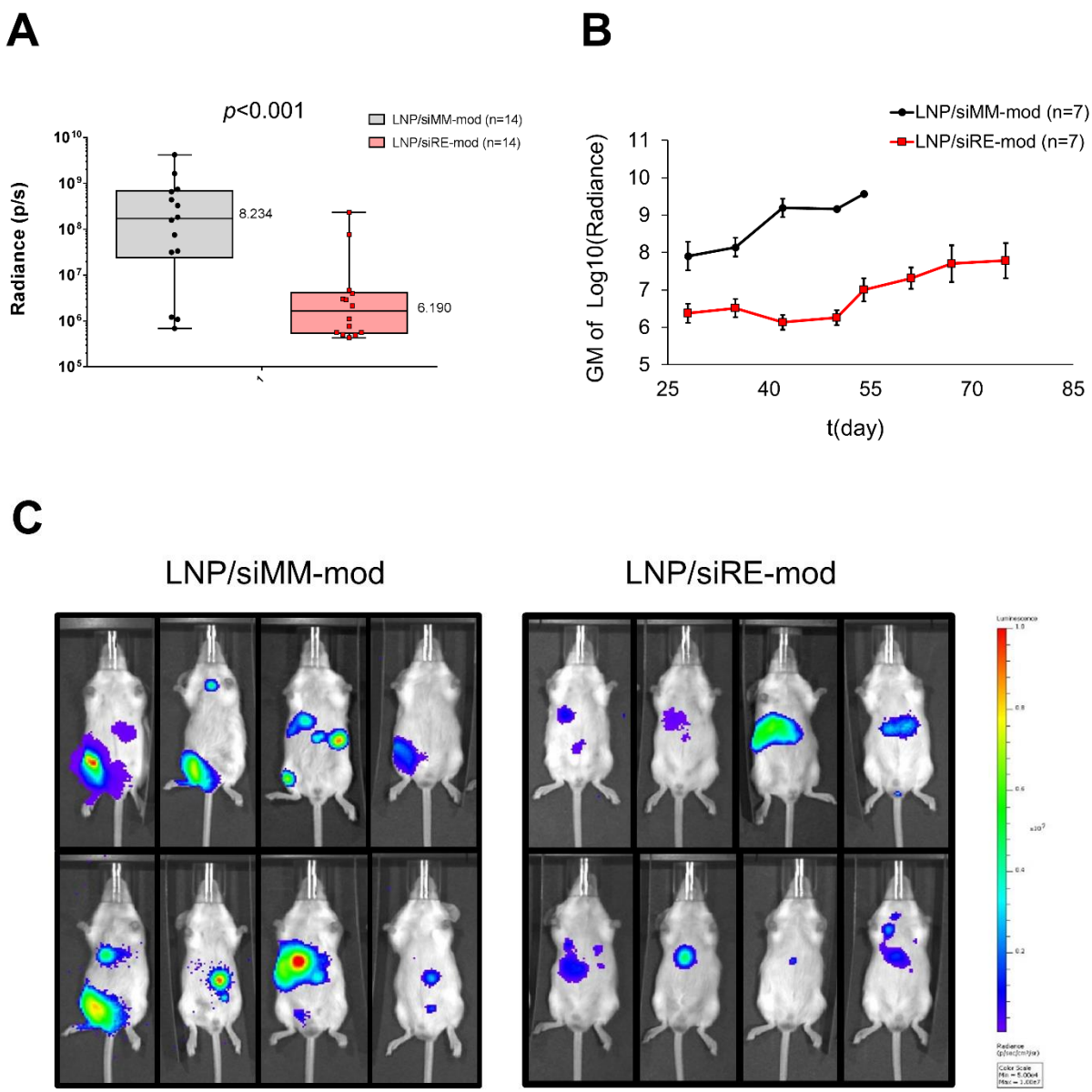

Fig 4-19: RUNX1/ETO depletion *in vivo* delays leukaemic cell engraftment. IVIS imaging of treated mice in the fourth in vivo experiment. (A) Analysis of bioluminescence at day 28 of the *RUNX1/ETO* targeted mice (LNP/siRE-mod) and control mice (LNP/siMM-mod). (B) Serial bioluminescent monitoring over 7 weeks showing a rapid increase in the signal of the control group and a slow increase in the signal of the *RUNX1/ETO* targeted group. Data represent the GM of the IVIS signals for each group (C) Representative IVIS images of 8 mice from each group. Scales are photons/second.

4.4.6 RUNX1/ETO knockdown in vivo impairs leukaemic cells self-renewal

Colony formation assay (CFA) of harvested Kasumi-1 p.SLIEW cells from treated mice showed a significant decrease in the colony formation ability of *RUNX1/ETO* knockdown cells (Fig 4-20). The reduction in clonogenicity was reproducible in all three *in vivo* experiments, regardless of the dosing regimen and the time of harvesting the cells (Fig 4-21).

The *ex vivo* colony formation showed slower progress than the *in vitro* assay. It took up to two weeks for single cells to form large colonies in the control samples, but the size and number of colonies in the *RUNX1/ETO* targeted group were significantly smaller. This could be due to the effect of P/S present in the methylcellulose media. Harvested colonies from the *RUNX1/ETO* targeted group did not provide sufficient number of cells to perform replating assay. Some samples in the *RUNX1/ETO* targeted arm did not form any colonies even after four weeks.

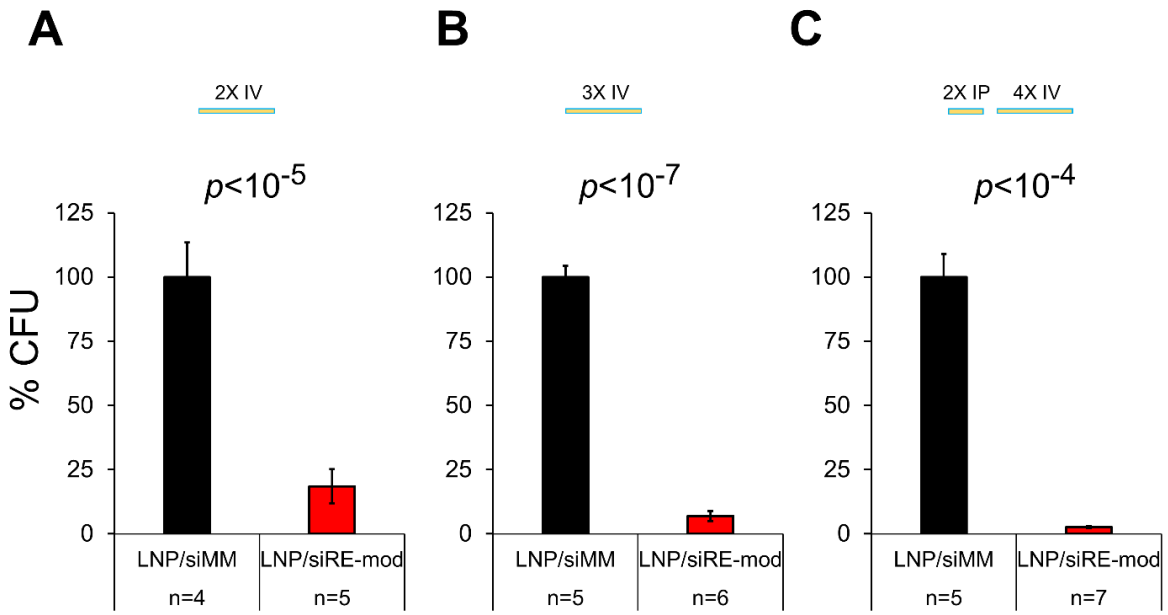

Fig 4-20: *Ex vivo* colony formation assay upon *RUNX1/ETO* knockdown *in vivo*. Harvested Kasumi-1 p.SLIEW from treated mice were seeded for colony formation in methylcellulose media. (A), (B) and (C) represent the normalised colonies number to the control group of the first, second and third *in vivo* experiments, respectively. Colony number was determined approximately after two weeks of incubation and four wells were counted per sample. Error bars represent SEM of the counted colonies in each group, **P*<0.05, ***P*<0.01, ****P*<0.001, two-tailed Student's *t*-test.

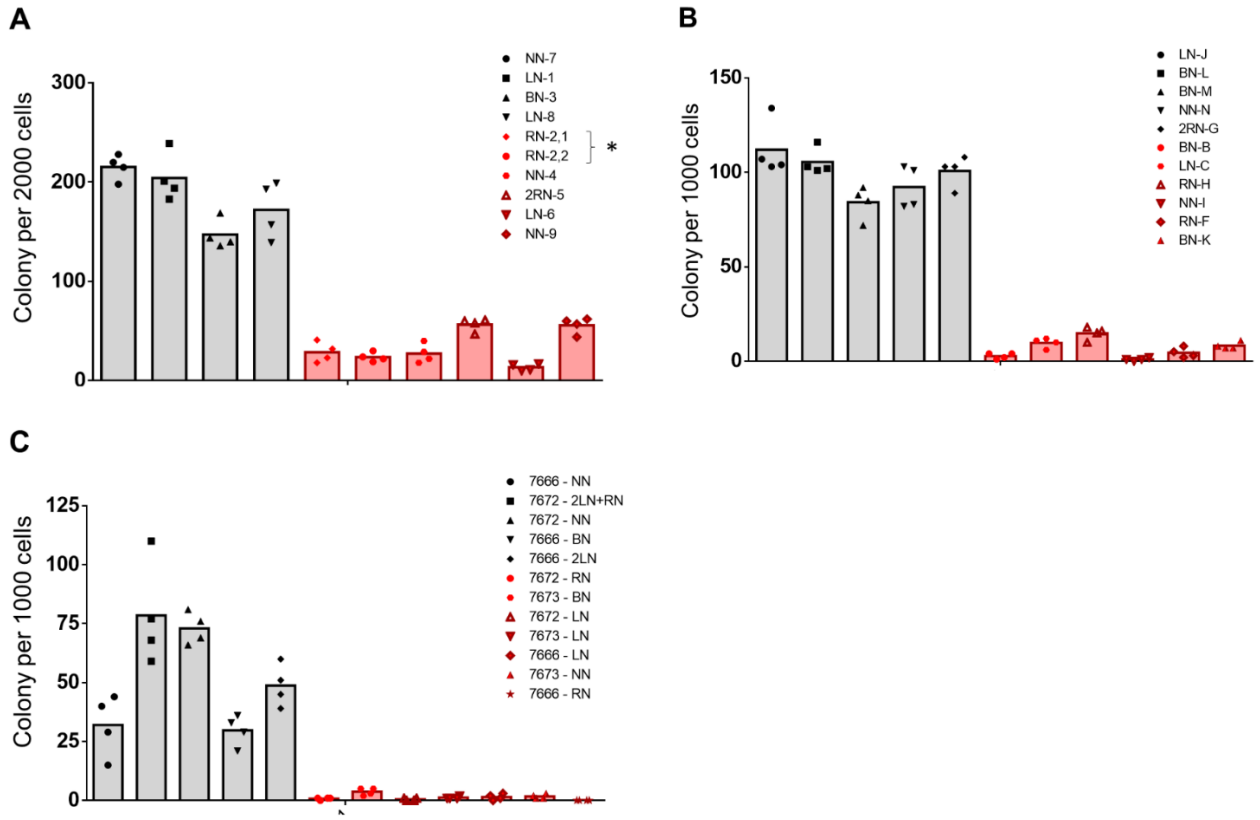

Fig 4-21: Detailed e*x vivo* colony formation assay. Colony formation was performed as described in Fig 4-20. (A), (B) and (C) show the total number of colonies in the first, second and third *in vivo* experiments, respectively. The grey and red bars represent the mean of counted colonies from the LNP/siMM, and LNP/siRE-mod treated groups, respectively. Mice identification codes are shown on the right side of the graphs. The star on the graph (A) refers to two samples collected from the same mouse.

In order to investigate the long-term effect of RUNX1/ETO depletion on self-renewal, harvested Kasumi-1 p.SLIEW cells from treated mice were retransplanted in secondary recipients. The retransplantation experiment of harvested cells from the third *in vivo* experiment showed that *in vivo* depletion of *RUNX1/ETO* severely impaired engraftment in the secondary recipient (p=0.0016) (Fig 4-22).

Two sets of secondary transplantation experiments were conducted. The first attempt consisted of transplanting two Rag2$^{-/-}$ɣC$^{-/-}$ litters, 3 and 5 days old. Each litter contained 4 pups. Three days after the last IV injection, four mice were culled for the secondary transplantation, and 0.25 x 10^6 cells of harvested viable Kasumi-1

p.SLIEW cells were intrahepatically transplanted on the same day into new newborn recipient mice. Injected samples were distributed evenly between the two litters where each litter contained both treatment groups. The 3 days old litter showed engraftment in the control group while the 5 days old litter did not engraft. The skin of the 5 days old mice was thick and it was difficult to perform the intrahepatic injection. There is a possibility that the cells were not injected into the liver. Thus, the 5 days old litter dropped from the analysis.

Given that one litter in the first retransplantation experiment did engraft, a 2 days old litter was transplanted in a second attempt. In this experiment, 2 harvested Kasumi-1 p.SLIEW samples from each group (*RUNX1/ETO* targeted group and control group) were thawed, and 0.25 x 10^6 cells were intrahepatically transplanted. Each sample was transplanted into two pups.

Remarkably, the retransplantation experiment showed that all harvested cells from LNP/siMM treated mice engrafted with short latency (Fig 4-22A, B). However, transplantation of cells taken from LNP/siRE-mod treated mice resulted in significantly prolonged survival (Fig 4-22B).

The first IVIS imaging after weaning the mice showed that all control mice (LNP/siMM primary treatment) had significantly high IVIS signal ~ 10^7 p/s, which increased over time until all mice reached the protocol endpoints. On the other hand, the IVIS signal of the *RUNX1/ETO* targeted group (LNP/siRE-mod treatment), however, had nonquantitative (<10^6) signal (Fig 4-22A). Moreover, transplantation of freshly harvested cells or previously frozen and thawed cells did not impact the IVIS signal or the overall survival of the control group. The median survival of the control group was 62 days, where the median survival of the *RUNX1/ETO* targeted group was beyond 210 days (p<0.0016).

Interestingly, in the *RUNX1/ETO* targeted group, one mouse engrafted after 80 days. The mouse had a quantitative IVIS signal that increased gradually until the tumour size reached the protocol endpoint. The last mouse in this group at day 210 had a fivefold enlarged spleen and leukaemic cells invaded the right ovary while the left ovary and the uterus were normal (Fig 4-22C). Half of the mice in the *RUNX1/ETO* targeted group did not engraft until the point of terminating the experiment at day 300.

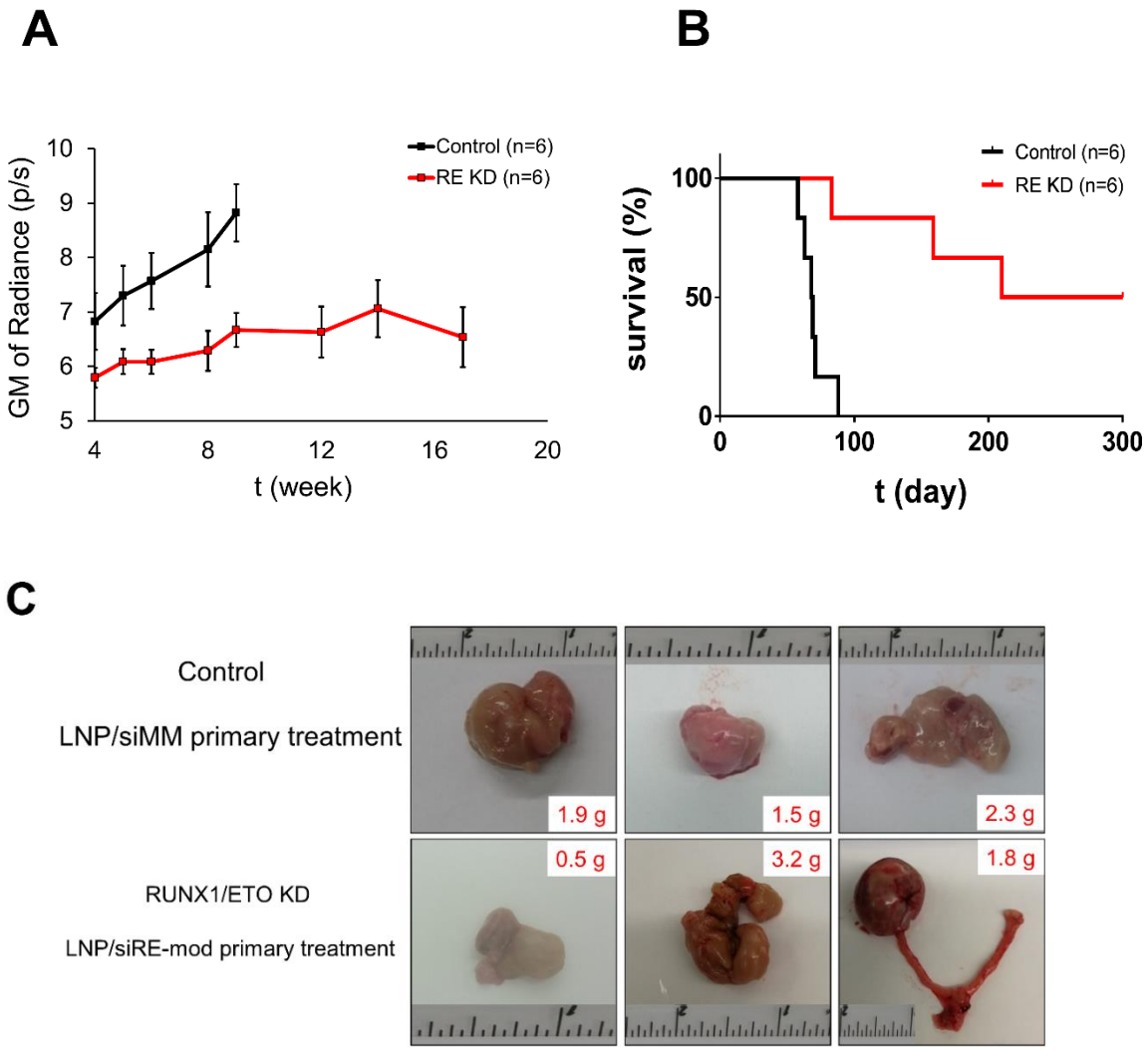

Fig 4-22: *In vivo* depletion of *RUNX1/ETO* impairs engraftment in secondary recipients. Harvested Kasumi-1 p.SLIEW cells from the primary treatment were intrahepatically injected in 2 or 3 days old Rag2$^{-/-}$ɣC$^{-/-}$ mice. Treatment of the primary mice was performed as described in scheme Fig 4-5. (A) Serial bioluminescent monitoring over 12 weeks to assess leukaemia burden in the secondary retransplanted mice showing increase in the IVIS signal of the control group. Data represent the GM of the IVIS signal for each group. Error bars represent SEM of the IVIS signal of each group. (B) Kaplan–Meier graph of the retransplantation experiment. (C) Images of representative tumours harvested from the secondary transplanted mice.

4.4.7 RUNX1/ETO knockdown initiates myeloid differentiation in vivo

Harvested cells from the secondary transplantation experiment indicted an initiation of a myeloid differentiation programme (Fig 4-23). Despite there was not reduction in *RUNX1/ETO* expression level, the *RUNX1/ETO* targeted group showed significant upregulation of *CEBPA* and downregulation of *CD34* at mRNA level (Fig 4-23A). Moreover, the *RUNX1/ETO* targeted group showed less surface expression of the stem cell marker CD34 (~ 6 to 8-fold reduction in the geometric mean), and a marked increase (> 90%) in the monocytes markers CD14 and CD11b (Fig 4-22B).

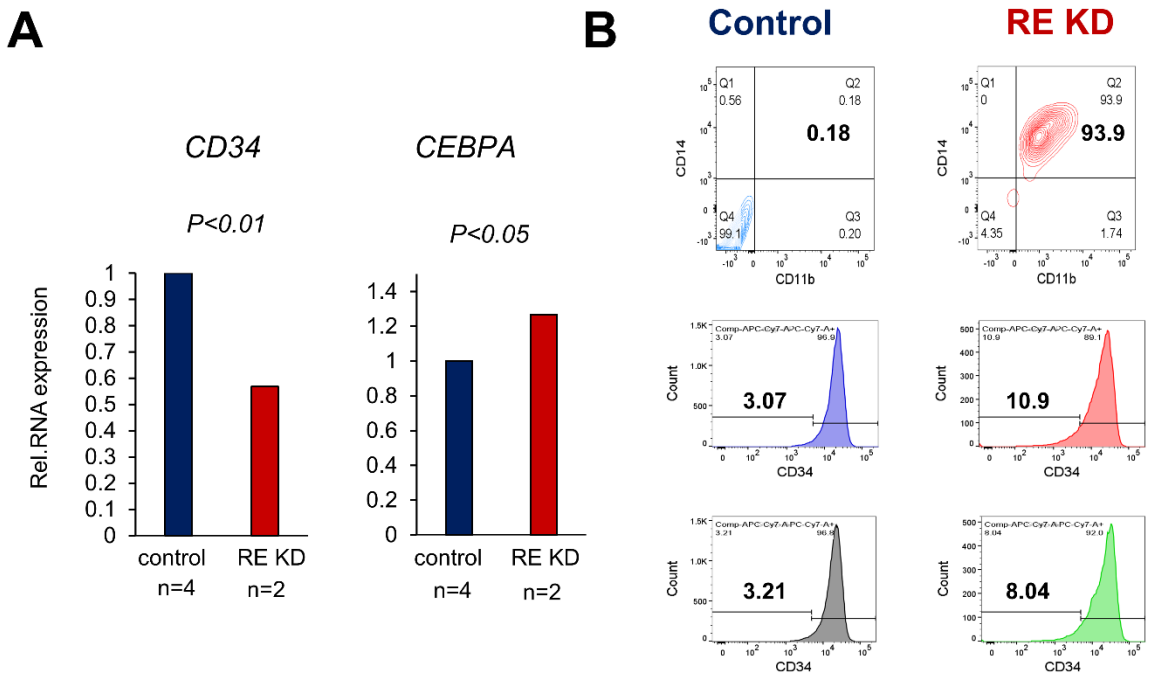

Fig 4-23: *In vivo* depletion of *RUNX1/ETO* triggers myeloid differentiation in the secondary recipient. Harvested Kasumi-1 p.SLIEW cells from the secondary retransplanted mice demonstrate initiation of the myeloid differentiation programme. (A) qRT-PCR analysis shows the expression level of *CD34* and *CEBPA* in four mice in the control group, and two mice in the *RUNX1/ETO* targeted group. (B) Multicolour FACS analysis of harvested cells from control mice (left) and *RUNX1/ETO* targeted group (right) showing an increase in the CD11b and CD14 surface expression in the *RUNX1/ETO* knockdown mouse (top), and a decrease in the CD34 geometric mean in two *RUNX1/ETO* knockdown mice.

4.4.8 RUNX1/ETO knockdown in vivo alters t(8;21) transcriptome

Harvested cells from the third *in vivo* experiment were sent for RNA sequencing (RNA-seq). Two mice from each treatment arm were culled three days after completing the treatment followed by sorting Kasumi-1 p.SLIEW cells based on eGFP expression. One *RUNX1/ETO* targeted mouse did not give sufficient cell number for RNA extraction, thus cells from another mouse was collected. Following sorting and RNA extraction, four samples were sent for sequencing.

Dr. Sirintra Nakjang performed the bioinformatic analysis of the RNA-seq data.

Gene expression analysis showed that *RUNX1/ETO* knockdown mice (RE KD-1, RE KD-2 had different transcriptome from the control mice (MM ctr-1, MM ctr-2) (Fig 4-24). Principle component analysis (PC1 and PC2) showed that control mice had similar gene expression while *RUNX1/ETO* knockdown mice differed in gene expression between each other and in comparison with the controls.

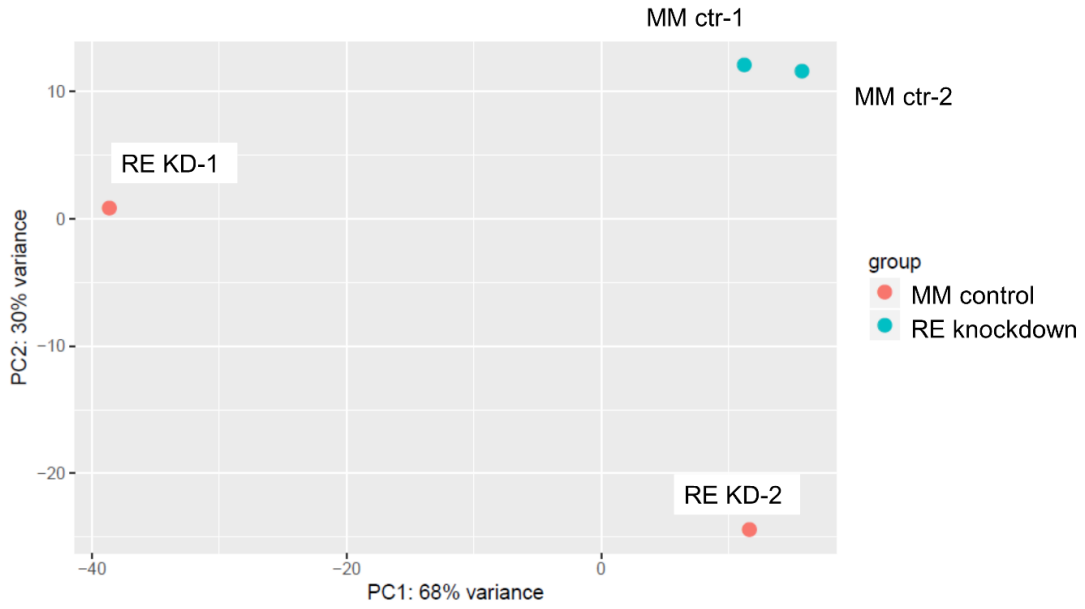

Fig 4-24: Principal component analysis of *RUNX1/ETO* knockdown *in vivo*. Mice were transplanted with Kasumi-1 p.SLIEW cells ,and treated with the nanoparticles as shown in the ligand of Fig 4-5. Cells were collected from treated mice, sorted based on the eGFP expression followed by RNA extraction and RNA sequencing. MM ctr-1 and MM ctr-2 represent the control group, and *RUNX1/ETO* knockdown group consists of RE KD-1 and RE KD-2.

RNA-seq data were analysed using several computational analysis platforms including, Gene set enrichment analysis (GSEA), Gene Ontology (GO) and Kyoto Encyclopedia of Genes and Genomes (KEGG). Analyses were performed on the top differentially upregulated genes and differentially downregulated genes. Only genes which had more than twofold log2 change with p values <0.05 were included in the pathway analyses.

KEGG pathway analysis showed that *RUNX1/ETO* knockdown *in vivo* induces several canonical pathways common in cancers including NF-κB, MAPK and others as shown in (Fig 4-25). The KEGG proved the on-target effect, and mapping the differentially expressed genes on KEGG pathways showed several known targets of RUNX1/ETO as shown in the supplementary figures (s-Fig 2 to 12). Moreover, GO and GSEA analyses on the differentially expressed protein-coding genes also revealed similar pathways to those shown in KEGG. The top 20 enriched pathways in KEGGG, GO, and GSEA can be attributed to 6 common functional categories as revealed by PANTHER classification system. These categories were, NF-κB induced pro-inflammatory response, TGF-β signalling, cytokine-receptor signalling, pathways in cancers, cell cycle regulation and metabolism as depicted in (Fig 4-26).

RNA sequencing was performed only on 4 samples, 2 in each group. This small cohort is the main limitation of the experiment. It was not possible to send more samples for sequencing because sorting based on eGFP expression failed to give sufficient amounts of cells for downstream processing. Moreover, it was also not feasible to sequence more samples from other *in vivo* knockdown experiments due to time constraints.

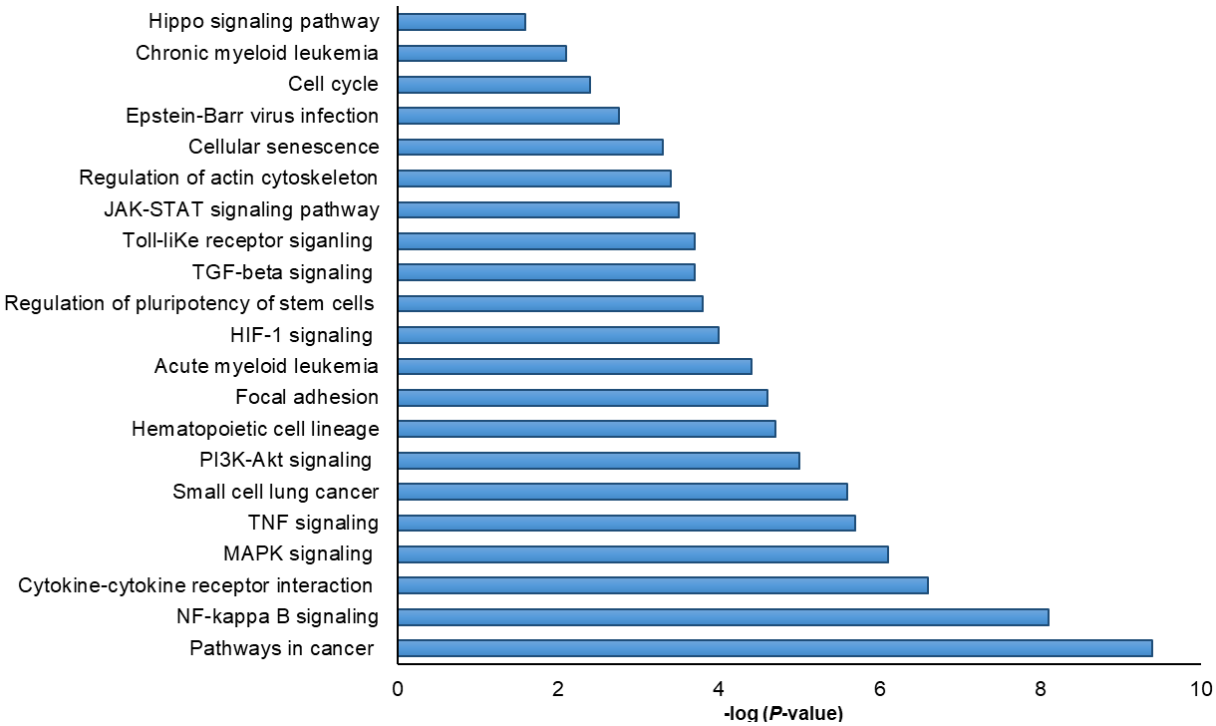

Fig 4-25: Pathway analysis of *RUNX1/ETO* knockdown *in vivo*. Pathways analysis was performed on the differentially regulated genes with $P < 0.05$ using KEGG pathways analysis platform.

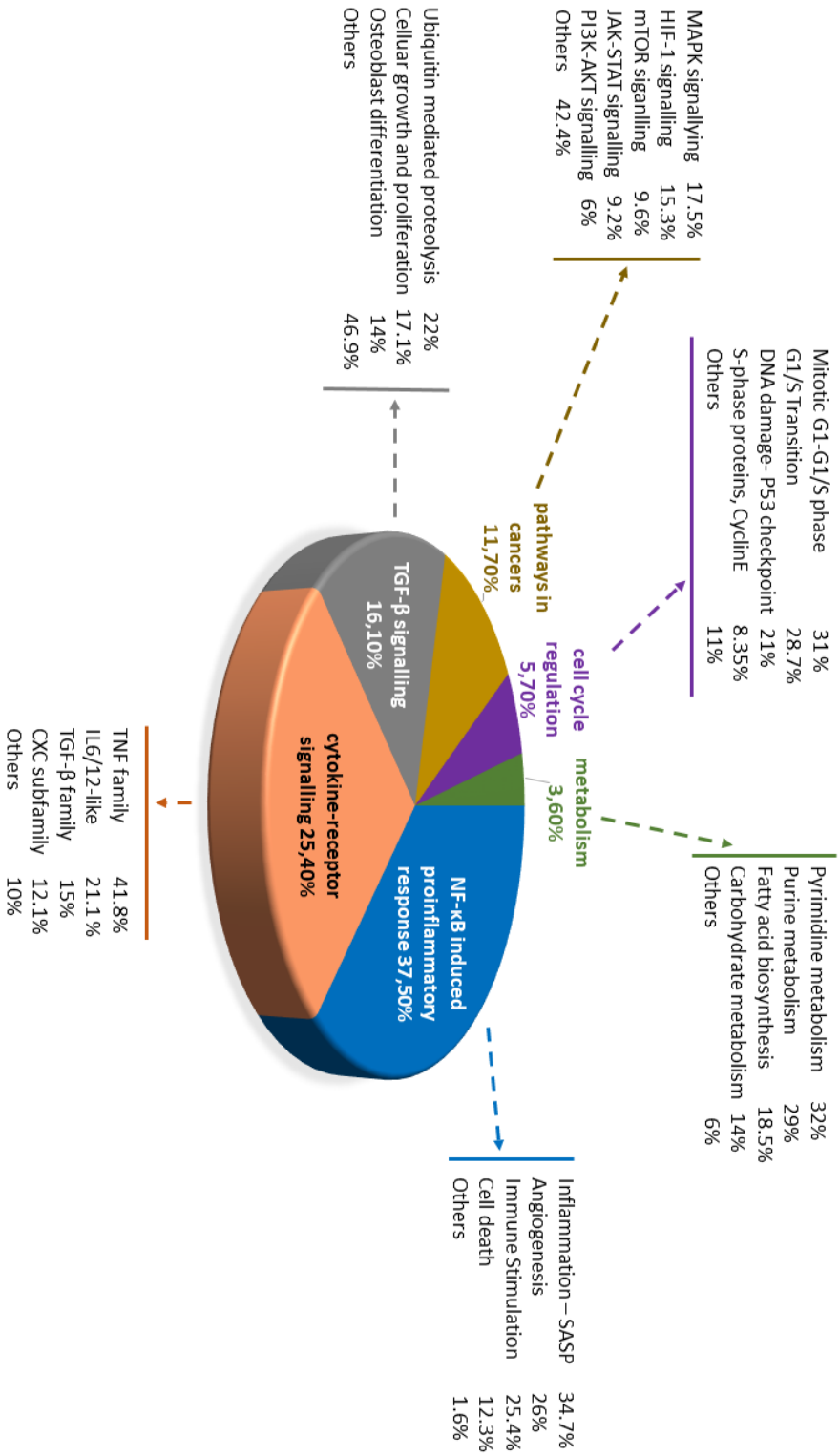

Fig 4-26: Classification of the functional pathways of *RUNX1/ETO* knockdown *in vivo*. Pathway analysis was performed using KEGG, GO and GSEA platforms. The resulted top 20 canonical pathways from pathway analyses were re-analysed using the PANTHER classification system. Statistical significance was determined by Fisher Exact test.

4.5 Results summary

The main challenges facing siRNA therapeutics are the poor pharmacokinetics and pharmacodynamics of naked siRNA. Lipid-based delivery systems such as liposomes and nanoparticles are among the promising strategies to improve the siRNA bioavailability and pharmacokinetics (Leung, Tam et al. 2014, Park, Park et al. 2016, Viger-Gravel, Schantz et al. 2018). The second part of this project utilised a lipid nanoparticle system encapsulating the potent modified siRNA to study the effect of modulating *RUNX1/ETO* expression *in vivo*.

Following siRNA chemical modification and optimisation of RUNX1/ETO knockdown using the lipid nanoparticles, the second aim of the study was to investigate the effect of *RUNX1/ETO* knockdown using lipid nanoparticles *in vivo*. The xenotransplantation model of t(8;21) AML was generated by intrahepatic injection of Kasumi-1 cells stably expressing *luciferase* into newborn Rag2$^{-/-}$ɣC$^{-/-}$ mice. This xenotransplantation model is not optimal because transplanted mice develop solid tumours, and Kasumi-1 cells are rarely detected in the peripheral blood. The model also has low engraftment in the spleen and bone marrow. However, the engraftment behaviour is highly reproducible and consistent. Moreover, the tumours mainly consist of Kasumi-1 cells expressing CD34 and CD33 surface markers, and they can engraft serially in further transplantations (Soria, Tussiwand et al. 2009). This model was suitable for this project, particularly because Kasumi-1 cells do not lose the self-renewal properties *in vivo*.

The optimisation of in-house click reaction protocol, LNP/siRNA was successfully labelled with the SulfoCyanine7.5 dye. The methods of labelling did not significantly affect the nanoparticles parameters. The pharmacodynamics and biodistribution study indicated that the nanoparticles have global body distribution. Although the liver was enriched with the nanoparticles as shown by IVIS, the particles were detected in several organs, including the brain and the bone marrow.

Although Kasumi-1 p.SLIEW cells form abdominal extra-medullary tumours, RUNX1/ETO knockdown was successfully achieved on the mRNA and protein levels. The systemic treatment proved that the LNP/siRNA reached the tumour site and provided on-target effect.

LNP/siRNA treatment did not affect the biological development of treated mice, and no toxicity was observed. This finding has high relevance for further *in vivo* studies as the toxicity has been confirmed not to be an obstacle. *RUNX1/ETO* knockdown *in vivo* significantly enhanced the median survival of the mice, implying that *RUNX1/ETO* is required for leukaemia expansion *in vivo*.

The knockdown of RUNX1/ETO was associated with changes in RUNX1/ETO direct target genes including *ANGPT1*, *CD34* and *LAPTM5*. The knockdown also significantly reduced CCND2 and TERT protein levels and triggered senescence. Moreover, RNA-seq showed that the most upregulated genes after *RUXN1/ETO* silencing correlated with the induction of pro-inflammatory response, deregulated angiogenesis and induction of C/EBPα-associated myeloid differentiation. The downregulated genes identified by RNA-seq have also been linked to pathways relevant for self-renewal, clonogenicity and G-CSF induced proliferation.

The transient depletion of *RUNX1/ETO in vivo* inhibited leukaemic cells proliferation *ex vivo* and severely impaired clonogenicity. The knockdown *in vivo* also remarkably impaired engraftment in secondary recipient mice. These findings emphasise the role of RUNX1/ETO in maintaining leukaemic self-renewal.

Furthermore, *RUNX1/ETO* knockdown *in vivo* led to downregulation of the stem cell marker CD34 in the secondary recipient mice. The knockdown also elevated the expression level of the transcription factor *CEBPA.* Further characterisation of harvested cells revealed that *RUNX1/ETO* knockdown increased CD14 and CD11b expression. These findings imply that *RUNX1/ETO* knockdown *in vivo* led to monocytic differentiation. Giemsa stain would have proved the monocytic phenotype, but due to the time limit, it was not feasible to characterise the differentiation status on cytospin slides.

Chapter 5.

RUNX1/ETO knockdown effects on drug sensitivity

5.1 Introduction

AML is a clonal disease with complex genomic aberrations that lead to drug resistance, primarily upon relapse. (Sabbath, Ball et al. 1985, Blair, Hogge et al. 1998, Siddiqui, Hogge et al. 2016). AML treatments account for a broad spectrum of short- and long-term side effects including neurotoxicity, cardiotoxicity and infertility (Boyd, Aslostovar et al. 2018). It is, therefore, necessary to enhance chemosensitivity to achieve a higher cure rate with a less toxic burden. Currently, AML treatment focuses on eliminating leukaemic blast cells following two strategies, inducing DNA damage or enhancing mitochondrial apoptotic pathways. Despite the favourable prognoses of t(8;21) AML, approximately 30% of patients relapse with poor prognoses, which highlights the importance of finding new therapeutic strategies (Burnett, Hills et al. 2010).

This project proved that *RUNX1/ETO* depletion by siRNA prevents leukaemia propagation and severely impairs self-renewal and expansion in secondary receipt mouse model. *RUNX1/ETO* knockdown *in vivo* did not lead to cell death. However, it caused a cytostatic phenotype indicated by G1 cell cycle arrest. Since RUNX1/ETO mandates the G1 to S phase progression in t(8;21) AML by regulating the CCND2-CDK4/6 complex and its inhibitors p21 and p27 (Goel, DeCristo et al. 2018, Martinez-Soria 2018), we have hypothesised that the imbalance between the cyclins and the cyclin-dependent kinase inhibitors upon *RUNX1/ETO* suppression may prime leukaemic cells for apoptosis.

Senescence and apoptosis are evolved to suppress tumorigenesis, and several senescence-causing effectors are oncogenic (Childs, Baker et al. 2014). *RUNX1/ETO* knockdown *in vivo* induced cellular senescence. However, in contrast to apoptotic cells, senescence is imperfect tumour-suppressive fate because senescent cells secrete many cytokines and factors that promote tissue and organ dysfunction (Maciel-Baron, Morales-Rosales et al. 2016, Ritschka, Storer et al. 2017). Analysis of our RNA-seq data obtained from *RUNX1/ETO* knockdown *in vivo* showed a strong pro-inflammatory response marked by a signature of the senescence-associated secretory phenotype (SASP). Additionally, senescent cells are stably viable and some of the SASP inducers such as NF-κB may have tumour-promoting effect (Salminen, Kauppinen et al. 2012, Nelson, Kucheryavenko et al.

2018). Since recent studies have shown that potent drug combinations could eliminate senescent cells (Chaikovsky and Sage 2018, Xu, Pirtskhalava et al. 2018), we aimed to explore whether *RUNX1/ETO* knockdown makes leukaemic cells more susceptible to apoptosis.

For these reason, in this chapter we explored the therapeutic potential of several clinically relevant chemotherapies combined with *RUNX1/ETO* knockdown. It was hypothesised that if *RUNX1/ETO* repression sensitises leukaemic cells to chemotherapies, this might stratify dose reduction in current t(8;21) AML treatment to fully irradiate leukaemia with reduced side-effects.

5.2 Aim

The combination of *RUNX1/ETO* knockdown with different chemotherapy agents was investigated. The aims were as follow;

1. To investigate the effectiveness of combinational treatment with *RUNX1/ETO* knockdown *in vitro.*
2. To elucidate the relationship between RUNX1/ETO expression and possible synergy or additive effect.
3. To test the combination of *RUNX1/ETO* depletion and the chemotherapy agent *in vivo*.

5.3 Experimental designs

5.3.1 Drug treatment experiments

Drug treatment with AraC, Rucaparib, and ABT-199 was performed on Kasumi-1 and SKNO-1 cell lines as well as on the stably transduced cell lines Kasumi-1 p.SLIEW and SKNO-1 p.SLIEW. Drug treatment was applied either with or without *RUNX1/ETO* knockdown (Fig 5-1). The knockdown of *RUNX1/ETO* was achieved by serial electroporation using 100 nM siRNA on day 0 and 3. On day 4, cells were counted and resuspended at 0.1 x 10^6 cells/ml density, and 90 µl of cell suspension was seeded into a 96-well plate. Drug treatment was performed by addition of 10 µl of 10X stock solution. Depending on the type of the drug solvent (e.g. DMSO), the concentration of the solvent was maintained at 0.1% for each well. The effect of the drug was determined either by reporter luciferase assay or fluorescent resazurin assay.

RUNX1/ETO knockdown *in vitro* was achieved by electroporation due to the limited amount and high cost of lipid nanoparticles.

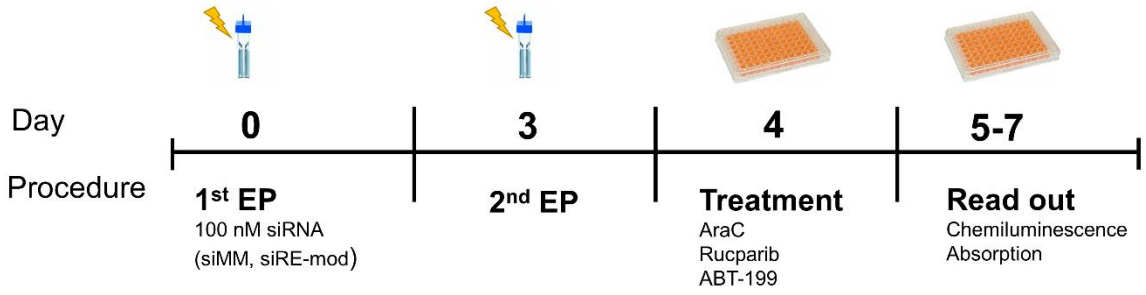

Fig 5-1: Experimental set up of *RUNX1/ETO* knockdown and chemotherapies combinations. AML cell lines were serially electroporated on days 0 and 3 with siRNA. On day 4, cells were seeded into a 96-well pate and treated with the chemotherapy agent for 2 - 3 days. The bioluminescence luciferase assay and the fluorescence resazurin assay were used to determine the activity of the drug.

5.3.2 The effect of G1 cell cycle arrest in response to BCL2 inhibition

In order to test the effect of G1 cell cycle arrest on BCL2 inhibition, two experiments were performed in SKNO-1 cell line. We have chosen SKNO-1 to perform these experiments because we found that SKNO-1 cells require stronger *RUNX1/ETO* knockdown to cause G1 cell cycle arrest in comparison with Kasumi-1 cells, and they recover faster from the cycle arrest (Fig 3-10). Thus, conducting the experiments in this cell line will allow us to observe any changes in the sensitivity to the treatment.

First, the cell cycle arrest in SKNO-1 cells was achieved by depleting *RUNX1/ETO* or *CCND2*. The repression was achieved by serial electroporation with 100 nM siRE-mod, or a mixture of 200 nM (siCCND2_2 and siCCND2_4) as shown in Fig 5-2. Both siCCND2_2 and siCCND2_4 are validated siRNAs targeting *CCND2* transcript (Martinez-Soria 2018). Drug treatment was applied 24 hours after two serial electroporations on day 0 and 3. The effect of BCL2 inhibition was assessed by resazurin assay on day 6. Cell cycle profiling was also performed on day 6 to quantify the level of cell cycle arrest.

Second, RUNX1/ETO was depleted by single electroporation and cells were seeded in two sequential colony formation assays. At the end of the second replating, cells were collected, washed twice with PBS, seeded into a 96-well plate and treated with the BCL2 inhibitor ABT-199 (Fig 5-3). Cell cycle profiling was also performed within one hour after harvesting the colonies. The effect of BCL2 inhibition was assessed by resazurin assay after 2 days.

5.3.4 Investigating BCL2 inhibition at protein level

We have investigated the effect of ABT-199 treatment at the protein level *in vitro* in Kasumi-1 p.SLIEW cells because our *in vivo* knockdown experiments were performed on these cells. Furthermore, the RNA-seq data were obtained from Kasumi-1 p.SLIEW cells as well, making the interpretation of the Western blotting data admissible.

Kasumi-1 p.SLIEW cells were electroporated with 100 nM of either siRE-mod or siMM on days 0 and 3. On day 4, ABT-199 treatment was applied and cells were collected for Western blotting on day 5.

Fig 5-2: BCL2 inhibition sensitivity to the cell cycle arrest effect on. SKNO-1 cells were serially electroporated on days 0 and 3 with siRNA and seeded for drug testing on day 4. After two days of continues treatment with ABT-199, drug activity was assessed by resazurin assay. PI cell cycle profiling was performed on day 4 before applying ABT-199 treatment.

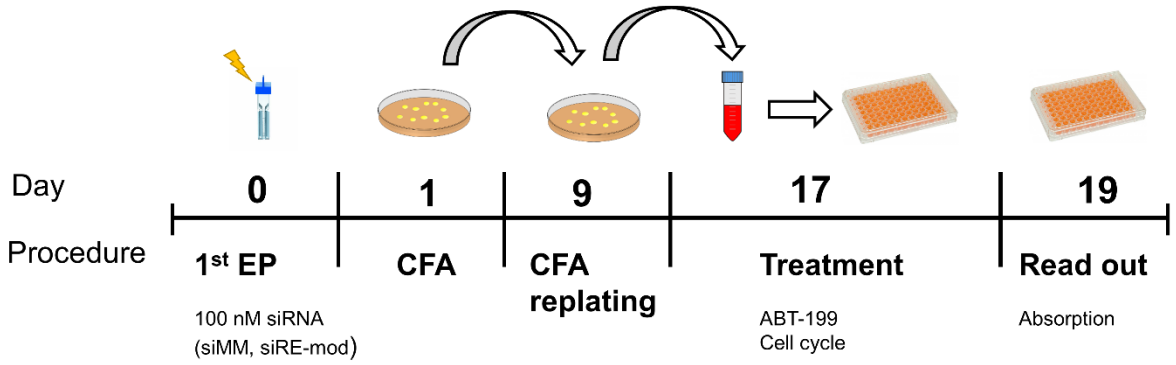

Fig 5-3: Prolonged *RUNX1/ETO* depletion effect on BCL2 inhibition. SKNO-1 cells were electroporated with siRNA and seeded seeded in colony formation after 24 hours. After 8 days, colonies were collected, washed twice with PBS and replated in a secondary colony formation assay. On day 17, colonies were collected followed by plating in a 96-well plate for drug testing. Cells were treated with ABT-199 for two days and drug activity assessed by resazurin assay. Cells were also stained with PI for cell cycle analysis on day 17.

5.3.5 ABT-199 treatment in vivo

The fourth *in vivo* experiment (Fig 4-6) consisted of 28 mice divided into two primary treatment groups, 14 mice in each group, *RUNX1/ETO* treated group (LNP/siRE-mod) and a control group (LNP/siMM-mod). After weaning, the leukaemic burden was assessed by IVIS imaging, then mice were randomised into four groups according to the IVIS signal. Mice were dosed with 100 mg/kg of ABT-199 or a control vehicle (CV) as shown in Fig 5-4.

The treatment groups were as follows;

LNP/siMM-mod + CV (7 mice; 3 females and 4 males)

LNP/siMM-mod + ABT-199 (7 mice; 5 females and 2 males)

LNP/siRE-mod + CV (7 mice; 4 females and 3 males)

LNP/siRE-mod + ABT-199 (7 mice; 3 females and 4 males)

Leukaemia propagation was monitored by IVIS every week. Mice were culled when they reached any of the protocol endpoints stated in 4.3.3.

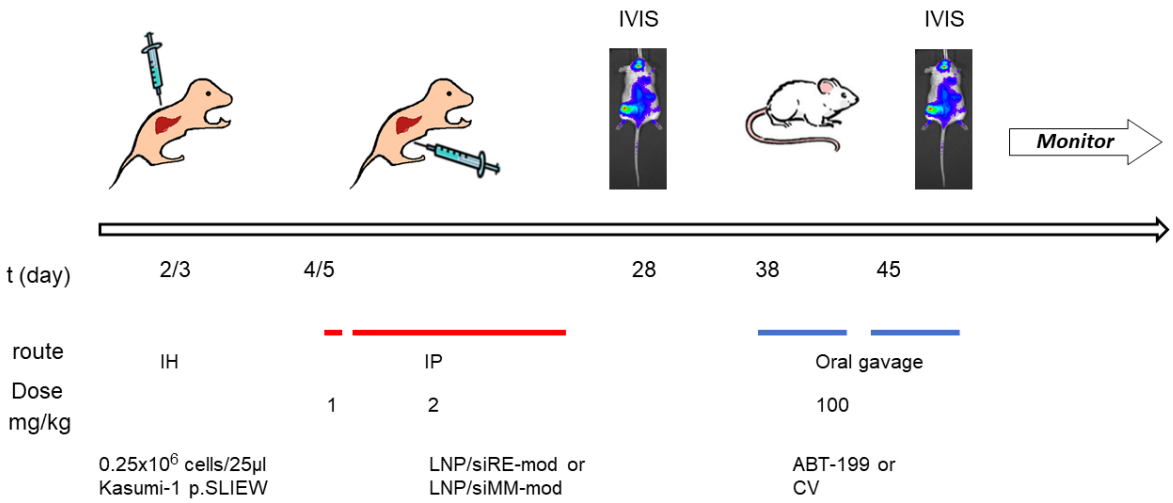

Fig 5-4: Experimental set up of ABT-199 treatment *in vivo* upon. Mice were transplanted and treated with lipid nanoparticles as described in Fig 4-6 and shown in the scheme above. Upon weaning, leukaemia engraftment was assessed by IVIS imaging on days 28 and 33. On day 38, the *RUNX1/ETO* targeted group and the control group were divided into two subgroups (7 mice each) as indicated in 5.3.5. Mice received 10 oral gavage doses of 100 mg/kg of ABT-199 or CV over two weeks. Mice monitored by IVIS during and after the treatment and culled when they reached the protocol endpoints.

5.4 Results

5.4.1 Sensitivity to AraC in response to RUNX1/ETO knockdown

Sensitivity towards AraC was investigated only in Kasumi-1 p.SLIEW cells with and without *RUNX1/ETO* knockdown. The viability of Kasumi-1 p.SLIEW was measured after 3 days of continuous treatment with AraC. The control cells (siMM electroporated cells) were responsive to AraC with 540 nM (IC_{50}). The depletion of *RUNX1/ETO* by siRE-mod reduced the sensitivity to AraC, and the IC_{50} became aournd1600 nM (Fig 5-5).

Since *RUNX1/ETO* knockdown did not sensitise Kasumi-1 cells to AraC treatment, no further experiments were perused.

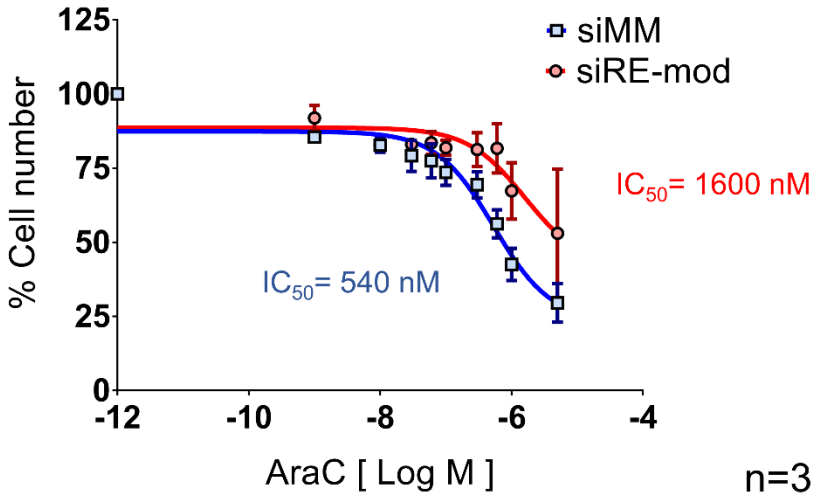

Fig 5-5: Cytotoxicity of AraC in Kasumi-1 p.SLIEW cells after *RUNX1/ETO* knockdown. The viability of Kasumi-1 p.SLIEW cells after AraC treatment with and without *RUNX1/ETO* knockdown. Data is presented as the percentage of viable cells after projecting the chemiluminescence intensity to the corresponding cell number. Error bars represent the SEM of three independent experiments.

5.4.2 RUNX1/ETO knockdown and sensitivity to Rucaparib

The response to the PARP inhibitor, Rucaparib, was also investigated following a similar approach to AraC experiments. The knockdown of *RUNX1/ETO* was achieved by two sequential electroporations and Rucaparib treatment was applied for 3 days. Kasumi-1 p.SLIEW cells were sensitive to Rucaparib at 3 µM (IC_{50}). Upon *RUNX1/ETO* knockdown, Kasumi-1 p.SLIEW responsiveness to Rucaparib was reduced and the IC_{50} was not achieved (IC_{50} >34 µM) (Fig 5-6). For this reason, no further experiments were conducted.

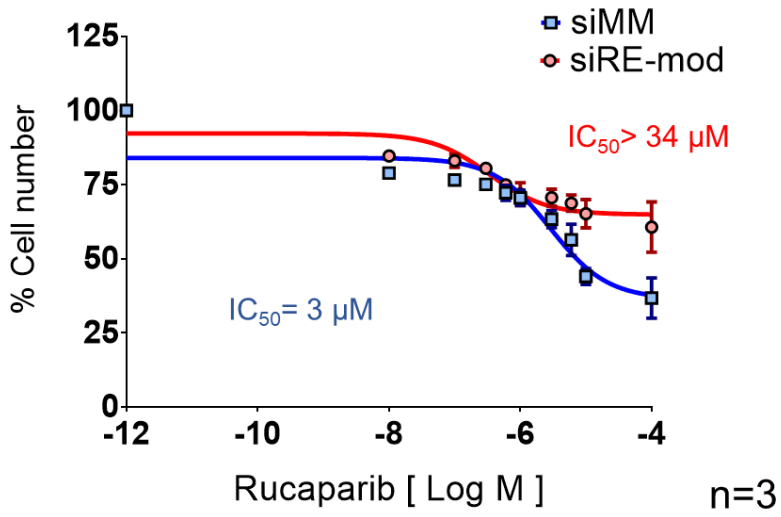

Fig 5-6: Cytotoxicity of Rucaparib in Kasumi-1 p.SLIEW cells after *RUNX1/ETO* knockdown. The viability of Kasumi-1 p.SLIEW cells after Rucaparib treatment with and without *RUNX1/ETO* knockdown. Data is presented as described in the legend to Fig 5-5. Error bars represent the SEM of three independent experiments.

5.4.3 RUNX1/ETO knockdown in t(8;21) AML cells lines and their sensitivity to ABT-199

BCL2 inhibition by ABT-199 was assessed using two independent assays, a fluorescent-based assay (resazurin) in Kasumi-1 and SKNO-1 cells lines, and a luciferase assay in both Kasumi-1 p.SLIEW and SKNO-1 p.SLIEW cells. Both AML cell lines, without electroporation, were sensitive in the nM range to BCL2 inhibition by ABT-199. The resazurin and luciferase assays both provided similar IC_{50} values. In Kasumi-1, the IC_{50} was 35 nM and 32 nM (Fig 5-7A) as measured by resazurin and luciferase, respectively. Similarly, SKNO-1 was sensitive to ABT-199 at IC_{50} of 24 nM and 25 nM as measured by resazurin and luciferase, respectively (Fig 5-7B). These experiments showed that t(8;21) AML cell lines are sensitive to ABT-199 treatment, and both luciferase and resazurin assays provide comparable results.

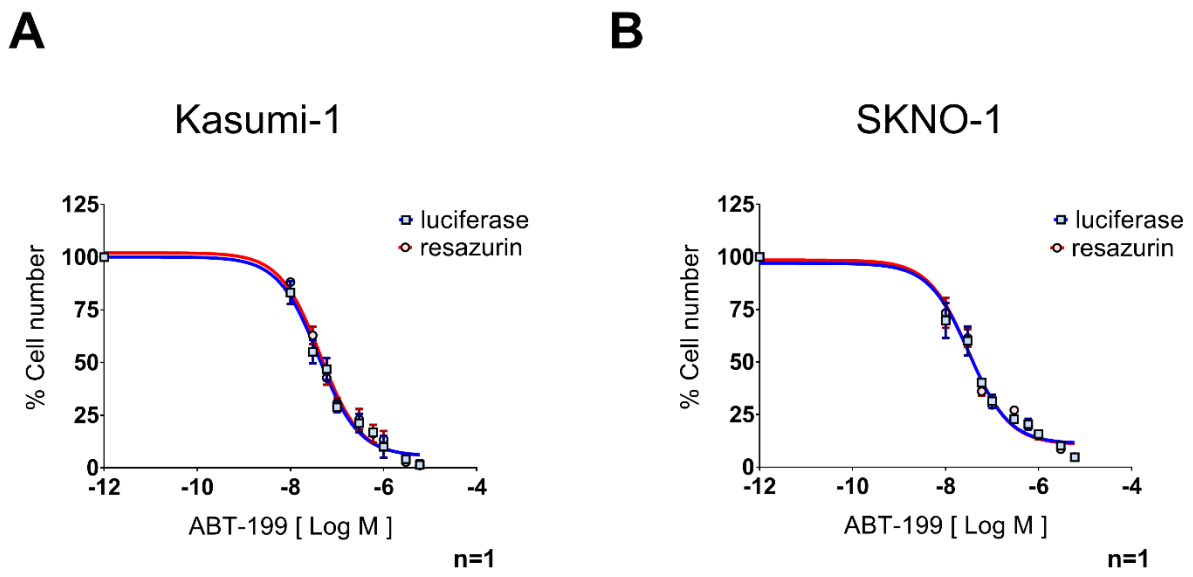

Fig 5-7: Cytotoxicity of ABT-199 in AML t(8;21) cell lines. The viability of Kasumi-1 (A) and SKNO-1 (B) cells to ABT-199 treatment. The luciferase assay data (blue line) is presented as described previously in the legend to Fig 5-5. The resazurin viability data (red line) is presented as the percentage of viable cells after projecting the fluorescence intensity to the corresponding cell number. Data presents the mean of three wells per treatment. Error bars represent the standard deviation of the mean of three wells per treatment.

The knockdown of *RUNX1/ETO* by siRNA enhanced the effect of ABT-199 treatment *in vitro*. The depletion of *RUNX1/ETO* in Kasumi-1 p.SLIEW cells reduced the IC_{50} from 28 nM to 10 nM as measured by the luciferase reporter assay (Fig 5-8A). This effect was confirmed with the resazurin assay, as shown in (Fig 5-8C). Similarly, treatment with ABT-199 was more effective when SKNO-1 p.SLIEW cells were under *RUNX1/ETO* knockdown by siRNA. Luciferase assays showed a fivefold reduction in the IC_{50} (from 28 nM to 5 nM) upon *RUNX1/ETO* knockdown (Fig 5-8B). The resazurin assay confirmed that the IC_{50} was reduced from 18 nM to 7 nM in SKNO-1 pSLIEW cells (Fig 5-8D).

Notably, the effect of ABT-199 did not differ significantly between naïve cells without electroporation and cells under mismatch siRNA (siMM) transfection (Fig 5-7 & Fig 5-8). The IC_{50} of the naïve cell line and the mismatch electroporated Kasumi-1 was 35 and 37 nM, respectively (Fig 5-7A & Fig 5-8C). In SKNO-1 p.SLIEW cells, the IC_{50} was 25 and 28 nM for naïve and siMM electroporated cells, respectively, as measured by luciferase assay (Fig 5-7B & Fig 5-8B).

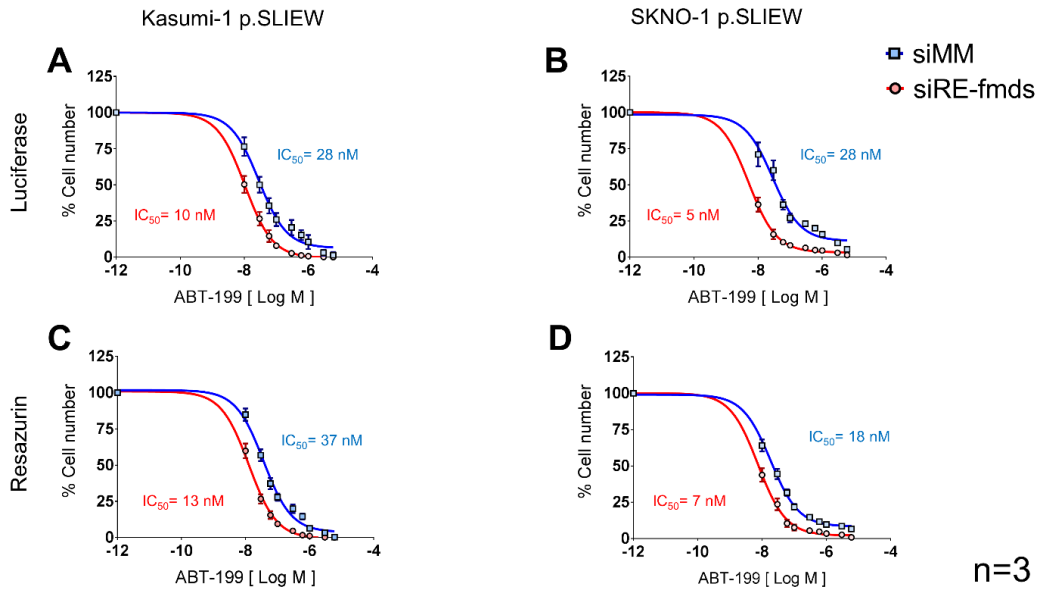

Fig 5-8: Cytotoxicity of ABT-199 in AML t(8;21) cell lines after *RUNX1/ETO* knockdown. The viability of Kasumi-1 (A, C) and SKNO-1 (B, D) cells to ABT-199 treatment with (red line) and without (blue line) *RUNX1/ETO* knockdown. The luciferase assay data (A, B) is presented as described previously in the legend to Fig 5-5. The resazurin viability data (C, D) is presented as described previously in the legend to Fig 5-7. Data presents the mean of three independent experiments. Error bars represent the SEM of three independent experiments.

5.4.4 The effect of the G1 cell cycle arrest on BCL2 inhibition

RUNX1/ETO repression resulted in an enhanced response to ABT-199 treatment but not to DNA damage agents AraC and Rucaparib. Given that *RUNX1/ETO* knockdown leads to a cytostatic phenotype governed by G1 cell cycle arrest, we investigated the relationship between the cell cycle status and sensitivity to ABT-199 treatment. We introduced the cell cycle arrest directly by deleting the cell cycle gene *CCND2* by siRNA, or indirectly by *RUNX1/ETO* knockdown.

The knockdown of either *RUNX1/ETO* by siRE-mod, or *CCND2* by (siCCND2_2 & siCCND2_4) induced the same level of the G1 cell cycle arrest in SKNO-1 cells. The G1 phase increased to 60.5% and 63% after *RUNX1/ETO* and *CCND2* knockdown, respectively, compared to 48% in the mismatch control (Fig 5-9A). The resazurin assay showed that *CCND2* knockdown did not enhance the sensitivity to ABT-199. On the other hand, *RUNX1/ETO* knockdown enhanced the sensitivity to ABT-199 treatment by fivefold (Fig 5-9B and Fig 5-8B, D). It cannot be concluded from one experiment that the G1 cell cycle arrest status does not influence the sensitivity to BCL2 inhibition. However, the results obtained from SKNO-1 cells reaffirm that *RUNX1/ETO* knockdown sensitises the cells to ABT-199.

In order to elucidate the effect of *RUNX1/ETO* expression on BCL2 inhibition, *RUNX/ETO* was repressed by siRNA, and cells were plated in two serial replating of colony formation assay followed by treatment with ABT-199. Cell cycle profiling of harvested colonies showed that the knockdown cells do not have cell cycle arrest after two replatings (Fig 5-10A). Surprisingly, the *RUNX1/ETO* knockdown cells showed a twofold enhanced sensitivity to ABT-199 treatment. Harvested cells from the replated control colonies (siMM transfection) had an IC_{50} of 29 nM, while the *RUNX1/ETO* targeted cells (siRE-mod transfection) showed an IC_{50} of 16 nM (Fig 5-10B). The prolonged effect of *RUNX1/ETO* repression on BCL2 inhibition has further confirmed our observation that the enhanced response to ABT-199 is independent of the G1 cell cycle arrest. For this reason, the effect of cell cycle arrest was not investigated any further. Additional experiments would have deciphered the relation between *RUNX1/ETO* expression and BCL2 inhibition, which was not pursued due to time constraint.

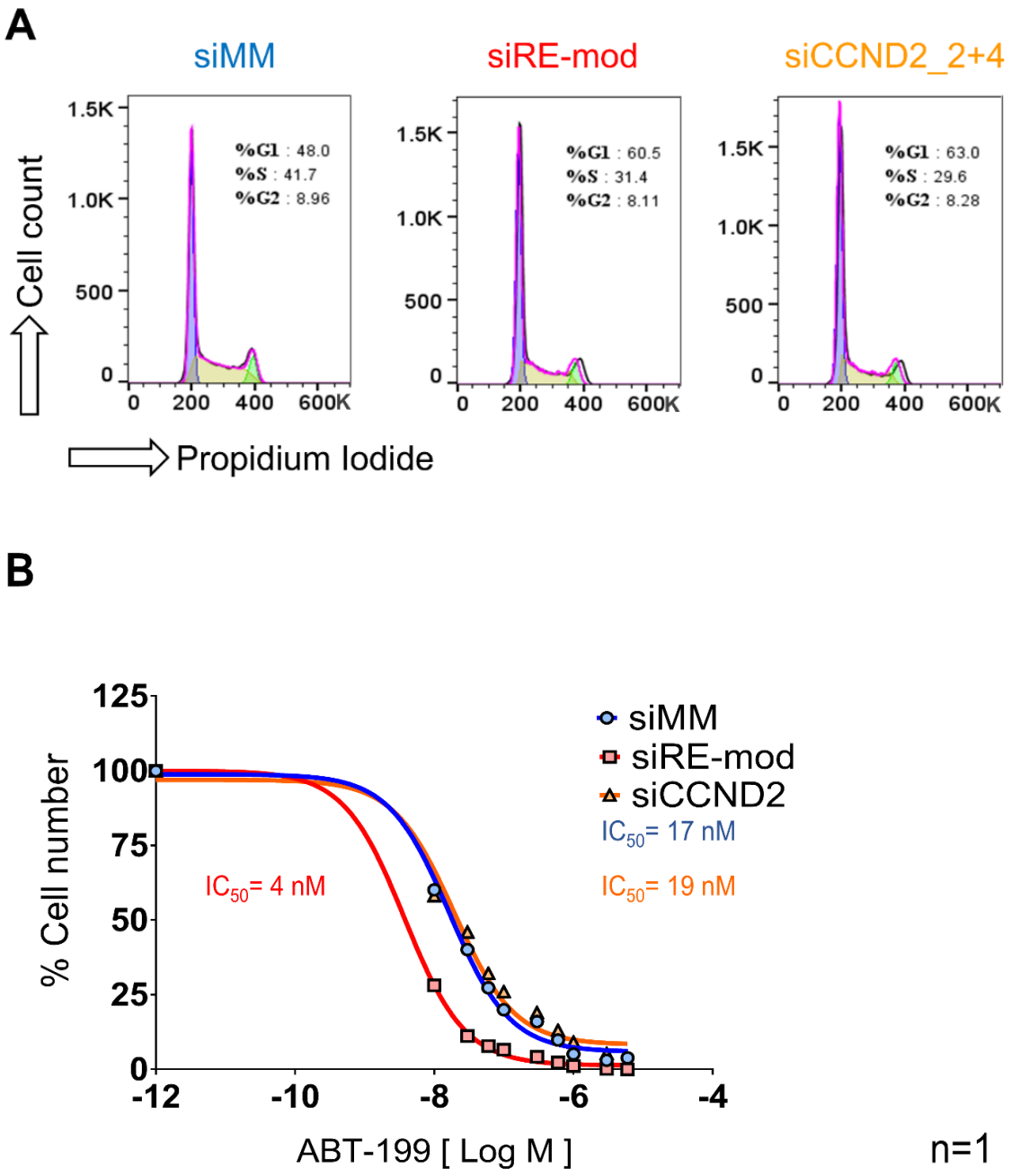

Fig 5-9: Cytotoxicity of ABT-199 in SKNO-1 cells after the induction of G1 cell cycle arrest. The effect of G1 cell cycle arrest on SKNO-1 response to ABT-199 treatment. The cell cycle arrest was induced by depleting *RUNX1/ETO* or *CCND2* by siRNA. (A) Cell cycle profiling by PI staining. (B) The viability of SKNO-1 cells after ABT-199 treatment, and the depletion of *RUNX1/ETO* (red line), *CCND2* (orange line) and without gene knockdown (blue line). The resazurin viability data is presented as described previously in the legend to Fig 5-7. Data presents the mean of three wells per treatment. Error bars represent the standard deviation of the mean of three wells per treatment.

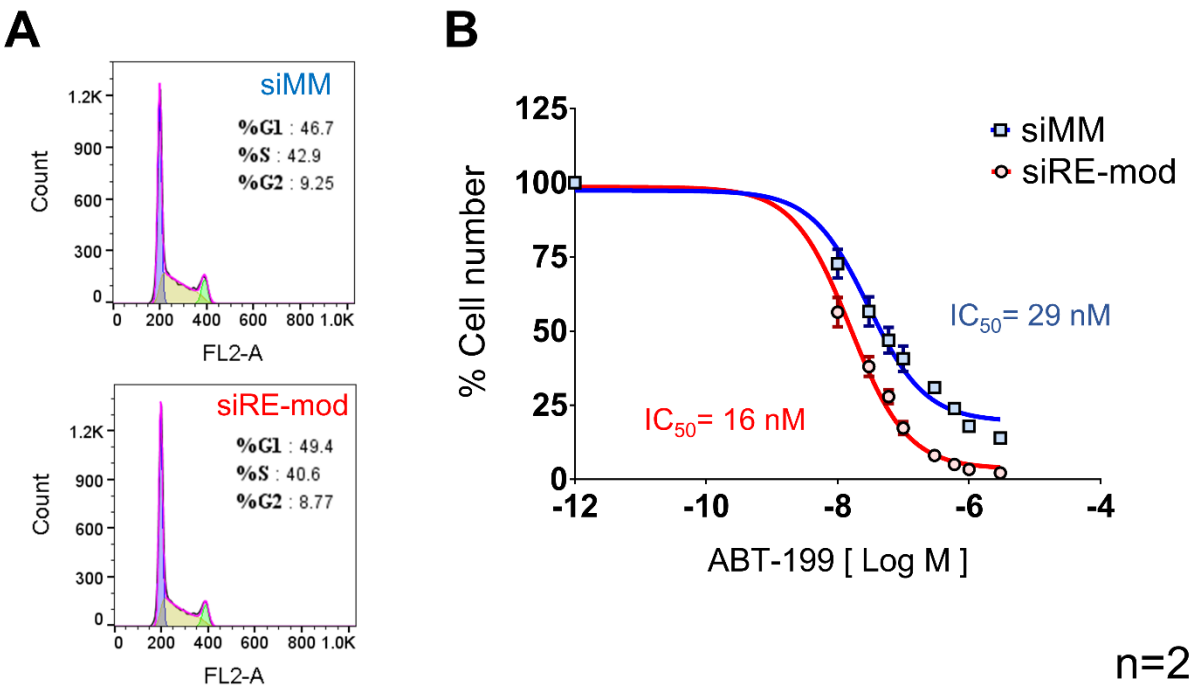

Fig 5-10: Long-term effect of *RUNX1/ETO* knockdown on sensitivity to ABT-199. SKNO-1 cells susceptibility to ABT-199 cytotoxicity after perennial *RUNX1/ETO* knockdown. The *RUNX1/ETO* knockdown-associated G1 cell cycle arrest disappears after two rounds of colony formation replatings but the sensitivity to ABT-199 remains. (A) PI cell cycle profiling of cells harvested from the *RUNX1/ETO* knockdown colonies and the mismatch control showing similar distributions of the cell cycle phases. (B) The viability of harvested SKNO-1 cells from the colony formation assays followed by ABT-199 treatment. The RUNX1/ETO-knockdown colonies are presented in the red line and the negative control in the blue line. The resazurin viability data was presented as described previously in the legend to Fig 5-7. Data represents the mean of two independent experiments. Error bars represents the standard deviation of the mean of two independent experiments.

5.4.5 BCL2 inhibition and RUNX1/ETO knockdown and effect on apoptosis

Given that BLC2 is localised on the mitochondria surface and regulates cell survival by inhibiting pro-apoptotic proteins, we assessed the expression of various proteins involved in the mitochondrial apoptosis pathways in response to ABT-199 treatment and *RUNX1/ETO* knockdown.

Western blotting showed that the depletion of RUNX1/ETO did not change BCL2 level in Kasumi-1 p.SLIEW cells, but a slight increase in BCLXL and MCL1 was observed (Fig 5-11). The knockdown was also associated with an increase in BIM protein expression. Treatment with ABT-199 resulted in a general reduction in RUNX1/ETO as well as RUNX1 level with and without *RUNX1/ETO* knockdown. Interestingly, the combination of RUNX1/ETO and ABT-199 treatment led to a marked MCL1 reduction in comparison with the control siMM transfected cells. Furthermore, the depletion of RUNX1/ETO and ABT-199 treatment did not affect the expression of BCL2 and BCLXL as well as BIM.

Due to experimental procedures, including stripping and reprobing of the membrane serval times, it was not possible to quantify the level of the housekeeping proteins. Nevertheless, Ponceau S red staining shows relatively equal loading and transfer.

Interestingly, Ponceau S red staining showed a prominent band around 70 kDa, which disappeared after ABT-199 treatment. This band is unlikely to be serum albumin (~ 66.5 kDa) because the cell pellets were washed twice with PBS to remove any traces of FCS before lysing the cells with RIPA buffer. Ponceau S red is unselective stain for proteins and polypeptides (Stochaj, Berkelman et al. 2006). Thus, it is very difficult to assign this band to a specific protein. We have extensively searched the literature to explain this observation but we could not find a conclusive answer.

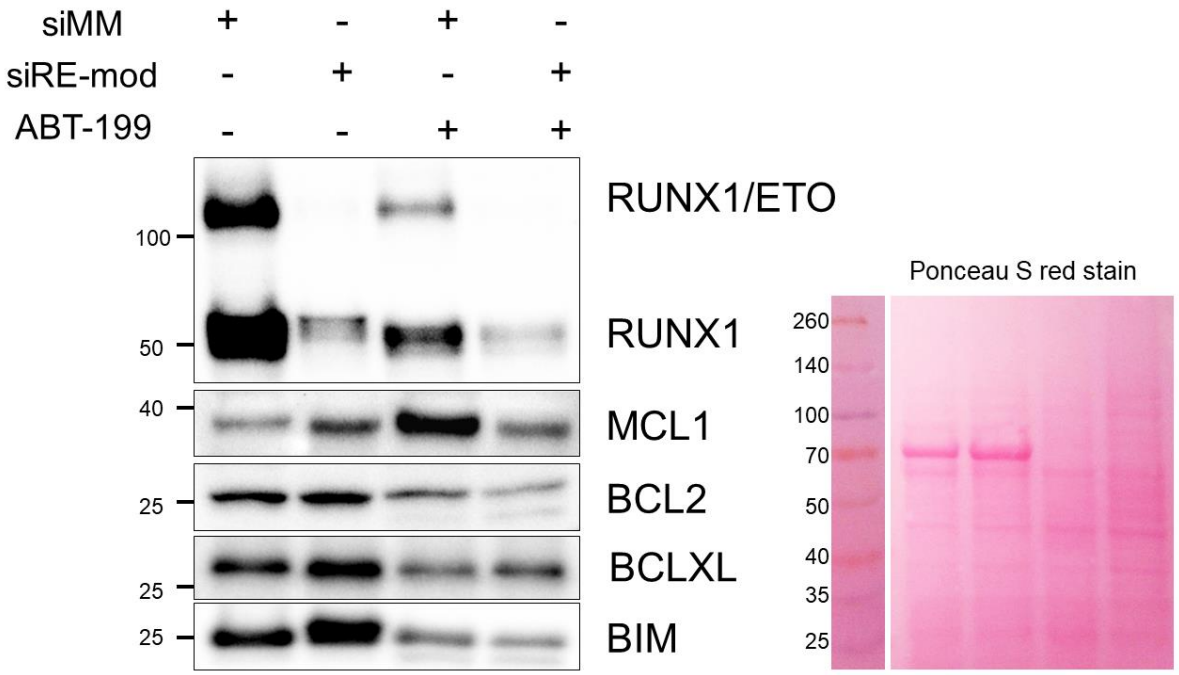

Fig 5-11: RUNX1/ETO knockdown and BCL2 inhibition effects on apoptosis proteins. Western blotting was performed to examine the expression of several proteins associated with the mitochondrial apoptosis pathways in Kasumi-1 p.SLIEW cells. The modulation of the apoptosis pathway was introduced by RUNX1/ETO knockdown followed by ABT-199 treatment. Membrane was blotted against α-RUNX1, α-MCL1, α-BCL2, α-BCLXL, and α-BIM antibodies. Ponceau S red stain was used to show the loading quality. Marker size in kDa is presented on the left side of the membrane.

5.4.6 ABT-199 treatment in vivo

In vitro experiments suggested that t(8;21) AML cell lines are sensitive to BCL2 inhibition by ABT-199. The combination of ABT-199 treatment and *RUNX1/ETO* knockdown was more effective than ABT-199 treatment alone. For this reason, the combination treatment was investigated *in vivo*.

Following the LNP/siRNA treatment in the fourth *in vivo* experiment, each treatment group was further divided into two secondary treatment arms. The randomisation was performed based on the mean of two consecutive IVIS imaging after weaning. The ABT-199 treatment was applied after 10 days from completion of the LNP/siRNA treatment.

After 10 doses of 100 mg/kg of ABT-199 or CV by oral gavage, the ABT-199 treatment showed increase in the IVIS of all treated groups. Unexpectedly, Kasumi-1 p.SLIEW cells were not sensitive to ABT-199 *in vivo* (Fig 5-12A). ABT-199 did not reduce the leukaemic burden of the LNP/siMM-mod control group, as the IVIS signal was similar to the LNP/siMM-mod + CV treatment group. Moreover, the combination of ABT-199 treatment and *RUNX1/ETO* knockdown led to a rapid increase in the IVIS signal in comparison with a combination of CV treatment and *RUNX1/ETO* knockdown.

ABT-199 treatment resulted in only 10 days (p=0.057) increase in the median survival of the knockdown-control arm (LNP/siMM-mod) in comparison with the control group (LNP/siMM-mod+ CV treatment).

The combination of BCL2 inhibition and *RUNX1/ETO* knockdown was therapeutically disadvantageous, as the median survival of the *RUNX1/ETO* targeted group was reduced (p=0.1) from 80 to 67 days in the LNP/siRE-mod + CV group and LNP/siRE-mod + ABT-199 group, respectively. Moreover, the median survival of the ABT-199 treated arms LNP/siMM-mod, and LNP/siRE-mod were 55 and 67 days, respectively, with no significant difference (Fig 5-12B).

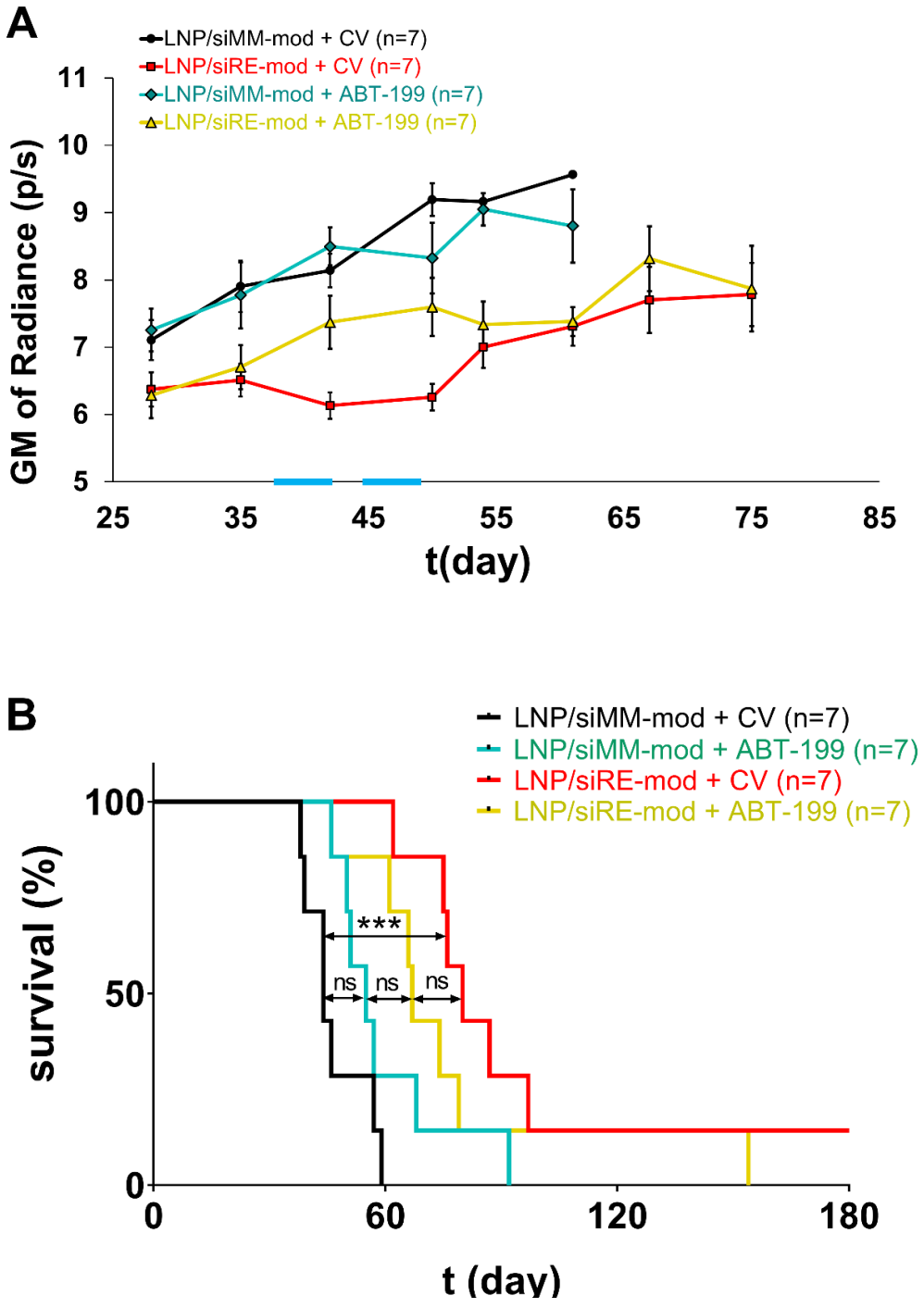

Fig 5-12: The effect of ABT-199 treatment *in vivo*. (A) Leukaemia burden was assessed by the bioluminescence of engrafted mice. Data is presented as the mean of total bioluminescence from 7 mice in each of the fours treatment arms. Error bars represent the SEM of the geometric mean of the total bioluminescence in each treatment arm. (B) Kaplan–Meier graph of the four treated arms. *P<0.05, **P<0.01, ***P<0.001.

5.5 Results summary

The heterogeneity of AML cytogenetic demands for more research on targeted and personalised treatment. Although t(8;21) AML is a favourable cytogenetic abnormality, a considerable cohort of patients has a poor prognosis if presented with additional mutations such as *FLT3-ITD* and *C-KIT* (Itzykson, Gardin et al. 2011, Ryotokuji, Yamaguchi et al. 2016). Patients with t(8;21) leukaemia are treated with combination therapies of high dose AraC and anthracyclines in the consolidation phase. Approximately 75% of treated patients have complete remission and some present disease-free survival. However, the current treatment options are highly toxic, which justifies the need for new therapeutic approaches (Schlenk, Dohner et al. 2008, Dohner, Estey et al. 2010, Vu and Kharas 2018). Given that *RUNX1/ETO* is a leukaemic specific fusion gene, and repression of the oncoprotein leads to a cytostatic phenotype, combination chemotherapies with *RUNX1/ETO* targeting may have a therapeutic advantage.

The DNA damage agents AraC and Rucaparib showed an antagonistic effect when combined with *RUNX1/ETO* knockdown. The depletion of *RUNX1/ETO* led to G1 cell cycle arrest, and subsequently a reduction in the S phase. Given that, AraC and Rucaparib are both active in the S phase of the cell cycle, the reduced sensitivity to the DNA damage after *RUNX1/ETO* knockdown is expected. The obtained IC_{50} of AraC treatment in Kasumi-1 could potentially be achievable in clinical setting (Wang, Harrison et al. 2016), but the depletion of *RUNX1/ETO* reduced the sensitivity dramatically. Moreover, Kasumi-1 cells poorly responded to high doses of Rucaparib, suggesting that PARP inhibition by Rucaparib alone may not provide any therapeutic window for t(8;21) positive leukaemias. Nevertheless, a combination of AraC and Rucaparib together, or with other inhibitors might be beneficial, but this is beyond this project's research questions.

MCL1 expression is crucial for healthy haematopoietic stem cell expansion, but leukaemic stem cells rely on BCL2 expression for survival (Vairo, Innes et al. 1996, Opferman, Iwasaki et al. 2005). Recent clinical data shows that AML patients benefit from BCL2 inhibition by ABT-199 (Pan, Hogdal et al. 2014, Teh, Nguyen et al. 2018). Previous *in vivo* work performed in our group has also shown that inhibition of BCL2 significantly prolonged the survival of immunocompromised mice bearing t(4;11)

AML leukaemia (unpublished data). For these reasons, the sensitivity of Kasumi-1 and SKNO-1 cell lines to ABT-199 was investigated. The luciferase reporter assay, as well as the cytotoxicity fluorescence-based assay, equally showed that t(8;21) AML cell lines are sensitive to BCL2 inhibition by ABT-199 in the low nanomolar range. Interestingly, the depletion of *RUNX1/ETO* by siRNA enhanced the effect of ABT-199 treatment *in vitro.* Throughout the ABT-199 treatment experiments, the knockdown of *RUNX1/ETO* was achieved by a 100 nM siRNA. Therefore, we cannot conclude whether the enhanced sensitivity to BCL2 inhibition is synergistic or additive when combined with *RUNX1/ETO* knockdown.

The enhanced cell death in the combination of *RUNX1/ETO* depletion and BCL2 inhibition was independent of the G1 cell cycle arrest since the knockdown of the cell cycle gene *CCND2* did not enhance the sensitivity to ABT-199. Furthermore, the pharmacological inhibition of the CDK4/6 complex by palbociclib does not change the sensitivity to ABT-199 treatment in t(8;21) and t(4;11) AML cell lines (unpublished data). Interestingly, BCL2 inhibition was susceptible to prolonged *RUNX1/ETO* depletion. The effect of *RUNX1/ETO* knockdown on BCL2 inhibition was detectable after two rounds of colony formation replatings. This finding may suggest a relationship between *RUNX1/ETO* expression and the mitochondrial apoptosis network.

Despite the improved toxicity of ABT-199 treatment after *RUNX1/ETO* knockdown *in vitro*, this combination therapy was disadvantageous *in vivo*. ABT-199 dosing scheme was obtained from collaborators, and relevant to recent published literature (Scherr, Kirchhoff et al. 2019). However, ABT-199 monotherapy did not significantly increase the survival of the mice. Kasumi-1 cells were sensitive to ABT-199 *in vitro* but not *in vivo*. Several factors might have contributed to the low potency of ABT-199 *in vivo*, including the pharmacodynamics, microenvironment, and the xenotransplantation model. Thus, it cannot be confirmed that BCL2 inhibition occurred in the cells *in vivo*. Unexpectedly, the combination of *RUNX1/ETO* knockdown by siRNA and ABT-199 treatment resulted in a faster expansion of leukaemia in comparison with *RUNX1/ETO* knockdown alone.

Chapter 6.

Concluding discussion

6.1 Introduction

The chromosomal translocation t(8;21) is linked to over 12% of *de novo* AML cases. The translocation product RUNX1/ETO is an oncogenic transcription factor (Ptasinska, Assi et al. 2014). Although patients with t(8;21)-positive leukaemia have favourable prognoses, current treatment accounts for a broad spectrum of side effects (Burnett, Hills et al. 2010, Grimwade, Hills et al. 2010). The *RUNX1/ETO* transcript is leukaemia-specific and thus serves as an ideal model for specific targeting with siRNA (Heidenreich, Krauter et al. 2003). Former RNAi-based functional studies identified some of the mechanisms underlying the leukaemogenesis of RUNX1/ETO. Although these *in vitro* studies successfully proved that RUNX1/ETO initiates and maintains leukaemia propagation via complex transcriptional networks (Martinez, Drescher et al. 2004, Ptasinska, Assi et al. 2012), it was not possible to confirm these finding *in vivo* due to the lack of potent siRNA delivery systems. The first aim of this project was to silence *RUXN1/ETO in vivo* by a clinically compatible siRNA delivery system.

The hallmark of t(8;21) leukaemia is associated with transformed haematopoietic stem cells (HSCs) characterised by hyperproliferation, enhanced self-renewal, high genomic stability and epigenetic changes in the myeloid lineage-specific transcription factors (Peterson and Zhang 2004, Loke, Assi et al. 2017). Chemoresistance in relapsed patients is widely postulated to be driven by malignant leukaemic stem cells, known as the leukaemic initiating cells (LICs). These LICs are intrinsically capable of escaping the toxic microenvironment caused by chemotherapy, altering their metabolic programme and resting in dormancy (Viale and Pelicci 2009, Cordeiro Gomes, Hara et al. 2016). Since RUNX1/ETO transforms the HSCs into a leukaemic reservoir, its knockdown might ultimately reduce leukaemia expansion and impair relapse (Soria, Tussiwand et al. 2009, Gessner, Thomas et al. 2010). The second aim of this study was to exploit the therapeutic potential of silencing *RUNX1/ETO in vivo* and study the consequences of modulating *RUNX1/ETO* expression.

6.2 Specific silencing of *RUNX1/ETO* by chemically modified siRNA

6.2.1 The specificity of siRNA to RUNX1/ETO transcript

The translocation between chromosomes 8 and 21 produces a single chimaeric transcript, with one unique breakpoint (Rulina, Spirin et al. 2010). The fusion site of *RUNX1/ETO* was targeted by siRNA (si*RUNX1/ETO*) composed of 21 nucleotides. The antisense of si*RUNX1/ETO* spans over the fusion breakpoint, and it has only seven nucleotides complementary to *RUNX1*. Given that a full complementarity between siRNA and mRNA is required for RISC activity (Haley and Zamore 2004, Ameres, Martinez et al. 2007), si*RUNX1/ETO* should eventually have no effect on the wild type *RUNX1* which is highly expressed in haematopoietic cells (Zhang, Fujioka et al. 1994, Zhang, Hetherington et al. 1996, Lorsbach, Moore et al. 2004). Moreover, upon swapping two nucleotides in the antisense of si*RUNX1/ETO*, we observed that there was no effect on *RUNX1/ETO* or *RUNX1,* suggesting the mutated siRNA an appropriate mismatch control (Fig 3-4 & 3-5). The knockdown of *RUNX1/ETO* by single or serial electroporation resulted in specific depletion of the fusion without changing RUNX1 level, which proved the specific silencing of si*RUNX1/ETO* (Fig 3-6 & 3-7).

6.2.2 Rational design of siRNA chemical modifications

The use of chemically modified siRNA was inevitable since therapeutic interventions require maximal on-target activity with the lowest possible dose. The activity of siRNA comprises of three main processes, first access of the siRNA to its action site in the cells, second specific binding to the target mRNA within the RISC complex, and finally post-binding events including RISC recycling and mRNA degradation (Lee, Seok et al. 2015, Kaczmarek, Kowalski et al. 2017, Khvorova and Watts 2017). From this perspective, we have rationally placed several chemical modifications on si*RUNX1/ETO* and evaluated the activity of the siRNA in a series of comprehensive *in vitro* experiments. The modifications on the antisense strand were placed outside the seed region and towards the 3'-nt overhang in order to avoid interfering with the complementarity to the *RUNX1/ETO* transcript. The modifications of the sense strand were placed in several locations in order to increase the stability and reduce

the off-target binding. We have shown that the chemically modified si*RUNX1/ETO* had enhanced potency indicated by prolonged knockdown and robust changes in RUNX1/ETO downstream targets (Fig 3-4, 3-8,), thereby providing potential for reducing the siRNA dose and improved therapeutic index.

I. Phosphorothioate modification (PS) enhances nuclease resistance

RNA and oligodeoxyribonucleotides are susceptible to degradation by 3' to 5' intracellular exonucleases and endonucleases (Dagle, Weeks et al. 1991). Phosphorothioate modification, which is achieved by substituting one of the nonbridging oxygen atoms with sulphur in the phosphate backbone, is the most common modification in the toolbox of oligonucleotides chemistry. PS modifications protect the single-stranded antisense and the double-stranded siRNA from serum 3' to 5' exonucleases and intracellular nucleases (Eder, DeVine et al. 1991).

Modified siRNA with PS linkage binds plasma proteins and has a higher affinity for cell surface proteins in comparison with unmodified siRNA. Modulation of this property is a tricky task. It is desirable to have high interaction with some serum proteins to improve the siRNA pharmaceutical profile, but not high enough to trigger unspecific internalisation. PS unspecific interactions with proteins may be therapeutically disadvantageous on its own due to the interaction with undesirable toxic proteins (Schlundt, Tants et al. 2017).

While this study aimed to develop a therapeutic siRNA delivery system, the influence of PS modifications on si*RUNX1/ETO* serum stability, and nonspecific cellular uptake were not obstacles. For these reasons, only two PS linkers were introduced to each of the 3'-dT-dT overhangs in si*RUNX1/ETO*. The reduced PS content provided excellent nuclease stability as well as mitigated the drawback of nonspecific interactions with intracellular proteins.

II. 3'-end modification influences the siRNA specificity

The thermostability of siRNA duplex determines the on-target knockdown efficiency of the antisense strand and influences the off-target silencing of the sense stand

(Cerutti, Mian et al. 2000). Within RISC, PAZ domain selects the antisense exclusively based on the differential thermostability between the two ends. The PAZ domain retains the strand with the lowest melting temperature at the 3'-end and more stable 5'-end (Lingel, Simon et al. 2003, Haley and Zamore 2004). PS modifications on the 3'-end equitably reduce the melting temperature of the siRNA duplex in each end (Jaroszewski, Clausen et al. 1996). Moreover, modified 3'-overhang was shown to increase the binding affinity to the PAZ domain (Sipa, Sochacka et al. 2007). On that account, we speculated that the modified overhangs (3'-$dT_{PS}dT$) of si*RUNX1/ETO* should not impair the target specificity. Indeed, the knockdown experiment have proven the on-target activity and demonstrated enhanced gene knockdown (Fig 3-6, Fig 3-7).

The influence of the 3'-end is minimal in the ''two-state'' model of RISC catalytic activity. This model proposes that AGO2 first binds the mRNA by direct contact with the seed sequence, whereas the PAZ domain retains the 3'-end of the antisense. Then in the second step, PAZ releases the 3'-end while the mRNA-antisense duplex remains stable until the PIWI domain starts the endonucleolytic cleavage (Tomari and Zamore 2005). Recent structural studies support the this mechanism and suggest a favourable minimal kinetic model for AGO2 turnover by a series of consecutive 3'-end retention and release from the PAZ domain during each cleavage cycle (Somoza, Terrazas et al. 2010, Maiti, Nauwelaerts et al. 2011, Xu, Wang et al. 2015).

Arguably, weak interactions between the antisense and the PAZ domain enhance the siRNA catalytic activity and specificity, as previously reported in mechanistic and computational studies (Wang, Juranek et al. 2009, Tian, Simanshu et al. 2014). On the contrary, studies on 3'-end modified nucleosides analogues have shown that strong antisense-PAZ domain interactions substantially reduce the off-target activity without affecting the on-target potency (Valenzuela, Onizuka et al. 2016).

Taken together, given that the PAZ domain is not involved in the contact between the seed region and the targeted mRNA (Wang, Juranek et al. 2009, Valenzuela, Onizuka et al. 2016), the $dT_{PS}dT$ motifs at the 3'-end antisense of si*RUNX1/ETO* perhaps has improved the binding affinity of the antisense to the RISC complex without compromising the specificity. Of note, this conclusion does not propose that

the affinity of the antisense to the PAZ domain is a good predictor of the siRNA specificity.

III. 2'-sugar modifications

The 2'-sugar modifications significantly alter siRNA duplex stability. The addition of a steric bulk by introducing 2'-F results in a *North* confirmation of the sugar (Pieken, Olsen et al. 1991, Beigelman, Karpeisky et al. 1995). This modification also enhances the thermal stability and reduces the melting temperature of the siRNA duplex (Watts, Martin-Pintado et al. 2010). Although the 2'-F modifications do not enhance the resistance towards exonucleases, it may confer some protection against endonucleases. For this reason, we have utilised the entropic advantage of the 2'-F modifications at 5'-end on the sense strand to improve the thermal stability of si*RUNX1/ETO* and entice the PAZ domain for recognition of the antisense (Lee, Seok et al. 2015).

The naturally occurring 2'-O-Me modification changes the sugar puckering toward *North* and improves the siRNA duplex stability. Importantly, the 2'-O-Me enhances the resistance towards endonuclease for both single-stranded and double-stranded RNAs (Hernandez, Stockdale et al. 2012, Shen and Corey 2018). Towards this direction, we have modified all the pyrimidine nucleotides on the sense strand of si*RUNX1/ETO* with 2'-O-Me residues.

The focus of this project was to enhance *RUNX1/ETO* knockdown by a modified siRNA. We did not pursue endonuclease stability assays but utilised gene knockdown as an indication of the modification potency. That is because the 2'-sugar modifications on si*RUNX1/ETO* require specific endonucleases that are not expressed in the cellular cytoplasm. Furthermore, the manufacturing cost of the chemically modified siRNAs was high, resulting in a limited quantity for the *in vitro* testing.

6.2.3 Modified siRNA has a potent activity

The repression of *RUNX1/ETO* have already been described in previous studies, including former work in our group, in which unmodified si*RUNX1/ETO* was used to achieve transient gene knockdown. However, serial transfections with up to 500 nM siRNA were required to achieve prolonged repression of *RUNX1/ETO*, thereby limiting the applicability of the siRNA in the therapeutic applications (Heidenreich, Krauter et al. 2003, Martinez, Drescher et al. 2004). In contrast, our modified si*RUNX1/ETO* has provided stronger efficacy and long-lasting effect at fivefold lower concentration and less frequent transfections (Fig 3-3 & 3-7). Having developed and functionally validated modified si*RUNX1/ETO*, gene knockdown *in vivo* has become more approachable.

The enhanced potency of the chemically modified si*RUNX1/ETO* was not surprising. The PS and 2'-sugar modifications at the 5'-end of the sense strand meant to reduce the off-target effect as discussed above. Importantly, these modifications stabilised the 5'-end against nucleases. Recent *in vivo* studies have reported that siRNAs isolated from several organs after systemic administration were degraded at the 5'-end (Jiang, Zhu et al. 2017). This may explain the potent activity at lower doses, as less siRNA molecules per cell are needed to achieve robust knockdown, and generating our modified si*RUNX1/ETO* has supposed to improve the clinical performance and herein associated dose toxicity.

6.2.4 RUNX1/ETO repression beyond mRNA cleavage

We have noticed that the reduction in *RUNX1/ETO* mRNA did not reflect the knockdown at the protein level on several occasions (Fig 3-20A, 3-21A & 3-22). A possible explanation would be RNAi non-silencing pathways were performed by the RISC complex (Filipowicz 2005, Matzke and Birchler 2005). Furthermore, the RNA-seq data of *RUNX1/ETO* depletion *in vivo* and RNA-seq data generated under shRNA gene knockdown *in vitro* (unpublished data and not the focus of this project), have revealed that RUNX1/ETO regulates some genes involved in the RNAi machinery. Furthermore, the repression of *RUNX1/ETO* also has an impact on the expression of genes involved in the regulation of protein synthesis, such as the eukaryotic initiation factor (eIF2). Therefore, we hypothesise that mRNA cleavage by

si*RUNX1/ETO* is partly contributing to *RUNX1/ETO* downregulation, and other non-silencing mechanisms might be involved in the gene knockdown. Further functional studies are recommended to identify possible regulatory pathways involved in stabilisation of *RUNX1/ETO* transcript and protein translation.

Furthermore, previous studies showed that acetylation of RUNX1/ETO hinders the ubiquitin-mediated degradation and stabilises RUNX1/ETO and RUNX1 proteins. (Jin, Jeon et al. 2004, Bali, Pranpat et al. 2005, Wang, Huang et al. 2009). Disturbing the physical interaction between RUNX1/ETO and the heat shock protein 90 (HSP90) has been reported to destabilise RUNX1/ETO. HDACs inhibitors treatment in Kasumi-1 cells have shown hyperacetylation of RUNX1/ETO-interacting proteins, such as HSP90, destabilisation of RUNX1/ETO and once the degradation triggered, a positive feedback for further RUNX1/ETO protein degradation is generated (Bali, Pranpat et al. 2005, Yang, Thompson et al. 2007). Therefore, the knockdown of RUNX1/ETO by si*RUNX1/ETO* to a certain threshold might shift the equilibrium of RUNX1/ETO and its interacting partners towards proteasomal degradation.

6.3 Lipid nanoparticle is a robust siRNA delivery system

With the exception of the liver, systemic delivery remains the main challenge to implement siRNA therapeutics. The low stability and poor pharmacokinetics of intravenously administered siRNA have limited its therapeutic use (Huang, Cheng et al. 2016). Having generated a potent chemically modified si*RUNX1/ETO,* and taking in consideration the recent advances in ionisable lipid nanoparticles (LNPs) (Adams, Gonzalez-Duarte et al. 2018), we have utilised the Dlin-MC3-DMA lipid to encapsulate the siRNAs and investigate gene knockdown in *in vitro* and *in vivo*.

6.3.1 LNPs have a prolonged stability

Regardless of targeted gene or tissue, the siRNA delivery system should be amenable to upscaling and should exhibit a reasonable shelf life and preservation of the cargo activity. Despite the fact that different formulations of LNP/siRNA were used during this project, the nanopractices had consistently low polydispersity index (Table 3-2). We have noticed that one LNP/siRNA formulation was stable over one year without significant changes in the particles size and charge (Fig 3-15). The chosen lipid nanoparticle seemed to be suitable for *RUNX1/ETO* knockdown with the potential for clinical use.

6.3.2 The chemistry and physics of Dlin-MC3-DMA nanoparticles

The lipid pKa determines the potency of the lipid nanoparticles. Dlin-MC3-DMA lipid has a dimethylamine (DMA) head group with pKa = 6.2 to 6.5, which has been validated as a suitable cationic head group for gene silencing *in vivo* including non-human primates animal models (Jayaraman, Ansell et al. 2012). In a broader perspective, the lipid head group influences the nanoparticle structure, siRNA packaging efficiency, cytotoxicity, and mechanism of endosomal release.

I. LNP/siRNA formulation efficacy

Within the context of Dlin-MC3-DMA nanoparticles, the DMA head group grants to the formed particles a nitrogen to phosphate ratio (N/P) of 3 to 6 depending on the formulation parameters. These N/P values are optimal for siRNA encapsulation and gene silencing *in vivo* (Semple, Akinc et al. 2010, Belliveau, Huft et al. 2012). During the LNP/siRNA formulation, loading of the negatively charged siRNA was performed under pH = 4. The acidic conditions ensure that all the lipid amino groups are fully protonated. This allows efficient electrostatic interactions and complexation between the siRNA and the lipid. During this project, we have produced four independent LNP/siRNA formulations with relatively consistent encapsulation efficiencies in three batches (~ 90%). This confirms that the lipid nanoparticle is a reliable and cost-effective siRNA delivery system.

Neutral lipid-based delivery systems may have up to 20% of the siRNA attached to the outer surface and not adequately protected inside the vehicles (Stuart and Allen 2000, Bartsch, Weeke-Klimp et al. 2004). This might results in an overestimation of the encapsulation efficiency. In contrast, the Dlin-MC3-DMA nanoparticles are formulated under a rapid mixing in a microfluidic system that forces the siRNA to be entrapped into the hydrophilic pockets inside the nanoparticle (Semple, Akinc et al. 2010, Belliveau, Huft et al. 2012). For this reason, it can be surmised that the LNP/siRNA formulations had a small amount of surface-bound siRNA, which have improved the accuracy of the encapsulation quantification.

II. PEG influence on the LNP/siRNA size and charge

Structure and size of lipid nanoparticles are good indicators of their potency. Additionally, composition of the lipid mixture and the formulation procedures determine the diameter of the lipid nanoparticles. Dlin-MC3-DMA lipid has a relatively small hydrophilic heads group (DMA) which enables the lipid molecules to form inverted and non-bilayer structures (Gilleron, Querbes et al. 2013). The polyethylene glycol (PEG) ratio also influences the particles size, charge, and potency. Several studies have suggested that 10 - 30% PEG is required to provide stable steric shielding effect (Mu, Hu et al. 2013, Guan, Guo et al. 2017). However, high PEG ratios have prohibitive toxicity, insufficient siRNA-endosomal release, and immuno-stimulation (Mui, Tam et al. 2013, Chen, Tam et al. 2016). The lipid nanoparticles mixture consisted of only 1.5% PEG but still sufficient to significantly stabilise the nanoparticles without compromising the gene knockdown (Fig 3-14, 3.4.5). For these reasons, we propose that the lipid nanoparticles acquired the desired properties for siRNA gene knockdown *in vitro* and *in vivo*.

6.3.3 LNP/siRNA uptake mechanisms

Size and charge of lipid nanoparticle accounts for its cellular uptake mechanism. A 50 nm nanoparticle triggers active cellular endocytosis upon close to the cell surface (Hoarau, Delmas et al. 2004, Mund, van der Beek et al. 2018). The surface shielding also influences the uptake rate of the nanoparticles. It was shown that a high surface

density of PEG is associated with increased steric repulsion and slower uptake, and PEGylated neutral nanoparticles have been suggested to have the poorest uptake. Furthermore, surface charge significantly affects the particle uptake in a way that positively charged nanoparticles induce active phagocytic endocytosis when compared with negatively charged ones (Papisov 1998, Vonarbourg, Passirani et al. 2006).

Whilst the used lipid nanoparticles had a relatively small negative charge (Table 3-2), counter ions near the surface heavily influence the zeta potential measurement of particles in solution and possibly affect the estimation of the surface charge (Delgado, Gonzalez-Caballero et al. 2007). Furthermore, the nanoparticles may not retain their naïve charge under the physiological conditions *in vitro*. Our *in vitro* cell culture media contained up to 20% FCS, and serum proteins can incorporate into the surface of the nanoparticles and change their charge (Tadin-Strapps, Peterson et al. 2011). We showed that the induction of *RUNX1/ETO* knockdown was rapid and potent during short periods, which may suggest that the lipid nanoparticles have fast cellular uptake (Fig 3-20A & 3-21A).

Liposomes with phospholipid bilayers greater than 200 nm were shown to fuse into the cellular membrane and slowly release their cargo (Ziello, Huang et al. 2010). The Dlin-MC3-DMA lipid nanoparticles we have used are less than 100 nm in diameter. Moreover, these lipid nanoparticles have a solid condense core rather than a bilayer structures as it was shown in previous studies (Leung, Hafez et al. 2012, Leung, Tam et al. 2015). Therefore, we can assume that the fusion of the lipid nanoparticles into the cell membrane is less probable.

Clathrin-mediated endocytosis (CME) is considered the main uptake pathway of particles less than 100 nm in diameter with relatively small positive or negative charge (-10 to +10 mV), such as positively charged PEI polyplexes (Rejman, Bragonzi et al. 2005, Rejman, Conese et al. 2006, Shi, Chou et al. 2013). Owing to the nanoparticles diameter (< 100 nm) and the negative charge (-8 to 0.25 mV), it can be sensibly assumed that the uptake mechanism is clathrin-mediated endocytosis (Ziello, Huang et al. 2010, Oh and Park 2014, Jyotsana, Sharma et al. 2018, Mund, van der Beek et al. 2018). Slow siRNA release from liposomes and nanoparticles is associated with caveolin-mediated endocytosis (He, Bennett et al.

2014). We, however, have shown that LNP/siRNA treatment *in vitro* resulted in a rapid *RUXN1/ETO* silencing within less than 24 hours, even with as little as 15 min of exposure time (Fig 3-17A & 3-18A). This may suggest that caveolin-mediated endocytosis did not contribute largely to the uptake of the nanoparticles. Due to time constraints, it was not feasible to investigate the uptake mechanisms. Further experiments should be performed to validate this hypothesis by specific inhibition of the dynamin and clathrin, which are the regulatory proteins for caveolin and clathrin endocytosis, respectively.

In conclusion, endocytosis has been studied for over five decades, yet a full understanding of its multiple types of machinery remains elusive (Schlossman, Schmid et al. 1984, Kaksonen and Roux 2018). Selective blocking of specific uptake route might elucidate the possible cellular uptake pathways (Mettlen, Loerke et al. 2010, Fekri, Delos Santos et al. 2016). Nevertheless, such studies are performed in *in vitro*. This leaves the question of how these processes occur in a complex multicellular system *in vivo* considering factors such as the body fluids dynamics, cell membrane elasticity and immune system response.

6.3.4 LNP/siRNA has low cytotoxicity

Cytotoxicity of the delivery vehicle limits its therapeutic use. Our *in vitro* assessment of the toxicity (Fig 3-16) and *in vivo* work in adult and newborn mice (Fig 4-17) have demonstrated that the lipid nanoparticles has insignificant toxicity. This finding may not be surprising as Dlin-MC3-DMA cationic head group ‘’DMA’’ has the lowest toxicity amongst all the tertiary amino groups (Walker, Jones et al. 2010, Jayaraman, Ansell et al. 2012, Kanasty, Dorkin et al. 2013). Furthermore, the low ratio of PEG (1.5%) in the lipid mixture may have largely reduced the toxicity. The high siRNA encapsulation efficiency meant that the therapeutic dose could be achieved with fewer nanoparticles, which also minimise the cytotoxicity of the lipid mixture. Taken together, the Dlin-MC3-DMA nanoparticles provide a safe vehicle for siRNA delivery *in vitro* and *in vivo*.

It has been shown that the Dlin-MC3-DMA lipid nanoparticles are well tolerated in immunocompromised hosts. Previous research has demonstrated that lipid nanoparticles treatment does not alter the number of white blood cells, platelets, and haemoglobin. It was also shown that lipid nanoparticles treatment does not cause any significant changes in liver enzymes such as aspartate aminotransferase (ALT) and alanine aminotransferase (ALT), and has minimal effect on the kidney and pancreas functions. However, nanoparticles treatment was shown to significantly increase serum albumin in NSG mice due to the presence of the cationic amino group (DMA) in the lipids (Jyotsana, Sharma et al. 2019).

Furthermore, it has been recently shown that Dlin-MC3-DMA nanoparticles treatment in immunodeficient hosts may stimulate the innate immune system, but it does not increase immunogenicity. It was reported that extended systemic administration of the nanoparticles in non-human primates elevates IL-6 serum level and induces a potent innate immune response (Hassett, Benenato et al. 2019, Sune-Pou, Limeres et al. 2019). For the clinical implementation of the lipid nanoparticles, it is essential to ensure that prolonged exposure to the lipid does not evoke an immunological response. We did not investigate the immune stimulation of the nanoparticles treatment due to the time constraints. Therefore, we suggest investigating whether the nanoparticles treatment can act as immunostimulants in immunodeficient and immunocompetence mice. It is necessary to look at the different immune-modulatory mechanisms following the nanoparticles treatment by monitoring the changes in serum interleukins, cytokines and interferons such as IL-1, IL-6, IL-12, lL-16, TNF-α, INF-α, INF-β and INF-γ. We also recommend exploring the effect of the nanoparticles on activating non-immunological cells *in vitro*, such as endothelial cells and fibroblasts, which are known to secrete several cytokines and immunogens. Current state-of-the-art multiplex ELISA and high throughput capillary immunoassays can be used to determine simultaneously the serum level of serval interleukins and interferons using few microliters of the plasma.

6.3.5 LNP/siRNA efficiently releases the siRNA into the cytoplasm

The job of the siRNA delivery vehicle does not end with the internalisation onto the cellular membrane. Efficient delivery systems should promote destabilisation of the endosome and the release of siRNA simultaneously from the vehicle and the endosome. Potent lipid formulations are expected to maintain stable lamellar phase to protect the siRNA, but also have a fast transition between the lamellar and the hexagonal phases, known as the transition temperature, within the endosome (Koltover, Salditt et al. 1998). Amphiphilic properties of lipid molecules determine the transition temperature where small hydrophilic centres and long hydrophobic tails exponentially reduce the transition temperature. The nanoparticles are expected to facilitate quick endosomal release of siRNA into the cytoplasm. That is because the Dlin-MC3-DMA lipid has a low transition temperature from lamellar to hexagonal phase due to its small polar head group and large unsaturated hydrophobic tail. The other factor that contributes to the transition temperature is cholesterol content. Liposomes consisting of 17% cholesterol can release over 90% of their encapsulated cargo within 5 minutes upon endocytosis (Zhigaltsev, Maurer et al. 2002, Viger-Gravel, Schantz et al. 2018). The LNP/siRNA has 38.5% cholesterol, which is expected to lower the transition temperature further and fasten the siRNA release.

Furthermore, intra-endosomal positive surface charge is required for endosomal release via the proton sponge effect (Hafez, Maurer et al. 2001, Semple, Akinc et al. 2010). The pKa of Dlin-MC3-DMA is 6.2 to 6.5 meaning that the lipid molecules will be protonated inside the lysosome resulting in an increased proton sponge effect over time leading to the rapture of the endosome and siRNA release (Creusat, Rinaldi et al. 2010, Benjaminsen, Mattebjerg et al. 2013). Nevertheless, the understanding of endosomal release is not fully complete and many mechanistic gaps of the nanoparticles interactions with different stages of the endosome during maturations are still unknown.

Overall, we have shown a rapid deletion of *RUNX1/ETO* transcript upon treatment with the lipid nanoparticles (Fig 3-20, 3-21 & 3-22), which can be explained by efficient release of the siRNA from the particles and the endosome.

6.4 The consequences of *RUNX1/ETO* knockdown *in vitro*

6.4.1 RUNX1/ETO depletion inhibits proliferation

Fusion genes, namely those that act as transcription factors, can control malignant cell proliferation. The transit depletion of *RUNX1/ETO* by siRNA significantly inhibited t(8;21) cell lines proliferation. The notion of a fusion protein controlling the proliferation of haematopoietic stem cell is not new. For instance, RNAi-mediated knockdown of *BCR/ABL* by antisense or siRNA inhibit the proliferation of chronic myeloid leukaemia (CML) cells (Skorski, Szczylik et al. 1991, O'Brien, Kirkland et al. 1994, Scherr, Battmer et al. 2003).

We have shown that RUNX1/ETO enhances leukaemic cell proliferation (Fig 3-3 & 3-19). There is contradictory research arguing that RUNX1/ETO expression represses proliferation, and other oncogenic factors are responsible for the hyperproliferative phenotype of leukaemic cells (Amann, Nip et al. 2001, Burel, Harakawa et al. 2001). Nonetheless, RUNX1/ETO inhibited proliferation after forced ectopic expression of *RUNX1/ETO* in cell lines do not carry the t(8;21) translocation. Furthermore, t(8;21) AML phenotype requires a sequence of genomic alterations, beginning with the translocation, expression of the fusion protein RUNX1/ETO which dysregulates RUNX1 transcriptional activity and establishes its oncogenic transcriptional network (Loke, Assi et al. 2017). For these reasons, as shown by our experiments on AML cell lines in which t(8;21) is the main oncogenic event, RUNX1/ETO attributes to the proliferation of leukaemic cells.

Experiments performed in t(8;21) AML cell lines and primary patient cells showed that RUNX1/ETO renders leukaemic cell proliferation by deregulating microRNAs. RUNX1/ETO promotes overexpression of miR-23-27-24 cluster by replacing RUNX1 binding sites on miR-23-27-24 locus. It was found that miR-24 downregulates MAPK phosphatase-7 (MKP-7) leading to phosphorylation of p38 and JNK kinases, which stimulate leukaemic cell proliferation (Tanoue, Yamamoto et al. 2001, Zaidi, Dowdy et al. 2009). The regulation of MAP kinases by leukaemic fusion proteins is not exclusive to RUNX1/ETO, for example, BCR/ABL also regulates MKP-7 leading to enhanced proliferation (Hoornaert, Marynen et al. 2003).

Cytokines signalling pathways are dysregulated in leukaemia due to mutations and genomic alterations as an early event required to promote leukaemic stem cell survival and proliferation (Scholl, Gilliland et al. 2008). RUNX1/ETO drives proliferation independent of IL-3 by maintaining high expression level of its dominant negative regulator miR-24 (Zaidi, Dowdy et al. 2009). RUNX1/ETO also cooperate with several cytokines to induce proliferation. For instance, RUNX1/ETO has a synergetic effect with the thrombopoietin receptor (MPL), which is highly expressed in HSCs, progenitors and t(8;21) AML cells. Consequently, the addition of thrombopoietin (THPO) induces high proliferative properties to t(8;21) cells by activating the JAK/STAT and PI3K/AKT pathways (Kaushansky 2009, Pulikkan, Madera et al. 2012). Given that RUNX1/ETO activates and synergises with several cytokine-mediated signalling pathways, the repression of RUNX1/ETO may have a therapeutic benefit.

6.4.2 RUNX1/ETO depletion induces G1 cell cycle arrest

The depletion of *RUNX1/ETO* led to G1 cell cycle arrest (Fig 3-10, 3-23). We have found that RUNX1/ETO knockdown leads to downregulation of the cell cycle gene CCND2 at mRNA and protein levels (3-8, 3-18 & 3-22B). Latest findings in our lab identified *CCND2* as a downstream target of RUNX1/ETO where the fusion protein corporates with AP-1 to drive high expression level of *CCND2* in AML. RUNX1/ETO activates *CCND2* directly by binding to the transcription start site (TSS) and the -30 kb region. Moreover, RUNX1/ETO upregulates *CCND2* indirectly by reducing AP-1 occupancy on *CCND2* promotor resulting in histone deacetylation and increased RNA POL II binding (Mathas, Hinz et al. 2002). We have also assessed the effect of the pharmacological inhibition of CDK4/6 and found that palbociclib significantly impairs leukaemic cell expansion *in vivo* and t(8;21) primary cells. Thereby, we proposed RUNX1/ETO as a central regulator of the cell cycle via the CCND2-CDK4/6 complex (Martinez-Soria 2018).

The modified si*RUNX1/ETO* showed robust inhibition of RB1 phosphorylation at T-821 (Fig 3-8). Phosphorylation of RB1 is crucial to drive the cell cycle progression. The cyclin kinases CDK4 and CDK6 phosphorylate RB1 at different sites including T-

821 (Harbour, Luo et al. 1999). In our work, we showed that depletion of *RUNX1/ETO* or *CCND2* reduced RB1 phosphorylation (Martinez-Soria 2018).

We observed that modified si*RUNX1/ETO* induced stronger cell cycle arrest in Kasumi-1 cells, where SKNO-1 required continuous *RUNX1/ETO* depletion to effectively inhibit the cell cycle at G1 phase (Fig 3-10). Early studies suggested that the cell cycle of AML blasts is independent of GM-CSF, G-CSF, and IL-3 (Liesveld, Keng et al. 1994). However, it is now widely agreed that cytokines accelerate G1 to S transition and enhance proliferation (Herrmann, Oster et al. 1990, Matsuura, Yan et al. 2012). The prompt response of Kasumi-1 cells to *RUNX1/ETO* knockdown and repressing the cell cycle could be due to a KIT mutation in Asn(822)-Lys (Beghini, Magnani et al. 2002) combined with high expression of G-CSF (Gordon, Dias et al. 2014). The KIT activation mutation promotes legend-independent proliferation, and G-CSF coordinates with the mutant KIT signalling to enhance AML expansion. RUNX1/ETO was found to activate G-CSF expression, and depletion of G-CSF results in cell cycle arrest (Elsasser, Franzen et al. 2003). On the other hand, SKNO-1 cell line has fourfold less expression of G-CSF in comparison with Kasumi-1, which may explain the modest effect of *RUNX1/ETO* knockdown on the cell cycle.

Furthermore, the dependency of SKNO-1 cells on GM-CSF for proliferation might alleviate the effect of RUNX1/ETO on the CCND-CDK4/6 complex. We were able to enhance the G1 cell cycle arrest by simultaneously reducing the concentration of GM-CSF in SKNO-1 media and depleting *RUNX1/ETO*. Previous research in endothelial progenitors has shown that GM-CSF upregulates CCND1 leading to RB1 phosphorylation, which drives higher expression of CCNE1 and consequently promotes the cell cycle progression (Qiu, Xie et al. 2014). The mechanism behind GM-CSF-induced cell cycle progression and activation of CCND1 was proposed to be through the phosphorylation of GSK3β which activates PI3K/AKT and ERK pathways (Ono, Yanagawa et al. 2007, Giambelluca, Cloutier et al. 2013).

The leukaemic stem cell is characterised by high proliferative capacity where it undergoes up to 200 doublings (Cheng, Rodrigues et al. 2000). The presence of oncogenic regulatory element to activate the cell cycle and enhance the DNA repair pathways is crucial to correct the DNA damage and prevent leukaemic stem cell exhaustion (Cheng 2004). Fusion proteins such as PML/RARA were found to

activate the cell cycle inhibitor p21 independently of TP53 status (Viale, De Franco et al. 2009). The high expression of p21 accelerates cell cycle propagation by CDK2-CCNE1 complex and restricts the hyperproliferative phenotype, which accumulates a high level of DNA damage. It was suggested that RUNX1/ETO mimics PML/RARA by activating p21 and driving the cell cycle (Zhou, Li et al. 2006). Taking into account that the role of p21 in t(8;21) leukaemogenesis was obtained in *TP53* negative cells, we thus speculate that the delayed leukaemia initiation in the absence of p21 could be due to the DNA damage agents which exhausted the leukaemic stem cells. Moreover, the expression of p21 in t(8;21) AML cell lines is lower than other AML cell lines due to mutated *TP53* (Quintas-Cardama, Hu et al. 2017). Taken together, oncogenic mutations such as *KIT* and *TP53* may contribute to cell cycle progression in t(8;21) leukaemia, and the CDK2-CCNE1 complex may not play a significant role in cell cycle modulation.

6.4.3 RUNX1/ETO depletion induces cellular senescence

Beta-galactosidase is an essential enzyme for cellular function in which it hydrolyses the β-glycosidic linkages between galactose and its partners. Senescent cells specifically overexpress β-galactosidase in the lysosome, which can be detected by X-Gal staining at pH = 6 (Dimri, Lee et al. 1995). We showed that RUNX1/ETO knockdown in Kasumi-1 and SKNO-1 cell lines leads to substantial increase in senescence (Fig 3-11, 3-24). Furthermore, we have showen that induction of senescence was specifically due to the gene knockdown, and not stress-mediated given that the mismatch transfected cells as well as the mock control had the same basal level of senescent cells (Ben-Porath and Weinberg 2005).

Maintenance of genome integrity is essential for leukaemic stem cell survival. Stable telomerase (*TERT*) expression is required for stem cell self-renewal, but *TERT* expression does not lead to cancer. The enhanced proliferation and self-renewal capacity of leukaemic cells are prominently dependent on high *TERT* expression (Deng, Chan et al. 2008). Former work in our group showed that RUNX1/ETO directly binds *TERT* promotor and drives high expression of telomerase. The depletion of the *RUNX1/ETO* in Kasumi-1 cell line and t(8;21) primary cells was found to increase RUNX1 binding to TSS of *TERT* and reduce histone acetylation

(H3K9Ac) after prolonged knockdown (Ptasinska, Assi et al. 2012). Our data supported the previously reported findings that *TERT* has a delayed response to *RUNX1/ETO* knockdown (Fig 3-18, 3-20 & 3-21) where senescence was detected one week after *RUNX1/ETO* repression.

In a broader perspective, telomere shortening leads to a state of replicative senescence when the cells are metabolically inactive and under cell cycle arrest (Allsopp and Harley 1995, Deng, Chan et al. 2008). Former work in our lab has showen that the knockdown of *RUNX1/ETO* in t(8;21) cell lines leads to telomere shortening and induction of senescence (Martinez, Drescher et al. 2004, Gessner, Thomas et al. 2010).

Oncogenic stimuli control senescence (Campisi 2001), such as the p16/RB1 tumour suppressor pathway which supresses senescence (Collins and Sedivy 2003). On the other hand, t(8;21) AML cell lines harbour mutated *TP53* which cannot phosphorylate RB1 at T-821, suggesting that the induction of cellular senescence in Kasumi-1 and SKNO-1 cells is independent of *TP53* (Hangaishi, Ogawa et al. 1996, Gil and Peters 2006). Furthermore, we showed that the depletion of *RUNX1/ETO* leads to G1 cell cycle arrest via the CCND2-CDK4/6 complex upon RB1 dephosphorylation at T-821 (Fig 3-8). The pharmacological inhibition of the CDK4/6 complex in Kasumi-1 and SKNO-1 cell lines also reduces RB1 phosphorylation and induces senescence (Martinez-Soria 2018). Additionally, the knockdown of the fusion protein also results in upregulation of the cell cycle inhibitor p27, which leads to the G1 cell cycle arrest (Martinez, Drescher et al. 2004). For these reasons, we propose that the induction of cellular senescence following the cell cycle arrest in t(8;21) cells could be due to loss of RB1 phosphorylation at T-821.

6.4.4 RUNX1/ETO depletion impairs self-renewal

Clonogenicity is the anchorage-independent expansion of cells, which maintains the stem cell properties (Hamburger and Salmon 1977). The *in vitro* assays of colony formation replating, using methylcellulose or sloppy agar are considered the most stringent methods to assess the oncogenic transformation of haematopoietic stem cells (Lieber and Kovach 1982, Bizzari and Mackillop 1985, Coulombel 2004, Borowicz, Van Scoyk et al. 2014).

Several chromosomal translocations result in the expression of fusion proteins which drive leukaemia propagation and promote survival by upregulating the self-renewal genes and downregulating the differentiation pathways. The RNAi-mediated depletion of some fusion genes, such as *BCR/ABL* in t(9;22) and *MLL/AF4* in t(4;11) reduces the clonogenic potential of leukaemic cells (Scherr, Battmer et al. 2003, Thomas, Gessner et al. 2005). While previous work in our group showed that transient depletion of *RUNX1/ETO* by siRNA reduces clonogenicity of Kasumi-1 and SKNO-1 (Soria, Tussiwand et al. 2009), in this study we have shown that *RUNX1/ETO* depletion, using the modified *siRUNX1/ETO* delivered by electroporation or nanoparticles treatment, provides a stronger reduction in clonogenicity (Fig 3-13 & 3-25). The knockdown of *RUNX1/ETO* had a prolonged effect on clonogenicity until five sequential replatings (Fig 3-14). This confirms that *RUNX1/ETO* repression maintains the self-renewal ability of leukemic stem cells.

Conceptually, in order for a cell to form a colony, it should have an active cell cycle, enhanced proliferative capacity and high expression of self-renewal genes *(Katayama, Takenaka et al. 1998)*. Former work from our group, as well as this study, has shown that RUNX1/ETO regulates the cell cycle, proliferation and self-renewal (Martinez, Drescher et al. 2004, Soria, Tussiwand et al. 2009, Ptasinska, Assi et al. 2012, Martinez-Soria 2018). We looked at the transcriptional level of *RUNX1/ETO* and its downstream targets after performing the colony formation. Surprisingly, we found that *RUNX1/ETO* and its direct target genes were significantly deregulated (Fig 3-26 & 3-27). There could be several reasons that may contribute to this finding, such as efficient recycling of the antisense-RISC complex. The chemical modification of the siRNA does not only provide stable gene knockdown, but it also guarantees that a sufficient amount of the RNAi machinery is maintained after cell division and therewith-associated dilution. The robust repression of RUNX1/ETO also might have led to irreversible changes in RUNX1/ETO transcriptional network. One might argue that this is a matter of concern, as the knockdown cells are adapted to the new transformations and rescued the leukaemic phenotype. However, the new transformation of cells, with a new transcriptional network might also open new therapeutically druggable pathways.

6.5 Pharmacokinetics and biodistribution of LNP/siRNA

6.5.1 The rationale behind siRNAs delivery system

Naked and unmodified oligonucleotides have unfavourable biodistribution and pharmacokinetics due to the fast clearance upon administration. Pharmacokinetic studies in rodent and non-human primates have shown that naked siRNA displays fast initial accumulation in the liver and kidneys after intravenous injection. It was also found that intact or partially metabolised siRNA in the liver excretes and accumulates in the hepatobiliary system before being delivered to the intestines with no evidence of relevant enterohepatic recirculation. Moreover, siRNA can also be filtered by the kidney, and accumulate in the bladder before being eliminated in the urine where fully intact siRNA duplexes can be detected. The endothelial properties of the organs' vasculature, especially the presence of fenestrated or sinusoidal capillaries, facilitate siRNA transport out of the circulation. Thus, siRNA effectively accumulates in several organs, such as the submandibular and bulbourethral glands and the pancreas, here the siRNA remains for long periods suggesting that these glands may function as a second natural drug reservoir, with potential bioavailability implications. (Huang, Hong et al. 2011, Huang, Cheng et al. 2016).

Furthermore, leukaemic stem cells are hidden within a complex protective niche in the bone marrow sanctuary (Asada 2018). In this manner, it is most unlikely for any naked siRNA to be able to reach these malignant cells in therapeutic doses capable of causing gene knockdown. Furthermore, leukaemia is known to invade the central nervous system (CNS) (Suzuki, Ino et al. 2008). To date, there is no evidence of detecting siRNA in the CNS, suggesting that naked siRNA cannot cross the brain-blood barrier.

Taken together, our strategy for siRNA delivery was to use a lipid nanoparticle with relevant clinical settings. Of notice, such a delivery system would also eliminate the activation of the innate immune response to the siRNA, which would be clinically advantageous (Yoneyama, Kikuchi et al. 2004, Karpala, Doran et al. 2005). That is because the activation of TLRs pathways by siRNA disrupt the immune homeostasis leading to the development of autoimmune diseases (Gao, Xiong et al. 2017).

siRNA chemical modifications and introducing conjugates alter the biodistribution and affect the elimination routes. For instance, 2'-O-methylation modifications enhance siRNA uptake by the submandibular and bulbourethral glands and subsequent secretion of the siRNA with exosomes (Lendvai, Velikyan et al. 2005). Cholesterol conjugate prolongs retention of siRNA in the liver, lungs and heart (Huang, Hong et al. 2011). The retention of siRNA in the liver may be advantageous, considering its involvement in a plethora of human diseases. Indeed, specific conjugates, such as trivalent *N*-acetylgalactosamine (GalNAc), enhances hepatocytes uptake of siRNA (Geary, Norris et al. 2015, Janas, Schlegel et al. 2018). Our lipid nanoparticle consisted of 38.5% cholesterol, which may lead to retention of the siRNA in the liver. Therefore, it is possible that the siRNA was secreted inside exosomes, which aided *in vivo* knockdown. We suggest investigating the potential of detecting exosome encapsulating siRNA in circulation. We recommend isolating the extracellular vesicles and exosomes by ultracentrifugation. If the modified siRNA were detected, then examine their integrity and ability to cause gene knockdown.

6.5.2 Developing protocol for LNP/siRNA labelling

In order to study the biodistribution of the nanoparticles, we developed a method to label the surface of the nanoparticles with a NIR fluorescent dye. We have chosen SulfoCyanine7.5 to label the nanoparticles because the dye excitation and emission spectra do not overlap with the mice auto-fluorescence, and we were able to detect the NIR fluorescence by IVIS (Fig 4-9 & 4-10). To that end, we did not find a suitable protocol for coupling a ligand to the surface of the nanoparticles in the literature. Thus, we generated a protocol that relies on a click reaction, a copper-catalysed reaction between alkyne and azide. The protocol is versatile, where the dye can be substituted by other ligands, such as aptamers, peptides or antibodies. However, the position and orientation of the ligands on the surface and stability of the new-labelled nanoparticles will require an extensive investigation.

We found that our in-house labelling protocol did not affect the nanoparticles physical parameters, and both the diameter and the polydispersity index (PDI) did not change significantly after the addition of the NIR dye to the nanoparticles (Fig 4-7). However, as we have anticipated the surface charge became slightly negative,

given the fact that SulfoCyanine7.5 carries a negative charge (Fig 4-7C). The change in the surface charge was also in accordance with equivalent studies, where the addition of negatively charged ligands increased the negative charge of liposomes (Leung, Tam et al. 2014, Weinstein, Toker et al. 2016). Nevertheless, our technique might be superior to other approaches. That is because the click reaction did not change the nanoparticles diameter more than ±5 nm, while a previously published technique relied on thiol-maleimide crosslinking protocol led to a twofold increase in the size of the lipid nanoparticles (Weinstein, Toker et al. 2016). For this reason, we speculate that the structure of the nanoparticles remained unchanged, which is crucial to keep the cellular uptake efficiency (Viger-Gravel, Schantz et al. 2018).

The use of SulfoCyanine7.5 was strategic in which it allowed the *in vivo* imaging. However, we were not able to quantify the amount of coupled molecules on the surface of the nanoparticles because the dye spectra were beyond the detection limit of the microplate reader. It was also not feasible to measure the *in vitro* or *in vivo* uptake of the labelled nanoparticles for the same reason. Hence, we recommend replacing SulfoCyanine7.5 with other dye that is suitable for *in vivo* imaging, but also compatible with the *in vitro* assays such as flow cytometry and optical density measurements.

Although we were not able to quantify the NIR dye molecules after labelling, we included several control conditions to assure successful incorporation of the dye onto the lipid nanoparticle. For instance, elimination of the ascorbic acid or copper from the reaction mixture led to less association of the SulfoCyanine7.5 with the nanoparticles. This finding was based on observing the changes in the LNP/siRNA colour from pink (due to the presence of the Dil dye) into dark green (the colour of SulfoCyanine7.5) after performing the click reaction and purification. Furthermore, the labelled nanoparticles were dialysed overnight using a membrane with 3.5 kDa cut-off that is three times larger than the molecular weight of SulfoCyanine7.5 (MWCO~ 1.1 kDa). Thus, it is fair to claim that the labelled nanoparticles contained insignificant traces of the free dye. However, due to the hydrophobic properties of SulfoCyanine7.5, some molecules might have been intercalated into the lipid layers rather than being chemically clicked to the surface. We suggest further physical and chemical characterisation to quantify the amount of chemically-bound

SulfoCyanine7.5 molecules to the nanoparticles, such as HPLC-Mass Cytometry and Cryo-TEM.

6.5.3 Pharmacokinetics and biodistribution of LNP/siRNA

We studied the biodistribution of the nanoparticles after systemic administration (Fig 4-8). It was not surprising to detect the nanoparticles in the liver two hours after intravenous injection, given that the liver is a highly perfused organ with fenestrated endothelium making it the first reservoir to any particle larger than 50 nm in diameter (Zimmermann, Lee et al. 2006). It was reported that lipid nanoparticles acquire positive charge after interaction with apolipoproteins, which enhances the uptake by hepatocytes (Bogorad, Yin et al. 2014). Gene knockdown by siRNA encapsulated into nanoparticles is successfully achieved in several animal models including non-human primates (Akinc, Goldberg et al. 2009, Love, Mahon et al. 2010, Maier, Jayaraman et al. 2013). Furthermore, we detected the NIR dye fluorescence signal in the liver five days post-administration (Fig 4-8). Several PK studies in rodent have shown that the liver can retain siRNA encapsulated into cholesterol-enriched liposomes up to ten days after intravenous injection (Semple, Akinc et al. 2010, Novobrantseva, Borodovsky et al. 2012). Additionally, the liver could entrap hydrophobic fluorescence dyes up to one month after uptake (Akinc, Goldberg et al. 2009). For these reasons, our IVIS imaging cannot assure that the detected fluorescence signal is coming from intact nanoparticles or from the SulfoCyanine7.5 molecules that might have been released from the labelled nanoparticles.

To increase the circulation of the nanoparticles we aimed in the second PK study to saturate the liver by pre-treatment with unlabelled nanoparticles, but we did not see any change in labelled nanoparticles biodistribution (Fig 4-7 & 4-8). There might be several explanations why the liver did not absorb less labelled nanoparticles in that experiment, such as high liver cells turnover, and uncompleted saturation of the liver with the unlabelled lipid nanoparticles.

The nanoparticles were detected in the tumours, and we showed the overlap between the bioluminescence of leukaemic cells and the NIR fluorescence of the

nanoparticles. Moreover, our PK and biodistribution studies showed that the lipid nanoparticles were widely distributed throughout the body, and enriched in the haematological tissues and relevant leukaemic compartments such as the liver, spleen, vertebral column, bones, and brain (Fig 4-9 & 4-10). However, the IVIS imaging alone cannot confirm the exact localisation of the nanoparticles in the tumour. That is because the tumours are vascular with complex extracellular matrix assuring the blood supply (Kalluri 2016, De Palma, Biziato et al. 2017). Moreover, we cannot claim that the nanoparticles were accumulated within the bone tissue, as both the bone marrow and periosteum membrane are profusely vascularised (Saulacic, Schaller et al. 2012, Saulacic, Schaller et al. 2013). Even so, in contrast with the periosteal capillary system, the bone marrow is supplied by extensively specialised sinusoidal and fenestrated capillaries which are essential for its haematopoietic functions. Therefore, it is fair to assume that at least a significant part of the signal detected in the bones might have come from accumulation of the nanoparticles in the bone marrow.

Novel lipid nanoparticles have prolonged first phase elimination up to 3 days, and the lipid metabolites are detectable up to 28 days in the plasma (Christensen, Litherland et al. 2014). This favourable pharmacokinetic profile ensure that the nanoparticle can reach the leukaemic malignant niche. On the other hand, the enhanced permeation and retention of the nanoparticles in the reticuloendothelial system for a prolonged period of time might cause *in vivo* toxicity (Juliano, Bauman et al. 2009). For these reasons, we recommend performing dose-escalation experiments to study the stability and toxicity of the nanoparticles. Moreover, the pharmacokinetic and biodistribution of the nanoparticles alone do not confirm the efficacy of the delivery system. That is because the localisation of the nanoparticles in a specific site might not correlate with the efficient release of the siRNA (Wei, Jones et al. 2011). We advise performing pharmacokinetic experiments to establish the relationship between the gene knockdown and the dose regimen in the relevant leukaemic tissues.

6.6 LNP/siRNA has on-target effect on leukaemic cells *in vivo*

Having confirmed the pharmacokinetics and biodistribution of the nanoparticles, the next question for our *in vivo* experiments was: can the nanoparticles achieve *RUNX1/ETO* silencing *in vivo,* and what are the consequences? We showed a specific slicing of *RUNX1/ETO* by siRNA in t(8;21) *in vivo* model. The concept of using nanoparticles to target fusion genes *in vivo* was experimented previously by silencing *TCF3/PBX1* in a murine model of t(1;19) childhood acute lymphoblastic leukaemia. However, about 17-fold higher dose of the nanoparticles was used to achieve a comparable knockdown to *RUNX/ETO* (Jyotsana, Sharma et al. 2018). This may suggest that *RUNX1/ETO* is more prone to siRNA silencing than previously investigated fusion genes with potential clinical implications.

The relationship between pharmacokinetics and pharmacodynamics determines the clinical suitability of the drug. Ideally, the nanoparticles are expected to achieve a maximal therapeutic effect with minimal dosage. We rationalised that the therapeutic profile of the siRNA is assessed by the measured *RUNX1/TEO* knockdown and the half-life of the pharmacological effect. We found that despite the difference in the dosing schedules, one additional dose of the nanoparticles provided a more significant reduction in *RUNX1/ETO* mRNA (Fig 4-11), suggesting that the effect is dose-dependent. However, the enhanced knockdown, we have observed, could also be due to the discrepancy in the leukaemic burden between the two experiments.

The reduction in RUNX1/ETO protein level was comparable between the mice, which suggests that the pharmacological effect was similar regardless of the dosing schedule, or the time of the analysis (endpoint by culling the mice) (Fig 3-12). The consistent reduction in RUNX1/ETO between the mice also suggests that the half-life of the RISC-siRNA complex was similar. Arguably, given that *RUNX1/ETO* knockdown impairs proliferation, the RISC-siRNA complex should not be diluted over time, as cells do not proliferate. However, in our experiments, the nanoparticle treatment did not reduce the leukaemic burden (Fig 4-13 & 4-14). Therefore, mice culled 10 days after treatment should have more leukaemic cells, and consequently, the intracellular content of the siRNA is diluted with cell doubling. This implies that continues dosing in these experiments was unlikely to cause more gene knockdown, otherwise it would have been expected to find less RUNX1/ETO knockdown in the

mice culled after 10 days of treatment, but this was not the case. We explain the comparable knockdown *in vivo* by the enhanced stability and efficient recycling of the RISC-siRNA complex. The 2'-sugar modifications of the siRNA were supposed to prolong the siRNA duplex stability. The 3'-end antisense modifications also meant to enhance the selectivity and reduce the off-target effect (Morrissey, Blanchard et al. 2005). Therefore, we surmise that the modified siRNA intrinsic properties enhanced RUNX1/ETO knockdown *in vivo.*

Pharmacodynamics studies in rat have shown that 500 siRNA molecules per cells are adequate to achieve 50% gene knockdown in the hepatocytes, 10 days after systemic application of the nanoparticles (Landesman, Svrzikapa et al. 2010). Due to the time constraints and viability of the nanoparticles, it was not possible to perform pharmacodynamics studies. We recommend utilising the nanoparticles platform to determine, in a clinically relevant setting *in vivo,* the optimal dose regimen needed to achieve potent *RUNX1/ETO* knockdown. We suggest collecting plasma samples and relevant leukaemic tissues at several time points after applying the nanoparticles treatment. We also advise performing dose-escalation treatment *in vivo* followed by isolation of cells from the bone marrow and RISC pulldown assays to quantify the antisense of si*RUNX1/ETO* by qRT-PCR. The simultaneous quantification of *RUNX1/ETO* expressing and the siRNA in the leukaemic cells will determine the therapeutic profiles of our siRNA and nanoparticles.

6.7 *RUNX1/ETO* repression *in vivo* enhances the survival

Previous work in our lab has shown that transient depletion of *RUNX1/ETO in vitro* by electroporation significantly prolongs the survival of transplanted mice from 64 to 90 days ($p<0.02$) (Soria, Tussiwand et al. 2009). That study provided the concept that interfering with *RUNX1/ETO* expression might, be therapeutically beneficial, but the delivery method was unsuitable for clinical implementation. In this study, we implemented a clinically relevant approach to exploit the therapeutic potential of repressing *RUINX1/ETO*. Indeed, the siRNA-mediated knockdown *in vivo* significantly increased the median survival of mice from 44 to 80 days ($p<0.0001$) (Fig 4-18). Our result highlights the therapeutic potential of targeting *RUNX1/ETO* in

t(8;21) AML and presents a versatile siRNA delivery system that has a clinical relevance.

siRNA-mediated knockdown of leukaemic fusion genes *in vivo*, such as *TCF3/PBX1* in t(1;19) or *BCR/ABL* in t(9;22) increase the survival of leukaemic mice (Jyotsana, Sharma et al. 2015, Jyotsana, Sharma et al. 2018). Moreover, knockdown of proto-oncogenes that control proliferation, such as *CCND1* in t(11;14) B-ALL reduces cell proliferation *in vivo* and enhance the survival (Weinstein, Toker et al. 2016). We have shown for the first time that direct repression of *RUNX1ETO in vivo* suppressed leukaemia expansion in a xenotransplantation model of t(8;21) AML, but it did not eliminate the leukaemic cells as all mice developed leukaemia at the end.

6.8 The consequences of *RUNX1/ETO* knockdown *in vivo*

In vitro studies showed that *RUNX1/ETO* knockdown inhibits proliferation, induces cells cycle arrest and triggers senescence. The knockdown also dysregulates the leukaemic-specific transcriptional network by reducing the expression of self-renewal genes and activating the C/EBPα myeloid differentiation programme (Ptasinska, Assi et al. 2012, Ptasinska, Assi et al. 2014, Loke, Assi et al. 2017, Martinez-Soria 2018). However, due to the difficulty in achieving transient depletion of *RUNX1/ETO in vivo,* it has never been investigated that whether knocking down the fusion *in vivo* would recapitulate the *in vitro* effects. Our nanoparticle delivery system did not only prove that *RUNX1/ETO* depletion *in vivo* enhances the survival of leukaemic mice, but it also provided the opportunity to study the effect of modulating *RUNX1/ETO* expression under a complex microenvironment *in vivo*.

6.8.1 RUNX1/ETO knockdown dysregulates t(8;21) transcriptional network

The N-terminus of RUNX1/ETO shares with RUNX1 the RHD domain that controls binding to DNA. Former studies in our group have demonstrated that RUNX1 and RUNX1/ETO could activate gene expression by binding to the promotor or TSS of target genes. On the other hand, RUNX1/ETO can also repress transcription by the

ETO component of the fusion, which recruits histone deacetylases (Ptasinska, Assi et al. 2012, Ptasinska, Assi et al. 2014). Our *in vivo* knockdown experiments showed that repressing RUNX1/ETO alters the expression of its target genes such as *CCND2, TERT, CD34*, *ANGPT1* and *LAPTM5* in a similar manner to the *in vitro* knockdown (Fig 4-11, 4-12 & 4-23). Thus, the *in vivo* targeting of *RUNX1/ETO* might cause similar transcriptomic changes to those observed *in vitro*.

Principal component (PC) analysis of the RNA-seq data showed that the control mice cluster next to each other while the *RUXN1/ETO* targeted mice are separate apart from each other and from the control (Fig 4-24). This affirms that *RUNX1/ETO* knockdown has an impact on t(8;21) transcriptome *in vivo*. The *RUNX1/ETO* targeted mice were culled at different time points, which might explain why they scored differently in the PC analysis. Despite having only two mice in each group, making the statistical analysis inadequate, the RNA-seq data revealed some parts of the changes in RUNX1/ETO transcriptional network. A closer look into the RNA-seq most dysregulated genes we can propose that the repression of *RUNX1/ETO in vivo* downregulates the self-renewal genes and impairs stemness, and triggers a myeloid differentiation programme assisted by a pro-inflammatory response and senescence.

RUNX1/ETO knockdown *in vivo* recapitulated the *in vitro* knockdown in initiating the myeloid differentiation and repression of self-renewal programmes. However, there was some discrepancy in the expression of some genes in comparison with the *in vitro* knockdown. For instance, the *in vivo* knockdown did not upregulate *CEBPA*, but we found substantial changes in C/EBPα direct target genes. Hence, the transit repression of *RUNX1/ETO* might have modulated *CEBPA* expression temporarily but sufficiently to disturb C/EBPα transcriptional network. Further studies are needed to confirm this hypothesis, such as ChIP-Seq. Moreover, cell growth *in vivo* is affected by the microenvironment in which leukaemic niche promotes survival (Schmidt and Carmeliet 2011). The complex signalling pathways *in vivo* might have contributed to the differences between the *in vitro* and *in vivo* dysregulated genes, justifying our observation in the RNA-seq.

Furthermore, several microRNAs are also involved in t(8;21) leukaemogenesis (Jongen-Lavrencic, Sun et al. 2008, Li, Lu et al. 2008). In RUNX1/ETO-driven leukaemia, the tumour repressors microRNAs, such as miR-9, miR-193a, and miR-

223 are downregulated, and the proliferation inducer miR-126 is upregulated (Fazi, Racanicchi et al. 2007, Li, Lu et al. 2008, Li, Gao et al. 2013, Emmrich, Katsman-Kuipers et al. 2014). We observed changes in the expression of several microRNAs that are known to be regulated by RUNX1/ETO. For instance, RUNX1/ETO knockdown *in vivo* reproduced the previously described downregulation of miR-23a and miR-27a expression. The repression of *RUNX1/ETO* also upregulated miR-142 which has restricted expression in the haematopoietic system and regulates *RUNX1* expression in HSCs (Sun, Varambally et al. 2011). The transcription factor PU.1 stringently controls miR-142 expression by coordinating RUNX1, C/EBPβ and CBFβ binding to its promotor (Sun, Sun et al. 2013). Therefore, the upregulation of miR-142 can provide compelling evidence for retrieving RUNX1 and PU.1 transcriptional activity upon *RUNX1/ETO* knockdown.

Taken together, these findings confirm the specific-silencing of *RUNX1/ETO* after the nanoparticles treatment and present examples of the complex regulatory network of RUNX1/ETO in t(8;12) AML.

6.8.2. RUNX1/ETO knockdown induces senescent and cytostatic phenotype

We have previously proposed that the *in vitro* knockdown of *RUNX1/ETO* induces cellular senescence by RB1 dephosphorylation. In line with the *in vitro* experiments, we observed induction of senescence after depleting *RUNX1/ETO in vivo.* Moreover, we also found a significant decrease in CCND2 and TERT protein level (Fig 4-12), which were shown to predispose cellular senescence following *in vitro k*nockdown (Fig 4-16). Therefore, we surmise that senescence induction in *vitro* and *in vivo* after *RUNX1/ETO* knockdown follows a similar mechanism. Nevertheless, further experiments are required to support this hypothesis, such as cell cycle profiling and assessment of RB1 phosphorylation status by Western blotting or flow cytometry.

Senescent cells are characterised by a unique secretory signature, known as the senescence-associated secretory phenotype (SASP), which is regulated by the transcription factors nuclear factor (NF-κB) (Coppe, Desprez et al. 2010, Chien, Scuoppo et al. 2011). The SASP factors include interleukins (IL-6, IL-7, IL-1α/β, IL-13 and IL-15), chemokines (IL-8, HCC-4, MIP-1a and MCP-2/4), growth factors (HGF, VEGF; SCF and SDF-1), proteases (NMP-1/3/10/14, TIMP-2 and PAI-1), and

soluble or shed receptors or ligands (ICAM-1/3, OPG and EGF-R). The RNA-seq showed upregulation of the genes coding these inflammatory cytokines and growth factors. Moreover, analysis of RNA-seq revealed a strong pro-inflammatory response by NF-κB pathway (Fig 4-25). Specifically, we found upregulation in the expression of *NFKB1* and a set of genes known to activate NF-κB pathway, including *TNF* and several members of the TNF receptor superfamily (Hayden and Ghosh 2014, Munoz-Espin and Serrano 2014). We propose that *RUNX1/ETO* knockdown *in vivo* provides the SASP-associated pro-inflammatory signature that supports the cytostatic phenotype. This finding has a significant clinical relevance since it was shown recently that the senescence inflammatory microenvironment could be effectively targeted for the eradication of senescent cells and subsequently avoiding the tissue damage and dysfunction following chemotherapies (Xu, Pirtskhalava et al. 2018).

The translocation of the High Mobility Group Box-1 (HMGB1) protein from the nucleus to the cytoplasm is a senescence marker (Yamada and Maruyama 2007, Kumar, Singal et al. 2008). HMGB1 is an inflammatory mediator that controls the release of SASP cytokines (Davalos, Kawahara et al. 2013). Therefore, we suggest performing immunofluorescence staining to investigate the changes in HMGB1 expression in the nucleus, which supports our findings.

Senescent cells are characterised by a decrease in *LMNB1* expression and changes in the nuclear lamina (Shimi, Butin-Israeli et al. 2011, Freund, Laberge et al. 2012). In our *in vivo* experiments, *RUNX1/ETO* knockdown downregulated *LMNB2* while *LMNB1* remained unchanged. One explanation of this observation could be attributed to the mutated P53 in Kasumi-1 cells, as the activation of P53 is required for deregulating *LMNB1* (Sablina, Budanov et al. 2005, Shimi, Butin-Israeli et al. 2011). Moreover, the induction of senescence by *LMNB1* downregulation is independent of telomere dysfunction, but telomere shortening in t(8;21) cell lines leads to senescence (Martinez, Drescher et al. 2004, Shimi, Butin-Israeli et al. 2011). It is possible that the knockdown of *RUNX1/ETO in vivo* caused nuclear lamina aberrations by reducing LMNB2 expression. Further measurements are required to support this hypothesis, such as quantification of the nuclear Laminin B1 and B2 after *RUNX1/ETO* knockdown.

Furthermore, overexpression of the tumour-suppressor protein $p16^{INK4a}$, coded by *CDKN2A* gene (cyclin-dependent kinase inhibitor 2A), is a senescence marker in cells do develop SASP (Michaloglou, Vredeveld et al. 2005). Our RNA-seq data did not show any changes in *CDKN2A* expression, which complements the literature in which only the cells that harbour dysfunctional P53 secrete SASP (Coppe, Patil et al. 2008, Rodier, Coppe et al. 2009). We performed the *in vivo* known experiments on Kasumi-1 cells, which carries mutated P53 and resembles the SASP-induced senescence. However, the vast majority of t(8;21) AML patients have wild type P53. Therefore, the knockdown of *RUNX1/ETO in vivo* on PDXs with functional P53 may upregulate $p16^{INK4a}$ and induce senescence. Thus, we suggest investigating $p16^{INK4a}$ expression when performing *RUNX1/ETO* knockdown on PDXs in future experiments.

Overall, the induction of cellular senescence *in vivo* upon *RUNX1/ETO* depletion may provide a possible therapeutic avenue that prevents relapse and tissue dysfunction. Recent studies support the concept of ‘’Achilles’ heel of senescent cells’’ or senolytics which are potent drug combinations such as (dasatinib and quercetin) or potent siRNAs against proto-oncogenes such as *CDKN1A* or *SERPINB2*. These senolytics, under specific conditions, can eliminate the senescent cells and alleviate the physical dysfunction (Zhu, Tchkonia et al. 2015, Xu, Pirtskhalava et al. 2018).

6.8.3. RUNX1/ETO knockdown affects angiogenesis

RUNX1/ETO knockdown *in vitro* reduced *ANGPT1* mRNA in Kasumi-1, primary patient cells and PDXs (Fig 3-20F, 3-27C, 3-28 & 3-29). Our *in vivo* experiments have shown that the expression level of *ANGPT1* and *ANGPT2* were downregulated after *RUNX1/ETO* knockdown (Fig 4-11A). Pathway analysis of the RNA-seq data has also revealed a signature of dysregulated angiogenesis (Fig 4-26). Furthermore, we have observed the formation of leaky vessels in tumours collected from the *RUNX1/ETO* targeted mice (Fig 4-13D). We hypothesise that this could be due to dysregulated vascular angiogenesis (Fukuhara, Sako et al. 2009, Wu, Lee et al. 2015). The human ANGPT1 effectively binds murine Tie2 (endothelium-specific receptor tyrosine kinase 2) surface receptor, which mediates vascular maintenance

and remodelling (Davis, Aldrich et al. 1996). Therefore, reduction in *ANGPT1* expression might reduce the amount of secreted ANGPT1 and consequently impair the ANGPT1-Tie2 interaction.

Angiogenesis via ANGPT1-TIE2 crosstalk has been shown to be critical for haematopoietic lineage specification as well as HSCs activity and differentiation (Mendelson and Frenette 2014). On the other hand, leukaemic stem cells control neoangiogenesis by modulating the levels of secreted ANGPT1/2 and VEGF ligands and consequently affect the sinusoidal endothelium integrity and perivascular niche (de Bont, Rosati et al. 2001, Zhou, Ding et al. 2015, Itkin, Gur-Cohen et al. 2016, Asada 2018). The clinical implication of neoangiogenesis is that leukaemic stem cells can escape the toxic bone marrow environment caused by different chemotherapies. Thus, it is not surprising to find increasing evidences about the effectiveness of antiangiogenic therapeutics against leukaemia (Schmidt and Carmeliet 2011, Ikushima, Arai et al. 2013, Harney, Karagiannis et al. 2017). The infiltration of the bone marrow with leukaemic cells and induction of angiogenesis have been shown in several haematological malignancies including AML, ALL, CML, and myelodysplastic syndromes (Perez-Atayde, Sallan et al. 1997, Lundberg, Lerner et al. 1998, Aguayo, Kantarjian et al. 2000, Hussong, Rodgers et al. 2000). It has also been shown that blocking the ANGPT1-Tie2 interaction between the primary human AML cells and murine fibroblasts or osteoblasts effectively reduces AML cell expansion (Reikvam, Hatfield et al. 2010). In CML, BCR/ABL upregulates *VEGF* expression, and it has been proposed that pharmacological inhibition of the fusion protein reduces VEGF secretion, impairs angiogenesis and inhibits proliferation (Dias, Shmelkov et al. 2002, Mayerhofer, Valent et al. 2002). It can be speculated that similar to BCR/ABL, the depletion of *RUNX1/ETO* might dysregulate angiogenesis with potential therapeutic benefits.

Furthermore, Leupaxin (*LPXN*) is a member of the paxillin protein family was found upregulated after *RUNX1/ETO* knockdown. It was shown in bladder cancer that the overexpression of LPXN is associated with dysregulated angiogenesis and enhanced proliferation (Regha, Assi et al. 2015). Several studies have demonstrated that overexpression of LPXN induces high expression of *S100P* and *S100A4* (members of the S100 calcium-binding protein family), and secretion of S100P and S100A4 dysregulates angiogenesis (Semov, Moreno et al. 2005, Hernandez, Padilla

et al. 2013). The knockdown of *RUNX1/ETO in vivo* also upregulated both *S100P* and *S00A4* expressions. Therefore, we propose that overexpression of *LPXN, S100P,* and *S100A4* may affect angiogenesis in t(8;21) AML following *RUNX1/ETO* knockdown.

6.8.4 RUNX1/ETO knockdown impairs proliferation

We have shown in this thesis that *RUNX1/ETO* knockdown *in vitro* inhibits proliferation, but this effect was less dominant *in vivo*. Despite having on-target effects in three independent *in vivo* experiments, *RUNX1/ETO* knockdown did not reduce proliferation (Fig 4-13A-C & 4-14). We anticipated that the repression of *RUNX1/ETO* in a well-established leukaemic mass might not reduce proliferation due to the complex leukaemic niche which supports proliferation by cell to cell contact and secretion of stimulatory growth factors and cytokines (Schmidt and Carmeliet 2011). Indeed, upon removal from the niche support into a simple intercellular communication context, the *in vivo* knockdown showed a significant effect on proliferation *ex vivo* (Fig 4-15).

RUNX1/ETO knockdown *in vitro* and in *vivo* was associated with a marked reduction in the stem cell gene *CD34* at the transcript and protein levels (Fig 4-15). Downregulation of CD34 in haematopoietic stem cells precedes differentiation in which the cells make less interaction with the haematopoietic niche and gain enhanced migration potential (Salati, Zini et al. 2008). It is possible that the aforementioned dysregulated neoangiogenesis and improved migration capability of Kasumi-1 cells have promoted the proliferation, which can justify our observation that the *RUNX1/ETO* knockdown *in vivo* did not inhibit leukaemia expansion.

One aspect of tumorigenesis is the interplay between microRNAs and oncogenes to promote cell growth (Iorio and Croce 2012, Iorio and Croce 2017). Several microRNAs regulate leukaemic cell proliferation by modulating kinases or epigenetically interfering with the expression of key onto-oncogenes. For instance, it has been shown that RUNX1/ETO represses miR-193a by displacing RUNX1 on its promotor, while increased expression of miR-193a leads to repression *RUNX1/ETO, KIT, CCND1, DNMT3A, and HDAC3 and* activation *of PTEN* (Li, Gao et al. 2013). Although our RNA-seq did not show a substantial increase in miR-193a expression,

several microRNAs were modulated, including miR-4534 and miR-570. It was shown that miR-4534 targets *PTEN* and represses PTEN/PI3K pathway, while its knockdown impairs proliferation and induces G1 cell cycle (Nip, Dar et al. 2016). Moreover, overexpression of miR-570 inhibits leukaemic cells proliferation and impairs glycolysis in CML cell lines (Zhao, Liu et al. 2017). Therefore, changes in miR-4534 and miR-570 might have affected proliferation after *RUNX1/ETO* repression. Nevertheless, microRNAs have lineage-specific expressions, and they can act in *cis*- and *trans*-regulatory mechanisms. The role of miR-4534 and miR-570 in t(8;21) AML and their effect on proliferation require further validation.

6.8.5 RUNX1/ETO knockdown impairs leukaemic self-renewal

We have shown in several independent experiments that *RUNX1/ETO* knockdown *in vivo* downregulates several genes that play essential roles in self-renewal (Fig 4-11 & 4-23). We have also confirmed that the disruption of RUNX1/ETO transcriptional network *in vivo* severely impairs clonogenicity (Fig 4-20 & 4-21). These findings were consistent with the replating experiments *in vitro* as *RUNX1/ETO* knockdown showed a prolonged impact on the colony formation ability (Fig 3-14 & 3-25). Therefore, we followed a compelling approach to assess the impact of RUNX1/ETO on self-renewal by investigating the re-engraftment capacity of leukaemic cells upon the nanoparticles treatment. Our *in vivo* stringent retransplantation assay showed that *RUNX1/ETO* knockdown resulted in strikingly extended survival of transplanted mice (Fig 4-22B).

Furthermore, although half of the secondary transplanted mice had delayed engraftment spans over 7 months, the remaining 50% of the secondary recipients did not develop leukaemia or any sign of illness. The therapeutic effect of the nanoparticles depends on their pharmacodynamics and spatial location in the leukaemic tumours (Christensen, Litherland et al. 2014), this may lead to discrepancy in the level of *RUNX1/ETO* knockdown. For instance, cells located near the surface of the tumour might have had stronger *RUNX1/ETO* knockdown from those in the centre, which may explain our observation in the retransplantation assay.

In order for AML to engraft, a minimal population of leukaemic stem cells is needed, known as the leukaemia-initiating cells or the LICs (Bonnet and Dick 1997, Blair, Hogge et al. 1998). These cells are characteristically resistant to chemotherapy and result in relapse. The LIC number inversely correlates with leukaemia propagation and is conventionally determined by transplanting a limiting dilution of leukaemic cells followed by assessing the mice survival. Importantly, the LIC cells are exclusively capable of propagating leukaemia in secondary receipts (Taussig, Vargaftig et al. 2010). Therefore, we suggest that *RUNX1/ETO* knockdown significantly reduced the LICs number of Kasumi-1 cells. Based on our finding in the re-engraftment assay, *ex vivo* colony formation, and the *in vitro* replating experiments, we propose that *RUNX1/ETO* is critical for LICs maintenance and consequently targeting t(8;12) cells with nanoparticles as a second-line treatment might be potentially an effective therapy to prevent relapse.

Over 70% of AML patients have overexpression of *CITED2*, which is critically involved in HSCs maintenance and affects pluripotency by controlling the octamer-binding transcription factor (*OCT4)* (Li, Ramirez-Bergeron et al. 2012, Schepers, Korthuis et al. 2013, Kranc, Oliveira et al. 2015). It has been shown that leukaemic stem cells transformation depends on the interplay between overexpression of CITED2 and low level of the myeloid transcription factor PU.1. The ectopic expression of *CITED2* in normal CD34+ progenitors enhances clonogenicity and accelerates engraftment in immunodeficient hosts (Schepers, Korthuis et al. 2015). Our RNA-seq have revealed downregulation of *CITED2* expression upon *RUNX1/ETO* knockdown *in vivo.* Moreover, *RUNX1* mutations require a high expression of *CITED2* to impair myeloid differentiation and enhance self-renewal (Gerritsen, Tijchon et al. 2016). Hence, it can be assumed that downregulation of *CITED2* gene contributed to the prolonged survival of the secondary transplant mice and the severe reduction in clonogenicity. We propose that RUNX1/ETO leukaemogenesis requires a consecutive expression of *CITED2* to enhance the LSCs self-renewal capacity.

6.8.6 RUNX1/ETO knockdown in vivo triggers myeloid differentiation

Previous work in our group have revealed the molecular mechanism in which RUNX1/ETO competes with RUNX1 binding to DNA and causes a differentiation block on the myeloid lineage by repressing *CEBPA* (Ptasinska, Assi et al. 2014). The knockdown of *RUNX1/ETO in vivo* led to changes in genes that are known to induce myeloid differentiation as revealed by the RNA-seq, such as *SMAD3*, *Src* kinases, *S100* family, *GPRIN3* and others. Most of these upregulated genes are known to control signal transduction, extracellular matrix remodelling and inhibition of proliferation by cytokine binding. Although we did not observe an apparent myeloid phenotype upon the lipid nanoparticles treatment, cells retrieved from the re-engraftment experiments manifested a mature phenotype (Fig 4-23).

Previous work has shown showed that *in vitro* knockdown of *RUNX1/ETO* followed by TGF-β1 and vitamin D3 treatment leads to growth inhibition and myeloid differentiation (Heidenreich, Krauter et al. 2003). KEGG pathway analysis of RNA-seq data revealed fourfold enrichment in TGF-β signalling upon *RUNX1/ETO* knockdown *in vivo* and 16% of the canonical pathways were downstream of TGF-β (Fig 4-25 & 4-26). Furthermore, we have observed in the RNA-seq upregulation of *SMAD3* expression, which is known to be the activator of TGF-β1 signalling. On the other hand, it was shown that RUNX1/ETO represses *SMAD3* and hence deactivates TGF-β1-mediated differentiation (Jakubowiak, Pouponnot et al. 2000). In our *in vivo* experiments, we did not apply TGF-β1 treatment after using the nanoparticles, but we found that 15% of the activated cytokine-receptor signalling were related to the TGF-β family (Fig 4-26). Therefore, it is possible that the murine Tgf-β1 provided the substrate for inducing differentiation following the priming of TGF-β1 signalling pathway by *SMAD3* overexpression.

The S100 calcium-binding protein family are expressed on the surface of mature myocytes. Members of the S100 family control proliferation, differentiation, angiogenesis, metastasis, and immune stimulation. The bone marrow CD11b+ cells express high levels of S100A8/9, which induce the serum amyloid A3 (*SAA3*) expression and secretion followed by TLR-6 activation. We found upregulation of *S100A8*, *S100A9* and *TLR-6* expression following *RUNX1/ETO* knockdown. Several studies suggested that overexpression of SAA3 and TLR-6 promotes a pro-

inflammatory response by NF-κB signalling (Hiratsuka, Watanabe et al. 2008, Shimizu, Kida et al. 2008, Liu, Kosaka et al. 2013). Furthermore, we also found upregulation of *S100A16* expression, which was shown to promote differentiation of oral squamous cell carcinoma (Sapkota, Bruland et al. 2015). However, the role of S100A16 is not fully understood as its overexpression in cancers has been shown to be associated with enhanced metastasis and poor prognoses in breast cancer and non-small cell lung adenocarcinoma (Tanaka, Ichikawa-Tomikawa et al. 2015, Chen, Luo et al. 2018). On the other hand, *S100A16* repression has been found to reduce the level of the pluripotent markers *Oct4* and *Nanog* (Tomiyama, Ikeda et al. 2018). Further validation of the S100 family members is required to elucidate the possible mechanisms of myeloid differentiation upon *RUNX1/ETO* repression.

Furthermore, several genes from the Src family kinases such as *HCK*, *FYN*, and *FGR* were upregulated in the RNA-seq. These kinases are involved in serval cell signalling and signal transduction pathways, including cell migration and adhesion (Corey, Dombrosky-Ferlan et al. 1998, Harder, Parsons et al. 2001). Some Src family members have a lineage-restricted expression such as *HCK* which is overexpressed in monocytes and granulocytes. Both HCK and FGR are potent inducers of G-CSF-dependent proliferation (Santini, Scappini et al. 2003, Mermel, McLemore et al. 2006). Moreover, Src kinases are negative regulators of myeloid differentiation (Miranda and Johnson 2007, Miranda, Redner et al. 2007, Jones, Wang et al. 2009). Taken together, the overexpression of Src family members upon the *in vivo RUNX1/ETO* depletion might have contributed to mature myeloid phenotype that were observed in our experiments.

The repression of *RUNX1/ETO in vivo* led to overexpression of 9 genes belonging to the C/EBPα-activation signature upon granulocytic differentiation (Liss, Ooi et al. 2014). RNA-seq showed upregulation of *IL18RAP, EPAS1, SAT1, ACSL1, FAM129A, TRIB3, CCL3, TNFRSF10B, and TNFRSF10D*. Some of the aforementioned genes are involved in signal transduction, immunostimulation and metastasises. For instance, activation of IL-18 was found to increase CD11b expression and enhance differentiation (Wyman, Dinarello et al. 2002). Although the RNA-seq did not show any changes in *CEBPA* expression upon *RUNX1/ETO* knockdown, the *CEBPA* mRNA level was significantly upregulated in the secondary transplant, as shown by qRT-PCR (Fig 4-19). This finding might indicate that a

modest upregulation of *CEBPA* expression could be sufficient to trigger the differentiation programme.

Interestingly, we found several interleukins modulated upon *RUNX1/ETO* repression *in vivo,* such as *IL1*, *IL4*, and *IL18*. The activation of these interleukins indicates self-renewal repression and enhanced differentiation, which might provide a window for therapeutic interventions. It has been reported that HSCs undergo a rapid transcriptional remodelling upon PU.1 induction of IL-1β signalling in which the stemness is severely impaired, and HSCs are forced to differentiate. Arguably, myeloid differentiation requires a low expression of PU.1 (Dahl, Walsh et al. 2003, Laslo, Spooner et al. 2006, Dakic, Wu et al. 2007). However, IL-1β signalling has been shown to be reversible and exclusive to chronic stress or induction of pro-inflammatory signalling by NF-κB or TLRs signals, where PU.1 activation proceeded the kinases induction (Sullivan, Porter et al. 2014, Pietras, Mirantes-Barbeito et al. 2016). Furthermore, *IL4R* expression was found upregulated in the RNA-seq. The signalling pathway of IL-4 predisposes myeloid differentiation (Feldman, Ruhl et al. 1991), and inhibits G-CSF-dependant proliferation of myeloid progenitors (Woytschak, Keller et al. 2016). Recent studies suggested that selective antibodies and cytokines, which can inhibit IL-4 signalling might have efficacy in several haematological cancers (Woytschak, Keller et al. 2016). Our data suggest the induction of immune-specific antigens upon *RUNX1/ETO* knockdown, which may be beneficial for AML patients.

Given that RUNX1/ETO regulates several microRNA clusters in AML, it was not surprising to find modulation of miR-23-24-27a cluster upon treatment with nanoparticles *in vivo*. Each microRNA form this cluster has a distinct function. For instance, miR-23a enhances proliferation and blocks myeloid differentiation (Zaidi, Dowdy et al. 2009, Chhabra, Dubey et al. 2010, Ptasinska, Assi et al. 2012). Moreover, miR-23a is one of the most potent regulators of haematopoiesis and its downregulation primes progenitors to myeloid lineage commitment (Kurkewich, Hansen et al. 2017). Our RNA-seq showed that the knockdown of *RUNX1/ETO in vivo* downregulated miR-23a expression, which further affirms our observations of the mature phenotype.

Collectively, the induction of myeloid differentiation upon *RUNX1/ETO* repression might increase the susceptibility of t(8;21) leukaemia to differentiation therapy or selective cytokines, providing potential therapeutic benefits for t(8;21) AML patients.

6.9 Possible combinational therapies with *RUNX1/ETO* repression

Several lines of evidence obtained during our comprehensive *in vitro* and *in vivo* experiments indicated that *RUNX1/ETO* knockdown might open a therapeutic window for patients with t(8;21) positive leukaemia. We have showed that inhibition of *RUNX1/ETO* conveys a cytostatic phenotype to leukaemic cells, which is characterised by G1 cell cycle arrest followed by senescence. We have also demonstrated that the knockdown severely impairs self-renewal and triggers myeloid differentiation. Although senescence is recognised as degenerative and irreversible cell fate, marked by permanent proliferative arrest (Futreal and Barrett 1991), current studies emphasise the adverse effect of senescence-associated secretory cytokines that cause local tissue dysfunction (Xu, Pirtskhalava et al. 2018). Searching for a therapeutic approach that assures a certain cell death and leukaemia eradication, we have investigated combinational treatments with *RUNX1/ETO* knockdown.

6.9.1 RUNX1/ETO repression in vitro desensitise AML to DNA damage agents

As a result of silencing *RUNX1/ETO*, Kasumi-1 cells lost their sensitivity to AraC (Fig 5-5). Kasumi-1 sensitivity to AraC was in concordance with the literature and clinically achievable (Xie, Edwards et al. 2010). The activity of AraC is driven by the incorporation of AraC-triphosphate into the elongating DNA strands, resulting in chain termination and consequently, inhibition of DNA synthesis (Grant 1998). The decreased sensitivity following *RUNX1/ETO* knockdown can be explained by the reduction in the S phase caused by the G1 cell cycle arrest (Kohn, Ruth et al. 2002). Recent work in our lab has shown that the pharmacological inhibition of CDK4/6 by palbociclib induces cell cycle arrest and senescence implying an effective therapeutic option for t(8;21) AML patients (Martinez-Soria 2018). Nucleoside analogues, including AraC, are recognised as potent inhibitors and standard chemotherapeutics for AML. Moreover, recent clinical studies suggested improving

the cytotoxicity by consecutive treatments of AraC followed by differentiation agents, such as Vitamin D analogues (Wang, Harrison et al. 2016). Based on these findings, we speculate that the inhibition of the cell cycle is not recommended to precede AraC treatment in t(8;21) leukaemia. However, repression of *RUNX1/ETO* following the treatment with DNA damage agents might be beneficial to reduce the leukaemic burden.

Although mutations in the DNA damage response genes (DDR) in AML are not as common as in other malignancies, such as ovarian or breast cancers, the pharmacological inhibition of poly (ADP-ribose) polymerase (PARP) using PARP potent inhibitors (such as olaparib or rucaparib) have shown to be effective in t(8;12) and t(15;17) AML (Alcalay, Meani et al. 2003, Esposito and So 2014). In parallel, RNAi knockdown or pharmacological inhibition of PARP by olaparib causes senescence and induces differentiation of Kasumi-1 cells (Esposito, Zhao et al. 2015). Although we have achieved PARP inhibition, in Kasumi-1 by rucaparib, with tenfold lower IC_{50} in comparison with olaparib (Wang, Cai et al. 2015), the effect appeared to be more cytostatic than cytotoxic. The repression of *RUNX1/ETO* also desensitised the cells to PARP inhibition (Fig-6). This could be due to the cytostatic phenotype and G1 cell cycle arrest upon *RUNX1/ETO* repression.

6.9.2 RUNX1/ETO repression enhances BCL2 inhibition in vitro

Inhibition of the B-cell lymphoma 2 (BCL2) has been implicated as an attractive approach to combat chemoresistance in AML. To date, the most selective single agent for BCL2 inhibition is ABT-199 (venetoclax). In line with the literature, we have observed a consistent activity of venetoclax in t(8;21) cell lines (Fig 5-7) (Pan, Hogdal et al. 2014). The combination of *RUNX1/ETO* knockdown and venetoclax treatment *in vitro* enhanced cytotoxicity to venetoclax by further reducing the protein level of MCL1 and BCLXL (Fig 5-11). While depleting *RUNX1/ETO* did not markedly change BCL2 level, we have noticed a slight increase in MCL1, suggesting that the increased cell death was possibly due to stabilisation of MCL1 level (Raje, Kumar et al. 2005). *In vitro* and *in vivo* RNA-seq data, as well as Chip-seq, (unpublished data and not included in this thesis) did not show any effect of *RUNX1/ETO* knockdown on *MCL1* expression. However,

RUNX1/ETO-downstream targets may regulate MCL1 post-translationally. We suggest performing immunoprecipitation to reveal the interaction between RUNX1/ETO and its targets with BCL2 and MCL1.

Furthermore, BCL2 inhibitors reduce BIM binding to BCL2, causing cell death (Del Gaizo Moore, Brown et al. 2007, Huang and Sinicrope 2008). The repression of RUNX1/ETO *in vitro* resulted in increased BIM protein level, which might have contributed to the cytotoxicity of venetoclax. Moreover, HDACs inhibitors which activate BIM, enhance BCL2 inhibition lethality (Zhao, Tan et al. 2005). The molecular mechanism of HDACs inhibitors and BIM activation was suggested to be dependent on acetylation of the forkhead box protein O1 (FOXO1) (Chen, Dai et al. 2009, Yang, Zhao et al. 2009). We hypothesise that RUNX1/ETO depletion mimics the HDACs inhibitor mechanism in overexpressing BIM. Indeed, RUNX1, RUNX1/ETO, and FOXO1 share many loci (Lin, Ptasinska et al. 2017, Loke, Assi et al. 2017). Thus, we speculate that the knockdown of *RUNX1/ETO* possibly changes the acetylation of *FOXO1* or other direct genes regulated by RUNX1 and FOXO1 transcription factors.

Since we did not further explore the mechanism of BCL2 inhibition in t(8;21) cell lines in downstream experiments, we cannot draw a definite conclusion or provide substantial evidence of our hypothesis that *RUNX1/ETO* regulates MCL1 and BCL2 indirectly. Further investigation is needed to confirm the changes in BIM isoforms and BCLXS protein levels. We suggest quantifying the level of apoptotic cells following venetoclax treatment by annexin V staining or caspase assays. Induction of apoptosis by caspase-3 and activation and PARP cleavage and translocation from the cytoplasm into the nucleus could also be a method to confirm the apoptosis using Western blotting.

6.9.3 BCL2 inhibition in SKNO-1 in vitro is independent from the cell cycle

Previous work in our lab has shown that RUNX1/ETO transcriptionally activates the cell cycle in t(8;21) leukaemic cells by causing overexpression of *CCND2*. Repression of either genes leads to G1 cell cycle arrest. In SKNO-1 cell line, we

showed that the depletion of *CCND2* by siRNA did not enhance the cytotoxicity of ABT-199. Inversely, *RUNX1/ETO* knockdown had a prolonged impact on the sensitivity to ABT-199 (Fig 5-9 & 5-10). These findings contradict previous studies which suggest that BCL2 affects the cell cycle by modulating p27 expression (Vairo, Innes et al. 1996, Vairo, Soos et al. 2000). Other studies have shown that BCL2 is more effective under a quiescent phenotype that is guarded by p27 overexpression (Brady, Gil-Gomez et al. 1996, Mazel, Burtrum et al. 1996). Arguably, the cell cycle machinery in t(8;21) is controlled by RUNX1/ETO, and the depletion of the fusion gene alone can upregulate p27 expression and induce senescence (Martinez, Drescher et al. 2004, Gu, Hu et al. 2014). Since we did not see any major increase in the G0 fraction after *RUNX1/ETO* knockdown in other work not reported in this thesis, we could reasonably propose that *RUNX1/ETO* depletion *in vitro* does not lead to increased G0 and quiescence. Thereby our observation of the increased sensitivity towards ABT-199 after *RUNX1/ETO* knockdown independently from the G1 cell cycle justifies the need to further experiments to unveil the relationship between the cell cycle and BCL2 inhibition in t(8;21) leukaemia.

6.9.4 RUNX1/ETO knockdown in vivo desensitises Kasumi-1 to BCL2 inhibition

Clinical and preclinical studies indicate that venetoclax has great therapeutic benefits in ALL, CLL and AML due to its selectivity and manageable toxicity (Roberts, Seymour et al. 2012, Souers, Leverson et al. 2013, Kipps, Eradat et al. 2015). The combinational treatment of venetoclax with AraC or hypomethylating agents has been shown to be synergistic in newly diagnosed, relapsed, or refractory adult AML patients (Mihalyova, Jelinek et al. 2018). While we observed potent toxicity of venetoclax in AML cell lines *in vitro*, the *in vivo* treatment showed minimal prolonged median survival by only 10 days (p=0.057) (Fig 5-12). For the *in vivo* experiments, we followed a recommended dose regimen from our collaborators to achieve the therapeutic plasma level (Scherr, Kirchhoff et al. 2019). However, we could not confirm that the maximal BCL2 inhibition was achieved. For future *in vivo* studies involving BCL2 inhibitors, we recommend

confirming the induction of apoptosis by quantifying changes in the mitochondrial membrane potential using tetramethylrhodamine ethyl ester (TMRE) staining.

Unexpectedly, venetoclax treatment antagonised *RUNX1/ETO* knockdown *in vivo* and reduced the median survival by two weeks (Fig 5-12). We noticed an increase in BCLXL protein level following *RUNX1/ETO* knockdown *in vitro,* but the enhanced BCLXL expression did not affect venetoclax toxicity (Fig 5-11). On the contrary, it is possible that *RUNX1/ETO* depletion *in vivo* led to a more significant increase in BLCXL which hijacked BCL2 inhibition and rescued the mitochondrial apoptosis. Clinical studies on AML patients have shown that BCLXL is immune to venetoclax (Souers, Leverson et al. 2013, Pan, Hogdal et al. 2014). In order to prevent BCLXL upregulation and effectively trigger the mitochondria apoptosis, ABT-263 (navitoclax) has been developed as a potent inhibitor for both BCL2 and BCLXL, which is considered as a senolytic agent as well (Tse, Shoemaker et al. 2008, Shafer and Grant 2016). Further experiments are required to evaluate the protein level of BCL family members, BIM isoforms and MCL1 after *RUNX1/ETO* depletion *in vivo*. We also propose to investigate the synergy between *RUNX1/ETO* knockdown and navitoclax *in vitro* and *in vivo*.

Although *RUXN1/ETO* knockdown *in vitro* did not change BCL2 protein level (Fig 5-11), RNA-seq obtained from the *in vivo* knockdown showed downregulation of *BCL2* expression. Typically, reduction in BCL2 protein level leads to adverse effect of venetoclax in which BCLXL can be upregulated and enhance the anti-apoptotic phenotype. Our RNA-seq did not show any changes in *BCLXL* expression, however this finding needs to be further investigated at protein level in future work. The depletion of *RUNX1/ETO in vivo* modulated the expression of genes involved in the mitochondria apoptosis pathways such as *BBC3, LPNX,* and *BMF*.

We found in our RNA-seq that *RUNX1/ETO* knockdown *in vivo* upregulated the BCL2 modifying factor (*BMF*). It has been shown that co-expression of the pro-apoptotic factors BMF and BIM enhances apoptosis in mutated *TP53* cells (Grespi, Soratroi et al. 2010, Hornsveld, Tenhagen et al. 2016). However, in our experiment, the increased expression of *BMF* did not enhance BCL2 inhibition. Additionally, upregulation of BBC3 in wild-type *TP53* malignant cells leads to a

robust pro-apoptotic phenotype as a response to various stimuli (Han, Flemington et al. 2001, Omori, Mitsuhashi et al. 2011). Although *TP53* is mutated in Kasumi-1, we found that *RUNX1/ETO* knockdown *in vivo* caused *BBC3* upregulation. The expression of *BBC3* in t(8;21) AML is higher than premature progenitors and HSCs, and it increases upon myeloid differentiation (Folkerts, Hilgendorf et al. 2017). It could be speculated that *RUNX1/ETO* knockdown may activate these pro-apoptotic regulators, which can compensate BCL2 inhibition. Further experiments are required to confirm the regulation of *BMF* and *BBC3* by RUNX1/ETO, and whether overexpression of either genes desensitise t(8;21) leukaemia to BCL2 inhibition.

Furthermore, we found that the *in vivo* depletion of *RUNX1/ETO* upregulated leupaxin (*LPXN*) expression, which is a member of the paxillin focal adhesion proteins family. Overexpression of LPXN is characteristic for aggressive tumours metastasise and migration (Kaulfuss, Grzmil et al. 2008, Chen and Kroog 2010). Moreover, BCL2 and LPXN share several complementary binning motifs, which their interaction leads to stabilisation of both proteins (Sheibani, Tang et al. 2008). It has been suggested that LPXN enhances AML invasion by upregulating BCL2 and downregulation of BAX (Dai, Zhu et al. 2016). Therefore, perhaps *RUNX1/ETO* knockdown *in vivo* led to upregulation of LPNX followed by stabilisation of BCL2 protein, hence reducing venetoclax activity. To prove our hypothesis, we recommend performing co-immunoprecipitation to evaluate the effect of *RUNX1/ETO* knockdown on the interaction of LPNX and BCL2 proteins in future studies.

Chapter 7.

Concluding remarks

7.1. General summary

RUNX1/ETO, the oncogenic transcription factor produced by the translocation t(8;21), represent an excellent example of the leukaemic-specific genes. Former work revealed that RUNX1/ETO dysregulates RUNX1 transcriptome to drive and maintain leukaemia by modulating genes involved in self-renewal, differentiation, cell cycle and genome stability. We showed that depleting *RUNX1/ETO* could provide a therapeutic window for t(8;21) AML patients, which may stratify for intervention and dose reduction in the current toxic chemotherapies.

To date, RNAi-mediated repression of several leukaemic fusion genes, such as *BCR/ABL*, *MLL/AF9*, *MLL/AF6*, and *PML/RARA* have been achieved by constitutive or conditional expression of shRNAs targeting these genes *(Ward, Sternsdorf et al. 2011, Deshpande, Chen et al. 2013, Goyama, Schibler et al. 2013, Barabe, Gil et al. 2017)*. For clinical implementation, it is not feasible to use shRNA to treat men. However, we have established transient gene knockdown using lipid nanoparticles encapsulating siRNA. Our approach has demonstrated the possibility to alter RUNX1/ETO leukaemogenesis *in vivo,* which could have the potential to be used in clinical setting. This thesis emphasises the functional importance of disrupting *RUNX1/ETO* transcriptional network, thereby confirming the therapeutic potential of targeting *RUNX1/ETO* to impair relapse.

Our findings provide a comprehensive picture on the consequences of RUNX1/ETO repression, despite the limitations of our xenotransplantation model, which partially recapitulates the niche-leukaemic stem cell interactions, and possible deceptively of cell lines. We have extensively proven the robustness of our siRNA delivery system in patient primary and patient-derived xenograft cells in a co-culture system that mimics the complex signalling pathways required to maintain leukaemic stem cells in a quiescent state. The intersection of our *in vitro*, *in vivo* and *ex vivo* findings with the results obtained from patient primary and PDXs cells that represent the patients clonal complexity, we provide valuable insight into understanding the underlying mechanism of RUNX1/ETO leukaemogenesis. The *in vivo* knockdown of *RUNX1/ETO* indicated a robust disruption of multipotent stem cells genes, thereby confirming the therapeutic potential of targeting *RUNX1/ETO* to impair relapse.

Patients with t(8;21) AML have a favourable prognosis, but recurrence of AML remains a major clinical obstacle. Development of novel drugs and improvement in diagnoses have improved the management of toxicity in standard AML chemotherapies. However, the vast majority of survivors still experience long-term side effects, such as cardiotoxicity and bone marrow failure (Siddiqui, Hogge et al. 2016). Relapse is driven by dormant cells, and it has been recently revealed that these cells remain susceptible to chemotherapies across a spectrum of genetically diverse AML (Boyd, Aslostovar et al. 2018).

Intriguingly, having proved the effectiveness of depleting *RUNX1/ETO* to inhibit leukaemia propagation, we tested the combinational effect of gene knockdown with current AML chemotherapies. Our observation of the reduced sensitivity of AML cell lines *in vitro* to the DNA damage agents after *RUNX1/ETO* inhibition complements the principle of ‘‘timed sequential therapy’’ in which the induction of chemotherapy must match the proliferative states of leukaemic cells in order to increase the effectiveness of treatments and improve the outcome for AML patients.

Evading apoptosis is an intrinsic feature of dormant leukaemic stem cells in which the anti- and pro-apoptotic machineries are modulated transcriptionally, translationally, and post-translationally to circumvent cell death. The mitochondrial apoptosis regulator BLC2 has been implicated as a critical pro-survival regulator in AML with great potential of venetoclax treatment. From another perspective, the elimination of senescent cells is an emerging topic in degenerative diseases (Xu, Pirtskhalava et al. 2018). Given that *RUNX1/ETO* repression is a potent senescence inducer, it is likely that treatment targeting the fusion protein alone would induce tissue damage. Thereby, we interrogated the possibility if RUNX1/ETO overrides the apoptotic resistance machinery of leukaemic cells, and aimed to eradicate leukaemia by testing the combinational therapy of *RUNX1/ETO* knockdown and venetoclax treatment. Although leukaemic cells were amenable to a combination of venetoclax and *RUNX1/ETO* knockdown *in vitro*, we could not conclusively prove that t(8;21) leukaemia is vulnerable to such combination. Due to time constraints, no further investigation into the combinational therapies could be performed in this project.

7.2 Considerations for future directions of siRNA therapeutics

The promise of siRNA targeted therapy is evolving rapidly with advances in oligonucleotides chemistry and siRNA delivery systems. RNAi-based therapeutics might be efficacious drugs to target leukaemic specific genes, such as *RUNX1/ETO*. Although some siRNA therapeutics are already approved for use in men, and dozens are now in clinical trials for several diseases, yet many challenges remain to be addressed. These include the low on-target activity, off-target effect by unintended silencing, immunogenic reaction to the siRNA duplex and toxicity of the excipient chemicals.

7.2.1 Sequence selection and the structural motif design

The antisense of siRNA is the putative strand for specific silencing of the targeted transcript. Hence, upon incorporation of the antisense in the RISC complex, the sequence of antisense is the exclusive determinant of gene knockdown. Additionally, sequence selection affects the on-target potency and off-target silencing. Nowadays, several software packages and databases are available to design selective siRNAs and predict their activity, such as Dharmacon's siDESIGN Center and IDT DNA custom DsiRNA design centre. These platforms screen the genomic and transcriptomic sequences to identify regions with extensive complementarity to the putative antisense. The algorithms in these platforms, such as blastn algorithms, can reliably predict the siRNA duplex thermodynamic stability and off-target matches. Generally, the ideal siRNA triggers are AU rich at the 5'-end of the antisense (Agrawal and Kandimalla 2001, Hu and Hu 2014, Hagedorn, Hansen et al. 2017).

The RNAi machinery has restrictive structural requirements in which RNA duplexes smaller than 15 bp do not incorporate into RISC, and those larger than 30 bp activate the PKR pathway and hereby the associated toxicity. The duplex structure affects siRNA processing and loading into RISC. Asymmetric siRNA, with two nucleotides at the 3'-overhangs at one side and a blunt end at the other, biases the selection of the antisense strand to the favour the strand carrying the 3'-overhangs. Moreover, the avoidance of immune stimulatory repeats, such as GU-rich motifs, is required to improve the safety profile of the siRNA (Zhang, Ohto et al. 2017, Seok, Lee et al. 2018).

7.2.2 siRNA chemical modifications

Oligonucleotides chemical modifications serve two vital functions. First, they improve the stability of the siRNA. Second, they attenuate the immunogenicity of the siRNA. In particular, introducing 2'-ribose and phosphorothioate modifications improve the siRNA pharmacokinetics and pharmacodynamics. Besides increasing the nuclease resistance, these modifications enhance the selective binding to RISC and reduce the off-target silencing (Lee, Seok et al. 2015, Kobayashi and Tomari 2016, Jiang, Zhu et al. 2017).

siRNAs stimulate and activate the TLR-dependent innate and adaptive immune responses primarily by TLR-7/8 in the endosome. Base modifications and introducing 2'-sugar modifications improve the safety of siRNA, especially 2'-O-Me modification by alleviating the TLR-mediated immune effects.

7.2.3 Delivery systems

Regardless of the sequence, duplex structure and chemical modifications, hydrophilicity, size and charge of the siRNA remain major obstetricals for stability in the systemic circulation, organs and tissue penetration, cellular uptake and endosomal escape. Therefore, biocompatible excipients are mandatory to overcome the siRNAs inherited poor pharmacokinetics.

Owing to the current vibrant research on delivery vehicles, siRNA therapeutics are moving through more mature clinical relevant development and pipelines. In particular, novel lipid nanoparticles formulations have proven to be efficacious in delivering several payloads, including siRNA. These nanoparticles allow the systemic administration of siRNA by intravenous infusion as well as site-specific injection. To treat leukaemia, the diameter of nanoparticles should be below 100 nm to ensure the delivery to the leukaemic niche through the endosteum membrane. Given that leukaemia may invade the CNS, the ability of the nanoparticles to pass the blood-brain barrier is also desirable.

In addition to the improved pharmacokinetics, the potency of siRNA could also benefit from enhanced targeted delivery. For instance, lipid nanoparticles allow for tissue-specific targeting by decorating the surface with ligands, such as antibodies,

scFv, aptamers or peptides, which ultimately increases the retention of the particles in the relevant tissues.

Chapter 8.

Supplementary Data

Cell lines authentication certificates.

NewGene Limited, Bioscience Building
International Centre for Life
Newcastle Upon Tyne
NE1 4EP
An ISO 15189 accredited Medical Laboratory
Company Number: 0673544
+44 (0)191 242 1923
info@newgene.org.uk

STR Profiling Report

Customer contact details: Claire Hutton, Northern Institute for Cancer Research

Tel: 07954138863 email: claire.hutton@ncl.ac.uk

Purchase Order number: 4200567749

Date received: 04 June 2018 Date reported: 11 June 2018

Sample lab ID code: 18-02675

Customer-submitted cell-line identification: KASUMI-1

NewGene STR profile-determined cell-line identification:
DSMZ Cell line #: 220 Name: KASUMI-1

Analysis performed by: Cara Shrimplin Checked by:

STR profiling data

Submitted sample profile					Reference database profile			
Loci	Sample profile ID:				Database profile ID:			
TH01	6	9			6	9		
TPOX	8	9			8	9		
vWA	14				14			
CSF1PO	10	12			10	12		
D16S539	9	12			9	12		
D7S820	8	11			8	11		
D13S317	11	13			11	13		
D5S818	9				9	11		
Amelogenin	X				X			
Complex electropherogram? (indicating sample is a mixture)								
Alleles shared between sample and reference profiles					15			
Total alleles in submitted sample profile					15			
Total alleles in reference database profile					16			
Percent allelic match between sample and reference profiles					**97%**			

s-Table 1: Kasumi-1 cell line authentication.

NewGene Limited, Bioscience Building
International Centre for Life
Newcastle Upon Tyne
NE1 4EP
An ISO 15189 accredited Medical Laboratory
Company Number: 0673544
+44 (0)191 242 1923
info@newgene.org.uk

STR Profiling Report

Customer contact details: Claire Hutton, Northern Institute for Cancer Research

Tel: 07954138863 email: claire.hutton@ncl.ac.uk

Purchase Order number: 4200567749

Date received: 04 June 2018 Date reported: 11 June 2018

Sample lab ID code: 18-02674

Customer-submitted cell-line identification: SKNO-1

NewGene STR profile-determined cell-line identification:
DSMZ Cell line #: 690 Name: SKNO-1

Analysis performed by: Cara Shrimplin Checked by:

STR profiling data

Submitted sample profile					Reference database profile			
Loci	Sample profile ID:				Database profile ID:			
TH01	7				7			
TPOX	8	9			8	9		
vWA	14	17			14	17		
CSF1PO	12	13			12	13		
D16S539	10	11			10	11		
D7S820	10	12			10	12		
D13S317	8	11			8	11		
D5S818	10	13			10	13		
Amelogenin	X				X			
Complex electropherogram? (indicating sample is a mixture)								
Alleles shared between sample and reference profiles					16			
Total alleles in submitted sample profile					16			
Total alleles in reference database profile					16			
Percent allelic match between sample and reference profiles					**100%**			

s-Table 2: SKNO-1 cell line authentication.

Plating efficiency of t(8;21) AML cell line.

Kasumi-1					
seeded cells	**500**	**1000**	**2000**	**5000**	**10000**
counted colonies	148	312	601	1409	3178
	140	289	593	1523	2268
	137	305	583	1331	2970
	141	308	600	1316	
Avg CFA	141.5	303.5	594.25	1394.75	2805.333
CFA%	28.3	30.35	29.7125	27.895	28.05333
stdv	4.031129	8.732125	7.189402	82.03162	389.3253
stdv%	2.848854	2.877142	1.209828	5.881457	13.87804

SKNO-1					
seeded cells	**500**	**1000**	**2000**	**5000**	**10000**
counted colonies	113	235	516	1003	2132
	125	215	487	973	2094
	99	261	525	1231	2346
	103	236	499	1167	
Avg CFA	110	236.75	506.75	1093.5	2190.667
CFA%	22	23.675	25.3375	21.87	21.90667
stdv	10.04988	16.31525	14.73728	108.4193	110.9274
stdv%	9.136251	6.891343	2.908196	9.91489	5.063637

s-Table 3: The plating efficiency of Kasumi-1 and SKNO-1 cell line. The exact colony number, normalisation and statistical analysis of data presented in Fig 3-12.

P.SLIEW vector map.

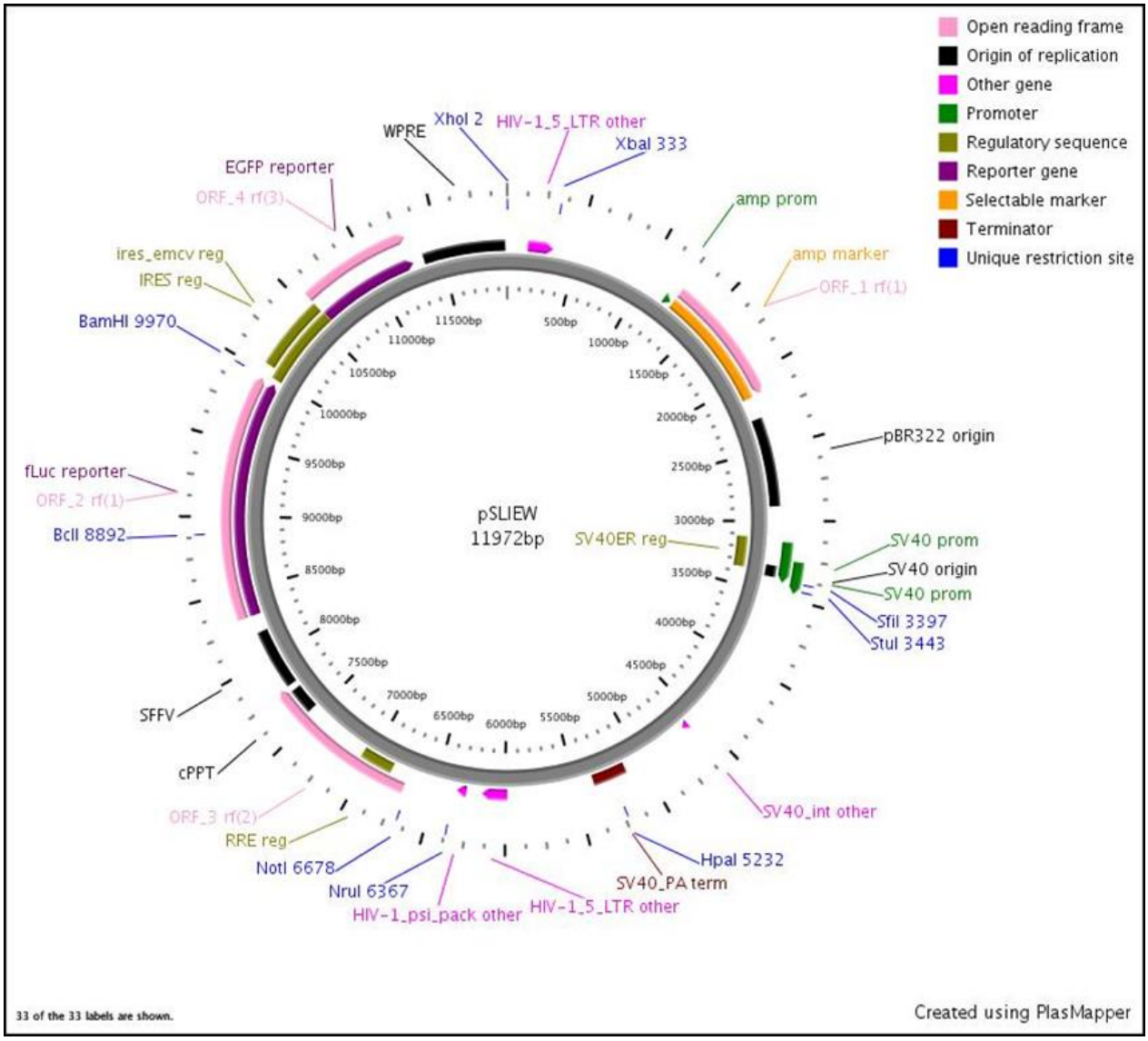

s-Fig 1: Vector map of the lentiviral expression vector p.SLIEW-shRNA.
Kasumi-1 p.SLIEW and SKNO-1 p.SLIEW cells were generated by Dr. Simon Bookmen as previously demonstrated in (Bomken, Buechler et al. 2013).

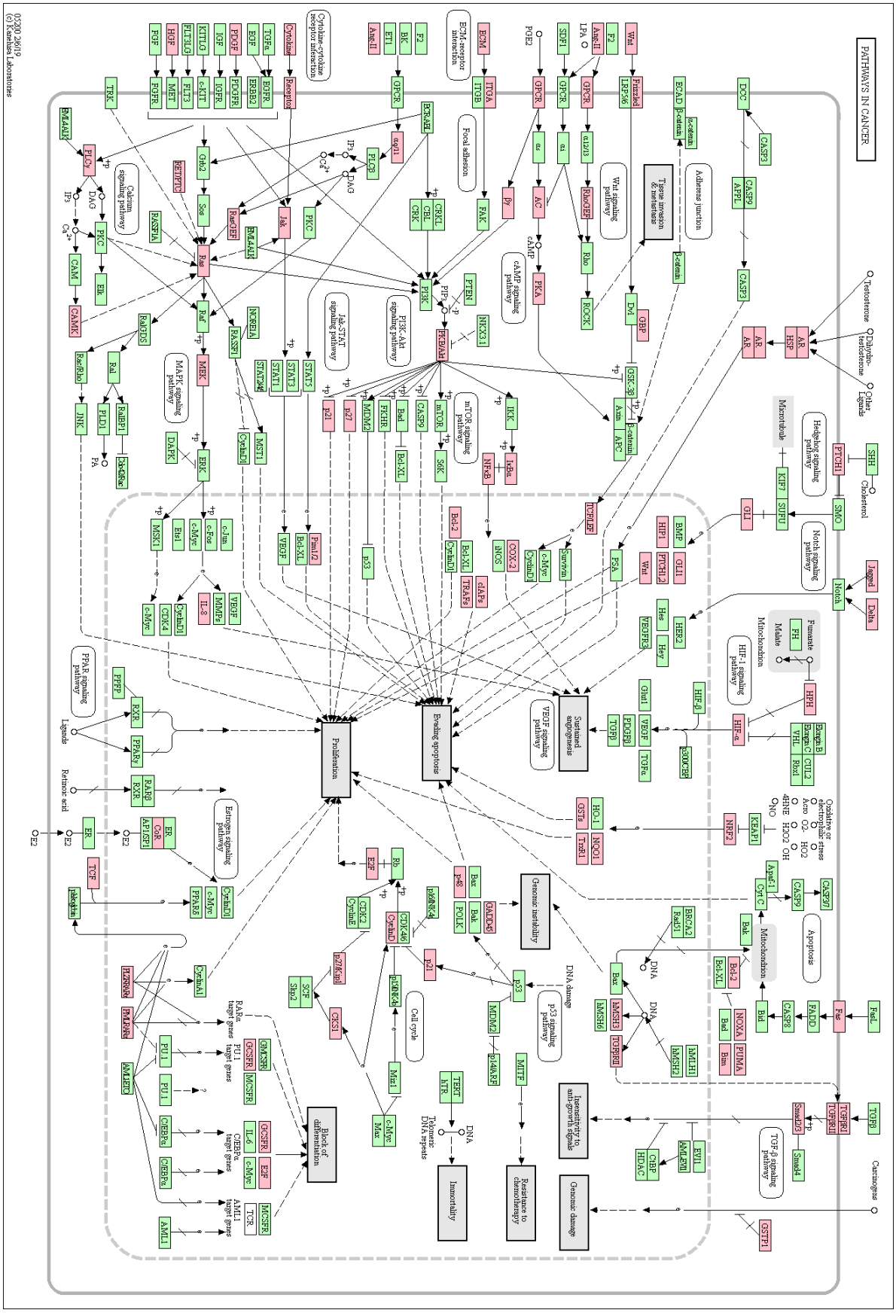

s-Fig 2: KEGG pathway analysis. Pathways in cancers.

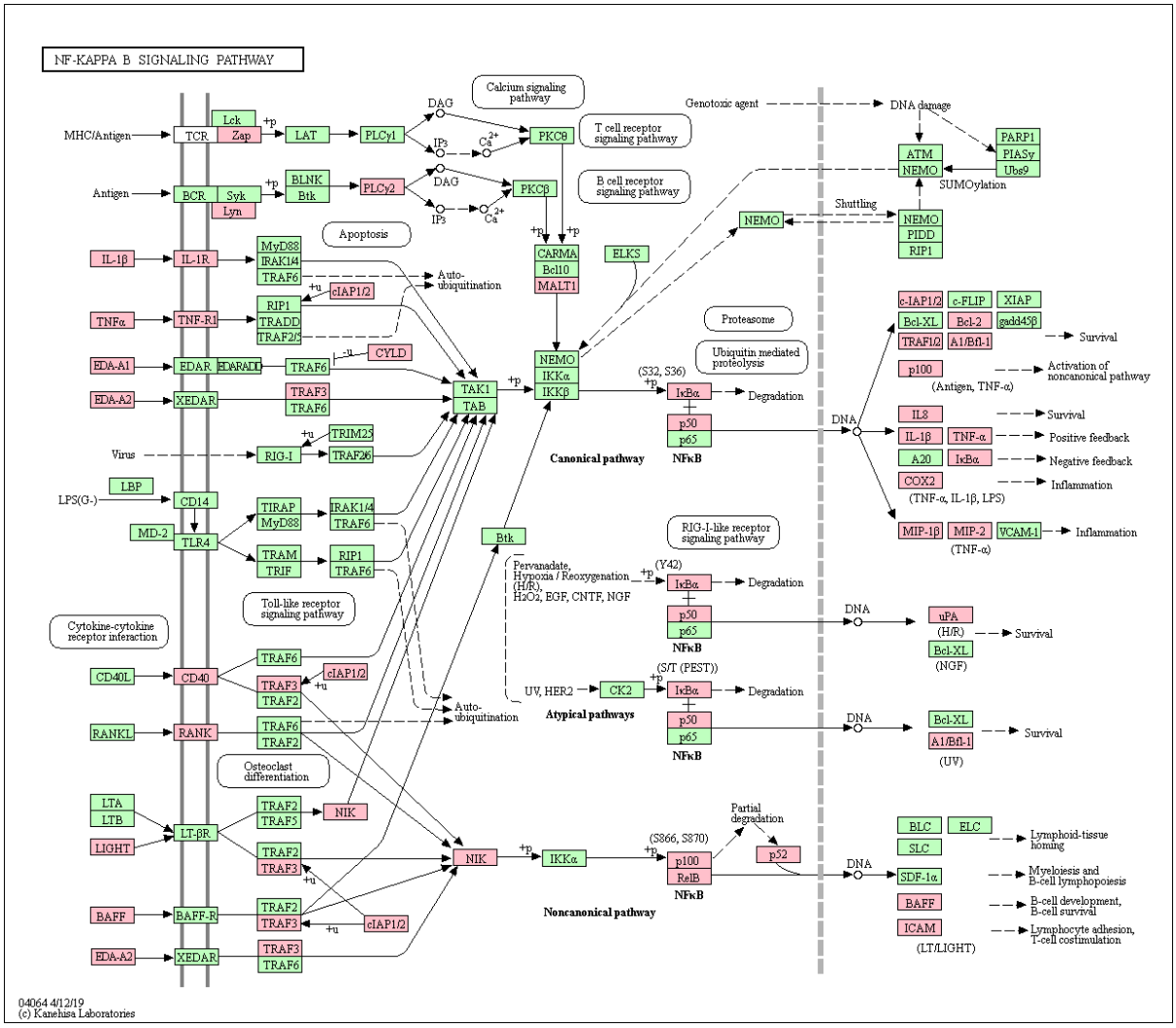

s-Fig 3: KEGG pathway analysis. NF-κB pathway.

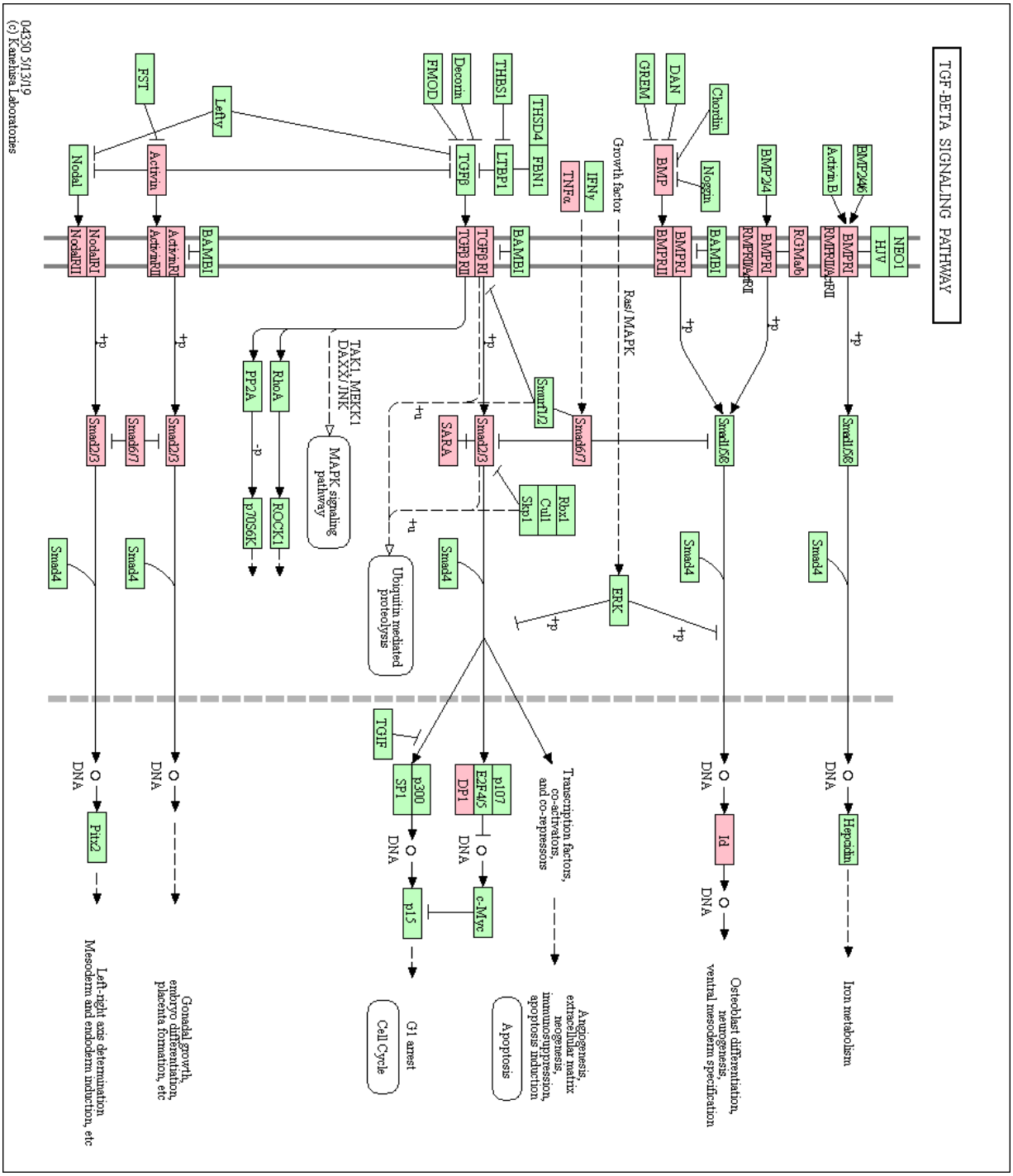

s-Fig 4: KEGG pathway analysis. TGF-β signalling.

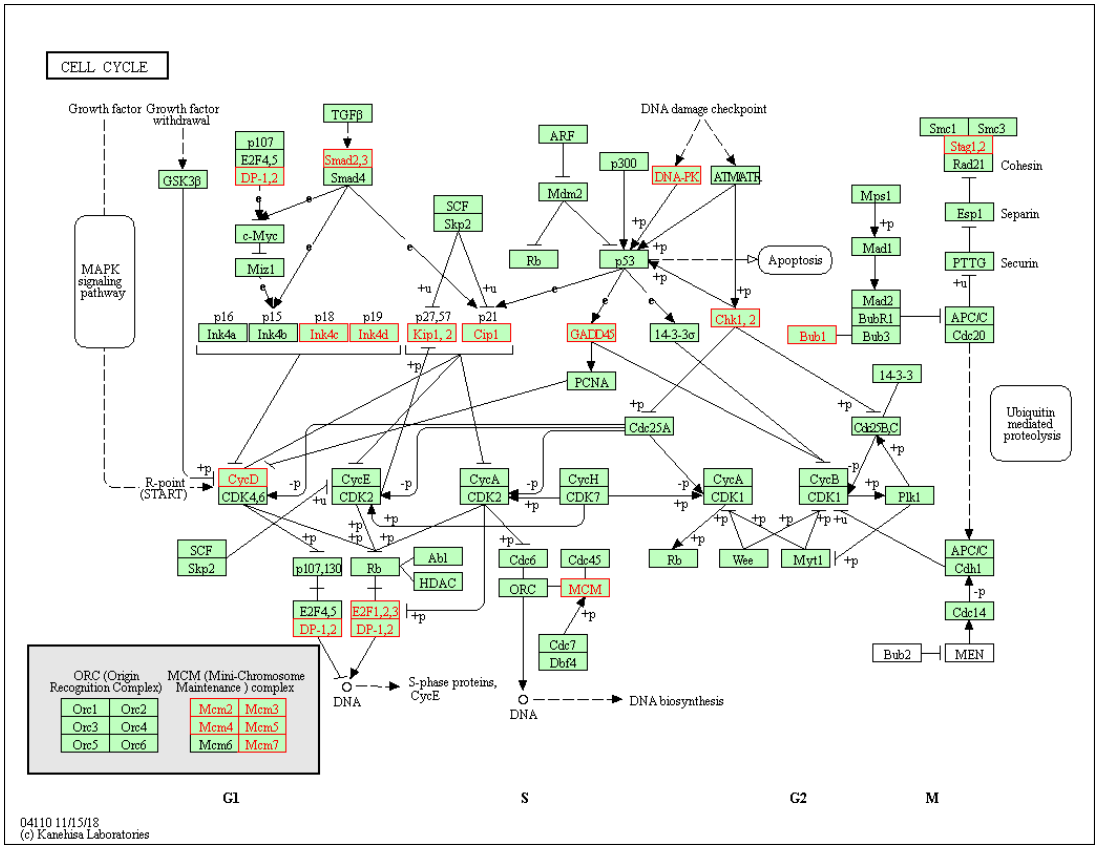

s-Fig 5: KEGG pathway analysis. Cell Cycle.

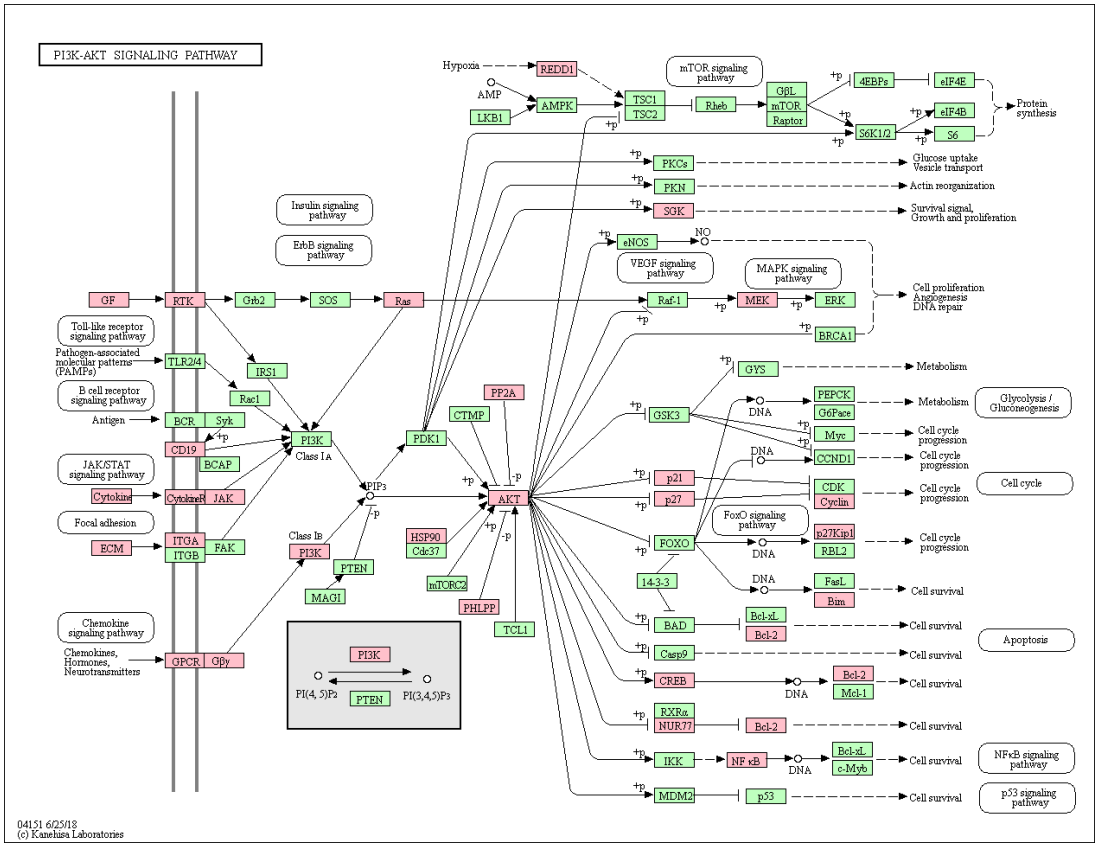

s-Fig 6: KEGG pathway analysis. PI3K-AKT signalling.

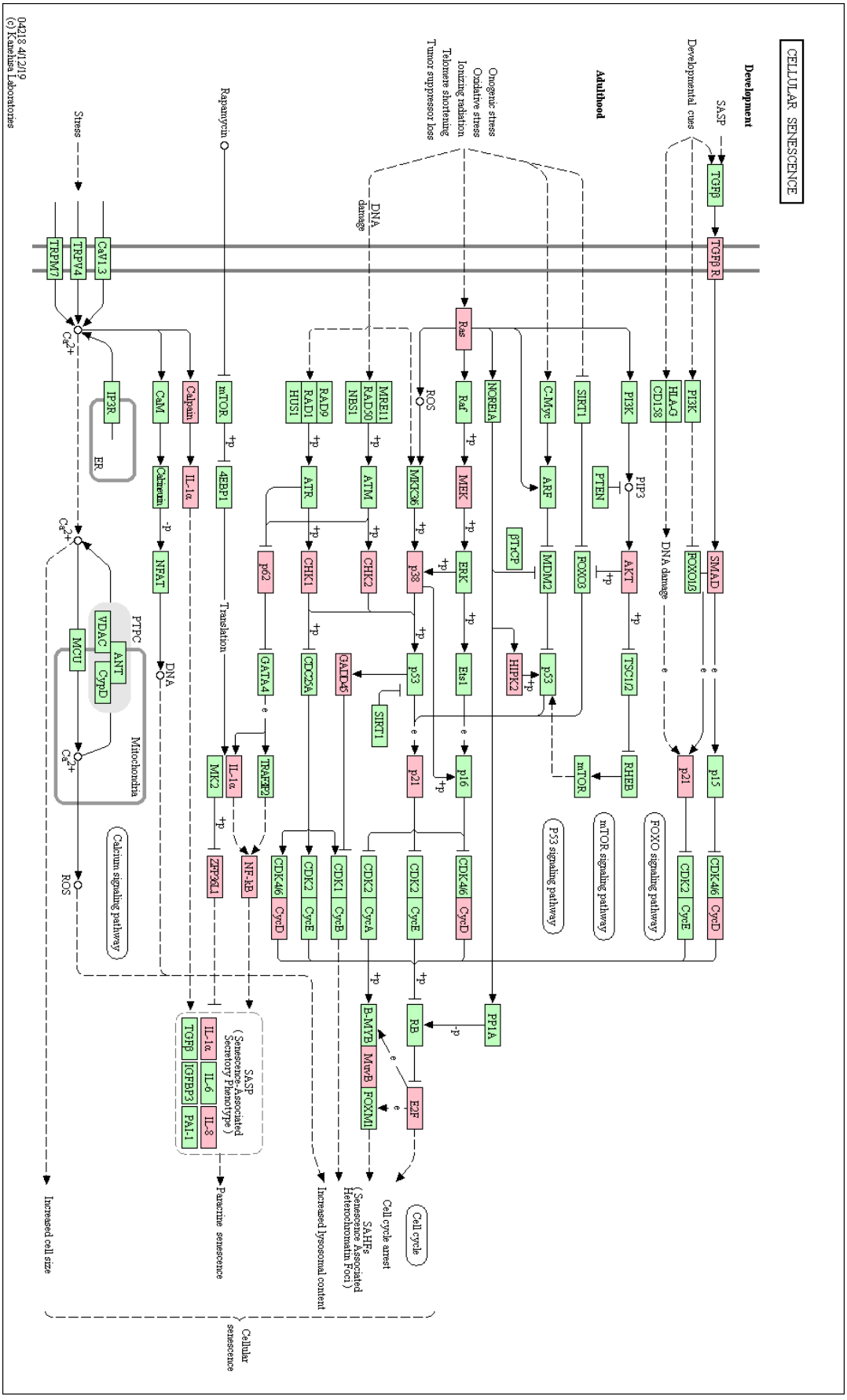

s-Fig 7: KEGG pathway analysis. Cellular senescence.

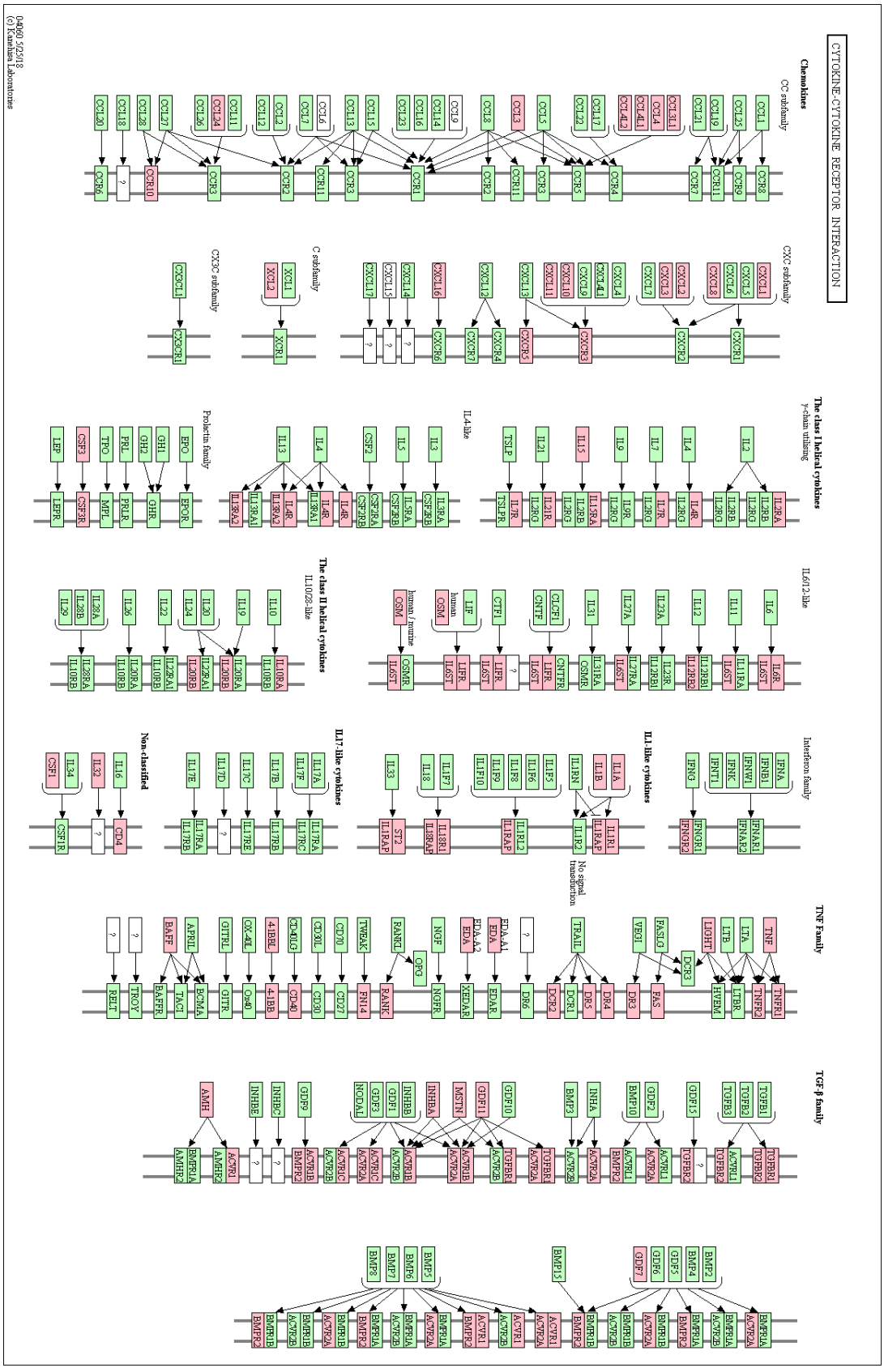

s-Fig 8: KEGG pathway analysis. Cytokine-receptor interaction.

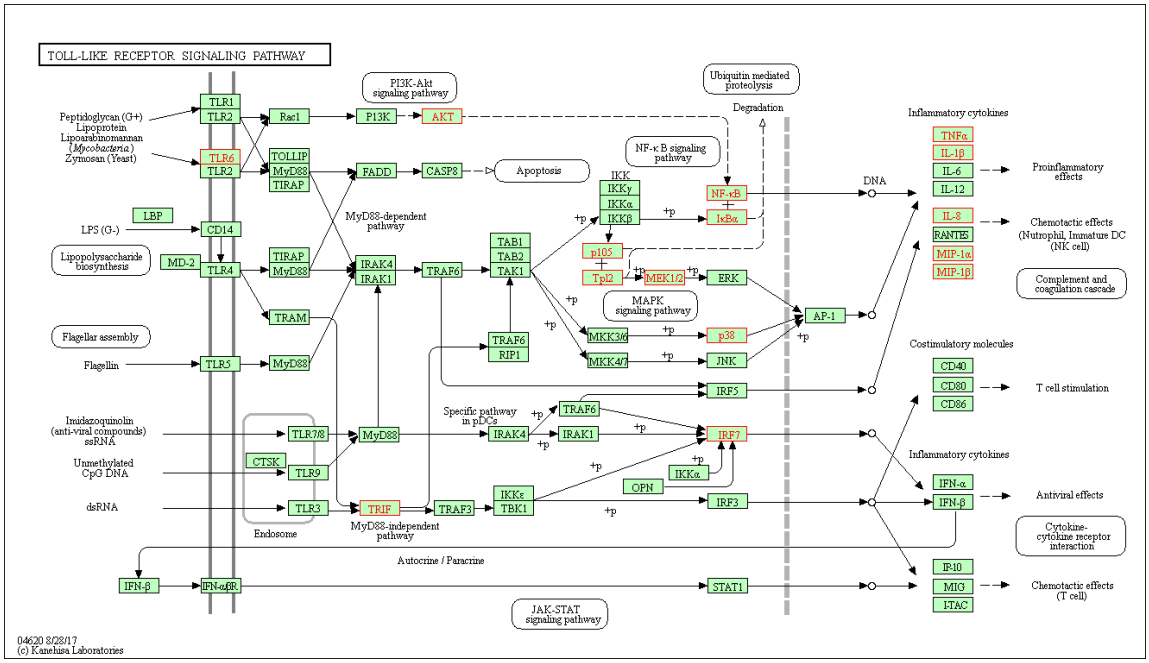

s-Fig 9: KEGG pathway analysis. Toll-like receptor signalling.

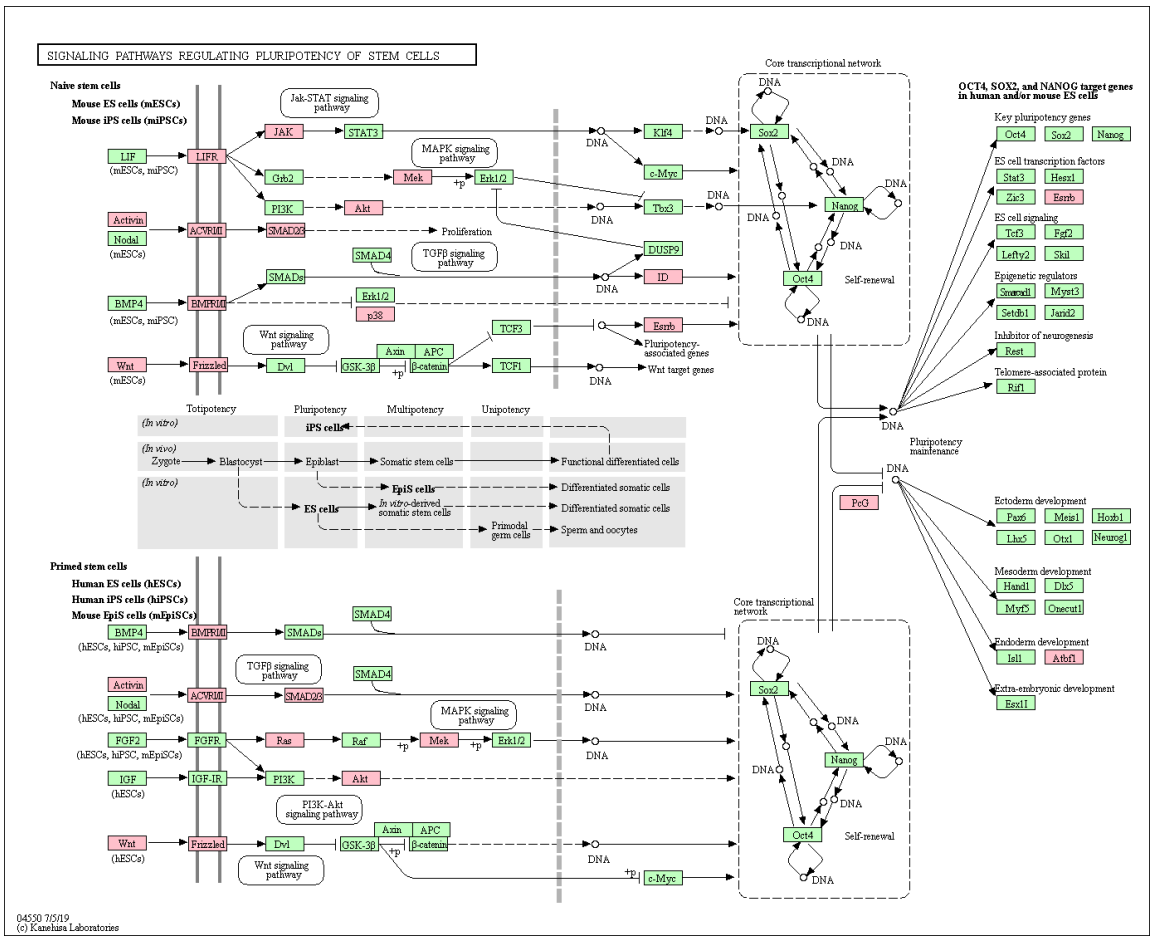

s-Fig 10: KEGG pathway analysis. Signalling pathways regulating pluripotency of stem cells.

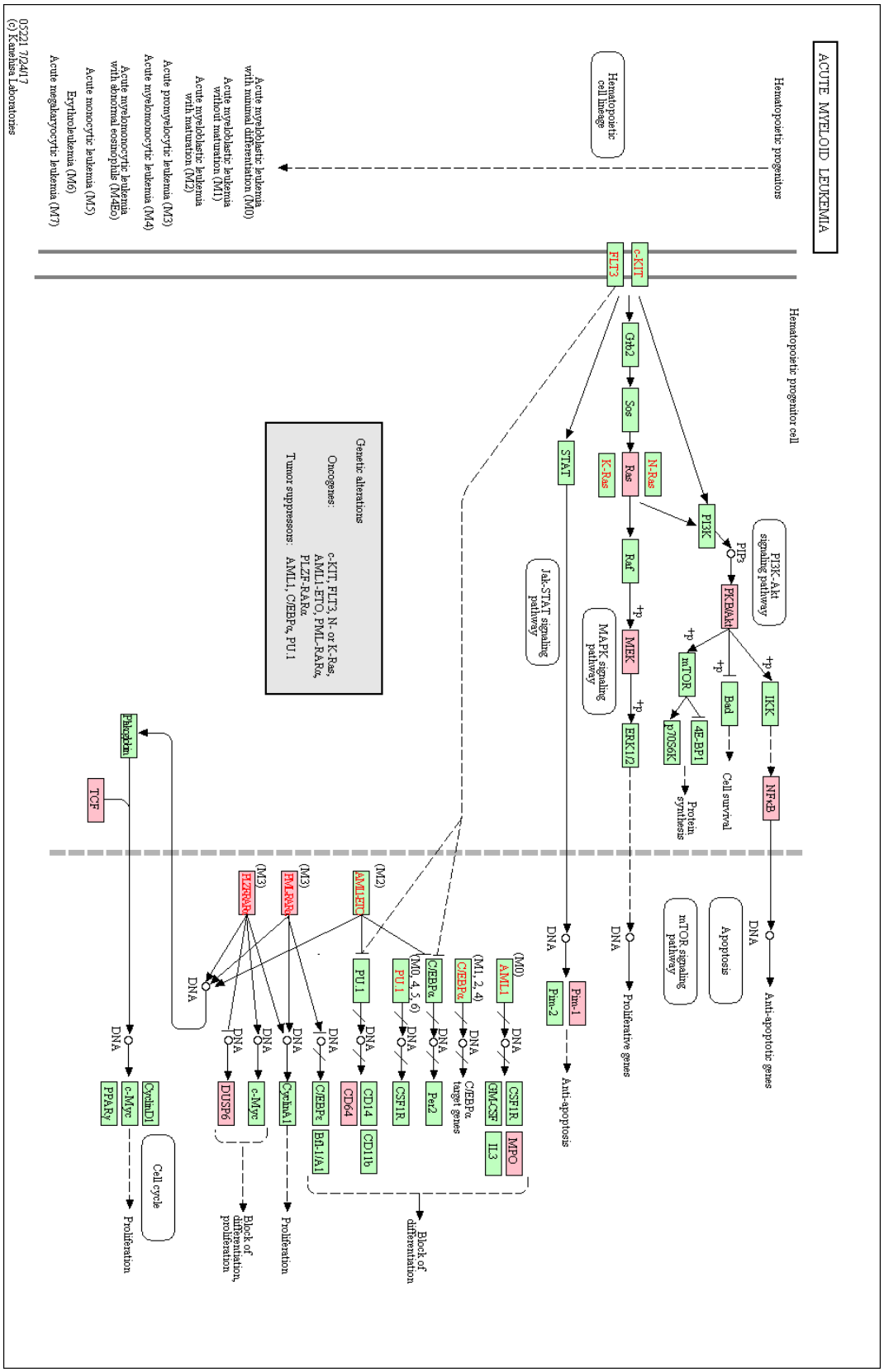

s-Fig 11: KEGG pathway analysis. Acute Myeloid Leukaemia.

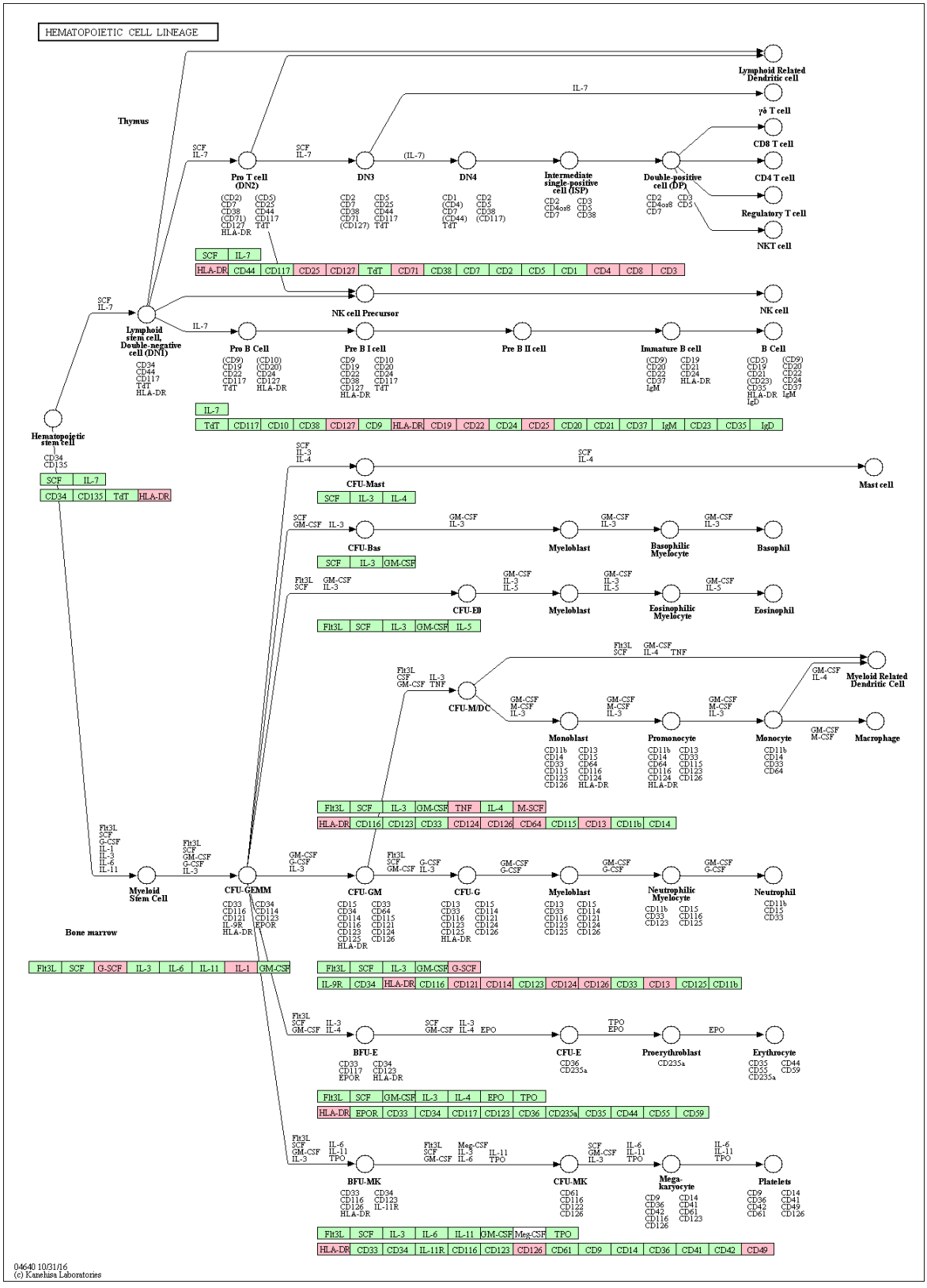

s-Fig 12: KEGG pathway analysis. Haematopoietic cell lineage.

Chapter 9.

References

Abu Lila, A. S. and T. Ishida (2017). "Liposomal Delivery Systems: Design Optimization and Current Applications." Biol Pharm Bull **40**(1): 1-10.
Adams, D., A. Gonzalez-Duarte, W. D. O'Riordan, C. C. Yang, M. Ueda, A. V. Kristen, I. Tournev, H. H. Schmidt, T. Coelho, J. L. Berk, K. P. Lin, G. Vita, S. Attarian, V. Plante-Bordeneuve, M. M. Mezei, J. M. Campistol, J. Buades, T. H. Brannagan, 3rd, B. J. Kim, J. Oh, Y. Parman, Y. Sekijima, P. N. Hawkins, S. D. Solomon, M. Polydefkis, P. J. Dyck, P. J. Gandhi, S. Goyal, J. Chen, A. L. Strahs, S. V. Nochur, M. T. Sweetser, P. P. Garg, A. K. Vaishnaw, J. A. Gollob and O. B. Suhr (2018). "Patisiran, an RNAi Therapeutic, for Hereditary Transthyretin Amyloidosis." N Engl J Med **379**(1): 11-21.
Agrawal, S. and E. R. Kandimalla (2001). "Antisense and/or immunostimulatory oligonucleotide therapeutics." Curr Cancer Drug Targets **1**(3): 197-209.
Aguayo, A., H. Kantarjian, T. Manshouri, C. Gidel, E. Estey, D. Thomas, C. Koller, Z. Estrov, S. O'Brien, M. Keating, E. Freireich and M. Albitar (2000). "Angiogenesis in acute and chronic leukemias and myelodysplastic syndromes." Blood **96**(6): 2240-2245.
Akinc, A., M. Goldberg, J. Qin, J. R. Dorkin, C. Gamba-Vitalo, M. Maier, K. N. Jayaprakash, M. Jayaraman, K. G. Rajeev, M. Manoharan, V. Koteliansky, I. Rohl, E. S. Leshchiner, R. Langer and D. G. Anderson (2009). "Development of lipidoid-siRNA formulations for systemic delivery to the liver." Mol Ther **17**(5): 872-879.
Al-Jamal, W. T. and K. Kostarelos (2011). "Liposomes: from a clinically established drug delivery system to a nanoparticle platform for theranostic nanomedicine." Acc Chem Res **44**(10): 1094-1104.
Alcalay, M., N. Meani, V. Gelmetti, A. Fantozzi, M. Fagioli, A. Orleth, D. Riganelli, C. Sebastiani, E. Cappelli, C. Casciari, M. T. Sciurpi, A. R. Mariano, S. P. Minardi, L. Luzi, H. Muller, P. P. Di Fiore, G. Frosina and P. G. Pelicci (2003). "Acute myeloid leukemia fusion proteins deregulate genes involved in stem cell maintenance and DNA repair." J Clin Invest **112**(11): 1751-1761.
Allsopp, R. C. and C. B. Harley (1995). "Evidence for a critical telomere length in senescent human fibroblasts." Exp Cell Res **219**(1): 130-136.
Amabile, G., R. S. Welner, C. Nombela-Arrieta, A. M. D'Alise, A. Di Ruscio, A. K. Ebralidze, Y. Kraytsberg, M. Ye, O. Kocher, D. S. Neuberg, K. Khrapko, L. E. Silberstein and D. G. Tenen (2013). "In vivo generation of transplantable human hematopoietic cells from induced pluripotent stem cells." Blood **121**(8): 1255-1264.
Amann, J. M., J. Nip, D. K. Strom, B. Lutterbach, H. Harada, N. Lenny, J. R. Downing, S. Meyers and S. W. Hiebert (2001). "ETO, a target of t(8;21) in acute leukemia, makes distinct contacts with multiple histone deacetylases and binds mSin3A through its oligomerization domain." Mol Cell Biol **21**(19): 6470-6483.
Ameres, S. L., J. Martinez and R. Schroeder (2007). "Molecular basis for target RNA recognition and cleavage by human RISC." Cell **130**(1): 101-112.
Andre, M. C., A. Erbacher, C. Gille, V. Schmauke, B. Goecke, A. Hohberger, P. Mang, A. Wilhelm, I. Mueller, W. Herr, P. Lang, R. Handgretinger and U. F. Hartwig (2010). "Long-term human CD34+ stem cell-engrafted nonobese diabetic/SCID/IL-2R gamma(null) mice show impaired CD8+ T cell maintenance and a functional arrest of immature NK cells." J Immunol **185**(5): 2710-2720.
Anzahaee, M. Y., J. K. Watts, N. R. Alla, A. W. Nicholson and M. J. Damha (2011). "Energetically important C-H...F-C pseudohydrogen bonding in water: evidence and application to rational design of oligonucleotides with high binding affinity." J Am Chem Soc **133**(4): 728-731.
Asada, N. (2018). "Regulation of Malignant Hematopoiesis by Bone Marrow Microenvironment." Front Oncol **8**: 119.
Bailey, J. K., W. Shen, X. H. Liang and S. T. Crooke (2017). "Nucleic acid binding proteins affect the subcellular distribution of phosphorothioate antisense oligonucleotides." Nucleic Acids Res **45**(18): 10649-10671.
Bali, P., M. Pranpat, J. Bradner, M. Balasis, W. Fiskus, F. Guo, K. Rocha, S. Kumaraswamy, S. Boyapalle, P. Atadja, E. Seto and K. Bhalla (2005). "Inhibition of histone deacetylase 6 acetylates and disrupts the chaperone function of heat shock protein 90: a novel basis for antileukemia activity of histone deacetylase inhibitors." J Biol Chem **280**(29): 26729-26734.

Bangham, A. D., M. M. Standish and J. C. Watkins (1965). "Diffusion of univalent ions across the lamellae of swollen phospholipids." Journal of Molecular Biology **13**(1): 238-IN227.
Bao, Y., Y. Jin, P. Chivukula, J. Zhang, Y. Liu, J. Liu, J. P. Clamme, R. I. Mahato, D. Ng, W. Ying, Y. Wang and L. Yu (2013). "Effect of PEGylation on biodistribution and gene silencing of siRNA/lipid nanoparticle complexes." Pharm Res **30**(2): 342-351.
Barabe, F., L. Gil, M. Celton, A. Bergeron, V. Lamontagne, E. Roques, K. Lagace, A. Forest, R. Johnson, L. Pecheux, J. Simard, J. Pelloux, A. Bellemare-Pelletier, E. Gagnon, J. Hebert, S. Cellot and B. T. Wilhelm (2017). "Modeling human MLL-AF9 translocated acute myeloid leukemia from single donors reveals RET as a potential therapeutic target." Leukemia **31**(5): 1166-1176.
Barata, P., A. K. Sood and D. S. Hong (2016). "RNA-targeted therapeutics in cancer clinical trials: Current status and future directions." Cancer Treat Rev **50**: 35-47.
Barseguian, K., B. Lutterbach, S. W. Hiebert, J. Nickerson, J. B. Lian, J. L. Stein, A. J. van Wijnen and G. S. Stein (2002). "Multiple subnuclear targeting signals of the leukemia-related AML1/ETO and ETO repressor proteins." Proc Natl Acad Sci U S A **99**(24): 15434-15439.
Bartsch, M., A. H. Weeke-Klimp, E. P. Hoenselaar, M. C. Stuart, D. K. Meijer, G. L. Scherphof and J. A. Kamps (2004). "Stabilized lipid coated lipoplexes for the delivery of antisense oligonucleotides to liver endothelial cells in vitro and in vivo." J Drug Target **12**(9-10): 613-621.
Beaudin, A. E., S. W. Boyer, J. Perez-Cunningham, G. E. Hernandez, S. C. Derderian, C. Jujjavarapu, E. Aaserude, T. MacKenzie and E. C. Forsberg (2016). "A Transient Developmental Hematopoietic Stem Cell Gives Rise to Innate-like B and T Cells." Cell Stem Cell **19**(6): 768-783.
Beghini, A., I. Magnani, C. B. Ripamonti and L. Larizza (2002). "Amplification of a novel c-Kit activating mutation Asn(822)-Lys in the Kasumi-1 cell line: a t(8;21)-Kit mutant model for acute myeloid leukemia." Hematol J **3**(3): 157-163.
Beigelman, L., A. Karpeisky, J. Matulicadamic, P. Haeberli, D. Sweedler and N. Usman (1995). "Synthesis of 2'-Modified Nucleotides and Their Incorporation into Hammerhead Ribozymes." Nucleic Acids Research **23**(21): 4434-4442.
Belair, C., S. Sim and S. L. Wolin (2018). "Noncoding RNA Surveillance: The Ends Justify the Means." **118**(8): 4422-4447.
Belliveau, N. M., J. Huft, P. J. Lin, S. Chen, A. K. Leung, T. J. Leaver, A. W. Wild, J. B. Lee, R. J. Taylor, Y. K. Tam, C. L. Hansen and P. R. Cullis (2012). "Microfluidic Synthesis of Highly Potent Limit-size Lipid Nanoparticles for In Vivo Delivery of siRNA." Mol Ther Nucleic Acids **1**: e37.
Ben-Porath, I. and R. A. Weinberg (2005). "The signals and pathways activating cellular senescence." Int J Biochem Cell Biol **37**(5): 961-976.
Benjaminsen, R. V., M. A. Mattebjerg, J. R. Henriksen, S. M. Moghimi and T. L. Andresen (2013). "The possible "proton sponge " effect of polyethylenimine (PEI) does not include change in lysosomal pH." Mol Ther **21**(1): 149-157.
Benjaminsen, R. V., M. A. Mattebjerg, J. R. Henriksen, S. M. Moghimi and T. L. Andresen (2013). "The Possible "Proton Sponge" Effect of Polyethylenimine (PEI) Does Not Include Change in Lysosomal pH." Molecular Therapy **21**(1): 149-157.
Bennett, J. M., D. Catovsky, M. T. Daniel, G. Flandrin, D. A. Galton, H. R. Gralnick and C. Sultan (1976). "Proposals for the classification of the acute leukaemias. French-American-British (FAB) co-operative group." Br J Haematol **33**(4): 451-458.
Bertoli, C., J. M. Skotheim and R. A. de Bruin (2013). "Control of cell cycle transcription during G1 and S phases." Nat Rev Mol Cell Biol **14**(8): 518-528.
Bertrand, J. Y., S. Giroux, R. Golub, M. Klaine, A. Jalil, L. Boucontet, I. Godin and A. Cumano (2005). "Characterization of purified intraembryonic hematopoietic stem cells as a tool to define their site of origin." Proceedings of the National Academy of Sciences of the United States of America **102**(1): 134-139.
Bizzari, J. P. and W. J. Mackillop (1985). "The estimation of self-renewal in the clonogenic cells of human solid tumours: a comparison of secondary plating efficiency and colony size." Br J Cancer **52**(2): 189-195.

Blair, A., D. E. Hogge and H. J. Sutherland (1998). "Most acute myeloid leukemia progenitor cells with long-term proliferative ability in vitro and in vivo have the phenotype CD34(+)/CD71(-)/HLA-DR-." Blood **92**(11): 4325-4335.
Bloom, W. and G. W. Bartelmez (1940). "Hematopoiesis in young human embryos." American Journal of Anatomy **67**(1): 21-53.
Blumenthal, E., S. Greenblatt, G. Huang, K. Ando, Y. Xu and S. D. Nimer (2017). Covalent Modifications of RUNX Proteins: Structure Affects Function. RUNX Proteins in Development and Cancer. Y. Groner, Y. Ito, P. Liu et al. Singapore, Springer Singapore**:** 33-44.
Bobo, D., K. J. Robinson, J. Islam, K. J. Thurecht and S. R. Corrie (2016). "Nanoparticle-Based Medicines: A Review of FDA-Approved Materials and Clinical Trials to Date." Pharm Res **33**(10): 2373-2387.
Bogorad, R. L., H. Yin, A. Zeigerer, H. Nonaka, V. M. Ruda, M. Zerial, D. G. Anderson and V. Koteliansky (2014). "Nanoparticle-formulated siRNA targeting integrins inhibits hepatocellular carcinoma progression in mice." Nat Commun **5**: 3869.
Bolu, B. S., R. Sanyal and A. Sanyal (2018). "Drug Delivery Systems from Self-Assembly of Dendron-Polymer Conjugates (dagger)." Molecules **23**(7).
Bomken, S., L. Buechler, K. Rehe, F. Ponthan, A. Elder, H. Blair, C. M. Bacon, J. Vormoor and O. Heidenreich (2013). "Lentiviral marking of patient-derived acute lymphoblastic leukaemic cells allows in vivo tracking of disease progression." Leukemia **27**(3): 718-721.
Bonnet, D. and J. E. Dick (1997). "Human acute myeloid leukemia is organized as a hierarchy that originates from a primitive hematopoietic cell." Nature Medicine **3**(7): 730-737.
Borowicz, S., M. Van Scoyk, S. Avasarala, M. K. Karuppusamy Rathinam, J. Tauler, R. K. Bikkavilli and R. A. Winn (2014). "The soft agar colony formation assay." J Vis Exp(92): e51998.
Boyd, A. L., L. Aslostovar, J. Reid, W. Ye, B. Tanasijevic, D. P. Porras, Z. Shapovalova, M. Almakadi, R. Foley, B. Leber, A. Xenocostas and M. Bhatia (2018). "Identification of Chemotherapy-Induced Leukemic-Regenerating Cells Reveals a Transient Vulnerability of Human AML Recurrence." Cancer Cell **34**(3): 483-498 e485.
Bracht, J. R., X. Wang, K. Shetty, X. Chen, G. J. Uttarotai, E. C. Callihan, S. S. McCloud, D. M. Clay, J. Wang, M. Nowacki and L. F. Landweber (2017). "Chromosome fusions triggered by noncoding RNA." RNA Biol **14**(5): 620-631.
Brady, H. J., G. Gil-Gomez, J. Kirberg and A. J. Berns (1996). "Bax alpha perturbs T cell development and affects cell cycle entry of T cells." EMBO J **15**(24): 6991-7001.
Braunova, A., L. Kostka, L. Sivak, L. Cuchalova, Z. Hvezdova, R. Laga, S. Filippov, P. Cernoch, M. Pechar, O. Janouskova, M. Sirova and T. Etrych (2017). "Tumor-targeted micelle-forming block copolymers for overcoming of multidrug resistance." J Control Release **245**: 41-51.
Buess, H. (1959). "Albrecht von Haller and his Elementa Physiologiae as the beginning of pathological physiology." Med Hist **3**(2): 123-131.
Burel, S. A., N. Harakawa, L. Zhou, T. Pabst, D. G. Tenen and D. E. Zhang (2001). "Dichotomy of AML1-ETO functions: growth arrest versus block of differentiation." Mol Cell Biol **21**(16): 5577-5590.
Burnett, A. K., R. K. Hills, D. W. Milligan, A. H. Goldstone, A. G. Prentice, M. F. McMullin, A. Duncombe, B. Gibson and K. Wheatley (2010). "Attempts to optimize induction and consolidation treatment in acute myeloid leukemia: results of the MRC AML12 trial." J Clin Oncol **28**(4): 586-595.
Buschges, R., R. G. Weber, B. Actor, P. Lichter, V. P. Collins and G. Reifenberger (1999). "Amplification and expression of cyclin D genes (CCND1, CCND2 and CCND3) in human malignant gliomas." Brain Pathol **9**(3): 435-442; discussion 432-433.
Cairoli, R., A. Beghini, G. Grillo, G. Nadali, F. Elice, C. B. Ripamonti, P. Colapietro, M. Nichelatti, L. Pezzetti, M. Lunghi, A. Cuneo, A. Viola, F. Ferrara, M. Lazzarino, F. Rodeghiero, G. Pizzolo, L. Larizza and E. Morra (2006). "Prognostic impact of c-KIT mutations in core binding factor leukemias: an Italian retrospective study." Blood **107**(9): 3463-3468.
Campisi, J. (2001). "Cellular senescence as a tumor-suppressor mechanism." Trends in Cell Biology **11**(11): S27-S31.

Cao, J., M. Spielmann, X. Qiu, X. Huang, D. M. Ibrahim, A. J. Hill, F. Zhang, S. Mundlos, L. Christiansen, F. J. Steemers, C. Trapnell and J. Shendure (2019). "The single-cell transcriptional landscape of mammalian organogenesis." Nature **566**(7745): 496-502.
Carthew, R. W. and E. J. Sontheimer (2009). "Origins and Mechanisms of miRNAs and siRNAs." Cell **136**(4): 642-655.
Cech, T. R. and J. A. Steitz (2014). "The noncoding RNA revolution-trashing old rules to forge new ones." Cell **157**(1): 77-94.
Cerutti, L., N. Mian and A. Bateman (2000). "Domains in gene silencing and cell differentiation proteins: the novel PAZ domain and redefinition of the Piwi domain." Trends Biochem Sci **25**(10): 481-482.
Chaikovsky, A. C. and J. Sage (2018). "Beyond the Cell Cycle: Enhancing the Immune Surveillance of Tumors Via CDK4/6 Inhibition." Mol Cancer Res **16**(10): 1454-1457.
Charan, J. and N. Kantharia (2013). "How to calculate sample size in animal studies?" Journal of Pharmacology and Pharmacotherapeutics **4**(4): 303-306.
Charan, J. and N. D. Kantharia (2013). "How to calculate sample size in animal studies?" J Pharmacol Pharmacother **4**(4): 303-306.
Chen, D., L. J. Luo and C. Liang (2018). "Aberrant S100A16 expression might be an independent prognostic indicator of unfavorable survival in non-small cell lung adenocarcinoma." Plos One **13**(5).
Chen, L., G. Wang, Y. Luo, Y. Wang, C. Xie, W. Jiang, Y. Xiao, G. Qian and X. Wang (2017). "Downregulation of LAPTM5 suppresses cell proliferation and viability inducing cell cycle arrest at G0/G1 phase of bladder cancer cells." Int J Oncol **50**(1): 263-271.
Chen, P. W. and G. S. Kroog (2010). "Leupaxin is similar to paxillin in focal adhesion targeting and tyrosine phosphorylation but has distinct roles in cell adhesion and spreading." Cell Adhesion & Migration **4**(4): 527-540.
Chen, S., Y. Dai, X. Y. Pei and S. Grant (2009). "Bim upregulation by histone deacetylase inhibitors mediates interactions with the Bcl-2 antagonist ABT-737: evidence for distinct roles for Bcl-2, Bcl-xL, and Mcl-1." Mol Cell Biol **29**(23): 6149-6169.
Chen, S., Y. Y. Tam, P. J. Lin, A. K. Leung, Y. K. Tam and P. R. Cullis (2014). "Development of lipid nanoparticle formulations of siRNA for hepatocyte gene silencing following subcutaneous administration." J Control Release **196**: 106-112.
Chen, S., Y. Y. C. Tam, P. J. C. Lin, M. M. H. Sung, Y. K. Tam and P. R. Cullis (2016). "Influence of particle size on the in vivo potency of lipid nanoparticle formulations of siRNA." J Control Release **235**: 236-244.
Cheng, T. (2004). "Cell cycle inhibitors in normal and tumor stem cells." Oncogene **23**(43): 7256-7266.
Cheng, T., N. Rodrigues, H. Shen, Y. Yang, D. Dombkowski, M. Sykes and D. T. Scadden (2000). "Hematopoietic stem cell quiescence maintained by p21cip1/waf1." Science **287**(5459): 1804-1808.
Cheng, X. and R. J. Lee (2016). "The role of helper lipids in lipid nanoparticles (LNPs) designed for oligonucleotide delivery." Adv Drug Deliv Rev **99**(Pt A): 129-137.
Cheung, A. M., T. K. Fung, A. K. Fan, T. S. Wan, H. C. Chow, J. C. Leung, L. Y. Chan, Y. L. Kwong, R. Liang and A. Y. Leung (2010). "Successful engraftment by leukemia initiating cells in adult acute lymphoblastic leukemia after direct intrahepatic injection into unconditioned newborn NOD/SCID mice." Exp Hematol **38**(1): 3-10.
Chhabra, R., R. Dubey and N. Saini (2010). "Cooperative and individualistic functions of the microRNAs in the miR-23a~27a~24-2 cluster and its implication in human diseases." Mol Cancer **9**: 232.
Chiang, H. R., L. W. Schoenfeld, J. G. Ruby, V. C. Auyeung, N. Spies, D. Baek, W. K. Johnston, C. Russ, S. Luo, J. E. Babiarz, R. Blelloch, G. P. Schroth, C. Nusbaum and D. P. Bartel (2010). "Mammalian microRNAs: experimental evaluation of novel and previously annotated genes." Genes Dev **24**(10): 992-1009.

Chien, Y. C., C. Scuoppo, X. W. Wang, X. P. Fang, B. Balgley, J. E. Bolden, P. Premsrirut, W. J. Luo, A. Chicas, C. S. Lee, S. C. Kogan and S. W. Lowe (2011). "Control of the senescence-associated secretory phenotype by NF-kappa B promotes senescence and enhances chemosensitivity." Genes & Development **25**(20): 2125-2136.
Childs, B. G., D. J. Baker, J. L. Kirkland, J. Campisi and J. M. van Deursen (2014). "Senescence and apoptosis: dueling or complementary cell fates?" EMBO reports **15**(11): 1139-1153.
Christensen, J., K. Litherland, T. Faller, E. van de Kerkhof, F. Natt, J. Hunziker, J. Boos, I. Beuvink, K. Bowman, J. Baryza, M. Beverly, C. Vargeese, O. Heudi, M. Stoeckli, J. Krauser and P. Swart (2014). "Biodistribution and metabolism studies of lipid nanoparticle-formulated internally [3H]-labeled siRNA in mice." Drug Metab Dispos **42**(3): 431-440.
Clemens, M. J. and A. Elia (1997). "The double-stranded RNA-dependent protein kinase PKR: Structure and function." Journal of Interferon and Cytokine Research **17**(9): 503-524.
Collins, C. J. and J. M. Sedivy (2003). "Involvement of the INK4a/Arf gene locus in senescence." Aging Cell **2**(3): 145-150.
Cook, A. F., M. J. Holman and A. L. Nussbaum (1969). "Nucleoside S-alkyl phosphorothioates. II. Preparation and chemical and enzymatic properties." J Am Chem Soc **91**(6): 1522-1527.
Coppe, J. P., P. Y. Desprez, A. Krtolica and J. Campisi (2010). "The senescence-associated secretory phenotype: the dark side of tumor suppression." Annu Rev Pathol **5**: 99-118.
Coppe, J. P., C. K. Patil, F. Rodier, Y. Sun, D. P. Munoz, J. Goldstein, P. S. Nelson, P. Y. Desprez and J. Campisi (2008). "Senescence-associated secretory phenotypes reveal cell-nonautonomous functions of oncogenic RAS and the p53 tumor suppressor." PLoS Biol **6**(12): 2853-2868.
Cordeiro Gomes, A., T. Hara, V. Y. Lim, D. Herndler-Brandstetter, E. Nevius, T. Sugiyama, S. Tani-Ichi, S. Schlenner, E. Richie, H. R. Rodewald, R. A. Flavell, T. Nagasawa, K. Ikuta and J. P. Pereira (2016). "Hematopoietic Stem Cell Niches Produce Lineage-Instructive Signals to Control Multipotent Progenitor Differentiation." Immunity **45**(6): 1219-1231.
Corey, S. J., P. M. Dombrosky-Ferlan, S. Zuo, E. Krohn, A. D. Donnenberg, P. Zorich, G. Romero, M. Takata and T. Kurosaki (1998). "Requirement of Src kinase Lyn for induction of DNA synthesis by granulocyte colony-stimulating factor." J Biol Chem **273**(6): 3230-3235.
Coulombel, L. (2004). "Identification of hematopoietic stem/progenitor cells: strength and drawbacks of functional assays." Oncogene **23**(43): 7210-7222.
Creusat, G., A. S. Rinaldi, E. Weiss, R. Elbaghdadi, J. S. Remy, R. Mulherkar and G. Zuber (2010). "Proton sponge trick for pH-sensitive disassembly of polyethylenimine-based siRNA delivery systems." Bioconjug Chem **21**(5): 994-1002.
Cullen, P. (1811). "Case of splenitis acutus in which the serum of the blood drawn from the arm had the appearance of milk." Edinburgh Medical Journal **7**: 169-171.
Cullis, P. R. and M. J. Hope (2017). "Lipid Nanoparticle Systems for Enabling Gene Therapies." Mol Ther **25**(7): 1467-1475.
Dagle, J. M., D. L. Weeks and J. A. Walder (1991). "Pathways of degradation and mechanism of action of antisense oligonucleotides in Xenopus laevis embryos." Antisense Res Dev **1**(1): 11-20.
Dahl, R., J. C. Walsh, D. Lancki, P. Laslo, S. R. Iyer, H. Singh and M. C. Simon (2003). "Regulation of macrophage and neutrophil cell fates by the PU.1:C/EBPalpha ratio and granulocyte colony-stimulating factor." Nat Immunol **4**(10): 1029-1036.
Dai, H. P., G. H. Zhu, Q. Shen, L. L. Wu, Q. Wang, Q. R. Wang, L. J. Wen, H. Yao, H. Y. Qiu, S. N. Chen and D. P. Wu (2016). "Lpxn Regulates Proliferation, Adhesion and Invasion of Acute Myeloid Leukemic Cells." Blood **128**(22).
Dakic, A., L. Wu and S. L. Nutt (2007). "Is PU.1 a dosage-sensitive regulator of haemopoietic lineage commitment and leukaemogenesis?" Trends in Immunology **28**(3): 108-114.
Dalpke, A. and M. Helm (2012). "RNA mediated Toll-like receptor stimulation in health and disease." RNA Biol **9**(6): 828-842.

Davalos, A. R., M. Kawahara, G. K. Malhotra, N. Schaum, J. Huang, U. Ved, C. M. Beausejour, J. P. Coppe, F. Rodier and J. Campisi (2013). "p53-dependent release of Alarmin HMGB1 is a central mediator of senescent phenotypes." J Cell Biol **201**(4): 613-629.
Davis, M. E., J. E. Zuckerman, C. H. Choi, D. Seligson, A. Tolcher, C. A. Alabi, Y. Yen, J. D. Heidel and A. Ribas (2010). "Evidence of RNAi in humans from systemically administered siRNA via targeted nanoparticles." Nature **464**(7291): 1067-1070.
Davis, S., T. H. Aldrich, P. F. Jones, A. Acheson, D. L. Compton, V. Jain, T. E. Ryan, J. Bruno, C. Radziejewski, P. C. Maisonpierre and G. D. Yancopoulos (1996). "Isolation of angiopoietin-1, a ligand for the TIE2 receptor, by secretion-trap expression cloning." Cell **87**(7): 1161-1169.
de Bont, E. S., S. Rosati, S. Jacobs, W. A. Kamps and E. Vellenga (2001). "Increased bone marrow vascularization in patients with acute myeloid leukaemia: a possible role for vascular endothelial growth factor." Br J Haematol **113**(2): 296-304.
De Palma, M., D. Biziato and T. V. Petrova (2017). "Microenvironmental regulation of tumour angiogenesis." Nat Rev Cancer **17**(8): 457-474.
DeKelver, R. C., B. Lewin, K. Lam, Y. Komeno, M. Yan, C. Rundle, M. C. Lo and D. E. Zhang (2013). "Cooperation between RUNX1-ETO9a and novel transcriptional partner KLF6 in upregulation of Alox5 in acute myeloid leukemia." PLoS Genet **9**(10): e1003765.
Del Gaizo Moore, V., J. R. Brown, M. Certo, T. M. Love, C. D. Novina and A. Letai (2007). "Chronic lymphocytic leukemia requires BCL2 to sequester prodeath BIM, explaining sensitivity to BCL2 antagonist ABT-737." J Clin Invest **117**(1): 112-121.
Deleavey, G. F. and M. J. Damha (2012). "Designing chemically modified oligonucleotides for targeted gene silencing." Chem Biol **19**(8): 937-954.
Delgado, A. V., F. Gonzalez-Caballero, R. J. Hunter, L. K. Koopal, J. Lyklema, P. International Union of, P. Applied Chemistry and I. T. R. Biophysical Chemistry Division (2007). "Measurement and interpretation of electrokinetic phenomena." J Colloid Interface Sci **309**(2): 194-224.
Deng, Y., S. S. Chan and S. Chang (2008). "Telomere dysfunction and tumour suppression: the senescence connection." Nat Rev Cancer **8**(6): 450-458.
Deniz, E. and B. Erman (2017). "Long noncoding RNA (lincRNA), a new paradigm in gene expression control." Funct Integr Genomics **17**(2-3): 135-143.
Deshpande, A. J., L. Chen, M. Fazio, A. U. Sinha, K. M. Bernt, D. Banka, S. Dias, J. Chang, E. J. Olhava, S. R. Daigle, V. M. Richon, R. M. Pollock and S. A. Armstrong (2013). "Leukemic transformation by the MLL-AF6 fusion oncogene requires the H3K79 methyltransferase Dot1l." Blood **121**(13): 2533-2541.
Dias, S., S. V. Shmelkov, G. Lam and S. Rafii (2002). "VEGF(165) promotes survival of leukemic cells by Hsp90-mediated induction of Bcl-2 expression and apoptosis inhibition." Blood **99**(7): 2532-2540.
Diederichs, S. (2014). "The four dimensions of noncoding RNA conservation." Trends Genet **30**(4): 121-123.
Dimri, G. P., X. H. Lee, G. Basile, M. Acosta, C. Scott, C. Roskelley, E. E. Medrano, M. Linskens, I. Rubelj, O. Pereirasmith, M. Peacocke and J. Campisi (1995). "A Biomarker That Identifies Senescent Human-Cells in Culture and in Aging Skin in-Vivo." Proceedings of the National Academy of Sciences of the United States of America **92**(20): 9363-9367.
Dohner, H., E. H. Estey, S. Amadori, F. R. Appelbaum, T. Buchner, A. K. Burnett, H. Dombret, P. Fenaux, D. Grimwade, R. A. Larson, F. Lo-Coco, T. Naoe, D. Niederwieser, G. J. Ossenkoppele, M. A. Sanz, J. Sierra, M. S. Tallman, B. Lowenberg, C. D. Bloomfield and L. European (2010). "Diagnosis and management of acute myeloid leukemia in adults: recommendations from an international expert panel, on behalf of the European LeukemiaNet." Blood **115**(3): 453-474.
Eder, P. S., R. J. DeVine, J. M. Dagle and J. A. Walder (1991). "Substrate specificity and kinetics of degradation of antisense oligonucleotides by a 3' exonuclease in plasma." Antisense Res Dev **1**(2): 141-151.
Elsasser, A., M. Franzen, A. Kohlmann, M. Weisser, S. Schnittger, C. Schoch, V. A. Reddy, S. Burel, D. E. Zhang, M. Ueffing, D. G. Tenen, W. Hiddemann and G. Behre (2003). "The fusion protein AML1-ETO in acute myeloid leukemia with translocation t(8;21) induces c-jun protein expression via the

proximal AP-1 site of the c-jun promoter in an indirect, JNK-dependent manner." Oncogene **22**(36): 5646-5657.
Emmrich, S., J. E. Katsman-Kuipers, K. Henke, M. E. Khatib, R. Jammal, F. Engeland, F. Dasci, C. M. Zwaan, M. L. den Boer, L. Verboon, J. Stary, A. Baruchel, V. de Haas, A. A. Danen-van Oorschot, M. Fornerod, R. Pieters, D. Reinhardt, J. H. Klusmann and M. M. van den Heuvel-Eibrink (2014). "miR-9 is a tumor suppressor in pediatric AML with t(8;21)." Leukemia **28**(5): 1022-1032.
Esposito, M. T. and C. W. So (2014). "DNA damage accumulation and repair defects in acute myeloid leukemia: implications for pathogenesis, disease progression, and chemotherapy resistance." Chromosoma **123**(6): 545-561.
Falini, B., E. Tiacci, M. P. Martelli, S. Ascani and S. A. Pileri (2010). "New classification of acute myeloid leukemia and precursor-related neoplasms: changes and unsolved issues." Discov Med **10**(53): 281-292.
Fazi, F., S. Racanicchi, G. Zardo, L. M. Starnes, M. Mancini, L. Travaglini, D. Diverio, E. Ammatuna, G. Cimino, F. Lo-Coco, F. Grignani and C. Nervi (2007). "Epigenetic silencing of the myelopoiesis regulator microRNA-223 by the AML1/ETO oncoprotein." Cancer Cell **12**(5): 457-466.
Fazi, F., G. Zardo, V. Gelmetti, L. Travaglini, A. Ciolfi, L. Di Croce, A. Rosa, I. Bozzoni, F. Grignani, F. Lo-Coco, P. G. Pelicci and C. Nervi (2007). "Heterochromatic gene repression of the retinoic acid pathway in acute myeloid leukemia." Blood **109**(10): 4432-4440.
Fekri, F., R. C. Delos Santos, R. Karshafian and C. N. Antonescu (2016). "Ultrasound Microbubble Treatment Enhances Clathrin-Mediated Endocytosis and Fluid-Phase Uptake through Distinct Mechanisms." PLoS One **11**(6): e0156754.
Feldman, G. M., S. Ruhl, M. Bickel, D. S. Finbloom and D. H. Pluznik (1991). "Regulation of interleukin-4 receptors on murine myeloid progenitor cells by interleukin-6." Blood **78**(7): 1678-1684.
Ferrara, F. F., F. Fazi, A. Bianchini, F. Padula, V. Gelmetti, S. Minucci, M. Mancini, P. G. Pelicci, F. Lo Coco and C. Nervi (2001). "Histone deacetylase-targeted treatment restores retinoic acid signaling and differentiation in acute myeloid leukemia." Cancer Res **61**(1): 2-7.
Festing, M. F. and D. G. Altman (2002). "Guidelines for the design and statistical analysis of experiments using laboratory animals." Ilar j **43**(4): 244-258.
Filipowicz, W. (2005). "RNAi: the nuts and bolts of the RISC machine." Cell **122**(1): 17-20.
Fisher, R. K., S. I. Mattern-Schain, M. D. Best, S. S. Kirkpatrick, M. B. Freeman, O. H. Grandas and D. J. H. Mountain (2017). "Improving the efficacy of liposome-mediated vascular gene therapy via lipid surface modifications." J Surg Res **219**: 136-144.
Folkerts, H., S. Hilgendorf, A. T. J. Wierenga, J. Jaques, A. B. Mulder, P. J. Coffer and J. J. Schuringa (2017). "Inhibition of autophagy as a treatment strategy for p53 wild-type acute myeloid leukemia." **8**(7): e2927.
Fontana, F., D. Liu, J. Hirvonen and H. A. Santos (2017). "Delivery of therapeutics with nanoparticles: what's new in cancer immunotherapy?" Wiley Interdiscip Rev Nanomed Nanobiotechnol **9**(1).
Forsbach, A., J. G. Nemorin, C. Montino, C. Muller, U. Samulowitz, A. P. Vicari, M. Jurk, G. K. Mutwiri, A. M. Krieg, G. B. Lipford and J. Vollmer (2008). "Identification of RNA sequence motifs stimulating sequence-specific TLR8-dependent immune responses." J Immunol **180**(6): 3729-3738.
Frank, F. and B. Nagar (2017). "Structural and Functional Characterization of Plant ARGONAUTE MID Domains." Methods Mol Biol **1640**: 227-239.
Freund, A., R. M. Laberge, M. Demaria and J. Campisi (2012). "Lamin B1 loss is a senescence-associated biomarker." Molecular Biology of the Cell **23**(11): 2066-2075.
Fukuhara, S., K. Sako, K. Noda, K. Nagao, K. Miura and N. Mochizuki (2009). "Tie2 is tied at the cell-cell contacts and to extracellular matrix by Angiopoietin-1." Experimental and Molecular Medicine **41**(3): 133-139.
Futreal, P. A. and J. C. Barrett (1991). "Failure of senescent cells to phosphorylate the RB protein." Oncogene **6**(7): 1109-1113.

Gao, W., Y. Xiong, Q. Li and H. Yang (2017). "Inhibition of Toll-Like Receptor Signaling as a Promising Therapy for Inflammatory Diseases: A Journey from Molecular to Nano Therapeutics." Frontiers in Physiology **8**.
Garg, M., Y. Nagata, D. Kanojia, A. Mayakonda, K. Yoshida, S. H. Keloth, Z. J. Zang, Y. Okuno, Y. Shiraishi, K. Chiba, H. Tanaka, S. Miyano, L. W. Ding, T. Alpermann, Q. Y. Sun, D. C. Lin, W. W. Chien, V. Madan, L. Z. Liu, K. T. Tan, A. Sampath, S. Venkatesan, K. Inokuchi, S. Wakita, H. Yamaguchi, W. J. Chng, S. K. Y. Kham, A. E. J. Yeoh, M. Sanada, J. Schiller, K. A. Kreuzer, S. M. Kornblau, H. M. Kantarjian, T. Haferlach, M. Lill, M. C. Kuo, L. Y. Shih, I. W. Blau, O. Blau, H. Yang, S. Ogawa and H. P. Koeffler (2015). "Profiling of somatic mutations in acute myeloid leukemia with FLT3-ITD at diagnosis and relapse." Blood **126**(22): 2491-2501.
Geary, R. S., D. Norris, R. Yu and C. F. Bennett (2015). "Pharmacokinetics, biodistribution and cell uptake of antisense oligonucleotides." Adv Drug Deliv Rev **87**: 46-51.
Gerritsen, M., E. Tijchon, A. Mandoli, J. H. A. Martens, J. J. Schuringa and E. Vellenga (2016). "RUNX1 Mutations Cause a Myeloid Differentiation Block Leading to the Formation of a Long Term Expanding CD34(+) / CD33(+) / CD45RA(+) / CD123(+) Cell Population." Blood **128**(22).
Gessner, A., M. Thomas, P. G. Castro, L. Buchler, A. Scholz, T. H. Brummendorf, N. M. Soria, J. Vormoor, J. Greil and O. Heidenreich (2010). "Leukemic fusion genes MLL/AF4 and AML1/MTG8 support leukemic self-renewal by controlling expression of the telomerase subunit TERT." Leukemia **24**(10): 1751-1759.
Gialesaki, S., A. K. Mahnken, L. Schmid, M. Labuhn, R. Bhayadia, D. Heckl and J. H. Klusmann (2018). "GATA1s exerts developmental stage-specific effects in human hematopoiesis." Haematologica **103**(8): e336-e340.
Giambelluca, M. S., N. Cloutier, E. Rollet-Labelle, E. Boilard and M. Pouliot (2013). "Expression and regulation of glycogen synthase kinase 3 in human neutrophils." Int J Biochem Cell Biol **45**(11): 2660-2665.
Gil, J. and G. Peters (2006). "Regulation of the INK4b-ARF-INK4a tumour suppressor locus: all for one or one for all." Nature Reviews Molecular Cell Biology **7**(9): 667-677.
Gilleron, J., W. Querbes, A. Zeigerer, A. Borodovsky, G. Marsico, U. Schubert, K. Manygoats, S. Seifert, C. Andree, M. Stoter, H. Epstein-Barash, L. Zhang, V. Koteliansky, K. Fitzgerald, E. Fava, M. Bickle, Y. Kalaidzidis, A. Akinc, M. Maier and M. Zerial (2013). "Image-based analysis of lipid nanoparticle-mediated siRNA delivery, intracellular trafficking and endosomal escape." Nat Biotechnol **31**(7): 638-646.
Goel, S., M. J. DeCristo, S. S. McAllister and J. J. Zhao (2018). "CDK4/6 Inhibition in Cancer: Beyond Cell Cycle Arrest." Trends Cell Biol **28**(11): 911-925.
Gordon, P. M., S. Dias and D. A. Williams (2014). "Cytokines secreted by bone marrow stromal cells protect c-KIT mutant AML cells from c-KIT inhibitor-induced apoptosis." Leukemia **28**(11): 2257-2260.
Goyama, S., J. Schibler, L. Cunningham, Y. Zhang, Y. Rao, N. Nishimoto, M. Nakagawa, A. Olsson, M. Wunderlich, K. A. Link, B. Mizukawa, H. L. Grimes, M. Kurokawa, P. P. Liu, G. Huang and J. C. Mulloy (2013). "Transcription factor RUNX1 promotes survival of acute myeloid leukemia cells." J Clin Invest **123**(9): 3876-3888.
Graf, T. (2002). "Differentiation plasticity of hematopoietic cells." Blood **99**(9): 3089-3101.
Grant, S. (1998). "Ara-C: cellular and molecular pharmacology." Adv Cancer Res **72**: 197-233.
Grespi, F., C. Soratroi, G. Krumschnabel, B. Sohm, C. Ploner, S. Geley, L. Hengst, G. Hacker and A. Villunger (2010). "BH3-only protein Bmf mediates apoptosis upon inhibition of CAP-dependent protein synthesis." Cell Death Differ **17**(11): 1672-1683.
Grimwade, D., R. K. Hills, A. V. Moorman, H. Walker, S. Chatters, A. H. Goldstone, K. Wheatley, C. J. Harrison, A. K. Burnett and G. National Cancer Research Institute Adult Leukaemia Working (2010). "Refinement of cytogenetic classification in acute myeloid leukemia: determination of prognostic significance of rare recurring chromosomal abnormalities among 5876 younger adult patients treated in the United Kingdom Medical Research Council trials." Blood **116**(3): 354-365.

Gu, S., L. Jin, Y. Huang, F. Zhang and M. A. Kay (2012). "Slicing-independent RISC activation requires the argonaute PAZ domain." Curr Biol **22**(16): 1536-1542.
Gu, X., Z. Hu, Q. Ebrahem, J. S. Crabb, R. Z. Mahfouz, T. Radivoyevitch, J. W. Crabb and Y. Saunthararajah (2014). "Runx1 regulation of Pu.1 corepressor/coactivator exchange identifies specific molecular targets for leukemia differentiation therapy." J Biol Chem **289**(21): 14881-14895.
Guan, X., Z. Guo, T. Wang, L. Lin, J. Chen, H. Tian and X. Chen (2017). "A pH-Responsive Detachable PEG Shielding Strategy for Gene Delivery System in Cancer Therapy." Biomacromolecules **18**(4): 1342-1349.
Haas, S., A. Trumpp and M. D. Milsom (2018). "Causes and Consequences of Hematopoietic Stem Cell Heterogeneity." Cell Stem Cell **22**(5): 627-638.
Hafez, I. M., N. Maurer and P. R. Cullis (2001). "On the mechanism whereby cationic lipids promote intracellular delivery of polynucleic acids." Gene Ther **8**(15): 1188-1196.
Hagedorn, P. H., B. R. Hansen, T. Koch and M. Lindow (2017). "Managing the sequence-specificity of antisense oligonucleotides in drug discovery." Nucleic Acids Res **45**(5): 2262-2282.
Haley, B. and P. D. Zamore (2004). "Kinetic analysis of the RNAi enzyme complex." Nat Struct Mol Biol **11**(7): 599-606.
Hamburger, A. W. and S. E. Salmon (1977). "Primary bioassay of human tumor stem cells." Science **197**(4302): 461-463.
Han, J. W., C. Flemington, A. B. Houghton, Z. M. Gu, G. P. Zambetti, R. J. Lutz, L. Zhu and T. Chittenden (2001). "Expression of bbc3, a pro-apoptotic BH3-only gene, is regulated by diverse cell death and survival signals." Proceedings of the National Academy of Sciences of the United States of America **98**(20): 11318-11323.
Hangaishi, A., S. Ogawa, N. Imamura, S. Miyawaki, Y. Miura, N. Uike, C. Shimazaki, N. Emi, K. Takeyama, S. Hirosawa, N. Kamada, Y. Kobayashi, Y. Takemoto, T. Kitani, K. Toyama, S. Ohtake, Y. Yazaki, R. Ueda and H. Hirai (1996). "Inactivation of multiple tumor-suppressor genes involved in negative regulation of the cell cycle, MTS1/p16(INK4A)/CDKN2, MTS2/p15(INK4B), p53, and Rb genes in primary lymphoid malignancies." Blood **87**(12): 4949-4958.
Harada, Y., D. Inoue, Y. Ding, J. Imagawa, N. Doki, H. Matsui, T. Yahata, H. Matsushita, K. Ando, G. Sashida, A. Iwama, T. Kitamura and H. Harada (2013). "RUNX1/AML1 mutant collaborates with BMI1 overexpression in the development of human and murine myelodysplastic syndromes." Blood **121**(17): 3434-3446.
Harbour, J. W., R. X. Luo, A. D. Santi, A. A. Postigo and D. C. Dean (1999). "Cdk phosphorylation triggers sequential intramolecular interactions that progressively block Rb functions as cells move through G1." Cell **98**(6): 859-869.
Harder, K. W., L. M. Parsons, J. Armes, N. Evans, N. Kountouri, R. Clark, C. Quilici, D. Grail, G. S. Hodgson, A. R. Dunn and M. L. Hibbs (2001). "Gain- and loss-of-function Lyn mutant mice define a critical inhibitory role for Lyn in the myeloid lineage." Immunity **15**(4): 603-615.
Harney, A. S., G. S. Karagiannis, J. Pignatelli, B. D. Smith, E. Kadioglu, S. C. Wise, M. M. Hood, M. D. Kaufman, C. B. Leary, W. P. Lu, G. Al-Ani, X. Chen, D. Entenberg, M. H. Oktay, Y. Wang, L. Chun, M. De Palma, J. G. Jones, D. L. Flynn and J. S. Condeelis (2017). "The Selective Tie2 Inhibitor Rebastinib Blocks Recruitment and Function of Tie2(Hi) Macrophages in Breast Cancer and Pancreatic Neuroendocrine Tumors." Mol Cancer Ther **16**(11): 2486-2501.
Hashiba, K., Y. Sato and H. Harashima (2017). "pH-labile PEGylation of siRNA-loaded lipid nanoparticle improves active targeting and gene silencing activity in hepatocytes." J Control Release **262**: 239-246.
Hassett, K. J., K. E. Benenato, E. Jacquinet, A. Lee, A. Woods, O. Yuzhakov, S. Himansu, J. Deterling, B. M. Geilich, T. Ketova, C. Mihai, A. Lynn, I. McFadyen, M. J. Moore, J. J. Senn, M. G. Stanton, Ö. Almarsson, G. Ciaramella and L. A. Brito (2019). "Optimization of Lipid Nanoparticles for Intramuscular Administration of mRNA Vaccines." Molecular therapy. Nucleic acids **15**: 1-11.
Hayden, M. S. and S. Ghosh (2014). "Regulation of NF-kappaB by TNF family cytokines." Semin Immunol **26**(3): 253-266.

He, W., M. J. Bennett, L. Luistro, D. Carvajal, T. Nevins, M. Smith, G. Tyagi, J. Cai, X. Wei, T. A. Lin, D. C. Heimbrook, K. Packman and J. F. Boylan (2014). "Discovery of siRNA lipid nanoparticles to transfect suspension leukemia cells and provide in vivo delivery capability." Mol Ther **22**(2): 359-370.
Heemskerk, H. A., C. L. de Winter, S. J. de Kimpe, P. van Kuik-Romeijn, N. Heuvelmans, G. J. Platenburg, G. J. van Ommen, J. C. van Deutekom and A. Aartsma-Rus (2009). "In vivo comparison of 2'-O-methyl phosphorothioate and morpholino antisense oligonucleotides for Duchenne muscular dystrophy exon skipping." J Gene Med **11**(3): 257-266.
Heidenreich, O., J. Krauter, H. Riehle, P. Hadwiger, M. John, G. Heil, H. P. Vornlocher and A. Nordheim (2003). "AML1/MTG8 oncogene suppression by small interfering RNAs supports myeloid differentiation of t(8;21)-positive leukemic cells." Blood **101**(8): 3157-3163.
Helsten, T., S. Kato, M. Schwaederle, B. N. Tomson, T. P. Buys, S. K. Elkin, J. L. Carter and R. Kurzrock (2016). "Cell-Cycle Gene Alterations in 4,864 Tumors Analyzed by Next-Generation Sequencing: Implications for Targeted Therapeutics." Mol Cancer Ther **15**(7): 1682-1690.
Hernandez, F. J., K. R. Stockdale, L. Huang, A. R. Horswill, M. A. Behlke and J. O. McNamara, 2nd (2012). "Degradation of nuclease-stabilized RNA oligonucleotides in Mycoplasma-contaminated cell culture media." Nucleic Acid Ther **22**(1): 58-68.
Hernandez, J. L., L. Padilla, S. Dakhel, T. Coll, R. Hervas, J. Adan, M. Masa, F. Mitjans, J. M. Martinez, S. Coma, L. Rodriguez, V. Noe, C. J. Ciudad, F. Blasco and R. Messeguer (2013). "Therapeutic targeting of tumor growth and angiogenesis with a novel anti-S100A4 monoclonal antibody." PLoS One **8**(9): e72480.
Herrmann, F., W. Oster and R. Mertelsmann (1990). "Control of blast cell proliferation and differentiation in acute myelogenous leukemia by soluble polypeptide growth factors." Klin Padiatr **202**(4): 212-217.
Hiratsuka, S., A. Watanabe, Y. Sakurai, S. Akashi-Takamura, S. Ishibashi, K. Miyake, M. Shibuya, S. Akira, H. Aburatani and Y. Maru (2008). "The S100A8-serum amyloid A3-TLR4 paracrine cascade establishes a pre-metastatic phase." Nat Cell Biol **10**(11): 1349-1355.
Hirschi, K. K. (2012). "Hemogenic endothelium during development and beyond." Blood **119**(21): 4823-4827.
Hoarau, D., P. Delmas, S. David, E. Roux and J. C. Leroux (2004). "Novel long-circulating lipid nanocapsules." Pharm Res **21**(10): 1783-1789.
Hoornaert, I., P. Marynen, J. Goris, R. Sciot and M. Baens (2003). "MAPK phosphatase DUSP16/MKP-7, a candidate tumor suppressor for chromosome region 12p12-13, reduces BCR-ABL-induced transformation." Oncogene **22**(49): 7728-7736.
Hope, K. J., L. Jin and J. E. Dick (2004). "Acute myeloid leukemia originates from a hierarchy of leukemic stem cell classes that differ in self-renewal capacity." Nat Immunol **5**(7): 738-743.
Hornsveld, M., M. Tenhagen, R. A. van de Ven, A. M. Smits, M. H. van Triest, M. van Amersfoort, D. E. Kloet, T. B. Dansen, B. M. Burgering and P. W. Derksen (2016). "Restraining FOXO3-dependent transcriptional BMF activation underpins tumour growth and metastasis of E-cadherin-negative breast cancer." Cell Death Differ **23**(9): 1483-1492.
Hoy, S. M. (2018). "Patisiran: First Global Approval." Drugs **78**(15): 1625-1631.
Hu, W. and J. Hu (2014). "Prediction of siRNA potency using sparse logistic regression." J Comput Biol **21**(6): 420-427.
Huang, S. and F. A. Sinicrope (2008). "BH3 mimetic ABT-737 potentiates TRAIL-mediated apoptotic signaling by unsequestering Bim and Bak in human pancreatic cancer cells." Cancer Res **68**(8): 2944-2951.
Huang, Y., Q. Cheng, J. L. Ji, S. Zheng, L. Du, L. Meng, Y. Wu, D. Zhao, X. Wang, L. Lai, H. Cao, K. Xiao, S. Gao and Z. Liang (2016). "Pharmacokinetic Behaviors of Intravenously Administered siRNA in Glandular Tissues." Theranostics **6**(10): 1528-1541.
Huang, Y., J. Hong, S. Zheng, Y. Ding, S. Guo, H. Zhang, X. Zhang, Q. Du and Z. Liang (2011). "Elimination pathways of systemically delivered siRNA." Mol Ther **19**(2): 381-385.

Hussong, J. W., G. M. Rodgers and P. J. Shami (2000). "Evidence of increased angiogenesis in patients with acute myeloid leukemia." Blood **95**(1): 309-313.
Hyde, R. K., L. Zhao, L. Alemu and P. P. Liu (2015). "Runx1 is required for hematopoietic defects and leukemogenesis in Cbfb-MYH11 knock-in mice." Leukemia **29**(8): 1771-1778.
Iannitti, T., J. C. Morales-Medina and B. Palmieri (2014). "Phosphorothioate oligonucleotides: effectiveness and toxicity." Curr Drug Targets **15**(7): 663-673.
Ichikawa, M., A. Yoshimi, M. Nakagawa, N. Nishimoto, N. Watanabe-Okochi and M. Kurokawa (2013). "A role for RUNX1 in hematopoiesis and myeloid leukemia." Int J Hematol **97**(6): 726-734.
Ikushima, Y. M., F. Arai, Y. Nakamura, K. Hosokawa, Y. Kubota, M. Hirashima, H. Toyama and T. Suda (2013). "Enhanced Angpt1/Tie2 signaling affects the differentiation and long-term repopulation ability of hematopoietic stem cells." Biochem Biophys Res Commun **430**(1): 20-25.
Incarnato, D., F. Anselmi, E. Morandi, F. Neri, M. Maldotti, S. Rapelli, C. Parlato, G. Basile and S. Oliviero (2017). "High-throughput single-base resolution mapping of RNA 2-O-methylated residues." Nucleic Acids Res **45**(3): 1433-1441.
Indovina, P., F. Pentimalli, N. Casini, I. Vocca and A. Giordano (2015). "RB1 dual role in proliferation and apoptosis: cell fate control and implications for cancer therapy." Oncotarget **6**(20): 17873-17890.
Inoue, J., A. Misawa, Y. Tanaka, S. Ichinose, Y. Sugino, H. Hosoi, T. Sugimoto, I. Imoto and J. Inazawa (2009). "Lysosomal-associated protein multispanning transmembrane 5 gene (LAPTM5) is associated with spontaneous regression of neuroblastomas." PLoS One **4**(9): e7099.
Iorio, M. V. and C. M. Croce (2012). "MicroRNA dysregulation in cancer: diagnostics, monitoring and therapeutics. A comprehensive review." EMBO Mol Med **4**(3): 143-159.
Iorio, M. V. and C. M. Croce (2017). "MicroRNA dysregulation in cancer: diagnostics, monitoring and therapeutics. A comprehensive review." EMBO Mol Med **9**(6): 852.
Ishihara, T., M. Goto, K. Kodera, H. Kanazawa, Y. Murakami, Y. Mizushima and M. Higaki (2009). "Intracellular delivery of siRNA by cell-penetrating peptides modified with cationic oligopeptides." Drug Deliv **16**(3): 153-159.
Itkin, T., S. Gur-Cohen, J. A. Spencer, A. Schajnovitz, S. K. Ramasamy, A. P. Kusumbe, G. Ledergor, Y. Jung, I. Milo, M. G. Poulos, A. Kalinkovich, A. Ludin, O. Kollet, G. Shakhar, J. M. Butler, S. Rafii, R. H. Adams, D. T. Scadden, C. P. Lin and T. Lapidot (2016). "Distinct bone marrow blood vessels differentially regulate haematopoiesis." Nature **532**(7599): 323-328.
Ito, M., H. Hiramatsu, K. Kobayashi, K. Suzue, M. Kawahata, K. Hioki, Y. Ueyama, Y. Koyanagi, K. Sugamura, K. Tsuji, T. Heike and T. Nakahata (2002). "NOD/SCID/gamma(c)(null) mouse: an excellent recipient mouse model for engraftment of human cells." Blood **100**(9): 3175-3182.
Itzykson, R., C. Gardin, C. Pautas, X. Thomas, P. Turlure, E. Raffoux, C. Terre, P. Fenaux, S. Castaigne, H. Dombret, N. Boissel and A. Acute Leukemia French (2011). "Impact of post-remission therapy in patients aged 65-70 years with de novo acute myeloid leukemia: a comparison of two concomitant randomized ALFA trials with overlapping age inclusion criteria." Haematologica **96**(6): 837-844.
Ivanovs, A., S. Rybtsov, E. S. Ng, E. G. Stanley, A. G. Elefanty and A. Medvinsky (2017). "Human haematopoietic stem cell development: from the embryo to the dish." Development **144**(13): 2323-2337.
Jakubowiak, A., C. Pouponnot, F. Berguido, R. Frank, S. F. Mao, J. Massague and S. D. Nimer (2000). "Inhibition of the transforming growth factor beta 1 signaling pathway by the AML1/ETO leukemia-associated fusion protein." Journal of Biological Chemistry **275**(51): 40282-40287.
Janas, M. M., M. K. Schlegel, C. E. Harbison, V. O. Yilmaz, Y. Jiang, R. Parmar, I. Zlatev, A. Castoreno, H. Xu, S. Shulga-Morskaya, K. G. Rajeev, M. Manoharan, N. D. Keirstead, M. A. Maier and V. Jadhav (2018). "Selection of GalNAc-conjugated siRNAs with limited off-target-driven rat hepatotoxicity." Nat Commun **9**(1): 723.
Jaroszewski, J. W., V. Clausen, J. S. Cohen and O. Dahl (1996). "NMR investigations of duplex stability of phosphorothioate and phosphorodithioate DNA analogues modified in both strands." Nucleic Acids Res **24**(5): 829-834.

Jayaraman, M., S. M. Ansell, B. L. Mui, Y. K. Tam, J. Chen, X. Du, D. Butler, L. Eltepu, S. Matsuda, J. K. Narayanannair, K. G. Rajeev, I. M. Hafez, A. Akinc, M. A. Maier, M. A. Tracy, P. R. Cullis, T. D. Madden, M. Manoharan and M. J. Hope (2012). "Maximizing the potency of siRNA lipid nanoparticles for hepatic gene silencing in vivo." Angew Chem Int Ed Engl **51**(34): 8529-8533.
Jhaveri, A. M. and V. P. Torchilin (2014). "Multifunctional polymeric micelles for delivery of drugs and siRNA." Front Pharmacol **5**: 77.
Jiang, H., L. Zhu, A. Heliou, X. Gao, J. Bernauer and X. Huang (2017). "Elucidating Mechanisms of Molecular Recognition Between Human Argonaute and miRNA Using Computational Approaches." Methods Mol Biol **1517**: 251-275.
Jin, Y. H., E. J. Jeon, Q. L. Li, Y. H. Lee, J. K. Choi, W. J. Kim, K. Y. Lee and S. C. Bae (2004). "Transforming growth factor-beta stimulates p300-dependent RUNX3 acetylation, which inhibits ubiquitination-mediated degradation." Journal of Biological Chemistry **279**(28): 29409-29417.
Jones, J. E., L. Wang, P. L. Kropf, R. Duan and D. E. Johnson (2009). "Src family kinase gene targets during myeloid differentiation: identification of the EGR-1 gene as a direct target." Leukemia **23**(10): 1933-1935.
Jones, M. and J. Leroux (1999). "Polymeric micelles - a new generation of colloidal drug carriers." Eur J Pharm Biopharm **48**(2): 101-111.
Jongen-Lavrencic, M., S. M. Sun, M. K. Dijkstra, P. J. Valk and B. Lowenberg (2008). "MicroRNA expression profiling in relation to the genetic heterogeneity of acute myeloid leukemia." Blood **111**(10): 5078-5085.
Juliano, R., J. Bauman, H. Kang and X. Ming (2009). "Biological Barriers to Therapy with Antisense and siRNA Oligonucleotides." Molecular Pharmaceutics **6**(3): 686-695.
Juliano, R. L. (2016). "The delivery of therapeutic oligonucleotides." Nucleic Acids Res **44**(14): 6518-6548.
Jun, D. Y., H. Kim, W. Y. Jang, J. Y. Lee, K. Fukui and Y. H. Kim (2017). "Ectopic overexpression of LAPTM5 results in lysosomal targeting and induces Mcl-1 down-regulation, Bak activation, and mitochondria-dependent apoptosis in human HeLa cells." PLoS One **12**(5): e0176544.
Jyotsana, N., A. Sharma, A. Chaturvedi, R. Budida, M. Scherr, F. Kuchenbauer, R. Lindner, F. Noyan, K.-W. Sühs, M. Stangel, D. Grote-Koska, K. Brand, H.-P. Vornlocher, M. Eder, F. Thol, A. Ganser, R. K. Humphries, E. Ramsay, P. Cullis and M. Heuser (2019). "Lipid nanoparticle-mediated siRNA delivery for safe targeting of human CML in vivo." Annals of Hematology **98**(8): 1905-1918.
Jyotsana, N., A. Sharma, A. Chaturvedi, M. Scherr, F. Kuchenbauer, L. Sajti, A. Barchanski, R. Lindner, F. Noyan, K. W. Suhs, D. Grote-Koska, K. Brand, H. P. Vornlocher, M. Stanulla, B. Bornhauser, J. P. Bourquin, M. Eder, F. Thol, A. Ganser, R. K. Humphries, E. Ramsay, P. Cullis and M. Heuser (2018). "RNA interference efficiently targets human leukemia driven by a fusion oncogene in vivo." Leukemia **32**(1): 224-226.
Jyotsana, N., A. Sharma, A. Chaturvedi, C. Walsh, A. Thomas, M. Scherr, M. Eder, K. Battmer, F. Kuchenbauer, S. Laszlo, A. Barchanski, K. Goerlich, R. Lindner, F. Noyan, S. K. Wolfram, D. Grote-Koska, K. Brand, H. P. Vornlocher, A. Ganser, E. Ramsay, P. Cullis and M. Heuser (2015). "Effective Treatment of Human CML By RNAi In Vivo in a Xenotransplantation Mouse Model." Blood **126**(23).
Kaczmarek, J. C., P. S. Kowalski and D. G. Anderson (2017). "Advances in the delivery of RNA therapeutics: from concept to clinical reality." Genome Med **9**(1): 60.
Kaksonen, M. and A. Roux (2018). "Mechanisms of clathrin-mediated endocytosis." Nat Rev Mol Cell Biol **19**(5): 313-326.
Kalluri, R. (2016). "The biology and function of fibroblasts in cancer." Nat Rev Cancer **16**(9): 582-598.
Kanasty, R., J. R. Dorkin, A. Vegas and D. Anderson (2013). "Delivery materials for siRNA therapeutics." Nat Mater **12**(11): 967-977.
Karpala, A. J., T. J. Doran and A. G. Bean (2005). "Immune responses to dsRNA: implications for gene silencing technologies." Immunol Cell Biol **83**(3): 211-216.
Katayama, Y., K. Takenaka, N. Mahmut, T. Teshima, K. Shinagawa, E. Omoto and M. Harada (1998). "Replating potential of colony-forming units of granulocytes/macrophages (CFU-GM) expanded ex

vivo by stem cell factor, interleukin (IL)-3, IL-6, granulocyte colony-stimulating factor, erythropoietin with or without thrombopoietin." Int J Hematol **68**(2): 157-168.
Kaulfuss, S., M. Grzmil, B. Hemmerlein, P. Thelen, S. Schweyer, J. Neesen, L. Bubendorf, A. G. Glass, H. Jarry, B. Auber and P. Burfeind (2008). "Leupaxin, a novel coactivator of the androgen receptor, is expressed in prostate cancer and plays a role in adhesion and invasion of prostate carcinoma cells." Molecular Endocrinology **22**(7): 1606-1621.
Kaushansky, K. (2009). "Molecular mechanisms of thrombopoietin signaling." J Thromb Haemost **7 Suppl 1**: 235-238.
Kawamata, T. and Y. Tomari (2011). "Native gel analysis for RISC assembly." Methods Mol Biol **725**: 91-105.
Keskin, D. and A. Tezcaner (2017). "Micelles As Delivery System for Cancer Treatment." Curr Pharm Des **23**(35): 5230-5241.
Khvorova, A. and J. K. Watts (2017). "The chemical evolution of oligonucleotide therapies of clinical utility." Nat Biotechnol **35**(3): 238-248.
Kipps, T. J., H. Eradat, S. Grosicki, J. Catalano, W. Cosolo, I. S. Dyagil, S. Yalamanchili, A. Chai, S. Sahasranaman, E. Punnoose, D. Hurst and H. Pylypenko (2015). "A phase 2 study of the BH3 mimetic BCL2 inhibitor navitoclax (ABT-263) with or without rituximab, in previously untreated B-cell chronic lymphocytic leukemia." Leukemia & Lymphoma **56**(10): 2826-2833.
Klusmann, J. H., F. J. Godinho, K. Heitmann, A. Maroz, M. L. Koch, D. Reinhardt, S. H. Orkin and Z. Li (2010). "Developmental stage-specific interplay of GATA1 and IGF signaling in fetal megakaryopoiesis and leukemogenesis." Genes Dev **24**(15): 1659-1672.
Kobayashi, H. and Y. Tomari (2016). "RISC assembly: Coordination between small RNAs and Argonaute proteins." Biochim Biophys Acta **1859**(1): 71-81.
Kohn, E. A., N. D. Ruth, M. K. Brown, M. Livingstone and A. Eastman (2002). "Abrogation of the S phase DNA damage checkpoint results in S phase progression or premature mitosis depending on the concentration of 7-hydroxystaurosporine and the kinetics of Cdc25C activation." Journal of Biological Chemistry **277**(29): 26553-26564.
Koltover, I., T. Salditt, J. O. Radler and C. R. Safinya (1998). "An inverted hexagonal phase of cationic liposome-DNA complexes related to DNA release and delivery." Science **281**(5373): 78-81.
Kozu, T., T. Fukuyama, T. Yamami, K. Akagi and Y. Kaneko (2005). "MYND-less splice variants of AML1-MTG8 (RUNX1-CBFA2T1) are expressed in leukemia with t(8;21)." Genes Chromosomes Cancer **43**(1): 45-53.
Kranc, K. R., D. V. Oliveira, A. Armesilla-Diaz, I. Pacheco-Leyva, A. C. Matias, A. L. Escapa, C. Subramani, H. Wheadon, M. Trindade, J. Nichols, K. Kaji, T. Enver and J. Braganca (2015). "Acute Loss of Cited2 Impairs Nanog Expression and Decreases Self-Renewal of Mouse Embryonic Stem Cells." Stem Cells **33**(3): 699-712.
Kuang, H., S. H. Ku and E. Kokkoli (2017). "The design of peptide-amphiphiles as functional ligands for liposomal anticancer drug and gene delivery." Adv Drug Deliv Rev **110-111**: 80-101.
Kumar, K., A. Singal, M. M. Rizvi and V. S. Chauhan (2008). "High mobility group box (HMGB) proteins of Plasmodium falciparum: DNA binding proteins with pro-inflammatory activity." Parasitol Int **57**(2): 150-157.
Kurkewich, J. L., J. Hansen, N. Klopfenstein, H. Zhang, C. Wood, A. Boucher, J. Hickman, D. E. Muench, H. L. Grimes and R. Dahl (2017). "The miR-23a~27a~24-2 microRNA cluster buffers transcription and signaling pathways during hematopoiesis." PLoS Genet **13**(7): e1006887.
Kwak, P. B. and Y. Tomari (2012). "The N domain of Argonaute drives duplex unwinding during RISC assembly." Nat Struct Mol Biol **19**(2): 145-151.
Lam, K. and D. E. Zhang (2012). "RUNX1 and RUNX1-ETO: roles in hematopoiesis and leukemogenesis." Front Biosci (Landmark Ed) **17**: 1120-1139.
Landesman, Y., N. Svrzikapa, A. Cognetta, 3rd, X. Zhang, B. R. Bettencourt, S. Kuchimanchi, K. Dufault, S. Shaikh, M. Gioia, A. Akinc, R. Hutabarat and R. Meyers (2010). "In vivo quantification of

formulated and chemically modified small interfering RNA by heating-in-Triton quantitative reverse transcription polymerase chain reaction (HIT qRT-PCR)." Silence **1**(1): 16.
Lapidot, T., C. Sirard, J. Vormoor, B. Murdoch, T. Hoang, J. Caceres-cortes, M. Minden, B. Paterson, M. A. Caligiuri and J. E. Dick (1994). "A Cell Initiating Human Acute Myeloid-Leukemia after Transplantation into Scid Mice." Nature **367**(6464): 645-648.
Laslo, P., C. J. Spooner, A. Warmflash, D. W. Lancki, H. J. Lee, R. Sciammas, B. N. Gantner, A. R. Dinner and H. Singh (2006). "Multilineage transcriptional priming and determination of alternate hematopoietic cell fates." Cell **126**(4): 755-766.
Lee, H. S., H. Seok, D. H. Lee, J. Ham, W. Lee, E. M. Youm, J. S. Yoo, Y. S. Lee, E. S. Jang and S. W. Chi (2015). "Abasic pivot substitution harnesses target specificity of RNA interference." Nat Commun **6**: 10154.
Lendvai, G., I. Velikyan, M. Bergstrom, S. Estrada, D. Laryea, M. Valila, S. Salomaki, B. Langstrom and A. Roivainen (2005). "Biodistribution of 68Ga-labelled phosphodiester, phosphorothioate, and 2'-O-methyl phosphodiester oligonucleotides in normal rats." Eur J Pharm Sci **26**(1): 26-38.
Leung, A. K., I. M. Hafez, S. Baoukina, N. M. Belliveau, I. V. Zhigaltsev, E. Afshinmanesh, D. P. Tieleman, C. L. Hansen, M. J. Hope and P. R. Cullis (2012). "Lipid Nanoparticles Containing siRNA Synthesized by Microfluidic Mixing Exhibit an Electron-Dense Nanostructured Core." J Phys Chem C Nanomater Interfaces **116**(34): 18440-18450.
Leung, A. K., Y. Y. Tam, S. Chen, I. M. Hafez and P. R. Cullis (2015). "Microfluidic Mixing: A General Method for Encapsulating Macromolecules in Lipid Nanoparticle Systems." J Phys Chem B **119**(28): 8698-8706.
Leung, A. K., Y. Y. Tam and P. R. Cullis (2014). "Lipid nanoparticles for short interfering RNA delivery." Adv Genet **88**: 71-110.
Li, K., X. X. Lv, F. Hua, H. Lin, W. Sun, W. B. Cao, X. M. Fu, J. Xie, J. J. Yu, Z. Li, H. Liu, M. Z. Han and Z. W. Hu (2014). "Targeting acute myeloid leukemia with a proapoptotic peptide conjugated to a Toll-like receptor 2-mediated cell-penetrating peptide." Int J Cancer **134**(3): 692-702.
Li, L. M., Z. X. Chen, J. N. Cen, H. J. Shen, L. Yao, Y. Y. Wang and X. F. Qi (2012). "[Monitoring the expression ratio of AML1-ETO9a isoform in t(8;21) acute myeloid leukemia and its significance]." Zhonghua Xue Ye Xue Za Zhi **33**(1): 1-5.
Li, Q., D. L. Ramirez-Bergeron, S. L. Dunwoodie and Y. C. Yang (2012). "Cited2 gene controls pluripotency and cardiomyocyte differentiation of murine embryonic stem cells through Oct4 gene." J Biol Chem **287**(34): 29088-29100.
Li, Y., L. Gao, X. Luo, L. Wang, X. Gao, W. Wang, J. Sun, L. Dou, J. Li, C. Xu, L. Wang, M. Zhou, M. Jiang, J. Zhou, M. A. Caligiuri, C. Nervi, C. D. Bloomfield, G. Marcucci and L. Yu (2013). "Epigenetic silencing of microRNA-193a contributes to leukemogenesis in t(8;21) acute myeloid leukemia by activating the PTEN/PI3K signal pathway." Blood **121**(3): 499-509.
Li, Z., J. Lu, M. Sun, S. Mi, H. Zhang, R. T. Luo, P. Chen, Y. Wang, M. Yan, Z. Qian, M. B. Neilly, J. Jin, Y. Zhang, S. K. Bohlander, D. E. Zhang, R. A. Larson, M. M. Le Beau, M. J. Thirman, T. R. Golub, J. D. Rowley and J. Chen (2008). "Distinct microRNA expression profiles in acute myeloid leukemia with common translocations." Proc Natl Acad Sci U S A **105**(40): 15535-15540.
Lie, A. L. M., E. Marinopoulou, A. J. Lilly, M. Challinor, R. Patel, C. Lancrin and V. Kouskoff (2018). "Regulation of RUNX1 dosage is crucial for efficient blood formation from hemogenic endothelium." **145**(5).
Lieber, M. M. and J. S. Kovach (1982). "Soft agar colony formation assay for chemotherapy sensitivity testing of human solid tumors." Mayo Clin Proc **57**(8): 527-528.
Liesveld, J. L., P. C. Keng, J. M. Rowe, J. F. DiPersio and C. N. Abboud (1994). "Effects of GM-CSF on Ki67 expression and cell cycle traverse in acute myelogenous leukemia specimens and cell lines." Leuk Res **18**(8): 609-616.
Lim, K. H. and L. M. Staudt (2013). "Toll-like receptor signaling." Cold Spring Harb Perspect Biol **5**(1): a011247.

Lin, S., A. Ptasinska, X. Chen, M. Shrestha, S. A. Assi, P. S. Chin, M. R. Imperato, B. J. Aronow, J. Zhang, M. T. Weirauch, C. Bonifer and J. C. Mulloy (2017). "A FOXO1-induced oncogenic network defines the AML1-ETO preleukemic program." Blood **130**(10): 1213-1222.
Lingel, A., B. Simon, E. Izaurralde and M. Sattler (2003). "Structure and nucleic-acid binding of the Drosophila Argonaute 2 PAZ domain." Nature **426**(6965): 465-469.
Liss, A., C. H. Ooi, P. Zjablovskaja, T. Benoukraf, H. S. Radomska, C. Ju, M. Wu, M. Balastik, R. Delwel, T. Brdicka, P. Tan, D. G. Tenen and M. Alberich-Jorda (2014). "The gene signature in CCAAT-enhancer-binding protein alpha dysfunctional acute myeloid leukemia predicts responsiveness to histone deacetylase inhibitors." Haematologica **99**(4): 697-705.
Liu, J., T. Liu, X. Wang and A. He (2017). "Circles reshaping the RNA world: from waste to treasure." Mol Cancer **16**(1): 58.
Liu, Y., A. Kosaka, M. Ikeura, G. Kohanbash, W. Fellows-Mayle, L. A. Snyder and H. Okada (2013). "Premetastatic soil and prevention of breast cancer brain metastasis." Neuro Oncol **15**(7): 891-903.
Loke, J., S. A. Assi, M. R. Imperato, A. Ptasinska, P. Cauchy, Y. Grabovska, N. M. Soria, M. Raghavan, H. R. Delwel, P. N. Cockerill, O. Heidenreich and C. Bonifer (2017). "RUNX1-ETO and RUNX1-EVI1 Differentially Reprogram the Chromatin Landscape in t(8;21) and t(3;21) AML." Cell Rep **19**(8): 1654-1668.
Lorsbach, R. B., J. Moore, S. O. Ang, W. Sun, N. Lenny and J. R. Downing (2004). "Role of RUNX1 in adult hematopoiesis: analysis of RUNX1-IRES-GFP knock-in mice reveals differential lineage expression." Blood **103**(7): 2522-2529.
Love, K. T., K. P. Mahon, C. G. Levins, K. A. Whitehead, W. Querbes, J. R. Dorkin, J. Qin, W. Cantley, L. L. Qin, T. Racie, M. Frank-Kamenetsky, K. N. Yip, R. Alvarez, D. W. Y. Sah, A. de Fougerolles, K. Fitzgerald, V. Koteliansky, A. Akinc, R. Langer and D. G. Anderson (2010). "Lipid-like materials for low-dose, in vivo gene silencing (vol 107, pg 1864, 2010)." Proceedings of the National Academy of Sciences of the United States of America **107**(21): 9915-9915.
Lundberg, F. N. M. L. G., R. Lerner, P. Sundelin, R. Rogers, J. Folkman and J. Palmblad (1998). "Bone marrow in polycythemia vera, chronic myelocytic leukemia and myelofibrosis has an increased vascular density." Blood **92**(10): 425a-425a.
Maciel-Baron, L. A., S. L. Morales-Rosales, A. A. Aquino-Cruz, F. Triana-Martinez, S. Galvan-Arzate, A. Luna-Lopez, V. Y. Gonzalez-Puertos, N. E. Lopez-Diazguerrero, C. Torres and M. Konigsberg (2016). "Senescence associated secretory phenotype profile from primary lung mice fibroblasts depends on the senescence induction stimuli." Age (Dordr) **38**(1): 26.
Maier, M. A., M. Jayaraman, S. Matsuda, J. Liu, S. Barros, W. Querbes, Y. K. Tam, S. M. Ansell, V. Kumar, J. Qin, X. Zhang, Q. Wang, S. Panesar, R. Hutabarat, M. Carioto, J. Hettinger, P. Kandasamy, D. Butler, K. G. Rajeev, B. Pang, K. Charisse, K. Fitzgerald, B. L. Mui, X. Du, P. Cullis, T. D. Madden, M. J. Hope, M. Manoharan and A. Akinc (2013). "Biodegradable lipids enabling rapidly eliminated lipid nanoparticles for systemic delivery of RNAi therapeutics." Mol Ther **21**(8): 1570-1578.
Maiti, M., K. Nauwelaerts, E. Lescrinier and P. Herdewijn (2011). "Structural and binding study of modified siRNAs with the Argonaute 2 PAZ domain by NMR spectroscopy." Chemistry **17**(5): 1519-1528.
Martinez-Soria , L. M., Julia Draper, Anetta Ptasinska, Hasan Issa, Sandeep Potluri, Helen J. Blair, Anna Pickin, Asmida Isa, Paulynn Suyin Chin, Ricky Tirtakusuma, Daniel Coleman, Sirintra Nakjang, Salam Assi, Victoria Forster, Mojgan Reza, Ed Law, Philip Berry, Dorothee Mueller, Alex Elder, Simon N. Bomken, Deepali Pal, James M. Allan, Gareth J. Veal, Peter N. Cockerill, Christian Wichmann, Josef Vormoor, Georges Lacaud, Constanze Bonifer, Olaf Heidenreich (2018). "The Oncogenic Transcription Factor RUNX1/ETO Corrupts Cell Cycle Regulation to Drive Leukemic Transformation " Cancer Cell.
Martinez, J. and T. Tuschl (2004). "RISC is a 5 ' phosphomonoester-producing RNA endonuclease." Genes & Development **18**(9): 975-980.

Martinez, M., M. Hinojosa, D. Trombly, V. Morin, J. Stein, G. Stein, A. Javed and S. E. Gutierrez (2016). "Transcriptional Auto-Regulation of RUNX1 P1 Promoter." PloS one **11**(2): e0149119-e0149119.
Martinez, N., B. Drescher, H. Riehle, C. Cullmann, H. P. Vornlocher, A. Ganser, G. Heil, A. Nordheim, J. Krauter and O. Heidenreich (2004). "The oncogenic fusion protein RUNX1-CBFA2T1 supports proliferation and inhibits senescence in t(8;21)-positive leukaemic cells." BMC Cancer **4**: 44.
Mathas, S., M. Hinz, I. Anagnostopoulos, D. Krappmann, A. Lietz, F. Jundt, K. Bommert, F. Mechta-Grigoriou, H. Stein, B. Dorken and C. Scheidereit (2002). "Aberrantly expressed c-Jun and JunB are a hallmark of Hodgkin lymphoma cells, stimulate proliferation and synergize with NF-kappa B." EMBO J **21**(15): 4104-4113.
Matsuura, S., M. Yan, M. C. Lo, E. Y. Ahn, S. Weng, D. Dangoor, M. Matin, T. Higashi, G. S. Feng and D. E. Zhang (2012). "Negative effects of GM-CSF signaling in a murine model of t(8;21)-induced leukemia." Blood **119**(13): 3155-3163.
Matzke, M. A. and J. A. Birchler (2005). "RNAi-mediated pathways in the nucleus." Nat Rev Genet **6**(1): 24-35.
Mayerhofer, M., P. Valent, W. R. Sperr, J. D. Griffin and C. Sillaber (2002). "BCR/ABL induces expression of vascular endothelial growth factor and its transcriptional activator, hypoxia inducible factor-1alpha, through a pathway involving phosphoinositide 3-kinase and the mammalian target of rapamycin." Blood **100**(10): 3767-3775.
Mazel, S., D. Burtrum and H. T. Petrie (1996). "Regulation of cell division cycle progression by bcl-2 expression: a potential mechanism for inhibition of programmed cell death." J Exp Med **183**(5): 2219-2226.
Mazurier, F., A. Fontanellas, S. Salesse, L. Taine, S. Landriau, F. Moreau-Gaudry, J. Reiffers, B. Peault, J. P. D. Santo and H. D. Verneuil (1999). "A Novel Immunodeficient Mouse Model-RAG2 gamma Cytokine Receptor Chain Double Mutants-Requiring Exogenous Cytokine Administration for Human Hematopoietic Stem Cell Engraftment Common." Journal of Interferon & Cytokine Research **19**(5): 533-541.
Mendelson, A. and P. S. Frenette (2014). "Hematopoietic stem cell niche maintenance during homeostasis and regeneration." Nat Med **20**(8): 833-846.
Meng, Z. and M. Lu (2017). "RNA Interference-Induced Innate Immunity, Off-Target Effect, or Immune Adjuvant?" Front Immunol **8**: 331.
Mermel, C. H., M. L. McLemore, F. Liu, S. Pereira, J. Woloszynek, C. A. Lowell and D. C. Link (2006). "Src family kinases are important negative regulators of G-CSF-dependent granulopoiesis." Blood **108**(8): 2562-2568.
Mettlen, M., D. Loerke, D. Yarar, G. Danuser and S. L. Schmid (2010). "Cargo- and adaptor-specific mechanisms regulate clathrin-mediated endocytosis." J Cell Biol **188**(6): 919-933.
Metzeler, K. H. and C. D. Bloomfield (2017). Clinical Relevance of RUNX1 and CBFB Alterations in Acute Myeloid Leukemia and Other Hematological Disorders. RUNX Proteins in Development and Cancer. Y. Groner, Y. Ito, P. Liu et al. Singapore, Springer Singapore**:** 175-199.
Michaloglou, C., L. C. Vredeveld, M. S. Soengas, C. Denoyelle, T. Kuilman, C. M. van der Horst, D. M. Majoor, J. W. Shay, W. J. Mooi and D. S. Peeper (2005). "BRAFE600-associated senescence-like cell cycle arrest of human naevi." Nature **436**(7051): 720-724.
Mihalyova, J., T. Jelinek, K. Growkova, M. Hrdinka, M. Simicek and R. Hajek (2018). "Venetoclax: A new wave in hematooncology." Exp Hematol **61**: 10-25.
Miranda, M. B. and D. E. Johnson (2007). "Signal transduction pathways that contribute to myeloid differentiation." Leukemia **21**(7): 1363-1377.
Miranda, M. B., R. L. Redner and D. E. Johnson (2007). "Inhibition of Src family kinases enhances retinoic acid induced gene expression and myeloid differentiation." Mol Cancer Ther **6**(12 Pt 1): 3081-3090.

Morrissey, D. V., K. Blanchard, L. Shaw, K. Jensen, J. A. Lockridge, B. Dickinson, J. A. McSwiggen, C. Vargeese, K. Bowman, C. S. Shaffer, B. A. Polisky and S. Zinnen (2005). "Activity of stabilized short interfering RNA in a mouse model of hepatitis B virus replication." Hepatology **41**(6): 1349-1356.
Mu, Q., T. Hu and J. Yu (2013). "Molecular insight into the steric shielding effect of PEG on the conjugated staphylokinase: biochemical characterization and molecular dynamics simulation." PLoS One **8**(7): e68559.
Mui, B. L., Y. K. Tam, M. Jayaraman, S. M. Ansell, X. Du, Y. Y. Tam, P. J. Lin, S. Chen, J. K. Narayanannair, K. G. Rajeev, M. Manoharan, A. Akinc, M. A. Maier, P. Cullis, T. D. Madden and M. J. Hope (2013). "Influence of Polyethylene Glycol Lipid Desorption Rates on Pharmacokinetics and Pharmacodynamics of siRNA Lipid Nanoparticles." Mol Ther Nucleic Acids **2**: e139.
Mund, M., J. A. van der Beek, J. Deschamps, S. Dmitrieff, P. Hoess, J. L. Monster, A. Picco, F. Nedelec, M. Kaksonen and J. Ries (2018). "Systematic Nanoscale Analysis of Endocytosis Links Efficient Vesicle Formation to Patterned Actin Nucleation." Cell **174**(4): 884-896 e817.
Munoz-Espin, D. and M. Serrano (2014). "Cellular senescence: from physiology to pathology." Nat Rev Mol Cell Biol **15**(7): 482-496.
Nakanishi, K. (2016). "Anatomy of RISC: how do small RNAs and chaperones activate Argonaute proteins?" Wiley Interdiscip Rev RNA **7**(5): 637-660.
Naruse, K., E. Matsuura-Suzuki, M. Watanabe, S. Iwasaki and Y. Tomari (2018). "In vitro reconstitution of chaperone-mediated human RISC assembly." Rna **24**(1): 6-11.
Navarro, G., J. Y. Pan and V. P. Torchilin (2015). "Micelle-like Nanoparticles as Carriers for DNA and siRNA." Molecular Pharmaceutics **12**(2): 301-313.
Nelson, G., O. Kucheryavenko, J. Wordsworth and T. von Zglinicki (2018). "The senescent bystander effect is caused by ROS-activated NF-kappaB signalling." Mech Ageing Dev **170**: 30-36.
Nick, H. J., H. G. Kim, C. W. Chang, K. W. Harris, V. Reddy and C. A. Klug (2012). "Distinct classes of c-Kit-activating mutations differ in their ability to promote RUNX1-ETO-associated acute myeloid leukemia." Blood **119**(6): 1522-1531.
Nip, H., A. A. Dar, S. Saini, M. Colden, S. Varahram, H. Chowdhary, S. Yamamura, Y. Mitsui, Y. Tanaka, T. Kato, Y. Hashimoto, M. Shiina, P. Kulkarni, P. Dasgupta, M. Imai-Sumida, Z. L. Tabatabai, K. Greene, G. Deng, R. Dahiya and S. Majid (2016). "Oncogenic microRNA-4534 regulates PTEN pathway in prostate cancer." Oncotarget **7**(42): 68371-68384.
Novobrantseva, T. I., A. Borodovsky, J. Wong, B. Klebanov, M. Zafari, K. Yucius, W. Querbes, P. Ge, V. M. Ruda, S. Milstein, L. Speciner, R. Duncan, S. Barros, G. Basha, P. Cullis, A. Akinc, J. S. Donahoe, K. Narayanannair Jayaprakash, M. Jayaraman, R. L. Bogorad, K. Love, K. Whitehead, C. Levins, M. Manoharan, F. K. Swirski, R. Weissleder, R. Langer, D. G. Anderson, A. de Fougerolles, M. Nahrendorf and V. Koteliansky (2012). "Systemic RNAi-mediated Gene Silencing in Nonhuman Primate and Rodent Myeloid Cells." Mol Ther Nucleic Acids **1**: e4.
Nuylan, M., T. Kawano, J. Inazawa and J. Inoue (2016). "Down-regulation of LAPTM5 in human cancer cells." Oncotarget **7**(19): 28320-28328.
O'Brien, S. G., M. A. Kirkland, J. V. Melo, M. H. Rao, R. J. Davidson, C. McDonald and J. M. Goldman (1994). "Antisense BCR-ABL oligomers cause non-specific inhibition of chronic myeloid leukemia cell lines." Leukemia **8**(12): 2156-2162.
Obenauer, J. C., P. M. H. van Strien, R. M. Hoogenboezem, M. M. van den Heuvel-Eibrink and I. P. Touw (2015). "RUNX1 TAD and RHD Mutations Found in SCN/AML Differentially Affect HSPC Expansion in Conjunction with Truncated CSF3 Receptors." Blood **126**(23).
Oh, N. and J. H. Park (2014). "Endocytosis and exocytosis of nanoparticles in mammalian cells." Int J Nanomedicine **9 Suppl 1**: 51-63.
Ohbo, K., T. Suda, M. Hashiyama, A. Mantani, M. Ikebe, K. Miyakawa, M. Moriyama, M. Nakamura, M. Katsuki, K. Takahashi, K. Yamamura and K. Sugamura (1996). "Modulation of hematopoiesis in mice with a truncated mutant of the interleukin-2 receptor gamma chain." Blood **87**(3): 956-967.

Omori, K., M. Mitsuhashi, K. Ishiyama, I. Nair, J. Rawson, I. Todorov, F. Kandeel and Y. Mullen (2011). "mRNA of the pro-apoptotic gene BBC3 serves as a molecular marker for TNF-alpha-induced islet damage in humans." Diabetologia **54**(8): 2056-2066.
Ono, T., Y. Yanagawa, K. Iwabuchi, K. Nonomura and K. Onoe (2007). "Glycogen synthase kinase 3 activity during development of bone marrow-derived dendritic cells (DCs) essential for the DC function to induce T helper 2 polarization." Immunology **122**(2): 189-198.
Opferman, J. T., H. Iwasaki, C. C. Ong, H. Suh, S. Mizuno, K. Akashi and S. J. Korsmeyer (2005). "Obligate role of anti-apoptotic MCL-1 in the survival of hematopoietic stem cells." Science **307**(5712): 1101-1104.
Pal, D., H. J. Blair, A. Elder, K. Dormon, K. J. Rennie, D. J. Coleman, J. Weiland, K. S. Rankin, A. Filby, O. Heidenreich and J. Vormoor (2016). "Long-term in vitro maintenance of clonal abundance and leukaemia-initiating potential in acute lymphoblastic leukaemia." Leukemia **30**(8): 1691-1700.
Pal, D., H. J. Blair, A. Elder, K. Dormon, K. J. Rennie, D. J. L. Coleman, J. Weiland, K. S. Rankin, A. Filby, O. Heidenreich and J. Vormoor (2016). "Long-term in vitro maintenance of clonal abundance and leukaemia-initiating potential in acute lymphoblastic leukaemia." Leukemia **30**: 1691.
Pan, R., L. J. Hogdal, J. M. Benito, D. Bucci, L. Han, G. Borthakur, J. Cortes, D. J. DeAngelo, L. Debose, H. Mu, H. Dohner, V. I. Gaidzik, I. Galinsky, L. S. Golfman, T. Haferlach, K. G. Harutyunyan, J. Hu, J. D. Leverson, G. Marcucci, M. Muschen, R. Newman, E. Park, P. P. Ruvolo, V. Ruvolo, J. Ryan, S. Schindela, P. Zweidler-McKay, R. M. Stone, H. Kantarjian, M. Andreeff, M. Konopleva and A. G. Letai (2014). "Selective BCL-2 inhibition by ABT-199 causes on-target cell death in acute myeloid leukemia." Cancer Discov **4**(3): 362-375.
Pang, Q. S., W. Keeble, T. A. Christianson, J. Diaz, M. O'Dwyer, S. Fagerlie, K. Rathbun, G. R. Faulkner and G. C. Bagby (2000). "Interferon gamma (IFN-gamma) hypersensitivity of Fanconi anemia (FA) cells: The role of double-stranded RNA dependent protein kinase (PKR)." Blood **96**(11): 569a-+.
Papisov, M. I. (1998). "Theoretical considerations of RES-avoiding liposomes: Molecular mechanics and chemistry of liposome interactions." Adv Drug Deliv Rev **32**(1-2): 119-138.
Parikh, S. M. (2017). "Angiopoietins and Tie2 in vascular inflammation." Curr Opin Hematol **24**(5): 432-438.
Park, J., J. Park, Y. Pei, J. Xu and Y. Yeo (2016). "Pharmacokinetics and biodistribution of recently-developed siRNA nanomedicines." Adv Drug Deliv Rev **104**: 93-109.
Patan, S. (1998). "TIE1 and TIE2 receptor tyrosine kinases inversely regulate embryonic angiogenesis by the mechanism of intussusceptive microvascular growth." Microvasc Res **56**(1): 1-21.
Perez-Atayde, A. R., S. E. Sallan, U. Tedrow, S. Connors, E. Allred and J. Folkman (1997). "Spectrum of tumor angiogenesis in the bone marrow of children with acute lymphoblastic leukemia." Am J Pathol **150**(3): 815-821.
Peterson, L. F. and D. E. Zhang (2004). "The 8;21 translocation in leukemogenesis." Oncogene **23**(24): 4255-4262.
Pham, J. W. and E. J. Sontheimer (2005). "Molecular requirements for RNA-induced silencing complex assembly in the Drosophila RNA interference pathway." J Biol Chem **280**(47): 39278-39283.
Pieken, W. A., D. B. Olsen, F. Benseler, H. Aurup and F. Eckstein (1991). "Kinetic characterization of ribonuclease-resistant 2'-modified hammerhead ribozymes." Science **253**(5017): 314-317.
Pietras, E. M., C. Mirantes-Barbeito, S. Fong, D. Loeffler, L. V. Kovtonyuk, S. Zhang, R. Lakshminarasimhan, C. P. Chin, J. M. Techner, B. Will, C. Nerlov, U. Steidl, M. G. Manz, T. Schroeder and E. Passegue (2016). "Chronic interleukin-1 exposure drives haematopoietic stem cells towards precocious myeloid differentiation at the expense of self-renewal." Nat Cell Biol **18**(6): 607-618.
Piller, G. (2001). "Leukaemia - a brief historical review from ancient times to 1950." Br J Haematol **112**(2): 282-292.
Ptasinska, A., S. A. Assi, D. Mannari, S. R. James, D. Williamson, J. Dunne, M. Hoogenkamp, M. Wu, M. Care, H. McNeill, P. Cauchy, M. Cullen, R. M. Tooze, D. G. Tenen, B. D. Young, P. N. Cockerill, D. R. Westhead, O. Heidenreich and C. Bonifer (2012). "Depletion of RUNX1/ETO in t(8;21) AML cells leads

to genome-wide changes in chromatin structure and transcription factor binding." Leukemia **26**(8): 1829-1841.
Ptasinska, A., S. A. Assi, N. Martinez-Soria, M. R. Imperato, J. Piper, P. Cauchy, A. Pickin, S. R. James, M. Hoogenkamp, D. Williamson, M. Wu, D. G. Tenen, S. Ott, D. R. Westhead, P. N. Cockerill, O. Heidenreich and C. Bonifer (2014). "Identification of a dynamic core transcriptional network in t(8;21) AML that regulates differentiation block and self-renewal." Cell Rep **8**(6): 1974-1988.
Pulikkan, J. A., D. Madera, L. Xue, P. Bradley, S. F. Landrette, Y. H. Kuo, S. Abbas, L. J. Zhu, P. Valk and L. H. Castilla (2012). "Thrombopoietin/MPL participates in initiating and maintaining RUNX1-ETO acute myeloid leukemia via PI3K/AKT signaling." Blood **120**(4): 868-879.
Qiu, C., Q. Xie, D. Zhang, Q. Chen, J. Hu and L. Xu (2014). "GM-CSF induces cyclin D1 expression and proliferation of endothelial progenitor cells via PI3K and MAPK signaling." Cell Physiol Biochem **33**(3): 784-795.
Quintas-Cardama, A., C. Hu, A. Qutub, Y. H. Qiu, X. Zhang, S. M. Post, N. Zhang, K. Coombes and S. M. Kornblau (2017). "p53 pathway dysfunction is highly prevalent in acute myeloid leukemia independent of TP53 mutational status." Leukemia **31**(6): 1296-1305.
Raje, N., S. Kumar, T. Hideshima, A. Roccaro, K. Ishitsuka, H. Yasui, N. Shiraishi, D. Chauhan, N. C. Munshi, S. R. Green and K. C. Anderson (2005). "Seliciclib (CYC202 or R-roscovitine), a small-molecule cyclin-dependent kinase inhibitor, mediates activity via down-regulation of Mcl-1 in multiple myeloma." Blood **106**(3): 1042-1047.
Regha, K., S. A. Assi, O. Tsoulaki, J. Gilmour, G. Lacaud and C. Bonifer (2015). "Developmental-stage-dependent transcriptional response to leukaemic oncogene expression." Nat Commun **6**: 7203.
Reikvam, H., K. J. Hatfield, P. Lassalle, A. O. Kittang, E. Ersvaer and O. Bruserud (2010). "Targeting the angiopoietin (Ang)/Tie-2 pathway in the crosstalk between acute myeloid leukaemia and endothelial cells: studies of Tie-2 blocking antibodies, exogenous Ang-2 and inhibition of constitutive agonistic Ang-1 release." Expert Opinion on Investigational Drugs **19**(2): 169-183.
Reinhardt, D., K. Reinhardt, C. Neuhoff, A. Sander, J. H. Klusmann, A. Pekrun, A. Sauerbrey, A. von Stackelberg, C. Rossig, U. Creutzig and A. Kolenova (2012). "[GATA1-mutation associated leukemia in children with trisomy 21 mosaic]." Klin Padiatr **224**(3): 153-155.
Rejman, J., A. Bragonzi and M. Conese (2005). "Role of clathrin- and caveolae-mediated endocytosis in gene transfer mediated by lipo- and polyplexes." Mol Ther **12**(3): 468-474.
Rejman, J., M. Conese and D. Hoekstra (2006). "Gene transfer by means of lipo- and polyplexes: role of clathrin and caveolae-mediated endocytosis." J Liposome Res **16**(3): 237-247.
Ritschka, B., M. Storer, A. Mas, F. Heinzmann, M. C. Ortells, J. P. Morton, O. J. Sansom, L. Zender and W. M. Keyes (2017). "The senescence-associated secretory phenotype induces cellular plasticity and tissue regeneration." Genes Dev **31**(2): 172-183.
Rizk, M. and S. Tuzmen (2017). "Update on the clinical utility of an RNA interference-based treatment: focus on Patisiran." Pharmgenomics Pers Med **10**: 267-278.
Roberts, A. W., J. F. Seymour, J. R. Brown, W. G. Wierda, T. J. Kipps, S. L. Khaw, D. A. Carney, S. Z. He, D. C. Huang, H. Xiong, Y. Cui, T. A. Busman, E. M. McKeegan, A. P. Krivoshik, S. H. Enschede and R. Humerickhouse (2012). "Substantial susceptibility of chronic lymphocytic leukemia to BCL2 inhibition: results of a phase I study of navitoclax in patients with relapsed or refractory disease." J Clin Oncol **30**(5): 488-496.
Rodier, F., J. P. Coppe, C. K. Patil, W. A. Hoeijmakers, D. P. Munoz, S. R. Raza, A. Freund, E. Campeau, A. R. Davalos and J. Campisi (2009). "Persistent DNA damage signalling triggers senescence-associated inflammatory cytokine secretion." Nat Cell Biol **11**(8): 973-979.
Rongvaux, A., T. Willinger, J. Martinek, T. Strowig, S. V. Gearty, L. L. Teichmann, Y. Saito, F. Marches, S. Halene, A. K. Palucka, M. G. Manz and R. A. Flavell (2014). "Development and function of human innate immune cells in a humanized mouse model." Nat Biotechnol **32**(4): 364-372.
Rulina, A. V., P. V. Spirin and V. S. Prassolov (2010). "Activated leukemic oncogenes AML1-ETO and c-kit: role in development of acute myeloid leukemia and current approaches for their inhibition." Biochemistry (Mosc) **75**(13): 1650-1666.

Ryotokuji, T., H. Yamaguchi, T. Ueki, K. Usuki, S. Kurosawa, Y. Kobayashi, E. Kawata, K. Tajika, S. Gomi, J. Kanda, A. Kobayashi, I. Omori, A. Marumo, Y. Fujiwara, S. Yui, K. Terada, K. Fukunaga, T. Hirakawa, K. Arai, T. Kitano, F. Kosaka, H. Tamai, K. Nakayama, S. Wakita, T. Fukuda and K. Inokuchi (2016). "Clinical characteristics and prognosis of acute myeloid leukemia associated with DNA-methylation regulatory gene mutations." Haematologica **101**(9): 1074-1081.
Sabbath, K. D., E. D. Ball, P. Larcom, R. B. Davis and J. D. Griffin (1985). "Heterogeneity of clonogenic cells in acute myeloblastic leukemia." J Clin Invest **75**(2): 746-753.
Sablina, A. A., A. V. Budanov, G. V. Ilyinskaya, L. S. Agapova, J. E. Kravchenko and P. M. Chumakov (2005). "The antioxidant function of the p53 tumor suppressor." Nat Med **11**(12): 1306-1313.
Saito, Y., J. M. Ellegast, A. Rafiei, Y. Song, D. Kull, M. Heikenwalder, A. Rongvaux, S. Halene, R. A. Flavell and M. G. Manz (2016). "Peripheral blood CD34(+) cells efficiently engraft human cytokine knock-in mice." Blood **128**(14): 1829-1833.
Salati, S., R. Zini, E. Bianchi, A. Testa, F. Mavilio, R. Manfredini and S. Ferrari (2008). "Role of CD34 antigen in myeloid differentiation of human hematopoietic progenitor cells." Stem Cells **26**(4): 950-959.
Salminen, A., A. Kauppinen and K. Kaarniranta (2012). "Emerging role of NF-kappaB signaling in the induction of senescence-associated secretory phenotype (SASP)." Cell Signal **24**(4): 835-845.
Santini, V., B. Scappini, Z. K. Indik, A. Gozzini, P. R. Ferrini and A. D. Schreiber (2003). "The carboxy-terminal region of the granulocyte colony-stimulating factor receptor transduces a phagocytic signal." Blood **101**(11): 4615-4622.
Sapkota, D., O. Bruland, H. Parajuli, T. A. Osman, M. T. Teh, A. C. Johannessen and D. E. Costea (2015). "S100A16 promotes differentiation and contributes to a less aggressive tumor phenotype in oral squamous cell carcinoma." BMC Cancer **15**: 631.
Sasaki, H. M., H. Tadakuma and Y. Tomari (2018). "Single-Molecule Analysis for RISC Assembly and Target Cleavage." Methods Mol Biol **1680**: 145-164.
Saulacic, N., B. Schaller, D. D. Bosshardt, D. Buser, P. Jaun, H. Haeniwa and T. Iizuka (2012). "Periosteal distraction osteogenesis and barrier membrane application: an experimental study in the rat calvaria." J Periodontol **83**(6): 757-765.
Saulacic, N., B. Schaller, T. Iizuka, D. Buser, C. Hug and D. D. Bosshardt (2013). "Analysis of new bone formation induced by periosteal distraction in a rat calvarium model." Clin Implant Dent Relat Res **15**(2): 283-291.
Scheer, C., C. Kratz, O. Witt, U. Creutzig, D. Reinhardt and J. H. Klusmann (2016). "Hematologic Response to Vorinostat Treatment in Relapsed Myeloid Leukemia of Down Syndrome." Pediatr Blood Cancer **63**(9): 1677-1679.
Schepers, H., P. Korthuis, M. Geugien, J. Jaques, T. I. Todorova, U. Steidl, J. J. Schuringa and E. Vellenga (2015). "CITED2 Cooperates with Low PU.1 and DNMT3A to Maintain Self-Renewal in Hematopoietic Stem Cells." Blood **126**(23).
Schepers, H., P. M. Korthuis, J. J. Schuringa and E. Vellenga (2013). "Decreased PU.1 and Enhanced CITED2 Cooperate To Maintain Self-Renewal In Hematopoietic Stem/Progenitors." Blood **122**(21).
Scherr, M., K. Battmer, T. Winkler, O. Heidenreich, A. Ganser and M. Eder (2003). "Specific inhibition of bcr-abl gene expression by small interfering RNA." Blood **101**(4): 1566-1569.
Scherr, M., H. Kirchhoff, K. Battmer, K. Wohlan, C. W. Lee, M. Ricke-Hoch, S. Erschow, E. Law, A. Kloos, M. Heuser, A. Ganser, D. Hilfiker-Kleiner and O. Heidenreich (2019). "Optimized induction of mitochondrial apoptosis for chemotherapy-free treatment of BCR-ABL+acute lymphoblastic leukemia." **33**(6): 1313-1323.
Schirle, N. T., J. Sheu-Gruttadauria and I. J. MacRae (2014). "Structural basis for microRNA targeting." Science **346**(6209): 608-613.
Schlenk, R. F., K. Dohner, J. Krauter, S. Frohling, A. Corbacioglu, L. Bullinger, M. Habdank, D. Spath, M. Morgan, A. Benner, B. Schlegelberger, G. Heil, A. Ganser, H. Dohner and G. German-Austrian Acute Myeloid Leukemia Study (2008). "Mutations and treatment outcome in cytogenetically normal acute myeloid leukemia." N Engl J Med **358**(18): 1909-1918.

Schlossman, D. M., S. L. Schmid, W. A. Braell and J. E. Rothman (1984). "An Enzyme That Removes Clathrin Coats - Purification of an Uncoating Atpase." Journal of Cell Biology **99**(2): 723-733.
Schlundt, A., J. N. Tants and M. Sattler (2017). "Integrated structural biology to unravel molecular mechanisms of protein-RNA recognition." Methods **118-119**: 119-136.
Schmidt, T. and P. Carmeliet (2011). "Angiogenesis: A Target in Solid Tumors, Also in Leukemia?" Hematology-American Society of Hematology Education Program: 1-8.
Scholl, C., D. G. Gilliland and S. Frohling (2008). "Deregulation of signaling pathways in acute myeloid leukemia." Semin Oncol **35**(4): 336-345.
Schuck, J., T. Gursinsky, V. Pantaleo, J. Burgyan and S. E. Behrens (2013). "AGO/RISC-mediated antiviral RNA silencing in a plant in vitro system." Nucleic Acids Res **41**(9): 5090-5103.
Schwarz, D. S., Y. Tomari and P. D. Zamore (2004). "The RNA-induced silencing complex is a Mg2+-dependent endonuclease." Current Biology **14**(9): 787-791.
Semov, A., M. J. Moreno, A. Onichtchenko, A. Abulrob, M. Ball, I. Ekiel, G. Pietrzynski, D. Stanimirovic and V. Alakhov (2005). "Metastasis-associated protein S100A4 induces angiogenesis through interaction with annexin II and accelerated plasmin formation." Journal of Biological Chemistry **280**(21): 20833-20841.
Semple, S. C., A. Akinc, J. Chen, A. P. Sandhu, B. L. Mui, C. K. Cho, D. W. Sah, D. Stebbing, E. J. Crosley, E. Yaworski, I. M. Hafez, J. R. Dorkin, J. Qin, K. Lam, K. G. Rajeev, K. F. Wong, L. B. Jeffs, L. Nechev, M. L. Eisenhardt, M. Jayaraman, M. Kazem, M. A. Maier, M. Srinivasulu, M. J. Weinstein, Q. Chen, R. Alvarez, S. A. Barros, S. De, S. K. Klimuk, T. Borland, V. Kosovrasti, W. L. Cantley, Y. K. Tam, M. Manoharan, M. A. Ciufolini, M. A. Tracy, A. de Fougerolles, I. MacLachlan, P. R. Cullis, T. D. Madden and M. J. Hope (2010). "Rational design of cationic lipids for siRNA delivery." Nat Biotechnol **28**(2): 172-176.
Senac, J. B. (1926). "Traite de la structure du coeur, de son action, et de ses maladies, Vol 2, p 366. Paris, Breasson, 1749. As quoted by Beck CS: Wounds of the heart. The technic of suture." Arch Surg **13**: 205-227.
Seok, H., H. Lee, E. S. Jang and S. W. Chi (2018). "Evaluation and control of miRNA-like off-target repression for RNA interference." **75**(5): 797-814.
Setten, R. L., J. J. Rossi and S. P. Han (2019). "The current state and future directions of RNAi-based therapeutics." **18**(6): 421-446.
Shafer, D. and S. Grant (2016). "Update on rational targeted therapy in AML." Blood Rev **30**(4): 275-283.
Shajari, N., B. Mansoori, S. Davudian, A. Mohammadi and B. Baradaran (2017). "Overcoming the Challenges of siRNA Delivery: Nanoparticle Strategies." Curr Drug Deliv **14**(1): 36-46.
Sheibani, N., Y. Tang and C. M. Sorenson (2008). "Paxillin's LD4 motif interacts with bcl-2." J Cell Physiol **214**(3): 655-661.
Shen, X. and D. R. Corey (2018). "Chemistry, mechanism and clinical status of antisense oligonucleotides and duplex RNAs." Nucleic Acids Res **46**(4): 1584-1600.
Shen, Y., Y. M. Zhu, X. Fan, J. Y. Shi, Q. R. Wang, X. J. Yan, Z. H. Gu, Y. Y. Wang, B. Chen, C. L. Jiang, H. Yan, F. F. Chen, H. M. Chen, Z. Chen, J. Jin and S. J. Chen (2011). "Gene mutation patterns and their prognostic impact in a cohort of 1185 patients with acute myeloid leukemia." Blood **118**(20): 5593-5603.
Shi, J., B. Chou, J. L. Choi, A. L. Ta and S. H. Pun (2013). "Investigation of Polyethylenimine/DNA Polyplex Transfection to Cultured Cells Using Radiolabeling and Subcellular Fractionation Methods." Mol Pharm **10**(6): 2145-2156.
Shimi, T., V. Butin-Israeli, S. A. Adam, R. B. Hamanaka, A. E. Goldman, C. A. Lucas, D. K. Shumaker, S. T. Kosak, N. S. Chandel and R. D. Goldman (2011). "The role of nuclear lamin B1 in cell proliferation and senescence." Genes Dev **25**(24): 2579-2593.
Shimizu, T., Y. Kida and K. Kuwano (2008). "Ureaplasma parvum lipoproteins, including MB antigen, activate NF-{kappa}B through TLR1, TLR2 and TLR6." Microbiology **154**(Pt 5): 1318-1325.

Siddiqui, A., D. E. Hogge, T. J. Nevill, S. H. Nantel, M. J. Barnett, R. Broady, D. L. Forrest, S. Narayanan, M. M. Power, K. W. Song, C. L. Toze, Y. Abou Mourad, H. J. Sutherland, A. S. Gerrie and D. Sanford (2016). "Long-Term Outcomes of Patients with Acute Myeloid Leukemia Treated with Salvage High-Dose Etoposide and Cyclophosphamide." Blood **128**(22).
Singh, A. A., A. Mandoli, K. H. Prange, M. Laakso and J. H. Martens (2017). "AML associated oncofusion proteins PML-RARA, AML1-ETO and CBFB-MYH11 target RUNX/ETS-factor binding sites to modulate H3ac levels and drive leukemogenesis." Oncotarget **8**(8): 12855-12865.
Sipa, K., E. Sochacka, J. Kazmierczak-Baranska, M. Maszewska, M. Janicka, G. Nowak and B. Nawrot (2007). "Effect of base modifications on structure, thermodynamic stability, and gene silencing activity of short interfering RNA." RNA **13**(8): 1301-1316.
Skorski, T., C. Szczylik, L. Malaguarnera and B. Calabretta (1991). "Gene-targeted specific inhibition of chronic myeloid leukemia cell growth by BCR-ABL antisense oligodeoxynucleotides." Folia Histochem Cytobiol **29**(3): 85-89.
Somoza, A., M. Terrazas and R. Eritja (2010). "Modified siRNAs for the study of the PAZ domain." Chem Commun (Camb) **46**(24): 4270-4272.
Sontheimer, E. J. (2005). "Assembly and function of RNA silencing complexes." Nat Rev Mol Cell Biol **6**(2): 127-138.
Soria, N. M., R. Tussiwand, P. Ziegler, M. G. Manz and O. Heidenreich (2008). "Transient depletion of RUNX1/RUNX1T1 by RNA interference delays tumour formation in vivo." Leukemia **23**: 188.
Soria, N. M., R. Tussiwand, P. Ziegler, M. G. Manz and O. Heidenreich (2009). "Transient depletion of RUNX1/RUNX1T1 by RNA interference delays tumour formation in vivo." Leukemia **23**(1): 188-190.
Souers, A. J., J. D. Leverson, E. R. Boghaert, S. L. Ackler, N. D. Catron, J. Chen, B. D. Dayton, H. Ding, S. H. Enschede, W. J. Fairbrother, D. C. S. Huang, S. G. Hymowitz, S. Jin, S. L. Khaw, P. J. Kovar, L. T. Lam, J. Lee, H. L. Maecker, K. C. Marsh, K. D. Mason, M. J. Mitten, P. M. Nimmer, A. Oleksijew, C. H. Park, C. M. Park, D. C. Phillips, A. W. Roberts, D. Sampath, J. F. Seymour, M. L. Smith, G. M. Sullivan, S. K. Tahir, C. Tse, M. D. Wendt, Y. Xiao, J. C. Xue, H. C. Zhang, R. A. Humerickhouse, S. H. Rosenberg and S. W. Elmore (2013). "ABT-199, a potent and selective BCL-2 inhibitor, achieves antitumor activity while sparing platelets." Nature Medicine **19**(2): 202-208.
Sroczynska, P., C. Lancrin, V. Kouskoff and G. Lacaud (2009). "The differential activities of Runx1 promoters define milestones during embryonic hematopoiesis." Blood **114**(26): 5279-5289.
Stewart, J. C. (1980). "Colorimetric determination of phospholipids with ammonium ferrothiocyanate." Anal Biochem **104**(1): 10-14.
Stochaj, W. R., T. Berkelman and N. Laird (2006). "Staining membrane-bound proteins with ponceau s." CSH Protoc **2006**(5).
Strobel, S. L. and J. T. Brandt (1986). "The value of the Wright-Giemsa stain for diagnosing hairy cell leukemia in body cavity fluids." J Surg Oncol **33**(3): 182-185.
Stuart, D. D. and T. M. Allen (2000). "A new liposomal formulation for antisense oligodeoxynucleotides with small size, high incorporation efficiency and good stability." Biochim Biophys Acta **1463**(2): 219-229.
Sugamura, K., H. Asao, M. Kondo, N. Tanaka, N. Ishii, K. Ohbo, M. Nakamura and T. Takeshita (1996). "The interleukin-2 receptor gamma chain: its role in the multiple cytokine receptor complexes and T cell development in XSCID." Annu Rev Immunol **14**: 179-205.
Sullivan, C. B., R. M. Porter, C. H. Evans, T. Ritter, G. Shaw, F. Barry and J. M. Murphy (2014). "TNFalpha and IL-1beta influence the differentiation and migration of murine MSCs independently of the NF-kappaB pathway." Stem Cell Res Ther **5**(4): 104.
Sun, Y., J. Sun, T. Tomomi, E. Nieves, N. Mathewson, H. Tamaki, R. Evers and P. Reddy (2013). "PU.1-dependent transcriptional regulation of miR-142 contributes to its hematopoietic cell-specific expression and modulation of IL-6." J Immunol **190**(8): 4005-4013.
Sun, Y., S. Varambally, C. A. Maher, Q. Cao, P. Chockley, T. Toubai, C. Malter, E. Nieves, I. Tawara, Y. Wang, P. A. Ward, A. Chinnaiyan and P. Reddy (2011). "Targeting of microRNA-142-3p in dendritic cells regulates endotoxin-induced mortality." Blood **117**(23): 6172-6183.

Sune-Pou, M., M. J. Limeres, I. Nofrerias, A. Nardi-Ricart, S. Prieto-Sanchez, Y. El-Yousfi, P. Perez-Lozano, E. Garcia-Montoya, M. Minarro-Carmona, J. R. Tico, C. Hernandez-Munain, C. Sune and J. M. Sune-Negre (2019). "Improved synthesis and characterization of cholesteryl oleate-loaded cationic solid lipid nanoparticles with high transfection efficiency for gene therapy applications." Colloids Surf B Biointerfaces **180**: 159-167.
Suzuki, K., K. Ino, Y. Sugawara, M. Mizutani, T. Sekine and N. Katayama (2008). "[Acute myeloid leukemia invasion of the central nervous system, detected only along the Virchow Robin space]." Rinsho Ketsueki **49**(5): 340-343.
Tabe, Y., M. Konopleva, Y. Kondo, R. Contractor, L. Jin, V. Ruvolo, Y. Tsutsumi-Ishii, K. Miyake, N. Miyake, A. Ohsaka, I. Nagaoka, J. P. Issa and M. Andreeff (2006). "PML-RARalpha and AML1-ETO translocations are rarely associated with methylation of the RARbeta2 promoter." Ann Hematol **85**(10): 689-704.
Tadin-Strapps, M., L. B. Peterson, A. M. Cumiskey, R. L. Rosa, V. H. Mendoza, J. Castro-Perez, O. Puig, L. Zhang, W. R. Strapps, S. Yendluri, L. Andrews, V. Pickering, J. Rice, L. Luo, Z. Chen, S. Tep, B. Ason, E. P. Somers, A. B. Sachs, S. R. Bartz, J. Tian, J. Chin, B. K. Hubbard, K. K. Wong and L. J. Mitnaul (2011). "siRNA-induced liver ApoB knockdown lowers serum LDL-cholesterol in a mouse model with human-like serum lipids." J Lipid Res **52**(6): 1084-1097.
Takakura, N., T. Watanabe, S. Suenobu, Y. Yamada, T. Noda, Y. Ito, M. Satake and T. Suda (2000). "A role for hematopoietic stem cells in promoting angiogenesis." Cell **102**(2): 199-209.
Tanaka, M., N. Ichikawa-Tomikawa, N. Shishito, K. Nishiura, T. Miura, A. Hozumi, H. Chiba, S. Yoshida, T. Ohtake and T. Sugino (2015). "Co-expression of S100A14 and S100A16 correlates with a poor prognosis in human breast cancer and promotes cancer cell invasion." Bmc Cancer **15**.
Tanoue, T., T. Yamamoto, R. Maeda and E. Nishida (2001). "A Novel MAPK phosphatase MKP-7 acts preferentially on JNK/SAPK and p38 alpha and beta MAPKs." J Biol Chem **276**(28): 26629-26639.
Taussig, D. C., J. Vargaftig, F. Miraki-Moud, E. Griessinger, K. Sharrock, T. Luke, D. Lillington, H. Oakervee, J. Cavenagh, S. G. Agrawal, T. A. Lister, J. G. Gribben and D. Bonnet (2010). "Leukemia-initiating cells from some acute myeloid leukemia patients with mutated nucleophosmin reside in the CD34(-) fraction." Blood **115**(10): 1976-1984.
Teh, T. C., N. Y. Nguyen, D. M. Moujalled, D. Segal, G. Pomilio, S. Rijal, A. Jabbour, K. Cummins, K. Lackovic, P. Blombery, E. Thompson, P. G. Ekert, G. Lessene, S. P. Glaser, D. C. S. Huang, A. W. Roberts, M. A. Guthridge and A. H. Wei (2018). "Enhancing venetoclax activity in acute myeloid leukemia by co-targeting MCL1." Leukemia **32**(2): 303-312.
Teichert-Kuliszewska, K., P. C. Maisonpierre, N. Jones, A. I. Campbell, Z. Master, M. P. Bendeck, K. Alitalo, D. J. Dumont, G. D. Yancopoulos and D. J. Stewart (2001). "Biological action of angiopoietin-2 in a fibrin matrix model of angiogenesis is associated with activation of Tie2." Cardiovasc Res **49**(3): 659-670.
Thol, F., B. Kolking, F. Damm, K. Reinhardt, J. H. Klusmann, D. Reinhardt, N. von Neuhoff, M. H. Brugman, B. Schlegelberger, S. Suerbaum, J. Krauter, A. Ganser and M. Heuser (2012). "Next-generation sequencing for minimal residual disease monitoring in acute myeloid leukemia patients with FLT3-ITD or NPM1 mutations." Genes Chromosomes Cancer **51**(7): 689-695.
Thomas, M., A. Gessner, H. P. Vornlocher, P. Hadwiger, J. Greil and O. Heidenreich (2005). "Targeting MLL-AF4 with short interfering RNAs inhibits clonogenicity and engraftment of t(4;11)-positive human leukemic cells." Blood **106**(10): 3559-3566.
Thomson, S. P. and F. L. Meyskens, Jr. (1982). "Method for measurement of self-renewal capacity of clonogenic cells from biopsies of metastatic human malignant melanoma." Cancer Res **42**(11): 4606-4613.
Thwaites, M. J., M. J. Cecchini and D. T. Passos (2017). "Interchangeable Roles for E2F Transcriptional Repression by the Retinoblastoma Protein and p27KIP1-Cyclin-Dependent Kinase Regulation in Cell Cycle Control and Tumor Suppression." **37**(2).

Tian, Y., D. K. Simanshu, J. B. Ma, J. E. Park, I. Heo, V. N. Kim and D. J. Patel (2014). "A Phosphate-Binding Pocket within the Platform-PAZ-Connector Helix Cassette of Human Dicer." Molecular Cell **53**(4): 606-616.
Tomari, Y. and P. D. Zamore (2005). "Perspective: machines for RNAi." Genes Dev **19**(5): 517-529.
Tomiyama, N., R. Ikeda, Y. Nishizawa, S. Masuda, Y. Tajitsu and Y. Takeda (2018). "S100A16 up-regulates Oct4 and Nanog expression in cancer stem-like cells of Yumoto human cervical carcinoma cells." Oncol Lett **15**(6): 9929-9933.
Trombly, D. J., T. W. Whitfield, S. Padmanabhan, J. A. Gordon, J. B. Lian, A. J. van Wijnen, S. K. Zaidi, J. L. Stein and G. S. Stein (2015). "Genome-wide co-occupancy of AML1-ETO and N-CoR defines the t(8;21) AML signature in leukemic cells." BMC Genomics **16**: 309.
Tse, C., A. R. Shoemaker, J. Adickes, M. G. Anderson, J. Chen, S. Jin, E. F. Johnson, K. C. Marsh, M. J. Mitten, P. Nimmer, L. Roberts, S. K. Tahir, Y. Xiao, X. Yang, H. Zhang, S. Fesik, S. H. Rosenberg and S. W. Elmore (2008). "ABT-263: a potent and orally bioavailable Bcl-2 family inhibitor." Cancer Res **68**(9): 3421-3428.
Uffmann, M., M. Rasche, M. Zimmermann, C. von Neuhoff, U. Creutzig, M. Dworzak, L. Scheffers, H. Hasle, C. M. Zwaan, D. Reinhardt and J. H. Klusmann (2017). "Therapy reduction in patients with Down syndrome and myeloid leukemia: the international ML-DS 2006 trial." **129**(25): 3314-3321.
Vairo, G., K. M. Innes and J. M. Adams (1996). "Bcl-2 has a cell cycle inhibitory function separable from its enhancement of cell survival." Oncogene **13**(7): 1511-1519.
Vairo, G., T. J. Soos, T. M. Upton, J. Zalvide, J. A. DeCaprio, M. E. Ewen, A. Koff and J. M. Adams (2000). "Bcl-2 retards cell cycle entry through p27(Kip1), pRB relative p130, and altered E2F regulation." Molecular and Cellular Biology **20**(13): 4745-4753.
Valenzuela, R. A., K. Onizuka, A. A. Ball-Jones, T. Hu, S. R. Suter and P. A. Beal (2016). "Guide Strand 3'-End Modifications Regulate siRNA Specificity." Chembiochem **17**(24): 2340-2345.
Vaskova, J., K. Dubayova, G. Cakanova, I. Luckova, I. Bochova, G. Novotna, J. Sabo, S. Palasthy, E. Tothova, N. Stecova and A. Karabinos (2015). "Incidence and Prognostic Value of Known Genetic Aberrations in Patients with Acute Myeloid Leukemia--a Two Year Study." Klin Onkol **28**(4): 278-283.
Vasselon, T., M. Bouttier, A. Saumet and C. H. Lecellier (2013). "RNAi and retroviruses: are they in RISC?" Biomol Concepts **4**(1): 43-52.
Viale, A., F. De Franco, A. Orleth, V. Cambiaghi, V. Giuliani, D. Bossi, C. Ronchini, S. Ronzoni, I. Muradore, S. Monestiroli, A. Gobbi, M. Alcalay, S. Minucci and P. G. Pelicci (2009). "Cell-cycle restriction limits DNA damage and maintains self-renewal of leukaemia stem cells." Nature **457**(7225): 51-56.
Viale, A. and P. G. Pelicci (2009). "Awaking stem cells from dormancy: growing old and fighting cancer." EMBO Mol Med **1**(2): 88-91.
Viger-Gravel, J., A. Schantz, A. C. Pinon, A. J. Rossini, S. Schantz and L. Emsley (2018). "Structure of Lipid Nanoparticles Containing siRNA or mRNA by Dynamic Nuclear Polarization-Enhanced NMR Spectroscopy." J Phys Chem B **122**(7): 2073-2081.
Virchow, R. (1855). "Cellular-pathologie." Archiv für pathologische Anatomie und Physiologie und für klinische Medicin **8**(1): 3-39.
Vonarbourg, A., C. Passirani, P. Saulnier, P. Simard, J. C. Leroux and J. P. Benoit (2006). "Evaluation of pegylated lipid nanocapsules versus complement system activation and macrophage uptake." J Biomed Mater Res A **78**(3): 620-628.
Vu, L. P. and M. G. Kharas (2018). "Targeting the Residual Leukemia Cells after Chemotherapy." Cancer Cell **34**(3): 353-355.
Walker, D. K., R. M. Jones, A. N. R. Nedderman and P. A. Wright (2010). Chapter 4 Primary, Secondary and Tertiary Amines and their Isosteres. Metabolism, Pharmacokinetics and Toxicity of Functional Groups: Impact of Chemical Building Blocks on ADMET, The Royal Society of Chemistry**:** 168-209.

Wang, H., W. Li, R. Guo, J. Sun, J. Cui, G. Wang, A. R. Hoffman and J. F. Hu (2014). "An intragenic long noncoding RNA interacts epigenetically with the RUNX1 promoter and enhancer chromatin DNA in hematopoietic malignancies." Int J Cancer **135**(12): 2783-2794.
Wang, L., W. Cai, W. Zhang, X. Chen, W. Dong, D. Tang, Y. Zhang, C. Ji and M. Zhang (2015). "Inhibition of poly(ADP-ribose) polymerase 1 protects against acute myeloid leukemia by suppressing the myeloproliferative leukemia virus oncogene." Oncotarget **6**(29): 27490-27504.
Wang, L., G. Huang, X. Zhao, M. A. Hatlen, L. Vu, F. Liu and S. D. Nimer (2009). "Post-translational modifications of Runx1 regulate its activity in the cell." Blood Cells Mol Dis **43**(1): 30-34.
Wang, X., J. S. Harrison and G. P. Studzinski (2016). "Enhancement of arabinocytosine (AraC) toxicity to AML cells by a differentiation agent combination." J Steroid Biochem Mol Biol **164**: 72-78.
Wang, Y. L., S. Juranek, H. T. Li, G. Sheng, G. S. Wardle, T. Tuschl and D. J. Patel (2009). "Nucleation, propagation and cleavage of target RNAs in Ago silencing complexes." Nature **461**(7265): 754-U753.
Ward, S. V., T. Sternsdorf and N. B. Woods (2011). "Targeting expression of the leukemogenic PML-RARalpha fusion protein by lentiviral vector-mediated small interfering RNA results in leukemic cell differentiation and apoptosis." Hum Gene Ther **22**(12): 1593-1598.
Watts, J. K., N. Martin-Pintado, I. Gomez-Pinto, J. Schwartzentruber, G. Portella, M. Orozco, C. Gonzalez and M. J. Damha (2010). "Differential stability of 2'F-ANA*RNA and ANA*RNA hybrid duplexes: roles of structure, pseudohydrogen bonding, hydration, ion uptake and flexibility." Nucleic Acids Res **38**(7): 2498-2511.
Wei, J., J. Jones, J. Kang, A. Card, M. Krimm, P. Hancock, Y. Pei, B. Ason, E. Payson, N. Dubinina, M. Cancilla, M. Stroh, J. Burchard, A. B. Sachs, J. H. Hochman, W. M. Flanagan and N. A. Kuklin (2011). "RNA-induced silencing complex-bound small interfering RNA is a determinant of RNA interference-mediated gene silencing in mice." Mol Pharmacol **79**(6): 953-963.
Weinstein, S., I. A. Toker, R. Emmanuel, S. Ramishetti, I. Hazan-Halevy, D. Rosenblum, M. Goldsmith, A. Abraham, O. Benjamini, O. Bairey, P. Raanani, A. Nagler, J. Lieberman and D. Peer (2016). "Harnessing RNAi-based nanomedicines for therapeutic gene silencing in B-cell malignancies." Proc Natl Acad Sci U S A **113**(1): E16-22.
Werfel, T. A., M. A. Jackson, T. E. Kavanaugh, K. C. Kirkbride, M. Miteva, T. D. Giorgio and C. Duvall (2017). "Combinatorial optimization of PEG architecture and hydrophobic content improves ternary siRNA polyplex stability, pharmacokinetics, and potency in vivo." Journal of Controlled Release **255**: 12-26.
Whitehead, K. A., J. E. Dahlman, R. S. Langer and D. G. Anderson (2011). "Silencing or stimulation? siRNA delivery and the immune system." Annu Rev Chem Biomol Eng **2**: 77-96.
Wichmann, C., L. Chen, M. Heinrich, D. Baus, E. Pfitzner, M. Zornig, O. G. Ottmann and M. Grez (2007). "Targeting the oligomerization domain of ETO interferes with RUNX1/ETO oncogenic activity in t(8;21)-positive leukemic cells." Cancer Res **67**(5): 2280-2289.
Woronzoff-Dashkoff, K. K. (2002). "The wright-giemsa stain. Secrets revealed." Clin Lab Med **22**(1): 15-23.
Woytschak, J., N. Keller, C. Krieg, D. Impellizzieri, R. W. Thompson, T. A. Wynn, A. S. Zinkernagel and O. Boyman (2016). "Type 2 Interleukin-4 Receptor Signaling in Neutrophils Antagonizes Their Expansion and Migration during Infection and Inflammation." Immunity **45**(1): 172-184.
Wu, F. T., C. R. Lee, E. Bogdanovic, A. Prodeus, J. Gariepy and R. S. Kerbel (2015). "Vasculotide reduces endothelial permeability and tumor cell extravasation in the absence of binding to or agonistic activation of Tie2." EMBO Mol Med **7**(6): 770-787.
Wunderlich, M. and J. C. Mulloy (2016). "MISTRG extends PDX modeling to favorable AMLs." Blood **128**(17): 2111-2112.
Wyman, T. H., C. A. Dinarello, A. Banerjee, F. Gamboni-Robertson, A. A. Hiester, K. M. England, M. Kelher and C. C. Silliman (2002). "Physiological levels of interleukin-18 stimulate multiple neutrophil functions through p38 MAP kinase activation." J Leukoc Biol **72**(2): 401-409.
Xie, C. Z., H. Edwards, X. L. Xu, H. Zhou, S. A. Buck, M. L. Stout, Q. Yu, J. E. Rubnitz, L. H. Matherly, J. W. Taub and Y. B. Ge (2010). "Mechanisms of Synergistic Antileukemic Interactions between Valproic

Acid and Cytarabine in Pediatric Acute Myeloid Leukemia." Clinical Cancer Research **16**(22): 5499-5510.
Xu, L., X. Wang, H. He, J. Zhou, X. Li, H. Ma, Z. Li, Y. Zeng, R. Shao, S. Cen and Y. Wang (2015). "Structure-based design of novel chemical modification of the 3'-overhang for optimization of short interfering RNA performance." Biochemistry **54**(5): 1268-1277.
Xu, M., T. Pirtskhalava, J. N. Farr, B. M. Weigand, A. K. Palmer, M. M. Weivoda, C. L. Inman, M. B. Ogrodnik, C. M. Hachfeld, D. G. Fraser, J. L. Onken, K. O. Johnson, G. C. Verzosa, L. G. P. Langhi, M. Weigl, N. Giorgadze, N. K. LeBrasseur, J. D. Miller, D. Jurk, R. J. Singh, D. B. Allison, K. Ejima, G. B. Hubbard, Y. Ikeno, H. Cubro, V. D. Garovic, X. Hou, S. J. Weroha, P. D. Robbins, L. J. Niedernhofer, S. Khosla, T. Tchkonia and J. L. Kirkland (2018). "Senolytics improve physical function and increase lifespan in old age." Nat Med **24**(8): 1246-1256.
Yamada, S. and I. Maruyama (2007). "HMGB1, a novel inflammatory cytokine." Clin Chim Acta **375**(1-2): 36-42.
Yan, M., E. Kanbe, L. F. Peterson, A. Boyapati, Y. Miao, Y. Wang, I. M. Chen, Z. Chen, J. D. Rowley, C. L. Willman and D. E. Zhang (2006). "A previously unidentified alternatively spliced isoform of t(8;21) transcript promotes leukemogenesis." Nat Med **12**(8): 945-949.
Yan, M., E. Kanbe, L. F. Peterson, A. Boyapati, Y. Miao, Y. Wang, I. M. Chen, Z. X. Chen, J. D. Rowley, C. L. Willman and D. E. Zhang (2006). "A previously unidentified alternatively spliced isoform of t(8;21) transcript promotes leukemogenesis." Nature Medicine **12**(8): 945-949.
Yang, G., M. A. Thompson, S. J. Brandt and S. W. Hiebert (2007). "Histone deacetylase inhibitors induce the degradation of the t(8;21) fusion oncoprotein." Oncogene **26**(1): 91-101.
Yang, Y., Y. Zhao, W. Liao, J. Yang, L. Wu, Z. Zheng, Y. Yu, W. Zhou, L. Li, J. Feng, H. Wang and W. G. Zhu (2009). "Acetylation of FoxO1 activates Bim expression to induce apoptosis in response to histone deacetylase inhibitor depsipeptide treatment." Neoplasia **11**(4): 313-324.
Yi, T. (2018). "Identifying RISC Components Using Ago2 Immunoprecipitation and Mass Spectrometry." Methods Mol Biol **1720**: 149-159.
Yoneyama, M., M. Kikuchi, T. Natsukawa, N. Shinobu, T. Imaizumi, M. Miyagishi, K. Taira, S. Akira and T. Fujita (2004). "The RNA helicase RIG-I has an essential function in double-stranded RNA-induced innate antiviral responses." Nature Immunology **5**(7): 730-737.
Yuan, Y. Z., L. M. Zhou, T. Miyamoto, H. Iwasaki, N. Harakawa, C. J. Hetherington, S. A. Burel, E. Lagasse, I. L. Weissman, K. Akashi and D. E. Zhang (2001). "AML1-ETO expression is directly involved in the development of acute myeloid leukemia in the presence of additional mutations." Blood **98**(11): 565a-566a.
Yue, X. and Z. Dai (2018). "Liposomal Nanotechnology for Cancer Theranostics." Curr Med Chem **25**(12): 1397-1408.
Zaidi, S. K., C. R. Dowdy, A. J. van Wijnen, J. B. Lian, A. Raza, J. L. Stein, C. M. Croce and G. S. Stein (2009). "Altered Runx1 subnuclear targeting enhances myeloid cell proliferation and blocks differentiation by activating a miR-24/MKP-7/MAPK network." Cancer Res **69**(21): 8249-8255.
Zhang, D. E., K. I. Fujioka, C. J. Hetherington, L. H. Shapiro, H. M. Chen, A. T. Look and D. G. Tenen (1994). "Identification of a Region Which Directs the Monocytic Activity of the Colony-Stimulating Factor-1 (Macrophage-Colony-Stimulating Factor) Receptor Promoter and Binds Pebp2/Cbf (Aml1)." Molecular and Cellular Biology **14**(12): 8085-8095.
Zhang, D. E., C. J. Hetherington, S. Meyers, K. L. Rhoades, C. J. Larson, H. M. Chen, S. W. Hiebert and D. G. Tenen (1996). "CCAAT enhancer-binding protein (C/EBP) and AML1 (CBF alpha2) synergistically activate the macrophage colony-stimulating factor receptor promoter." Mol Cell Biol **16**(3): 1231-1240.
Zhang, Y., Y. Huang and S. Li (2014). "Polymeric micelles: nanocarriers for cancer-targeted drug delivery." AAPS PharmSciTech **15**(4): 862-871.
Zhang, Z., U. Ohto and T. Shimizu (2017). "Toward a structural understanding of nucleic acid-sensing Toll-like receptors in the innate immune system." FEBS Lett **591**(20): 3167-3181.

Zhao, H., F. Liu, R. Jia, H. Chang, H. Li, M. Miao, H. Wang and Z. Yang (2017). "MiR-570 inhibits cell proliferation and glucose metabolism by targeting IRS1 and IRS2 in human chronic myelogenous leukemia." Iran J Basic Med Sci **20**(5): 481-488.
Zhao, Y., J. Tan, L. Zhuang, X. Jiang, E. T. Liu and Q. Yu (2005). "Inhibitors of histone deacetylases target the Rb-E2F1 pathway for apoptosis induction through activation of proapoptotic protein Bim." Proceedings of the National Academy of Sciences of the United States of America **102**(44): 16090-16095.
Zhigaltsev, I. V., N. Maurer, K. F. Wong and P. R. Cullis (2002). "Triggered release of doxorubicin following mixing of cationic and anionic liposomes." Biochim Biophys Acta **1565**(1): 129-135.
Zhou, B. O., L. Ding and S. J. Morrison (2015). "Hematopoietic stem and progenitor cells regulate the regeneration of their niche by secreting Angiopoietin-1." Elife **4**.
Zhou, C., Z. Li, H. Diao, Y. Yu, W. Zhu, Y. Dai, F. F. Chen and J. Yang (2006). "DNA damage evaluated by gammaH2AX foci formation by a selective group of chemical/physical stressors." Mutat Res **604**(1-2): 8-18.
Zhu, Y., T. Tchkonia, T. Pirtskhalava, A. C. Gower, H. S. Ding, N. Giorgadze, A. K. Palmer, Y. Ikeno, G. B. Hubbard, M. Lenburg, S. P. O'Hara, N. F. LaRusso, J. D. Miller, C. M. Roos, G. C. Verzosa, N. K. LeBrasseur, J. D. Wren, J. N. Farr, S. Khosla, M. B. Stout, S. J. McGowan, H. Fuhrmann-Stroissnigg, A. U. Gurkar, J. Zhao, D. Colangelo, A. Dorronsoro, Y. Y. Ling, A. S. Barghouthy, D. C. Navarro, T. Sano, P. D. Robbins, L. J. Niedernhofer and J. L. Kirkland (2015). "The Achilles' heel of senescent cells: from transcriptome to senolytic drugs." Aging Cell **14**(4): 644-658.
Ziello, J. E., Y. Huang and I. S. Jovin (2010). "Cellular endocytosis and gene delivery." Mol Med **16**(5-6): 222-229.
Zimmermann, T. S., A. C. Lee, A. Akinc, B. Bramlage, D. Bumcrot, M. N. Fedoruk, J. Harborth, J. A. Heyes, L. B. Jeffs, M. John, A. D. Judge, K. Lam, K. McClintock, L. V. Nechev, L. R. Palmer, T. Racie, I. Rohl, S. Seiffert, S. Shanmugam, V. Sood, J. Soutschek, I. Toudjarska, A. J. Wheat, E. Yaworski, W. Zedalis, V. Koteliansky, M. Manoharan, H. P. Vornlocher and I. MacLachlan (2006). "RNAi-mediated gene silencing in non-human primates." Nature **441**(7089): 111-114.
Zon, G. and T. G. Geiser (1991). "Phosphorothioate oligonucleotides: chemistry, purification, analysis, scale-up and future directions." Anticancer Drug Des **6**(6): 539-568.